Electrode Processes

A Thesis Submitted for the Degree of Doctor of Philosophy in the University of Oxford

by

W. Joanne Aixill

Wolfson College

Trinity Term 1998

Electrode Processes
D. Phil. Thesis

W. Joanne Aixill
Trinity Term 1998

Abstract

The work presented in this thesis first characterises a high speed channel flow cell and then applies the system to the electro-reduction of nitromethane in aqueous solution.
Potential step transient measurements are carried out with the current-time transients simulated using a model based on the absence of axial diffusion. The excellent agreement between theory and experiment confirms the proposed mass transport model and further demonstrates that the combination of current-time transients recorded using the high speed channel flow cell and numerical simulations provide a powerful tool to access homogeneous rate constants of the order 1 x 10^6 s^{-1}.
The high speed channel flow cell is then used in combination with a range of complementary electrochemical techniques, numerical modelling, *in-situ* ESR, single crystal experiments and kinetic isotope measurements to infer a mechanistic scheme for the complex electro-reduction pathway of nitromethane in aqueous solution. Platinum, gold, mercury/copper and mercury/gold electrodes are investigated enabling the most conclusive description of the reduction mechanism to date. The reaction pathway is shown to follow an ECEEE type process with the chemical step proceeding at the electrode surface. The heterogeneous rate constant, k_{het}, describing the chemical step is calculated for each electrode surface. For platinum in the pH range 7.0 - 9.0 this value is 0.3 ± 0.06 cm s^{-1}. For mercury/copper it is 0.18 cm s^{-1}, for gold/mercury it is 0.06 cm s^{-1} and for Au it is 0.095 cm s^{-1}. Consideration of these values shows a surprising independence of the heterogeneous rate constant on the chemical identity of the surface with all of the values being similar to within less than an order of magnitude. The reason for the apparent paradox of the observed surface indifference of the chemical reaction step is explained by a homogeneous H transfer from the carbon to the oxygen of the nitromethane radical anion, formed form the initial electron transfer step, occurring in the layer of solution immediately adjacent to the electrode solution as shown in the scheme below. The resulting species, $^{\bullet}CH_2N(OH))^-$ then undergoes a rapid irreversible adsorption to the electrode surface and subsequent transformation to the final product the hydroxylamine, CH_3NHOH. It is proposed that if the energy barrier to the adsorption of $^{\bullet}CH_2N(OH))^-$ is less than that required for the H atom transfer then the reaction rate will be insensitive to the adsorption step and hence the chemical identity of the electrode. This introduces the concept of a whole new electrochemical process: *the surface indifferent electrocatalytic reaction.*

In loving memory of my father Hugh McNee Aixill

Acknowledgements

First I would like to thank Richard Compton for his supervision, encouragement and enthusiasm over the last three years.

Next I must say gracias to Paco for introducing me to the wonderful world of nitromethane which proved to be more of a mind bending mystery tour than any Inspector Morse. Cheers to Barry for all of his fast flow wisdom and the microbands that he churned out with painstaking precision. Thanks to John Freeman for pretty pictures. Staying on an academic theme I couldn't leave out the lovely Grimster who apart from being 'the most desirable' part II applied himself so well to Airy functions and Tetris. Also thanks to Pete for his informative chats on the rise and eventual plummet of Reading Football Club and sharing the whole nitromethane experience. I am also indebted to Dr. John Alden for his help in my execution of BI programs.

There is a unique bundle of beans in the lab that I must acknowledge for their entertainment and friendship during my days as the Wooster. The lovely Lilac for being a great mate every step of the way and defending my dignity on so many occasions, dearest Richie for his combat cavorting and always convincing me I had it in me, César who always supported my blonde campaign, Tommee for lucky tequila, lucky Alan and the not so lucky after effects, Coops for always reminding me of my vital statistics, age, height and hair colour, Jon Ball for his intriguing conversations (with the PC), Sarah for joining me on polishing marathons, Frank and his extensive library, Marco for his delicate touch with the single crystals, Jonny and Giles from the early days for exposing me to sights of St. John's that would have your eye out, and Lembit Nei for introducing the concept of fish fingers for breakfast. Thanks also to Jaya for sharing the wonders of Wolfson.

Outside of Oxford I must mention my dear friend Jon who's constant tales and antics would fill more chapters than any D.Phil. and Greenpea who's friendship has seen me through many hairy moments.

Last but by no means least I must thank my Mum and Keith for their constant love, support and trips in the Galaxy that without which this thesis would not have been possible. Many thanks also to the Baldwins, the Aixills and Kelv.

1. Introduction

2. Theory

3. Experimental

4. Transient Measurements and the High Speed Channel Flow Cell

5. The Reduction of Nitromethane in Basic Aqueous Solution

6. Heterogeneous ECE Processes at Channel Electrodes : Analytical Theory

7. The Application of Voltammetric Waveshape Theory to the Reduction of Nitromethane

CONTENTS

8. The Reduction of Nitromethane: A Surface Indifferent Electrocatalytic Reaction

Appendices

1. Introduction

Contents

1.1 Introduction

Over the past decade the introduction of microelectrodes has brought about a dramatic shrinkage of the voltammetric timescale. Such electrodes have at least one dimension on the micron scale resulting in greater mass transport to the electrode surface through enhanced diffusion. This increase has enabled the study of rapid electron transfer reactions along with fast coupled homogeneous and heterogeneous kinetics that were previously masked by mass transport control[1,2].

Until very recently the electrochemical measurements involving microelectrodes were carried out under diffusion only conditions. However, the merits of using convection in addition to diffusion in order to enhance the rate of mass transport to the electrode surface and hence decrease the voltammetric timescale further have now been investigated. This has resulted in the development of a novel system, the high speed channel flow cell[3] which has enabled the study of complex reaction mechanisms that were previously beyond the scope of voltammetric measurement. This experimental system represents a whole new genre of flow systems, using a pressurised chamber to produce very high solution flow rates across the microelectrode. The powerful combination of using convective mass transport with a microelectrode is demonstrated in the following chapters through a range of mechanistic investigations.

This first chapter introduces the challenges of studying electron transfer reactions and their coupled chemistry before moving on to look at the use of the channel flow cell in probing

---

1 J. Wang, *Microelectrodes*, VCH, New York, (1990)

2 M. Fleichman and S. Pons, *Ultramicroelectrodes*, Datatech, Morganton, North Carolina, (1987)

3 N. V. Rees, R. A. Dryfe, J. A. Cooper, B. A. Coles, R. G. Compton, S. G. Davies and T. D. McCarthy, *J. Phys. Chem.*, **99**, (1995), 7096

such processes. The introduction of microelectrodes and the subsequent development of the high speed channel flow cell are then discussed.

1.2 Mechanistic Electrochemistry

It is often found after the addition or removal of an electron from an electroactive species that the immediate electrolysis product formed is unstable. In such cases the initial electron transfer step is followed by a chemical reaction which can take on three different forms:

(1) Cleavage of a chemical bond

The addition of an anti-bonding electron to an electroactive species may weaken a bond to the point where the activation barrier of the bond cleavage is overcome resulting in the loss of the bond. This is the case for alkyl halides in which a one electron reduction is followed by the rapid loss of the halide ion[4]:

$$RX + e^- \rightleftharpoons RX^{\bullet -} \rightarrow R^{\bullet} + X^-$$

For the oxidative case the bond may be weakened due to the removal of an electron from a bonding orbital. An example of this is the Kolbe[5] hydrocarbon synthesis in which a partially neutralised carboxylic acid is oxidised to form an acyloxy radical intermediate. This then rapidly loses CO_2 and dimerises to give the hydrocarbon product.

(2) Rearrangement

Radical ions often undergo some form of rearrangement in order to distribute their excess charge over the atoms involved more effectively and hence lower the energy of the molecule.

---

4 M. Mohammad, J. Hadju and E. M. Kosower, *J. Am. Chem. Soc.*, **93**, (1971), 1792

5 H. Kolbe, *Ann.*, **69**, (1843), 257

The rearranged molecule may then undergo bond cleavage, mentioned previously or electrophilic/nucleophilic attack.

(3) Electrophilic/nucleophilic attack

Radical anions are strong nucleophiles and are therefore very susceptible to electrophilic attack. In protic solvents the most available electrophile is usually the hydrogen ion which results in protonation of the radical anion. Similarly radical cations undergo nucleophilic attack.

For the oxidation case involving the loss of an electron a fourth type of chemical reaction may occur, dimerisation. An example of this is:

$$Co(Me_2dtc)_3 \; - \; e^- \; \rightarrow \; Co_2(Me_2dtc)_3^+$$

$$2Co(Me_2dtc)_3^+ \rightarrow \; Co_2(Me_2dtc)_5^+ \; + \; \text{oxidised ligand}^6$$

When referring to electron transfer and chemical reaction steps the notation introduced by Testa and Reinmuth[7] is used. In this notation the heterogeneous electron transfer step is represented by the symbol E and the following chemical reaction by the symbol C. The chemical reactions discussed above may occur in solution or at the electrode surface, hence C steps may be homogeneous (C_{hom}) or heterogeneous (C_{het}). There are a variety of mechanistic schemes involving coupled electron transfer and chemical steps:

(1) EC Mechanism

This involves the transfer of an electron to/from the electroactive species followed by a chemical step as illustrated on the following page:

---

6 R. G. Compton, J. C. Eklund, L. Nei, A. Bond, R. Colton and Y. Mah, *J. Electroanal. Chem.*, **385**, (1995), 249

7 A. C. Testa and W. H. Reinmuth, *Anal Chem.*, **33**, (1961), 1320

$$E \quad A \pm e^- \rightleftharpoons B$$

$$C \quad B \rightarrow D$$

An example of an EC mechanism is the oxidation of *p*-aminophenol in aqueous, acidic conditions[8].

(2) CE Mechanism

In this mechanism the electroactive species shown as A is in equilibrium with an electroinactive precursor, Z:

$$C \quad Z \rightleftharpoons A$$

$$E \quad A \pm e^- \rightleftharpoons B$$

An example of a CE mechanism is the proton discharge from a weak acid such as acetic acid[9].

(3) EC' Mechanism

This is a particular type of EC mechanism in which the chemical step re-generates the initial electroactive species A from a reaction with an electroinactive species Y:

$$E \quad A \pm e^- \rightleftharpoons B$$

$$C' \quad B + Y \rightleftharpoons A + X$$

An example of the EC' mechanism is the reduction of 9,10-diphenylanthracene[10] (DPA) in the presence of 4,4-dibromobiphenyl (DBB) shown below:

$$E \quad DPA + e^- \rightleftharpoons DPA^{\bullet -}$$

$$C' \quad DPA^{\bullet -} + DBB \rightarrow DPA + DBB^{\bullet -}$$

---

8 A. J. Bard and L. R. Faulkner, *Electrochemical Methods: Fundamentals and Applications*, Wiley, New York, (1980)

9 S. Daniele, I. Lavagnini, M. A. Baldo and F. Magno, *J. Electroanal. Chem.*, **404**, (1996), 105

10 C. L. Miaw, J. F. Rusling and A. Owlia, *Anal. Chem.*, **62**, (1990), 268

(4) ECE and DISP Mechanisms

These mechanisms are similar to the EC case but the chemical step is followed by a further electron transfer step. There are three limiting cases that have been identified by Savéant and co-workers[11,12] as occurring from steps 1-4 shown in the scheme below. These are ECE, DISP 1 and DISP 2. The first two steps occur in all three of the mechanisms. However a second electron transfer step can occur at either the electrode (ECE) or in solution via disproportionation (DISP), giving steps 3 and 4 (below). Two different DISP mechanisms are possible depending on which of the steps, 2 or 4, is rate determining. If step 2 is rate determining the mechanism is DISP 1 and if step 4 is rate determining the method is DISP 2.

$$E \quad A \quad \pm \quad e^- \rightleftharpoons \quad B \qquad (1)$$

$$C \qquad\qquad B \quad \rightarrow \quad C \qquad (2)$$

$$E \quad C \quad \pm \quad e^- \rightleftharpoons \quad D \qquad (3)$$

$$C \quad B \quad + \quad C \quad \rightarrow \quad A + D \qquad (4)$$

Electron transfer reactions and coupled chemical reactions such as those described above provide a challenging area of investigation for electrochemists. The overall rate of such reactions is limited by the slowest step which may be the kinetics of the chemical step, the electron transfer step or the rate at which the species involved reach the electrode surface through mass transport. It follows that when rapid electrochemical reactions occur mass transport effects may become important in the investigation of such processes. Therefore before the techniques used to probe such kinetics are discussed it is important to understand how the electroactive species involved reach an electrode surface.

---

11 C. Amatore and J. M. Savéant, *J. Electroanal. Chem.*, **85**, (1977), 27

12 C. Amatore, M. Gareil and J. M. Savéant, *J. Electroanal. Chem.*, **147**, (1983), 1

1.3 Mass Transport

The three main types of mass transport of species to the electrode surface are diffusion, migration and convections.

(1) Diffusion

Diffusion involves the movement of species in solution due to an uneven concentration distribution. For electrode processes the uneven concentration distribution occurs in a region close to the electrode surface in which the solution is depleted of electroactive species, known as the diffusion layer. A mathematical description of diffusion is provided by Fick's[13] laws which link the flux of the species considered to the concentration present, as shown in the equation below:

$$J_d = -D_A \frac{\partial[A]}{\partial x} \qquad (1.1)$$

where D_A is the diffusion coefficient ($cm^2\ s^{-1}$) for a species A, [A] is the concentration of species A and J_d is the flux of the species to the electrode surface.

Experimentally it is the rate of change in the concentration of a species that is more commonly considered which is expressed in Fick's second law[14] given below:

$$\frac{\partial[A]}{\partial t} = D_A \frac{\partial^2[A]}{\partial x^2} \qquad (1.2)$$

(2) Migration

Migration occurs as the result of the electrostatic force on a charged particle in the electric field that exists at the interfacial region between the electrode and the solution. The migratory flux due to a potential gradient $\frac{\partial \Phi}{\partial x}$ is given by:

---

13 A. Fick, *Philosophical Mag. and Journal of Science*, **10**, (1855), 30

14 A. Fick, *Poggendorff's Annelen der Physik*, **94**, (1855), 59

$$J_m = -\frac{zF}{RT} D_A [A] \frac{\partial \Phi}{\partial x} \qquad (1.3)$$

where z is the charge of the ion, F is the Faraday constant, T is the temperature in Kelvin and R is the Universal Gas Constant.

Experimentally migration effects can be eliminated through the use of an inert 'supporting'[15] electrolyte which maintains electroneutrality in most of the interfacial region. A further result of adding supporting electrolyte is that the ionic strength of the solution remains effectively constant during an electron transfer reaction. Therefore the activity coefficients of the electroactive species, the potential necessary to bring about the electron transfer and the rate of chemical reactions are unchanged over the course of the experiment. An exceptional experimental case where supporting electrolyte may not be required is that of microelectrodes[1,2]. These are discussed in detail in section 1.6.

(3) Convection

There are two different types of convection that can occur, natural convection and forced convection. Natural convection arises from the differences in density or thermal gradients in the solution. Forced convection is achieved by an external force such as stirring or hydrodynamic flow which are often deliberately introduced to swamp the unpredictable effects of natural convection. For cases where forced convection is used the convective flux in one dimension may be written as:

$$J_c = [A] v_x \qquad (1.4)$$

15 J. Goodisman, *Electrochemistry: Theoretical Foundations*, Wiley-Interscience, (1987)

where J_c is the flux of species A due to convection and v_x is the velocity of the solution in the x-direction. This equation can then be substituted into equation (1.2) to yield an expression relating the concentration to time:

$$\frac{\partial[A]}{\partial t} = -\left[v_x \frac{\partial[A]}{\partial x} \right] \qquad (1.5)$$

It is the development and application of a hydrodynamic electrode system, the channel electrode, for the study of electrode processes that is reported in this thesis. The following section gives a brief introduction to the importance of hydrodynamic electrodes[16,17] before the channel electrode is looked at in detail.

1.4 Hydrodynamic Electrodes

As introduced in the previous section, hydrodynamic electrodes are based on controlled convective mass transport. This can be achieved through either stirring of the solution under investigation by rotation (rotating disk electrodes, RDE), vibration of the electrode or, for the case of channel electrodes, the flow of the solution over the stationary electrode.

The controlled movement of solution relative to the electrode surface leads directly to one of the biggest advantages when using hydrodynamic electrode systems to study electrode processes. The dominance of forced over natural convection means that the mass transport mechanisms in operation can be quantitatively described and controlled. The timescale of reactions that can be studied using such systems is greatly decreased enabling kinetic and

---

16 J. Newman, *J. Electroanal. Chem.*, 6, (1973), 187

17 R. B. Bird, W. E. Stewart and E. N. Lightfoot, *Transport Phenomena*, Wiley, New York, (1960)

mechanistic information about electrochemical reactions such as those discussed in section 1.2 to be probed.

1.5 The Channel Electrode

The channel electrode is an extremely useful and powerful tool for investigating electrochemical kinetics[18,19]. The system consists of an electrode embedded in a wall on a rectangular duct, the flow cell, through which electrolyte solution is flowed. A schematic diagram is shown in figure 1.1.

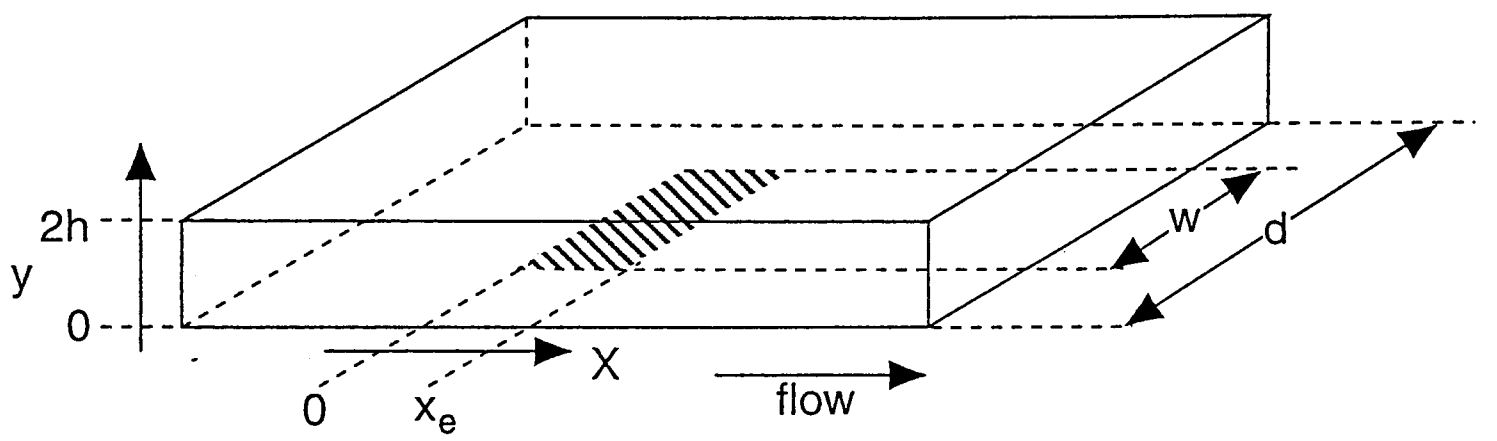

Figure 1.1. A schematic diagram of a channel flow cell.

This type of system offers several advantages over alternative types of hydrodynamic electrodes which are discussed below:

(1) The rate of mass transport to the electrode surface can be controlled over a very wide range. For example, volume flow rates between 10^{-4} and 10^{-1} cm^3 s^{-1} can easily be attained. This range has recently been extended with the introduction of a high speed channel flow cell, the details of which are discussed in section 1.7. Along with the variation in the

---

18 R. G. Compton and P. R. Unwin, *J. Electroanal. Chem.*, **205**, (1986), 1

19 P. R. Unwin and R. G. Compton, *Comprehensive Chemical Kinetics*, **29**, (1989), 173

volume flow rate, the mass transport can also be varied through changes in the electrode length, x_e, and the cell height, 2h, from microns to millimetres. This range of mass transport attainable with channel electrodes offers a huge advantage over other hydrodynamic electrodes such as rotating discs[20] and wall jets[21] which are much more limited.

(2) The channel flow cell can be operated under laminar flow conditions which are well defined and can be modelled mathematically. This allows accurate simulations to be carried out enabling discrimination between candidate reaction mechanisms.

(3) The channel electrode is easy to construct and can be used with a range of electrode materials.

(4) Channel flow cells can easily be adapted for electrochemical experiments to be carried out in conjunction with spectroscopic studies. This allows intermediates and the products of electrolytic reactions to be detected.

(5) The spent solution from the channel flow cell flows directly to a waste outlet preventing any stagnant zones from developing which is a problem with wall jet systems[22].

1.5.1 The Experimental Design of the Channel Electrode

1.5.1.1 The Channel Electrode Cell

Channel electrodes are designed as demountable units consisting of a channel unit and a coverplate which contains the working electrode. The two most commonly used designs are shown on the following page in figure 1.2. The first schematic illustrates a cell which is made

---

20 W. J. Albery, C. C. Jones and A. R. Mount, *Comprehensive Chemical Kinetics*, **29**, (1989), 129

21 M. B. Glauert, *J. Fluid Mech.*, **1**, (1956), 625

22 Y. Yamada and H. Matsuda, *J. Electroanal. Chem.*, **44**, (1973), 189

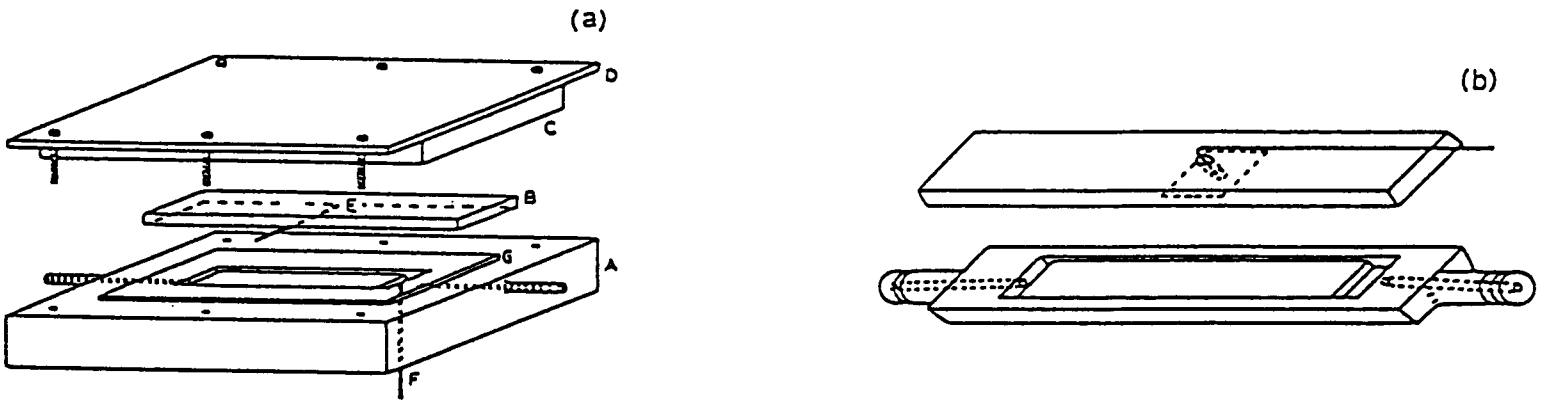

Figure 1.2. *(a)* *A schematic diagram of a perspex channel flow cell. A-channel unit, B-cover plate, C-rubber block, D-metal plate, E-working electrode, F-reference electrode.*

(b) *A schematic diagram of a silica channel flow cell.*

of perspex with the channel unit and coverplate joined by mechanical pressure[23]. A rubber layer acts as a seal between the two layers. The second schematic shows a silica channel unit which is cemented to the coverplate using either wax or adhesive. This has particular use in *in-situ* photochemical or UV/VIS studies[24]. Recently an alternative form of UV/VIS cell has been developed[25], which consists of a coverplate and a channel unit with a small circular silica window. The rest of the cell is optically opaque. The window is situated downstream of the electrode enabling *in-situ* detection of products generated instantaneously from a potential step electrode reaction. By monitoring the rate at which a peak appears in a spectrum generated form this type of experiment it is possible to gain information about the diffusion coefficient of the species under investigation in a very sensitive manner. Diffusion coefficients are vital in the modelling of electrochemical processes making this type of cell

---

23 R. G. Compton and B. A. Coles, *J. Electroanal. Chem.*, **144**, (1983), 87

24 R. G. Compton, R. A. W. Dryfe and A. C. Fisher, *J. Chem. Soc. Perkin Trans.*, **2**, (1994), 1581

25 K. Y. Tam, R. L. Wang, C. W. Lee and R. G. Compton, *Electroanalysis*, **9**, (1997), 219

invaluable when measuring the diffusion coefficient of radical species, which are not always the same as their natural parent.

The working electrode consists of a thin metal foil which is glued to the coverplate. A hole is drilled in the coverplate to allow electrical contact to the working electrode. Most working electrodes are made of Pt, Au, Cu or Ag. For such metals a rubber based glue is usually used for experiments carried out in aqueous solutions. Metal foils have also been cast in epoxy resin coverplates. This offers the advantage that after polishing there are no ridges between the edge of the electrode and the coverplate.

On assembling the channel electrode cell it is essential that the electrode is placed away from the edges of the channel ($w < d$) as in this region the flow in the x-direction deviates away from Poiseuille flow. The significance of this will become clear later. Another condition of Poiseuille flow is that the entry length is sufficient, requiring the electrode to be placed sufficiently downstream[23].

The final parts of the channel electrode cell are the reference and counter electrodes. These can be included in the cell itself or added in to the flow system. Meyer[26] designed a cell which incorporates all three electrodes in the channel unit.

1.5.1.2 The Flow System

Flow through channel electrode cells can be achieved by a gravity fed system or through pumping. In the case of the gravity fed system, figure 1.3, electrolyte is fed from a reservoir via a glass capillary. Each of the capillaries provide a different flow rate range and can be selected through the use of a multi-way tap. The flow rate range obtainable is generally

---

26 R. E. Meyer, M. C. Banta, P. M. Lanta and F. A. Posey, *J. Electroanal. Chem.*, **30**, (1971), 345

10^{-4} - 10^{-1} cm^2 s^{-1}. The flow rate range for each of the capillaries is obtained by varying the height between the reservoir and the capillary as shown in figure 1.3.

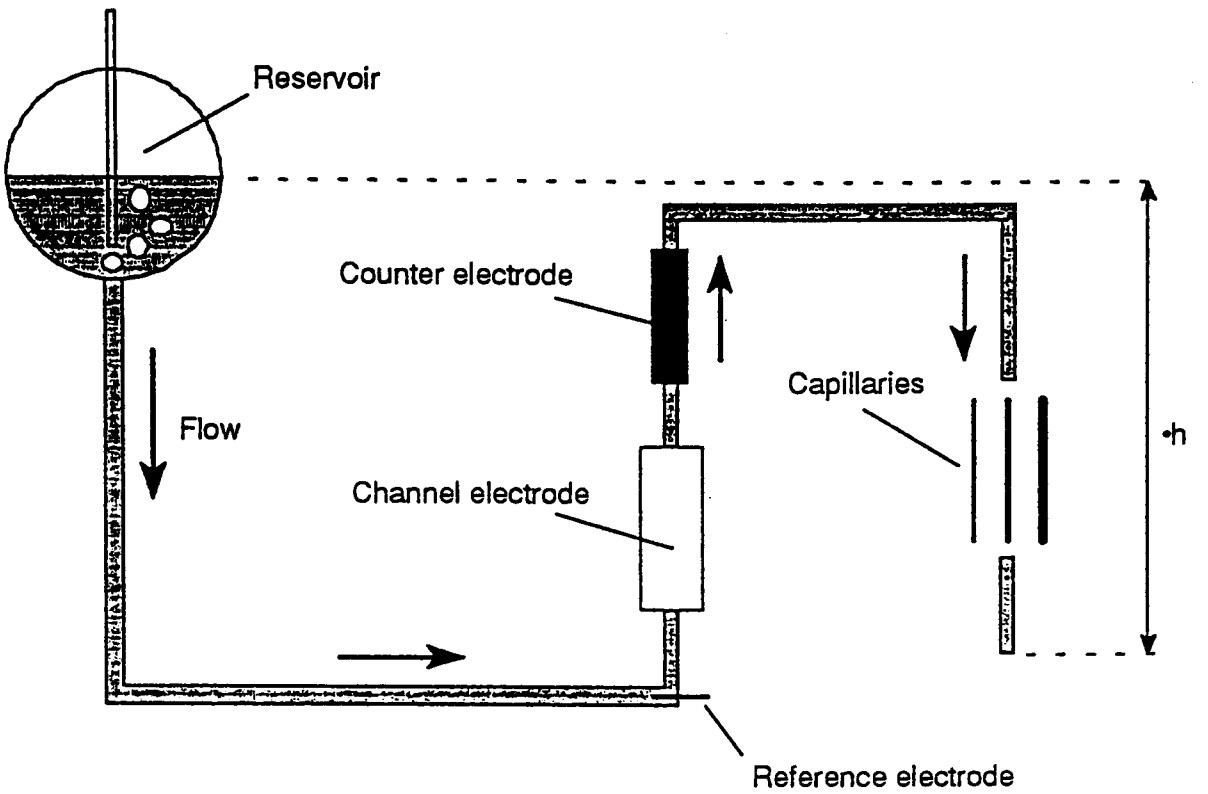

Figure 1.3. The gravity fed flow system.

In this system the solution runs into a waste container once it has passed through the channel cell. Brett and Oliveira Brett[27] have discussed the practicalities of designing flow systems in general.

Another type of flow system mentioned above is the pumped recirculating flow system[28], figure 1.4. This method is often preferred when large flow rates are needed. However, flow pulsation can be a problem. This is dampened by adding a thin tube and a hollow partially filled ball between the pump and the cell.

---

27 C. M. A. Brett and Oliveira Brett, *Comprehensive Chemical Kinetics*, **26**, Elsevier, Amsterdam

28 K. Aoki, K. Tokuda and H. Matsuda, *J. Electroanal. Chem.*, **76**, (1977), 217

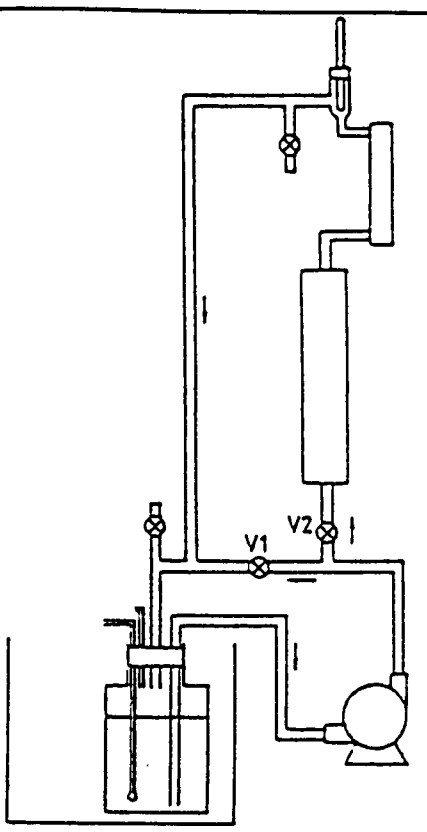

Figure 1.4. *The pumped recirculating flow system.*

1.5.2 The Mass Transport Equation for the Channel Flow Cell

As discussed previously, a major advantage when using channel flow cells is the accurate mathematical modelling of the electrochemical processes involved which can enable discrimination between mechanisms. This mathematical modelling is developed from the solution of the mass transport equations for the species involved. The mass transport of species in a channel flow cell can be modelled as the hydrodynamic flow and the dimensions of the cell can be measured with a high degree of accuracy. The introduction of the convective flow in the channel flow cell enhances the mass transport of the electroactive species considered to the electrode causing the diffusion layer to be restricted to a region close to the electrode surface. This enables the effects of natural convection in the cell to be eliminated which also ensures reproducible results and accurate modelling. As shown in figure 1.1, the direction of the flow over the electrode is designated as the x-direction and the direction normal to the electrode surface the y-direction.

The general equation describing the diffusion and convective behaviour of a species A at an electrode surface of any dimensions in a channel flow cell is given as follows:

$$\frac{\partial[A]}{\partial t} = D_A\left(\frac{\partial^2[A]}{\partial x^2}+\frac{\partial^2[A]}{\partial y^2}+\frac{\partial^2[A]}{\partial z^2}\right)-\left(\nu_x\frac{\partial[A]}{\partial x}+\nu_y\frac{\partial[A]}{\partial y}+\nu_z\frac{\partial[A]}{\partial z}\right) \qquad (1.6)$$

where [A] is the concentration of species A, D_A is the diffusion coefficient of species A, x, y and z are the co-ordinates defined in figure 1.1 and ν_x , ν_y, and ν_z are the solution velocity profiles in those directions.

1.5.2.1 Hydrodynamics

The following section describes the hydrodynamic flow within the channel electrode which can be characterised by the Reynolds number[19] :

$$R_e = \frac{h\nu_0}{\nu} \qquad (1.7)$$

where h is the half height of the channel flow cell, ν is the kinematic viscosity of the solution and ν_0 is the fluid velocity at the centre of the channel. Below a certain critical value[29], $R_{e\ crit.} < 2000$, the flow is described as being laminar and above this value the flow is turbulent. In the majority of channel flow experiments the flow is chosen to be laminar to enable mathematical modelling although turbulent systems can also be described with the introduction of modifications. Assuming the flow of solution entering the channel is laminar and the electrode 'edge effects' are negligible, ($h \leq d$), the flow profile can be considered to be 2-dimensional. The effect of friction at the channel walls slows down the flow close to the

---

29 V. G. Levich, *Physicochemical Hydrodynamics*, Prentice-Hall, Englewood Cliffs, New Jersey, USA, (1962)

walls, but after a lead in length of L_e, $L_e = (1 + 0.08R_e)h$, a Poiseuille flow is established in the channel[30]. This is parabolic in nature and is shown in figure 1.5.

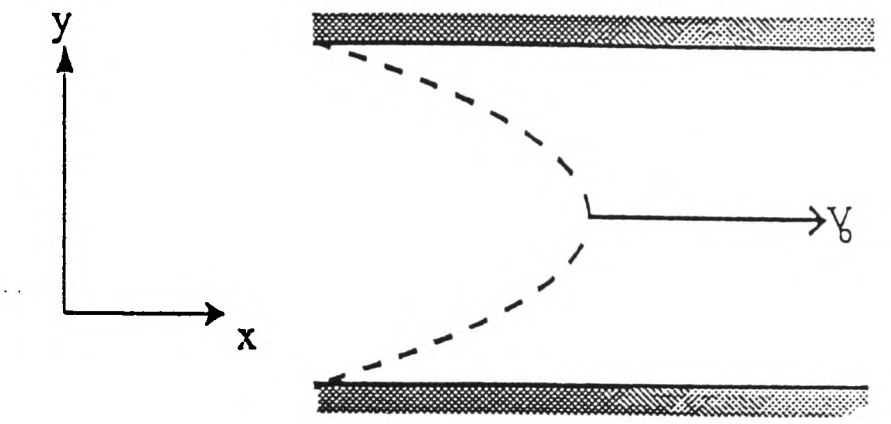

Figure 1.5. *The parabolic solution velocity profile in the channel flow cell.*

Mathematically for a parabolic flow:

$$v_x = v_0\left(1-\frac{(h-y)^2}{h^2}\right) \qquad (1.8)$$

1.5.2.2 Simplification of the Mass Transport Equation for the Channel Flow Cell

The complex mass transport equation, (1.6), can be simplified in several ways to produce an equation which is easier to work with:

(1) At steady state $\frac{\partial[A]}{\partial t} = 0$, hence the time dependence of the equation is removed.

(2) For the case of macroelectrodes it can be assumed that axial diffusion[31], diffusion in the x-drirection, is negligible. However, this is not the case for microelectrodes[32].

---

30 F. M. White, *Viscous Fluid Flow*: McGraw-Hill, New York, (1974)

(3) The Lévêque[33] approximation may be made, which approximates the parabolic flow of the solution to a linear flow close to the electrode surface, where the concentration changes take place.

Therefore taking into consideration approximations 1 and 2 the mass transport equation becomes:

$$\frac{\partial[A]}{\partial t} = 0 = D_A\left(\frac{\partial^2[A]}{\partial y^2}\right) - \left(v_x\frac{\partial[A]}{\partial x} + v_y\frac{\partial[A]}{\partial y} + v_z\frac{\partial[A]}{\partial z}\right) \qquad (1.9)$$

The change in the concentration of species A due to electrolysis is small enough to be limited to the channel wall (carrying the electrode) so that the parabolic velocity may be linearised using the Lévêque approximation mentioned in simplification 3, where:

$$v_x = v_0\left(1 - \frac{(h-y)^2}{h^2}\right) = v_0\left(\frac{h^2 - (h^2 - 2hy + y^2)}{h^2}\right) = v_0\frac{y}{h}\left(2 - \frac{y}{h}\right) \approx 2v_0\frac{y}{h} \qquad (1.10)$$

when $\left(\frac{y}{2h}\right) << 1$

The quadratic term in y is removed and the parabolic flow close to the electrode is seen to be approximately linear. Hence we arrive at the steady state mass transport equation for the channel flow cell:

$$D_A\frac{\partial^2[A]}{\partial y^2} = \frac{2v_0 y}{h}\frac{\partial[A]}{\partial x} \qquad (1.11)$$

---

33 M. Lévêque, *Ann. Mines Mem. Ser.*, **12/13**, (1928), 201

It is possible to solve this equation analytically for the case of a transport-limited oxidation/reduction with no preceding or following chemical kinetics, as represented by the reaction shown below.

$$A \pm ne^- \rightleftharpoons B$$

A detailed description of the mathematics involved is given in the following chapter of this thesis however the result is the equation shown below, the Levich[29] equation:

$$I_{lim} = 0.925nF[A]_{bulk} D_A^{2/3} \nu_f^{1/3} \left(h^2 d\right)^{-1/3} w x_e^{2/3} \qquad (1.12)$$

where n is the number of electrons transferred, F is the Faraday constant, $[A]_{bulk}$ is the bulk concentration of species A, ν_f is the solution volume flow rate, w is the width of the electrode, x_e is the length of the electrode and d is the width of the channel. This equation accurately describes the transport limited current produced as a result of an electron transfer reaction occurring at an electrode surface within a channel electrode cell. It is therefore fundamental to the work presented in this thesis.

It is straightforward to design channel electrode cells that accurately conform to the Levich equation and it can therefore be assumed that the channel electrode cells referred to in this thesis have been designed in such a way. For the case of channel electrode cells where the Levich equation holds it has been found that the replacement of the parabolic flow profile by a linear profile within the channel electrode diffusion layer, discussed previously, becomes more accurate as the length of the electrode decreases. This is due to the decrease in the thickness of the diffusion layer. It has also been shown by solving the full mass transport equation that at low flow rates the Levich equation is found to deviate. This is due to the

natural convection becoming more significant compared to the forced flow[34-38]. However, of the several assumptions made during the simplification of the mass transport equation in order to arrive at the Levich equation as listed previously, the most important is the assumption that diffusion in all directions other than that normal to the electrode surface can be neglected. This is not the case for microelectrodes and when considering such systems the diffusion in the same direction as the convective mass transport must be considered. It is possible to adapt the mass transport equation to include such axial diffusion effects but in doing so the solutions of the resulting mass transport become increasingly complex. As an alternative to using an analytical solution to the mass transport equation, recent advances in computer power have made numerical solutions increasingly popular. Such methods are discussed in the following chapter.

1.5.3 Applications of the Channel Flow Cell

Having introduced channel electrodes and some of the basic theory used to model the results obtained from them, the following section describes how a combination of the two results in a powerful tool in the study of mechanistic electrochemistry.

1.5.3.1 The Measurement of Diffusion Coefficients

Diffusion coefficients of electroactive species can be easily measured in a number of ways using electrochemical techniques. The channel flow cell offers a straightforward experimental procedure based on the Levich equation which involves recording the limiting

---

34 M. R. Goldman and L. R. Burnett, *Trans. Inst. Chem. Eng.*, **47**, (1969), T29
35 A. A. Wragg, *Electrochim. Acta*, **16**, (1971), 373
36 A. A. Wragg and T. K. Ross, *Electrochim. Acta.*, **12**, (1967), 1421
37 D. J. Robinson, *Electrochim. Acta.*, **17**, (1972), 791

current of a species generated at an electrode over a range of flow rates. This method has been used extensively for a range of electroactive species[3,6].

However, measuring the diffusion coefficients of species generated electrochemically is more difficult. A modified channel electrode system[25] has been developed for this purpose which fits inside an ordinary UV/VIS spectrometer. This type of experiment involves stepping the potential from a potential where no current flows to one where the limiting current for the species involved occurs. An absorbance spectrum of the electrogenerated species is then recorded as a function of time. Mathematical theory has been developed which predicts the shape of the absorbance/time curves produced enabling the elucidation of the diffusion coefficient of the electro-generated product. It usually follows that the faster the electro-generated species diffuses towards the centre of the cell where the solution flow is greatest, the quicker the absorbance reaches a steady-state value. Examples where this type of method has been applied include the radical cation of N,N,N,N-tetramethylphenylene diamine (TMPD)[39], the radical anion of benzoquinone and the methyl viologen monocation[25].

1.5.3.2 Voltammetric Waveshapes

The shape of voltammograms obtained from channel flow cell experiments can provide useful information about homogeneous kinetics coupled to electron transfer reactions. This type of analysis has been used by Compton et al.[6] who investigated the homogeneous dimerisation reaction that follows the oxidation of a colbalt(III) compound using a channel flow cell. Both the shift in the potential caused by the homogeneous kinetics and the change in voltammetric wave shape were used to derive the kinetic parameters of the dimerisation

---

38 J. L. Anderson and S. Moldoveanu, *J. Electroanal. Chem.*, **179**, (1984), 119

39 R. L. Wang, K. Y. Tam, F. Marken and R. G. Compton, *Electroanalysis*, **9**, (1997), 284

reaction. Good agreement was found between the data obtained and independently determined values.

Another more recent example of this type of experiment is the study of the reduction of *p*-chloranil (CA) in acetonitrile which is followed by complexation of the resulting radical anion by the metal ions Mg^{2+} and Ba^{2+} [40]. Mathematical modelling was used to predict the shape of the voltammetric wave which enabled the determination of the overall rate constant for the complexation. Again this value was in perfect agreement with independent values.

1.5.3.3 Photoelectrochemistry

Photochemistry and electrochemistry have been widely studied separately to bring about the reaction of species in solution through electronically excited states and radical ions. However, work has recently been carried out with the aim of combining the two individual methods to produce a dual activation process.

As described earlier, channel flow cells have been constructed from silica to enable the electrode area to be irradiated with UV or visible light. This results in the excitation of the species under investigation and the promotion of following reactions such as electron transfer, bond dissociation, disproportionation or just enhanced reactivity.

When using photoelectrochemistry steady-state data can be recorded as a function of the flow rate to reveal photochemical equivalents of familiar mechanisms, - photo EC, CE, ECE and DISP pathways. The effect of the added light can then be detected via the extra current which flows when the light is present, known as a photo-current. This technique has been used extensively by Compton et al. who have recently published a comprehensive account of the

---

[40] J. A. Cooper, R. G. Compton, J. A. Alden, M. Oyama and S. Okazaki, *J. Electroanal. Chem*, **442**, (1998), 201

literature in this field[41]. An example of a system which has been shown to produce a photo-current is the reduction of 9,10-diphenylanthracene (DPA) in the presence of 4-chlorobiphenyl (4-CBP). In this system the electrogenerated radical anion of DPA is excited by light of wavelength 295 nm which spontaneously transfers an electron to the 4-CBP. The species generated therefore becomes unstable and dissociates, losing a chloride ion. It is hoped that the work carried in this area can be developed to facilitate the dechlorination of polybiphenyls which can be an environmental hazard[42]. Compton has also used photoelectrochemistry to diagnose the photochemical reduction of *p*-bromonitrobenzene in acetonitrile. For this mechanistic study the evolution of a photocurrent in time was monitored after the system had been irradiated with light. The combination of this phototransient data with steady-state photo/current flow data enabled the discrimination of the mechanism which was found to be a photo-ECE mechanism rather that a photo-ECEEE[43].

More recently the study of photochemical reactions has resulted in a number of new electrochemical mechanisms which are similar to the DISP reaction described previously. These are known as Self-Inhibited Disproportionation (SID) reactions[44] and include a range of special cases depending on which of a number of possible steps is rate determining. The different types of step involved include dis- and conproportionation, quenching of photo-excited states by themselves or other species and a variety of reaction steps each of which have their own rate constant. One example of a reaction which has been found to include such steps is the electro-reduction of 9, 10-diphenylanthracene in the presence of 4-chlorobiphenyl discussed above whose full mechanism has recently been elucidated using

---

41 R. A. W. Dryfe and R. G. Compton, *Prog. Reaction Kinetics*, **20**, (1995), 245
42 J. F. Rusling and Q. D. Huang, *Environmental Science and Technology*, **5**, (1995), 1195
43 R. G. Compton and R. A. W. Dryfe, *J. Electroanal. Chem.*, **375**, (1994), 247
44 W. M. Leslie, R. G. Compton and T. Silk, *Electrochim. Acta.*, **42**, (1997), 3575

photoelectrochemistry. Another is the case of the photodebromination of 4-bromonitrobenzene[45]. The photochemical reduction of other *p*-halonitrobenzenes have been investigated by Compton[24] who has published a detailed and comparative mechanistic study of the four halonitrobenzenes, $X\text{-}C_6H_4\text{-}NO_2$ (X = F, Cl, Br and I) in acetonitrile.

1.5.3.4 Spectroelectrochemistry

Recently ESR spectroscopy experiments have been carried out in conjunction with channel flow cells[46,47]. This is due to the very useful information that can be gained from such experiments as radical and radical ion species are frequent intermediates in electrochemical reactions. The channel flow cells used with *in-situ* ESR experiments are made of silica. This keeps the amount of paramagnetic impurities to a minimum whilst enabling *in-situ* photochemical ESR studies to be carried out by shining light directly onto the electrode ESR cavity. The use of the channel flow cell in conjunction with ESR also has a huge advantage over other types of cell that are based on a stagnant thin layer geometry. These types of cell are known as optically transparent thin layer electrodes which often have the problem of electrochemical decomposition product build up.

Channel flow cells with *in-situ* ESR allow the deduction of whether or not a radical is stable or not as it is possible to show theoretically that under the Lévêque approximation for a stable radical,

---

45 R. G. Compton, R. A. W. Dryfe, J. C. Eklund, S. D. Page, J. Hirst, L. Nei, G. W. J. Fleet, K. Y. Hsua, D. Bethell and L. J. Martingale, *J. Chem. Soc. Perkin* II, (1995), 1673

46 R. D. Webster, R. A. W. Dryfe, J. C. Eklund, C. W. Lee and R. G. Compton, *J. Electroanal. Chem.*, **402**, (1996), 167

47 C. W. Lee, R. G. Compton, R. A. W. Dryfe and J. C. Eklund, *Bulletin Korean Chem. Soc.*, **17**, (1996), 162

$$S \propto \frac{I}{\nu_f^{2/3}} \qquad (1.13)$$

where S is the signal intensity and I is the limiting current. Hence by plotting Log(S/I) against Log(ν_f) a stable radical would have a gradient of (-2/3) but an unstable radical would have a less steep gradient[41]. Simulations of the case for unstable radicals can be used to produce kinetic and mechanistic information about the reaction under investigation.

Other experiments using *in-situ* ESR channel flow cells have involved monitoring the decay or growth of the signal obtained. This also enables mechanistic and kinetic information to be determined. Examples of electrochemical systems investigated using this technique include the photo-dehalogenation of haloanthraquinones[48,49].

1.5.3.5 Double Channel Electrodes

The double channel electrode was introduced by Gerisher et al.[50]. The set-up is the same as that for the conventional channel electrode but for double channel electrodes two neighbouring electrodes are contained within the cell, figure 1.6.

The main application of double electrodes is in the study of electron transfer reactions with coupled homogeneous kinetics. When used in this way the upstream electrode generates the species of interest which is detected at the downstream electrode. The detector electrode is held at a potential at which the destruction of the species produced upstream is diffusion-controlled.

---

48 R. G. Compton, B. A. Coles, M. B. G. Pilkington and D. Bethell, *J. Chem. Soc., Faraday Trans.*, **86**, (1990), 663

49 W. M. Leslie, R. G. Compton and T. Silk, *J. Electroanal. Chem.*, **424**, (1997), 165

50 H. Gerischer, I. Mattes and R. Braun, *J. Electroanal. Chem.*, **10**, (1965), 553

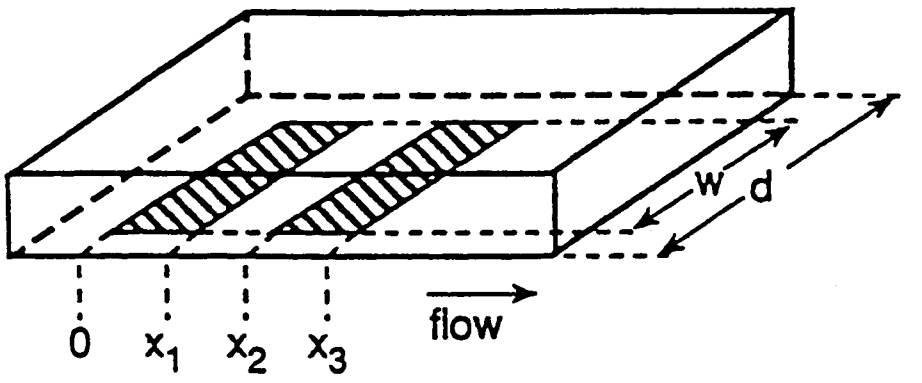

Figure 1.6. *A schematic diagram of a double electrode channel flow cell.*

Both kinetic and mechanistic information about the electrogenerated species can be gained by calculating the 'collection efficiency', N, which is the ratio of the current at the downstream electrode to that at the upstream electrode. In general the detector electrode is held at a potential which will destroy all of the species made at the upstream electrode. Compton and Fisher have provided a numerical model for channel electrode reactions involving first and second order homogeneous kinetics[51].

Compton et al. have also used double electrodes experimentally to measure heterogeneous rate constants. They investigated the case where a species generated at the upstream electrode underwent a heterogeneous reaction on the surface between the two electrodes[52]. A further area of investigation by Compton using double electrodes includes experiments carried out to investigate the current response of a downstream electrode to a potential step at an upstream generator electrode. These experiments[53] were used to demonstrate the value found for the diffusion coefficient of the electrochemically generated *p*-chloranil anion which was found to differ greatly from that of its parent molecule.

---

51 R. G. Compton and A. C. Fisher, *J. Appl. Electrochem.*, **21**, (1991), 208

52 R. G. Compton, G. M. Steam, P. R. Unwin and A. J. Barwise, *J. Appl. Electrochem.*, **18b**, (1988), 657

53 R. G. Compton, B. A. Coles, J. Gooding, A. C. Fisher and T. L. Cox, *J. Phys. Chem.*, **98**, (1994), 2446

1.5.3.6 Channel Microband Arrays.

Microband arrays have recently been successfully employed as a technique for mechanistic investigations[54]. A typical design consists of 13 electrodes ranging in size from 2 mm to 0.5 μm in length as shown in figure 1.7. In microband array investigations voltammograms are recorded at each of the electrodes at a range of flow rates, giving rise to a 3-dimensional plot of limiting currents, flow rate and size of the electrode. Numerical simulations can then provide theoretical values for the current as a function of flow rate and electrode size for a chosen mechanism. By comparing the 3-dimensional plot of the experimental data with that obtained from the numerical simulations it is then possible to determine whether or not the assumed mechanism is correct.

This technique has great potential to be developed into a powerful tool for the investigation of electrochemical kinetics.

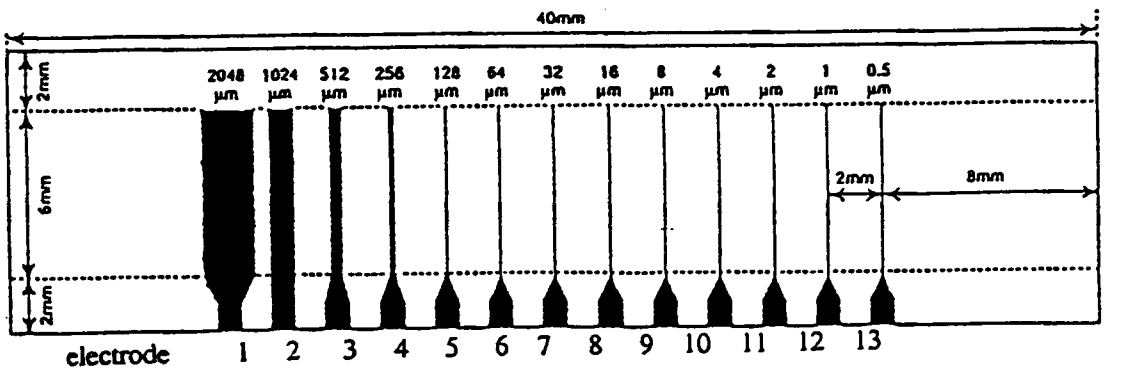

Figure 1.7. A schematic of a 13 electrode array.

1.6 Microelectrodes

The previous section gave an overview of the applications of channel electrodes. This next section considers the case of microelectrodes. Such electrodes have at least one dimension on the micron scale. The introduction of microelectrodes has brought about a

---

54 J. A. Alden, M. A. Feldman, E. Hill, F. Prieto, M. Oyama, B. A. Coles, R. G. Compton, P. J. Dobson and P. A. Leigh, *Anal. Chem.*, 70, (1998), 1707

dramatic shrinkage of the voltammetric timescale. Due to their size microelectrodes pass minute currents which induce a tiny amount of electrolysis in the solution. It therefore follows that the diffusion layers at such electrodes are very thin, inducing very large concentration gradients across them. As a result of this the relative mass transport to microelectrodes is considerably larger than that to conventional sized electrodes enabling the study of rapid electron transfer reactions at the electrode surface and subsequent kinetics that were previously masked by mass transport control[1,2]. The diagrams shown below, figure 1.8, illustrate the increase in diffusion to a microelectrode compared with a conventional macroelectrode.

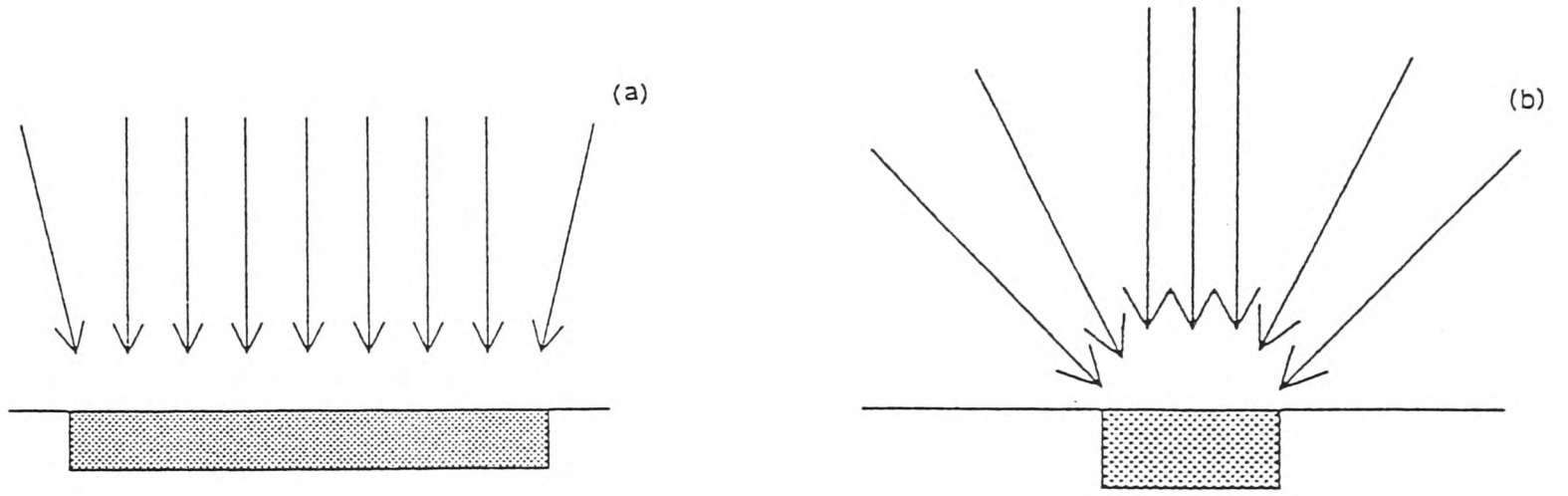

Figure 1.8. *(a)* *Planar diffusion to a macroelectrode.*

(b) *Convergent diffusion to a microelectrode.*

A further advantage of microelectrodes is that their reduced size decreases the amount of 'charging current' which occurs due to the change in ionic distribution near the electrode surface when a potential is applied. For macroelectrodes charging currents may be a problem as they can mask the reaction under investigation. Finally microelectrodes offer an advantage in resistive solutions when the passage of current causes the potential of the solution to be non-uniform. This can lead to distortions from the current/voltage responses from those

expected and is referred to as ohmic drop. However, as only tiny currents are passed at microelectrodes the ohmic drop at the electrode is reduced enabling experiments to be carried out with little or no background electrolyte. This enables experiments to be carried out in non-polar solvents such as benzene or toluene[55].

Montenegro[56] has carried out a comprehensive review on the applications of microelectrodes in the study of reaction kinetics. Magno et al.[57] have also reviewed kinetic investigations using microelectrodes that are supported by simulations.

Microelectrodes used in channel flow cells can take on the form of a microband or a microdisk, although little work has been carried out on microdisk[58,59] electrodes in comparison with microband electrodes. For the purpose of this thesis only microband electrodes are considered.

1.6.1 Microelectrodes in Channel Flow Cells

The determination of the heterogeneous rate constant for an electron transfer process requires the rate of the mass transport of the electroactive species to the electrode surface to be larger than that of the heterogeneous charge transfer step under investigation. Microelectrodes are very useful in achieving this in both potential step and steady-state measurements. Compton et al.[60] have considered the case of potential step measurements at channel microband electrodes using *p*-chloranil in acetonitrile. They presented a theoretical model using the hopscotch algorithm which enabled the results obtained to be numerically

---

55 J. B. Cooper, A. M. Bond and K. B. Oldham, *J. Electroanal. Chem.*, **331**, (1992), 877

56 M. I. Montenegro, , Eds. R. G. Compton and G. Hancock, *Research in Chemical Kinetics,* **2**, (1994)

57 F. Magno and I. Lavagnini, *Analytica Chimica Acta*, **305**, (1995), 96712

58 J. Booth, R. G. Compton, J. A. Cooper, R. A. W. Dryfe, A. C. Fisher, C. A. Davis and M. K. Walters, *J. Phys. Chem.*, **99**, (1995), 10943

59 R. G. Compton, J. C. Eklund and L. Lei, *J. Electroanaal. Chem.*, **381**, (1995), 87

modelled. The theoretical modelling techniques used for both microelectrodes and conventional electrodes in channel flow cells are discussed later in this thesis. The experimental and numerical results presented were found to be in good agreement whilst demonstrating that axial diffusion was significant when carrying out such experiments.

Microelectrodes have also revolutionised the study of very fast processes coupled with the heterogeneous electron transfer steps that were previously too rapid to be probed voltammetrically and were masked by diffusional control. Compton et al.[61] explored the use of microband channel electrodes for the study of electrode reaction mechanisms and kinetics in the anticipation that significantly shorter time domains would be accessible compared with conventional channel electrodes. They found that they were able to deduce the rate constant for the chemical step in the ECE reaction of *o*-bromonitrobenzene. At its time of publication this was the fastest chemical rate constant measured using steady-state channel electrode data. Compton et al. have also used the hopscotch algorithm to quantify the effects of electrode size and solution flow rate on the response of a microelectrode in a channel flow cell along with conditions where the mass transport occurs mainly by convection rather than diffusion. Having investigated the benefits of a system where the mass transport occurs predominantly by convection Coles et al.[3] then went on to design and use a high speed channel electrode. As a large amount of the work presented in this thesis is based on the high speed channel electrode the system is discussed in detail in the following section.

---

60 R. G. Compton, R. A. W. Dryfe, J. A. Alden, N. V. Rees, P. Dobson and P. A. Leigh, *J. Phys. Chem.*, **98**, (1994), 1270

61 R. G. Compton, R. G. Wellington, P. J. Dobson and P. A. Leigh, *J. Electroanal. Chem.*, **310,** (1994), 129

1.7 The High Speed Channel Flow Cell

The high speed channel electrode represents a new genre of channel flow systems as it optimises the rate of mass transport within the cell through the maximisation of the convective flow both through the cell and over the electrode surface. This is achieved using a pressurised chamber to produce very high solution flow rates through a miniature cell as described in detail below. It was anticipated that the high speed channel flow cell is capable of measuring rate constants under steady-state conditions which are significantly greater than those investigated using conventional channel flow cells.

1.7.1 The Design of the High Speed Channel Flow Cell

The high speed channel flow cell can be divided into three sections: the high speed channel, the accompanying microband electrode and the pressurised flow system.

1.7.1.1 The High Speed Channel Flow Cell

The flow cell, figure 1.9, is constructed from fused blocks of silica designed to minimise flow resistance. A smooth flow of solution from the cell inlet into the channel chamber is achieved using large bore entry tubes with low flow velocities. This flow is then accelerated by means of a taper section up to 35 times as it enters the channel. The channel length is chosen to be 2 mm to establish a stable flow pattern whilst keeping the required pressure drop within practical values of 150 kPa. The solution through the channel can reach values as high as 75 m s^{-1}, depending on the solvent used, at the centre of the channel.

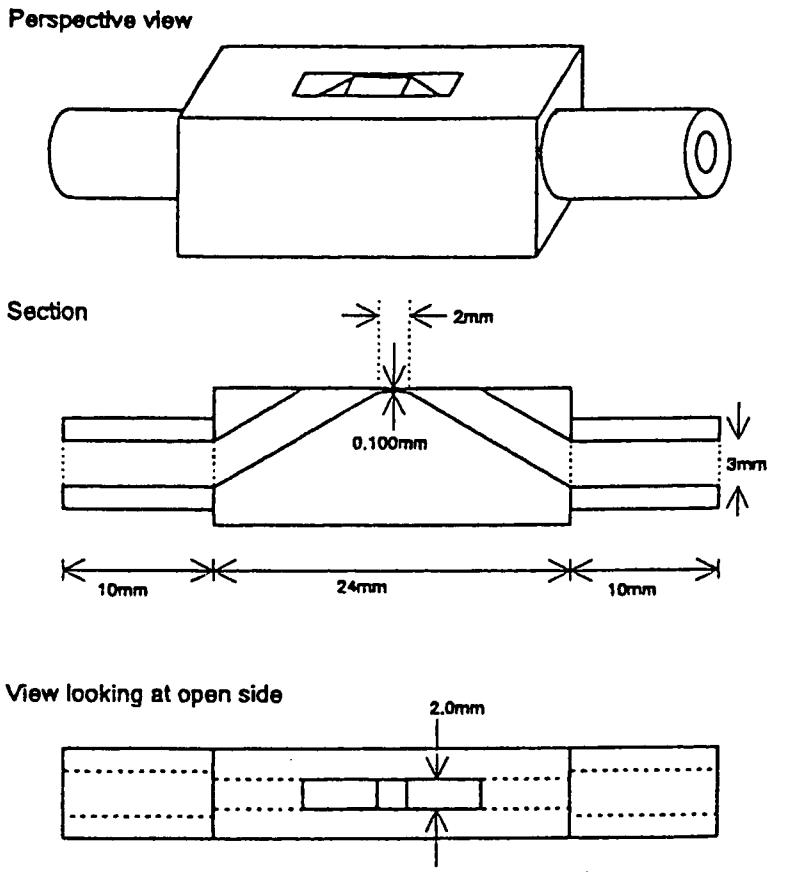

Figure 1.9. *The high speed channel flow cell showing a perspective view and the principal dimensions.*

1.7.1.2 The Microband Electrode

The cell is completed by the addition of a coverplate which carries the microband working electrode, figure 1.10. These two halves of the electrode assembly are sealed together by a gasket of silicone rubber. The cell is then mounted at one end of a pressure chamber. The microband electrodes, Au or Pt, are made by sealing a strip of foil between two glass rods. The section of glass carrying the electrode is then cut and ground to a rectangular shape, leaving a free end of the foil protruding on the side. This is then soldered to a Cu clip to make the electrical connection to the potentiostat. The counter electrode used in the high speed channel flow cell is a Pt coil placed 2 cm downstream of the working electrode and the pseudo reference is a Pt or Ag coil situated 2 cm upstream.

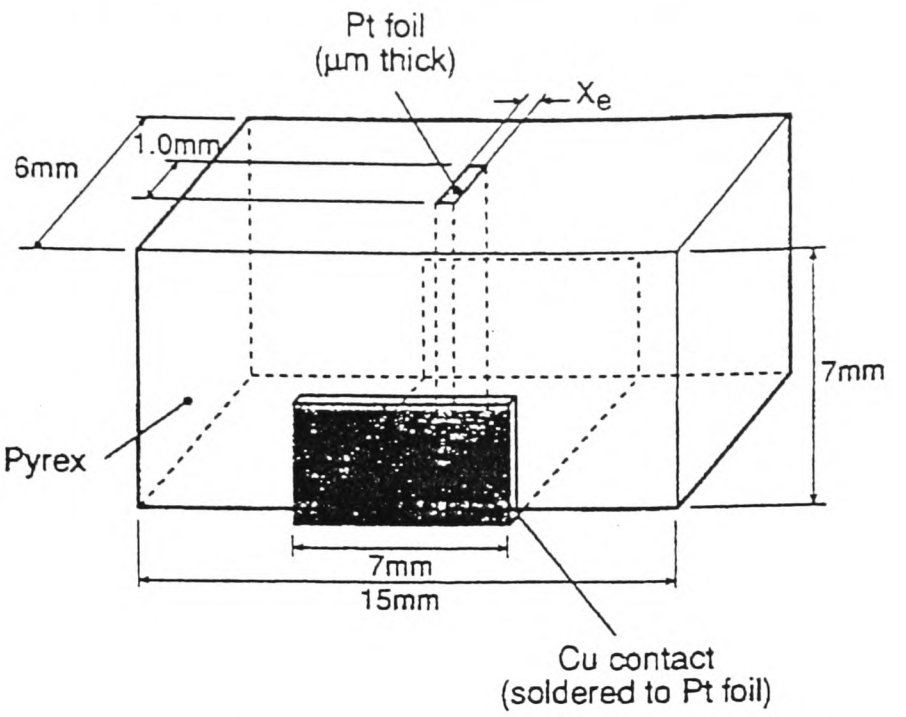

Figure 1.10. *A schematic diagram of the microband electrode.*

1.7.1.3 The Pressurised Flow System

The pressurised flow system shown in figure 1.11, is designed to force solution through the flow cell so as to induce velocity gradients at the electrode surface which are as high as possible. The flow rate of solution across the electrode is controlled by the combination of the chamber pressure with one of three different sized capillaries through which the waste solution flows. To avoid problems of operating the fragile cell assemblies at high pressures, the pressure differential is applied by enclosing the whole system including the solution reservoir, cell, reference and counter electrodes inside a pressure vessel. The waste solution produced is then discharged at atmospheric pressure. The chamber itself is pressurised using a cylinder of nitrogen which is computer controlled. The cell is then mounted at one end of the chamber in front of a silica window which enables inspection of the electrode surface.

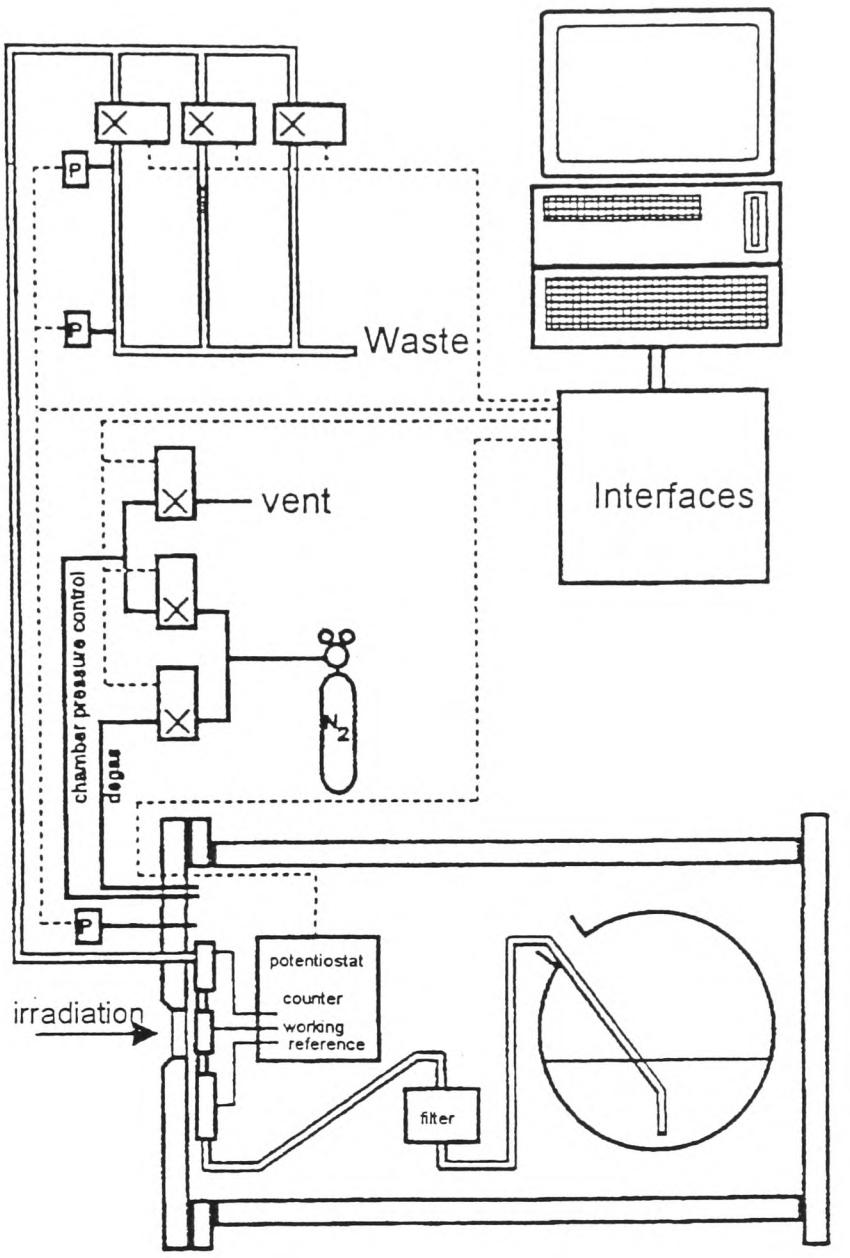

Figure 1.11. *A schematic diagram showing the main features of the high speed channel flow system.*

1.7.1.4 Experimental Advantages of the High Speed Channel Flow Cell

The main practical advantages of the high speed channel flow cell are listed on the following page:

(1) Due to the computer controlled pressure system the operation of the high speed channel flow cell is very clean and easy to use once the cell and solution reservoir have been mounted inside the chamber.

(2) Oxygen may easily be removed from the chamber by repeated cycles of pressurising and venting. The solution under investigation may also be deoxygenated by bubbling with nitrogen which is carried out with the chamber at atmospheric pressure to avoid supersaturation with nitrogen.

(3) The silica window that the cell is mounted next to enables the electrode surface to be irradiated with light if required for photochemical investigations.

1.7.2 Applications of the High Speed Channel Flow Cell

Coles et al.[3] carried out initial experiments using the high speed channel flow cell to investigate the fast kinetics coupled with the reduction of *p*-bromobenzophenone (*p*BBP). This process has been studied previously via fast scan cyclic voltammetry and was thought to undergo the following ECE mechanism[62]:

$p\text{-}BrC_6H_4COPh + e^- \rightarrow [p\text{-}BrC_6H_4COPh]^{\bullet -}$ E

$[p\text{-}BrC_6H_4COPh]^{\bullet -} \rightarrow Br^- + {}^{\bullet}C_6H_4COPh$ C

${}^{\bullet}C_6H_4COPh$ + "H" (from the supporting electrolyte) $\rightarrow$ PhCOPh C

$PhCOPh + e^- \rightarrow [PhCOPh]^{\bullet -}$ E

Using the high speed channel flow cell Compton et al. were able to probe the homogeneous kinetics of the formation of benzophenone which was known to have an extremely fast rate constant of $80000 \pm 24000\ s^{-1}$ [62]. Steady-state voltammograms were recorded at a range of

---

62 L. Nadjo and J. M. Savéant, *J. Electroanal. Chem.*, **30**, (1971), 41

flow rates enabling the rate constant for the chemical step to be deduced through the analysis of the number of electrons involved in the mechanism at the different flow rates, the details of which are described later in this thesis. *The rate constant was found to be 76500 s^{-1} which enters a new time domain in steady-state electrochemical measurements.*

Compton et al. then went on to use the high speed channel flow cell to study the rapid heterogeneous one electron transfer of *p*-benzoquinone[63], illustrating the power and versatility of the new technique. The standard rate constant for the one electron transfer was found to be 0.30 (± 0.04) cm s^{-1} again using steady-state measurements which was found to be in excellent agreement with independently determined values.

The application of the high speed channel flow cell has now been developed further and has been found to be extremely useful in the study of a range of electrochemical processes the details of which are presented in this thesis.

1.8 Work Presented in this Thesis

The purpose of this thesis is to investigate the application of the high speed channel flow cell to a range of electrochemical problems with the aim of elucidating electrochemical kinetics and mechanisms that were previously outside the scope of measurement by voltammetric means. This involves both steady-state and transient measurements for heterogeneous and homogeneous chemical kinetics and electron transfer processes.

The work is divided into three main parts. The first, including this chapter and chapters 2 and 3, describes the general theoretical and experimental background of the channel flow cell, in particular the high speed channel flow cell used in this thesis.

---

63 N. V. Rees, J. A. Alden, R. A. W. Dryfe, B. A. Coles and R. G. Compton, *J. Phys. Chem.*, **99**, (1995), 14813

Chapter 4, then introduces the application of the high speed channel flow cell to potential step transient measurements. This work was carried out with the aim of accessing even faster homogeneous rate constants than those previously attained from steady-state experiments. The one-electron reduction of *p*-bromonitrobenzene and *p*-chloronitrobenzene are reported along with the one-electron oxidation of N,N,N',N'-tetramethyl-1,4-phenyldiamine.

The final part made up of chapters 5, 6, 7 and 8, contains a complex study of the electrochemical kinetics involved in the reduction of nitromethane. The mechanism involved in the reduction of nitromethane has provided electrochemists with a challenging area of work for some time, representing the range of difficulties involved in the study of complex electrochemical processes. The work presented in this thesis demonstrates the unique ability of the high speed channel flow cell when applied to such investigations including the determination of rapid heterogeneous chemical kinetics and mechanistic discrimination. Complementary techniques have also been explored and developed including numerical modelling of the experimental results, single crystal experiments and isotopic effects.

2. Theory

Contents

2.1 Introduction

In this chapter the theory relating to the experimental results discussed in the following chapters is introduced. First the kinetics relating to an electrode transfer reaction are described along with the type of electrochemical measurements that can be carried out using a channel flow cell. The analytical solution of the mass transport equation for an electroactive species is then expanded to include coupled homogeneous kinetics before a general numerical approach to solving the mass transport equations coupled by homogeneous and heterogeneous reactions, the Backward Implicit method (BI), is introduced.

2.2 Basics - the Butler-Volmer Expression

In an electrochemical reaction the current produced at an electrode is proportional to the flux of the species involved. Considering a one electron transfer reaction:

$$A + e^- \rightleftharpoons B$$

the total flux can be written as:

$$J = k_f [A]_{surface} - k_b [B]_{surface} \qquad (2.1)$$

where k_f is the rate constant for the forward reaction and k_b is the rate constant for the backward reaction. It is possible to express each of these rate constants in terms of a standard rate constant, k_s, giving rise to the well known Butler-Volmer[1,2] expressions for the kinetic rate constants:

$$k_f = k_s e^{-\alpha F(E-E^0)/RT} \qquad (2.2)$$

$$k_B = k_s e^{\beta F(E-E^0)/RT} \qquad (2.3)$$

---

1 J. A. V. Butler, *Trans. Faraday Soc.*, **19**, (1924), 729

2 T. Erdey-Gruz and M. Volmer, *Z. Phys. Chem.*, **150A**, (1930), 203

where α and β are transfer coefficients, $\alpha + \beta = 1$, and E^0 is the standard electrode potential of the A/B redox couple. It follows from equations (2.1), (2.2) and (2.3) that at equilibrium, when no flux flows and the surface concentrations therefore equal their bulk values, that:

$$E = E_e = E^0 - \frac{RT}{F} \ln \frac{[B]}{[A]} \qquad (2.4)$$

This is the famous Nernst equation. However, when a net current is flowing through an electrochemical cell, the cell is not at equilibrium. The deviation of the half-cell potential, E, from the equilibrium potential, E_e, is known as the 'overpotential', η. As this overpotential is increased the flux of the electroactive species to the electrode surface changes to an extent dependent on the value of k_s. Figure 2.1. shows the variation of the flux with overpotential for the two limiting cases, considering in turn a small value and a large value of k_s. It can be seen, figure 2.1(a), that when k_s is large, little or no overpotential is required to drive the reaction and the current flows readily in both the anodic and cathodic directions. Such processes are termed 'electrochemically reversible' and the Nernst equation, (2.4), can be applied to any part of the voltammetric wave.

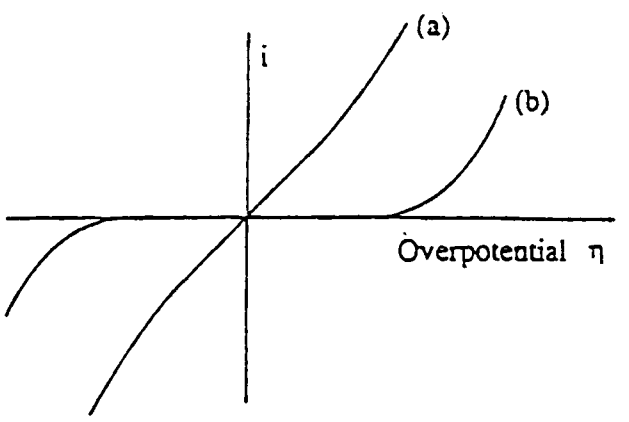

Figure 2.1. (a) Reversible reaction. (b) Irreversible reaction.

However, for processes that have a small value of k_s a high overpotential is required to induce current flow. Figure 2.1(b) shows that if the overpotential is increased to a value at which the anodic process is driven, the corresponding reductive current is very small and vice versa. Such processes are termed electrochemically 'irreversible'. The label 'quasi-reversible' is, obviously, applied to intermediate cases.

For irreversible reactions there is a region of potential where the flux of the electroactive species varies exponentially with potential. This region occurs when J is small so that at the surface the electroactive species concentrations deviate only a little from their bulk values. This is known as the Tafel region. For a reduction the relationship of the variation of the flux with potential is given by:

$$+\ln J = c - \frac{\alpha FE}{RT} \qquad (2.5)$$

where c is a constant. Similarly the relationship for an oxidation is given by:

$$+\ln J = c + \frac{\beta FE}{RT} \qquad (2.6)$$

The two expressions given above are forms of the Tafel law. Using the equation below, which relates the flux of electroactive species to the electrode to the current produced, by plotting ln(I) against the potential, E, it is possible to use the Tafel law to deduce the value of k_s. This will be considered in more detail in chapter 7.

$$I = nAFJ \qquad (2.7)$$

where A is the electrode area and F is the Faraday constant.

2.3 Voltammetry at Channel Electrodes

When using channel flow cells for electrochemical investigations two types of measurements can be made, steady-state or time-dependent measurements. The former of the two methods is more commonly known although time-dependent measurements can prove to be useful when increased sensitivity is required.

2.3.1 Linear Sweep Voltammetry

In linear sweep voltammetry experiments the potential at the electrode is scanned from a potential at which no electron-transfer occurs to one far anodic/cathodic of the formal potential (E^0), so as to observe the oxidation/reduction of the electroactive species under investigation. This produces a sigmoidal-shaped voltammogram, figure 2.2(a), with a corresponding transport limited plateau current (I_{lim}). A half wave potential is often quoted in experimental voltammetry which refers to the potential at half the I_{lim} value as shown in figure 2.2(a). Steady-state voltammograms are produced at sufficiently low scan rates (~1 $mV\,s^{-1}$) so that a true steady-state response is obtained. The steady-state current for a transport limited electron transfer is proportional to the concentration of the electroactive species undergoing the electron transfer as expressed in the Levich equation[3], (2.8), and hence can be used for analytical purposes.

$$I_{lim} = 0.925nF[A]_{bulk} D_A^{2/3} \nu_f^{1/3} \left(h^2 d\right)^{-1/3} w x_e^{2/3} \qquad (2.8)$$

---

3 V. G. Levich, *Physicochemical Hydrodynamics*, Prentice Hall, Englewood Cliffs, New Jersey, (1962)

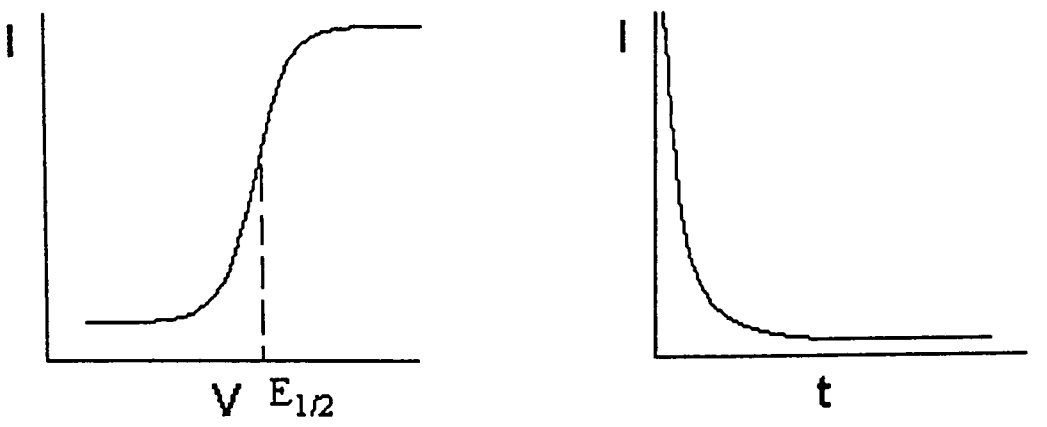

Figure 2.2. (a) A steady-state voltammogram. (b) A potential step transient.

2.3.2 Potential Step Transient Experiments

In potential step transient experiments the potential at the channel electrode is stepped, effectively instantaneously, from a potential corresponding to no reduction/oxidation of the electroactive species to a potential at which the oxidation/reduction usually occurs at a transport limited rate, (the potential corresponding to a point on the transport limited plateau of the sigmoidal-shaped voltammogram). Initially the current observed is very high before dropping off to a value corresponding to the mass transport limited current obtained when a steady-state voltammogram is recorded at the same flow rate, figure 2.2(b). This is explained by considering the thickness of the diffusion layer. After the potential step a very thin diffusion layer occurs due to the very small amount of the electroactive species that has undergone the redox process. As time progresses more of the electroactive species is oxidised/reduced resulting in a broadening on the diffusion layer and the observed drop in current.

A problem with potential step transient measurements is the loss in accuracy that can occur in comparison to highly reproducible steady-state measurements. This is a result of the rapid change in the current with time that induces an error in the time at which the current is measured.

2.4 The Development and Application of Working Curves

In the previous chapter we saw how the (simplified) mass transport equation for an electron transfer process at a conventional channel electrode can be solved analytically to produce the Levich equation. This analytical theory can be developed further to include electrochemical processes with following chemical kinetics.

2.4.1 The ECE Mechanism

First we consider the case of the ECE mechanism where the C step occurs in solution, C_{hom}. The reaction scheme for the reductive case of this mechanism is shown below:

$$A + e^- \rightleftharpoons B$$

$$B \xrightarrow{k} C$$

$$C + e^- \rightleftharpoons D$$

If the reduction potential of species A is such that species C is also reduced at that potential, then depending on the value of k for the homogeneous kinetics, the solution flow rate and the dimensions of the cell, the limiting current observed can vary between one and two times that for a simple one electron transfer process[4,5]. It therefore follows that at faster flow rates there is less time for B to react and form C before the solution is swept past the electrode, hence the possibility of C being reduced to D is removed. This results in a lowering of the current produced. It is possible to define the number of electrons transferred in the reaction, N_{eff}, as follows:

$$N_{eff} = \frac{I}{I_{1-electron}} \qquad 1 \leq N_{eff} \leq 2 \qquad (2.9)$$

---

4 C. Amatore and J. M. Savéant, *J. Electroanal. Chem.*, **85**, (1977), 27

5 C. Amatore, M. Gareil and J. M. Savéant, *J. Electroanal. Chem.*, **147**, (1983), 1

where $I_{1\text{-electron}}$ is the limiting current for a simple one-electron process.

The steady-state mass transport equations for the species involved in an $EC_{hom}E$ process, neglecting axial diffusion, are shown below. The case for microelectrodes where axial diffusion is significant has been investigated by Aoki[6] and Alden[7].

$$D_A \frac{\partial^2[A]}{\partial y^2} - v_x \frac{\partial[A]}{\partial x} = 0 \qquad (2.10)$$

$$D_B \frac{\partial^2[B]}{\partial y^2} - v_x \frac{\partial[B]}{\partial x} - k[B] = 0 \qquad (2.11)$$

$$D_C \frac{\partial^2[C]}{\partial y^2} - v_x \frac{\partial[C]}{\partial x} + k[B] = 0 \qquad (2.12)$$

In order to simplify these equations the Lévêque approximation is applied as described in section 1.5.2.2 of chapter 1. This results in the equations listed below:

$$D_A \frac{\partial^2[A]}{\partial y^2} = \frac{2v_0 y}{h} \frac{\partial[A]}{\partial x} \qquad (2.13)$$

$$D_B \frac{\partial^2[B]}{\partial y^2} - \frac{2v_0 y}{h} \frac{\partial[B]}{\partial x} - k[B] = 0 \qquad (2.14)$$

$$D_C \frac{\partial^2[C]}{\partial y^2} - \frac{2v_0 y}{h} \frac{\partial[C]}{\partial x} + k[B] = 0 \qquad (2.15)$$

To enable further simplification and the conversion of x and y to dimensionless terms the following variables are introduced:

$$\chi = \frac{x}{x_e} \qquad (2.16)$$

$$\xi = \left(\frac{2v_0}{hDx_e}\right)^{1/3} y \qquad (2.17)$$

---

6 K. Aoki, K. Tokuda and H. Matsuda, *J. Electroanal. Chem.*, **209**, (1986), 247

7 J. A. Alden and R. G. Compton, *J. Electroanal. Chem.*, **404**, (1996), 27

It is assumed that $D = D_A = D_B = D_C$.

These variables can then be substituted for x and y into equation (2.13) to give the equation below:

$$\frac{\partial^2[A]}{\partial\xi^2} = \xi\frac{\partial[A]}{\partial\chi} \tag{2.18}$$

This equation implies that the concentration of species A only depends on χ and ξ enabling a profile of the species concentration in (χ, ξ) space to describe all possible solution flow rates, cell geometries and diffusion coefficients.

Similarly, substituting equations (2.16) and (2.17) into equations (2.14) and (2.15) produces:

$$0 = \frac{\partial^2[B]}{\partial\xi^2} - \xi\frac{\partial[B]}{\partial\chi} - k\left(\frac{h^2 x_e{}^2}{4\nu_0{}^2 D}\right)^{1/3}[B] \tag{2.19}$$

and

$$0 = \frac{\partial^2[C]}{\partial\xi^2} - \xi\frac{\partial[C]}{\partial\chi} + k\left(\frac{h^2 x_e{}^2}{4\nu_0{}^2 D}\right)^{1/3}[B] \tag{2.20}$$

A dimensionless rate constant K_{norm} can now be defined as shown below:

$$K_{norm} = k\left(\frac{h^2 x_e{}^2}{4\nu_0{}^2 D}\right)^{1/3} \tag{2.21}$$

which simplifies equations (2.19) and (2.20) to:

$$0 = \frac{\partial^2[B]}{\partial\xi^2} - \xi\frac{\partial[B]}{\partial\chi} - K_{norm}[B] \tag{2.22}$$

and

$$0 = \frac{\partial^2[C]}{\partial\xi^2} - \xi\frac{\partial[C]}{\partial\chi} + K_{norm}[B] \tag{2.23}$$

Hence looking at the equations on the previous page it is possible to conclude that the concentrations of species B and C depend only on χ, ξ and K_{norm}. When calculating the current at the electrode surface, $\xi = 0$, the concentration of the species involved are integrated across the length of the electrode removing the dependence of χ and ξ. This results in the possibility of describing the response at a channel electrode of any geometry and flow rate, providing that the Lévêque approximation is applicable, by a *working curve* which relates theoretical values of N_{eff} to the normalised parameter K_{norm}, figure 2.3.

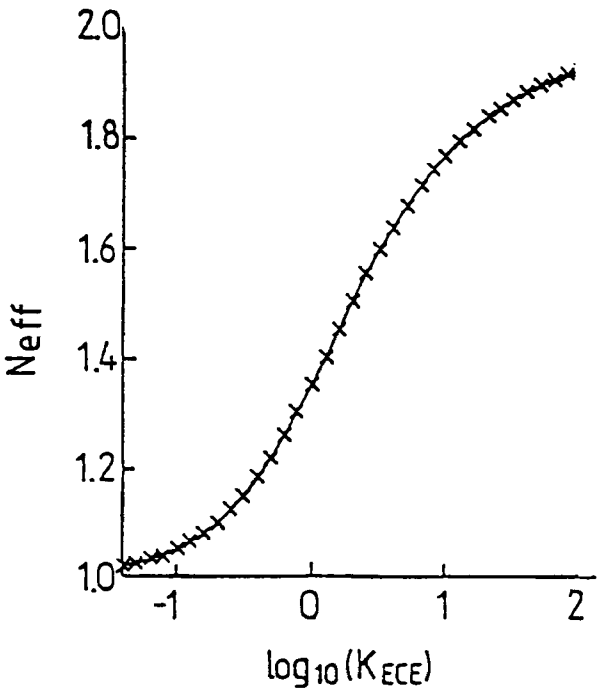

Figure 2.3. *The $EC_{hom}E$ working curve.*

A similar analytical treatment can be applied to an important variation of the ECE mechanism discussed above, namely the $EC_{het}E$ mechanism in which the chemical kinetics occur at the electrode surface. This is described in detail in chapter 6. Working curves for DISP 2, EC', EC_2E and DISP 1 mechanisms have also been generated[8,9,10].

---

8 J. A. Cooper and R. G. Compton, *J. Electroanal. Chem.*, **10**, (1998), 141

9 J. A. Alden, R. G. Compton, W. M. Leslie and T. Silk, *J. Phys. Chem.*, **100**, (1996), 14130

10 J. Alden and R. G. Compton, *J. Phys. Chem.*, **101**, (1997), 9741

2.4.2 The Use of Working Curves

Working curves are extremely useful tools for mechanistic investigations using channel electrodes in which axial diffusion can be neglected. Steady-state voltammograms recorded at a range of different flow rates enable N_{eff} values to be calculated from the Levich equation which can then be converted to their corresponding K_{norm} values using a working curve. A plot of these K_{norm} values against the (volume flow rate)$^{-2/3}$, (for $EC_{hom}E$, EC_2E, DISP 2 and DISP 1 mechanisms) generates a straight line graph providing that the correct working curve for the mechanism under investigation is chosen (enabling mechanistic discrimination). The gradient of the plot then allows the rate constant for the coupled kinetics under investigation to be calculated using the relevant definition of K_{norm} as discussed above.

2.5 Numerical Methods

It has been shown how approximate analytical solutions of the mass transport equation for channel electrodes such as the Levich equation and numerically simulated working curves are useful in the characterisation of electrochemical processes. However, by far the most general method of solving the mass transport equation in order to generate working curves and carry out other mechanistic investigations for a process of interest is through numerical methods. The recent advances in computer power have made numerical methods increasingly popular due to the complex mechanisms and microelectrode geometries that can now be successfully investigated.

The principal method that has been used to solve the mass transport equation numerically is the finite difference method[11]. There are several finite difference methods that have been

---

[11] J. B. Flanagan and L. Marcoux, *J. Phys. Chem.*, 78, (1974), 718

investigated by Anderson and Moldoveanu[12] who were able to conclude that providing axial diffusion can be neglected the space-marching Backwards Implicit finite difference method is the most efficient. This method results in a tri-diagonal matrix equation, as described in the following sections, which can be solved using the Thomas Algorithm[13]. Throughout this thesis the phrase 'Backwards Implicit' and the acronym BI refer to the space-marching application of this implicit method. The BI method retains the full parabolic flow pattern for the solution flow and so represents an improvement over analytical methods whilst being much simpler to implement and readily adapted to include complex homogeneous kinetics[14], unequal diffusion coefficients[15] and transient measurements[16]. An introduction to the BI method is given in the following section, 2.5.1. For the case of electrochemical investigations where axial diffusion is found to be significant, alternative numerical methods of solving the finite difference equations generated from the mass transport equations such as the strongly implicit procedure, SIP[17], or the Multigrid method, MGD1[18] are available. These are not discussed much further in this thesis as the experimental work presented does not involve significant axial diffusion effects.

2.5.1 The Backward Implicit Method - Steady-State Theory

The following sections describe how the BI method can be used to model the current generated at a conventional channel electrode. First, the time-independent (steady-state) case is considered with the time-dependent (transient) case discussed in section 2.5.2.

---

12 J. L. Anderson and S. Moldoveanu, *J. Electroanal. Chem.*, **179**, (1984), 107

13 L. Lapidus and G. F. Pinder, *Numerical Analysis of Partial Differential Equations in Engineering and Science*, Wiley, New York, (1982)

14 A. C. Fisher and R. G. Compton, *Electroanalysis*, **4**, (1992), 311

15 R. G. Compton, A. C. Fisher and R. A. Spackman, *Electroanalysis*, **4**, (1992), 167

16 R. G. Compton and R. G. Wellington, *Electroanalysis*, **4**, (1992), 695

17 H. L. Stone, *Siam J. Numerical Analysis*, **5**, (1968), 530

2.5.1.1 The Finite Difference Form of the Mass Transport Equation

In order to apply the BI method to electrochemical processes the mass transport equation for the species involved is put into finite difference form. This involves covering the region of the channel that is to be simulated with a grid of discrete nodes forming a mesh of points with small finite differences between them, figure 2.4.

The adjacent points in the x-direction are separated by Δx (shown above) and by Δy in the y-direction, resulting in a general point in the channel with co-ordinates (x_k, y_j) where:

$$x_k = k\Delta x \qquad k = 0, 1.....K, \text{ where } \Delta x = \frac{x_e}{K}$$

$$y_j = j\Delta y \qquad j = 0, 1.....J, \text{ where } \Delta y = \frac{2h}{J}$$

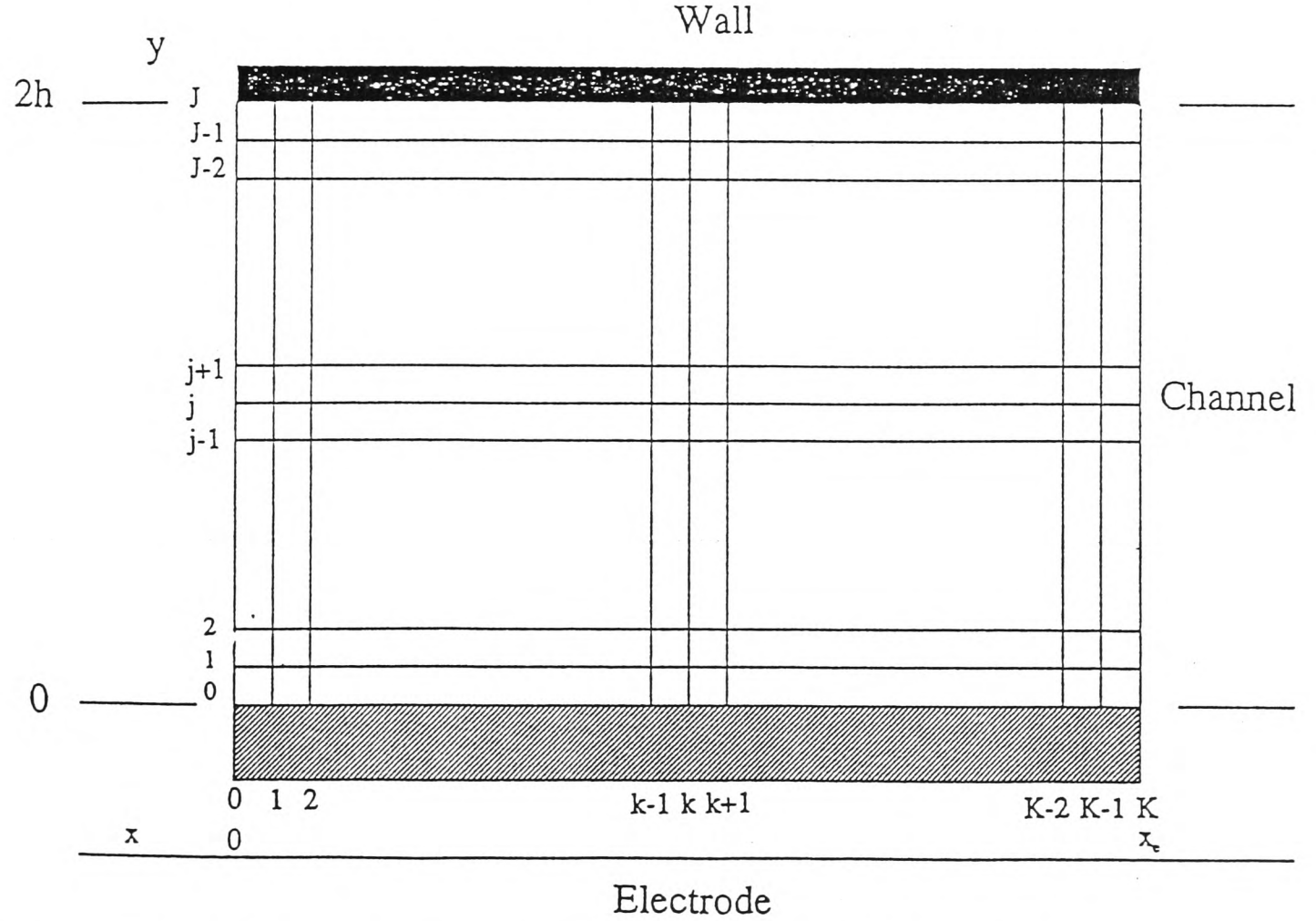

Figure 2.4. The finite difference grid employed for channel electrode modelling.

---

[18] M. J. Bidwell, J. A. Alden and R. G. Compton, *J. Electroanal. Chem.*, **414**, (1996), 247

Hence, the derivatives in the mass transport equation (2.13) for a simple one electron transfer

$$A \quad \pm \quad e^- \quad \rightleftharpoons \quad B$$

can be approximated as:

$$\frac{\partial g^A}{\partial x} \cong \frac{\left(g^A_{j,k+1} - g^A_{j,k}\right)}{\Delta x} \tag{2.24}$$

and

$$\frac{\partial^2 g^A}{\partial y^2} \cong \frac{\left(g^A_{j-1,k+1} - 2g^A_{j,k+1} + g^A_{j+1,k+1}\right)}{(\Delta y)^2} \tag{2.25}$$

where g^A is the normalised concentration, $g^A = [A]/[A]_{bulk.}$

Combining equations (2.13), (2.24) and (2.25) results in the equation shown below:

$$\left(\frac{D_A}{(\Delta y)^2}\right)(g^A_{j-1,k+1} - 2g^A_{j,k+1} + g^A_{j+1,k+1}) = \left(g^A_{j,k+1} - g^A{}_{j,k}\right)\left(\frac{D_A}{\lambda_j (\Delta y)^2}\right) \tag{2.26}$$

where:

$$\lambda_j = \frac{D_A \Delta x (2h)^3 d}{6 v_f j (\Delta y)^3 (2h - j\Delta y)} \tag{2.27}$$

and

$$v_0 = \frac{3 v_f}{4hd} \tag{2.28}$$

In order to solve the finite difference form of the steady-state mass transport equation, (2.26), the following boundary conditions for the mass transport limited current listed on the following page are used.

(1) $x = 0;\ [A] = [A]_{bulk};\quad g^{A}_{j,0} = 1$ (2.29)

At x = 0 (for all y) species A has not yet reached the electrode, hence the concentration of A is equal to that of the bulk concentration.

(2) $y = 0;\ [A]_{bulk} = 0;\quad g^{A}_{0,k} = 0$ (2.30)

At y = 0 the concentration of species A is 0 as it has all undergone an electron transfer reaction to form species B.

(3) $y = 2h;\ D_A \frac{\partial [A]}{\partial y} = 0;\quad g^{A}_{J,K} = g^{A}_{J-1,K}$ (2.31)

There is a no flux boundary at the channel wall as the material is constrained within the channel region.

Using the boundary conditions listed above equation (2.26) becomes:

$$g^{A}_{1,k} = (2\lambda_1 + 1)\, g^{A}_{1,k+1} - \lambda_1\, g^{A}_{2,k+1} \quad (2.32)$$

$$g^{A}_{j,k} = -\lambda_j\, g^{A}_{j-1,k+1} + (2\lambda_j + 1)\, g^{A}_{j,k+1} - \lambda_j\, g^{A}_{j+1,k+1} \qquad j = 2,3.....J\text{-}2 \quad (2.33)$$

$$g^{A}_{J-1,k} = -\lambda_{J-1}\, g^{A}_{J-2,k+1} + (\lambda_{J-1} + 1)\, g^{A}_{J-1,k+1} \quad (2.34)$$

with equation (2.33) describing the concentration of a species at a general point j, k.

2.5.1.2 The Matrix Equation

If we were to describe each of the nodes at a particular k value, J-1 simultaneous equations would be required. It is possible to express these (J-1) simultaneous (linear) equations as a (J-1) x (J-1) matrix equation:

$$\{d\} = [T]\{u\} \quad (2.35)$$

i.e.

$$\begin{bmatrix} d_1 \\ d_2 \\ \vdots \\ \vdots \\ \vdots \\ d_j \\ \vdots \\ \vdots \\ \vdots \\ d_{J-2} \\ d_{J-1} \end{bmatrix} = \begin{bmatrix} b_1 & c_1 & 0 & & & & & & \\ a_2 & b_2 & c_2 & 0 & & & & & \\ & \ddots & \ddots & \ddots & & & & & \\ & & \ddots & \ddots & \ddots & & & & \\ & & 0 & a_j & b_j & c_j & 0 & & \\ & & & & \ddots & \ddots & \ddots & & \\ & & & & & \ddots & \ddots & \ddots & \\ & & & & & & a_{J-2} & b_{J-2} & c_{J-2} \\ & & & & & & 0 & a_{J-1} & b_{J-1} \end{bmatrix} \begin{bmatrix} u_1 \\ u_2 \\ \vdots \\ \vdots \\ \vdots \\ u_j \\ \vdots \\ \vdots \\ \vdots \\ u_{J-2} \\ u_{J-1} \end{bmatrix}$$

where:

$$d_j = g^A_{j,k} \qquad j= 1, 2....J-1 \qquad (2.36)$$

$$u_j = g^A_{j,k+1} \qquad j= 1, 2....J-1 \qquad (2.37)$$

$$a_j = -\lambda_j \qquad j= 2, 3....J-1 \qquad (2.38)$$

$$b_j = 2\lambda_j + 1 \qquad j= 1, 2....J-2 \qquad (2.39)$$

$$b_{J-1} = \lambda_{J-1} + 1 \qquad (2.40)$$

$$c_j = -\lambda_j \qquad j= 1, 2....J-2 \qquad (2.41)$$

The matrix [T] is of tridiagonal form enabling $\{u\}_k$ to be calculated from $\{d\}_k$ using the Thomas algorithm[13] (appendix 1). The boundary condition described above where $g^A_{j,0} = 0$, (2.29), provides the first vector $\{d\}_0$ as every element in this vector is equal to 1. From this $\{u\}_0$ (corresponding to the next vector along, k = 1) can then be calculated using the matrix above as a_j, b_j and c_j are all known for each value of j. The calculation then sweeps downstream over the electrode with each $\{u\}_k$ being calculated from $\{d\}_k$ until the vector $\{u\}_{K-1}$ is calculated. At this point all of the values of $g^A_{j,k}$ (where j = 1, 2....J-1 and k = 1,

2,...K) have been evaluated in the course of the calculation describing the entire concentration profile for species A in the channel flow cell.

2.5.1.3 Current Evaluation

A knowledge of the concentration profile for each species in a channel flow cell enables the current produced at the electrode to be predicted[19]. This results in the expression shown below:

$$I \cong nwFD_A[A]_{bulk} \sum_{k-1}^{K} \left(\frac{g^A_{1,k} - g^A_{0,k}}{\Delta y} \right) \Delta x \qquad (2.42)$$

where n = 1 for the one electron transfer case considered.

From the mass transport limited current boundary condition $g^A_{0,k} = 0$, (2.30), equation (2.42), can be reduced to:

$$I \cong \frac{nwFD_A[A]_{bulk}\,\Delta x}{\Delta y} \sum_{k=1}^{K} g^A_{1,k} \qquad (2.43)$$

The limiting current data can be approximated from the theory described above using FORTRAN 77 programs on a Silicon Graphics Origin 2000 computer. The approximation of the partial derivatives in the mass transport equation as finite differences becomes more valid as the difference between the nodes decreases. This results in the numerical calculation converging to a true solution as the spaces between the nodes are reduced. Therefore, in order to ensure that the calculated current is converged, simulations are repeated with an increasing number of nodes until no significant change in the current is observed.

$$D_A \frac{\partial^2[A]}{\partial y^2} - v_0\left[1 - \frac{(y-h)^2}{h^2}\right]\frac{\partial[A]}{\partial x} = \frac{\partial[A]}{\partial t} \qquad (2.44)$$

As with the steady state case discussed in section 2.5.1, the region of the channel that is to be simulated is described by a finite difference grid, figure 2.4. However, the boundary conditions for a potential step transient are different to those for the steady-state case as shown below:

$t \leq 0$

$0 < y < 2h, \quad 0 < x < x_e; \quad [A] = [A]_{bulk}; \quad {}^{t}g^{A}_{j,k} = 1 \qquad (2.45)$

$t > 0$

$x = 0; \quad [A] = [A]_{bulk}; \quad {}^{t}g^{A}_{j,0} = 1 \qquad (2.46)$

$y = 0; \quad [A]_{bulk} = 0; \quad {}^{t}g^{A}_{0,k} = 0 \qquad (2.47)$

$y = 2h; \quad \frac{\partial[A]}{\partial y} = 0; \quad {}^{t}g^{A}_{J,k} = {}^{t}g^{A}_{J-1,k} \qquad (2.48)$

where ${}^{t}g^{A}_{j,k}$ is the normalised concentration of species A at a general point (j, k) in the finite difference grid at a time $t\Delta t$ where Δt is the time period between successive time steps in the BI calculation and t is the simple unitary counter (i.e. t = 0, 1, 2...NT, where $NT\Delta t$ is the time taken to complete the transient and t = 0 is the start of the transient).

The mass transport equation (2.44), can be written in finite difference form as shown on the following page:

$$\frac{{}^{t+1}g^{A}_{j,k} - {}^{t}g^{A}_{j,k}}{\Delta t} = \frac{D_A}{(\Delta y)^2}\left({}^{t+1}g^{A}_{j-1,k} - 2\,{}^{t+1}g^{A}_{j,k} + {}^{t+1}g^{A}_{j+1,k}\right) - \nu_0\left[1 - \frac{(y-h)^2}{h^2}\right]\left(\frac{{}^{t+1}g^{A}_{j,k} - {}^{t+1}g^{A}_{j,k-1}}{\Delta x}\right) \tag{2.49}$$

This equation may then be reduced to:

$${}^{t}g^{A}_{j,k} + \lambda^{c}_{j}\left({}^{t+1}g^{A}_{j,k-1}\right) = -\lambda^{y}\left({}^{t+1}g^{A}_{j-1,k}\right) + \left(2\lambda^{y} + \lambda^{c}_{j} + 1\right)\left({}^{t+1}g^{A}_{j,k}\right) - \lambda^{y}\left({}^{t+1}g^{A}_{j+1,k}\right) \tag{2.50}$$

where:

$$\lambda^{c}_{j} = \frac{6\nu_f \Delta y \Delta t j(2h - j\Delta y)}{\Delta x (2h)^3 d} \tag{2.51}$$

and:

$$\lambda^{y} = \frac{D_A \Delta t}{(\Delta y)^2} \tag{2.52}$$

Equation (2.50) is similar in form to equation (2.32) which enables the (J-1) simultaneous equations generated from equation (2.50) to be combined in the form of a matrix equation, as shown previously by equation (2.35). The matrix elements for the matrix are defined by the equations shown below:

$$d_j = {}^{t}g^{A}_{j,k} + \lambda^{c}_{j}\left({}^{t+1}g^{A}_{j,k-1}\right) \qquad j = 1, 2....J\text{-}1 \tag{2.53}$$

$$u_j = {}^{t+1}g^{A}_{j,k} \qquad j = 1, 2....J\text{-}1 \tag{2.54}$$

$$a_j = -\lambda^{y} \qquad j = 2, 3,...J\text{-}1 \tag{2.55}$$

$$b_j = 2\lambda^{y} + \lambda^{c}_{j} + 1 \qquad j = 1, 2....J\text{-}2 \tag{2.56}$$

$$b_{J-1} = \lambda^{y} + \lambda^{c}_{J-1} + 1 \tag{2.57}$$

$$c_j = -\lambda^{y} \qquad j = 1, 2....J\text{-}2 \tag{2.58}$$

As for the steady-state case the Thomas Algorithm[13] can be used to solve the matrix equation. However, the method used for the solution differs slightly as it is known that at t = 0, $g^{A}_{j,k}$ is equal to 1 at every node in the finite difference grid. This gives the starting concentration vectors, $\{d\}_k^{t=0}$, for every k co-ordinate at time t = 0. The vector $\{d\}_k^t$, representing the concentrations of A along the y-axis at a particular value of k at time tΔt, can then be used to calculate $\{u\}_k^t$, which represents the concentrations of A along the y-axis vector, at the same time value of k but at time (t + 1)Δt, using the matrix equation. The calculation can then be repeated for the y-axis concentration vectors along each of the k co-ordinates across the electrode, generating a full concentration profile of species A at time (t + 1)Δt from that at tΔt. The calculation continues in this manner until the concentration profile has been calculated at every point required to complete the transient (usually until a steady-state current is seen).

The current generated at the electrode surface at time tΔt is given by:

$$I^t = \frac{nwFD[A]_{bulk}\Delta x}{\Delta y}\sum_{k=1}^{K} {}^{t}g^{A}_{1,k} \qquad (2.59)$$

where n = 1.

2.5.2.1 The Inclusion of Coupled Kinetics

As for steady-state BI modelling it is possible to include homogeneous kinetics in the numerical modelling of potential step transients[24]. This is discussed in more detail in chapter 4 where an $EC_{hom}E$ mechanism is investigated.

---

24 F. Prieto, W. J. Aixill, J. A. Alden, B. A. Coles and R. G. Compton, *J. Phys. Chem.*, **101**, (1997), 5540

3. Experimental

Contents

3.1 Introduction

The aim of this chapter is to introduce the different experimental techniques used in the voltammetric investigations described in the following chapters. A comprehensive list of the chemicals used is also provided in section 3.11.

3.2 The Channel Electrode

A diagram of the conventional channel electrode used in the gravity flow investigations described in chapter 5 is shown in figure 3.1. The cell is a demountable unit, made of optical quality synthetic silica[1], consisting of a coverplate and channel unit as shown below.

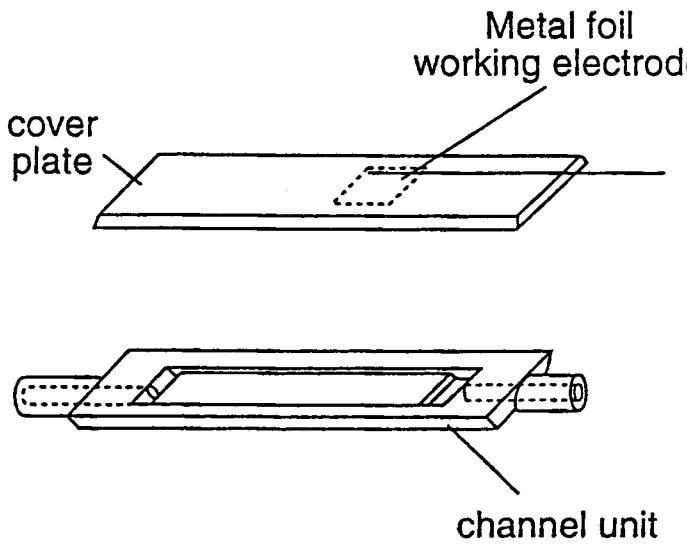

Figure 3.1. The channel electrode used for mechanistic electrochemical studies.

The two units were sealed together using a wax with a low melting point, "Wax-Away" (Vychem Ltd., Poole, Dorset). This offers three main advantages listed below:

(1) It adheres well to silica.

(2) It melts at 50°C and sets solid on cooling.

(3) It dissolves readily in ethanol making it easy to clean and dismantle the cell.

---

1 R. G. Compton and R. A. W. Dryfe, *Prog. Reaction Kinetics*, **20**, (1995), 245

The working electrode was fabricated from a Au foil (purity of 99.95%, thickness 0.025 mm) with dimensions of 4 mm x 6 mm (Goodfellow Metals, Cambridge). This was cemented onto the inside of the coverplate using Araldite epoxy resin with a thin adjoining 'tail' attached to enable electrical connection through a hole in the coverplate. The electrode foil was rolled with a steel caster until it was uniformly flat and essentially flush with the channel wall. The precise electrode dimensions, detailed in chapter 5, could then be determined using a travelling microscope. For the experiments described in chapter 5 the Au electrode was amalgamated with Hg using a 0.12 M KCN/ 0.115 M mercury nitrate (I) solution[2].

A Ag wire (Goodfellow Metals, Cambridge) pseudo reference electrode was positioned in the flow system in a glass T-piece upstream of the working electrode. The Pt gauze counter electrode (Goodfellow Metals, Cambridge) was located downstream of the channel electrode in order to flush any products formed away from the working electrode.

3.2.1 The Channel Electrode Flow System

A gravity fed flow system, figure 3.2, was used in conjunction with the conventional channel electrode to provide a regular flow of solution over the electrode surface. The dimensions of the channel cell easily satisfied the criterion for parabolic (Poiseuille) flow described in section 1.5.2.1 of chapter 1. The electrolyte solution flowed from a 250 cm^3 reservoir through Pyrex tubing with an internal diameter of 2 mm. The Pyrex tubing from the reservoir to the channel was constructed from two 1 m lengths joined with a B5 ground glass cone and socket joint using wax as a sealant. Small lengths of silicone rubber tubing were used to connect the channel to the Pyrex tubing. The downstream section of the flow system was constructed from flexible Teflon tubing, 3 mm in diameter (Anachem, Luton), which led

---

2 P. J. Daly, D. J. Page and R. G. Compton, *Anal. Chem.*, **55**, (1983), 1191

to three glass capillaries and a by-pass tube selected through the use of a four-way tap (V. A. Howe Ltd, Banbury). After passing through a selected capillary the solution dripped from a glass tip, connected using Teflon tubing, into a waste receptacle.

The flow rate of the solution could be varied in two ways:

(1) Selecting one of the three different sized calibrated capillaries incorporated into the flow system using the four way tap.

(2) Varying the height difference between the solution reservoir and the outlet tip by adjusting the vertical position of the outlet tip.

These enabled flow rates in the range of 10^{-4} - 10^{-1} $cm^3 s^{-1}$ to be routinely used.

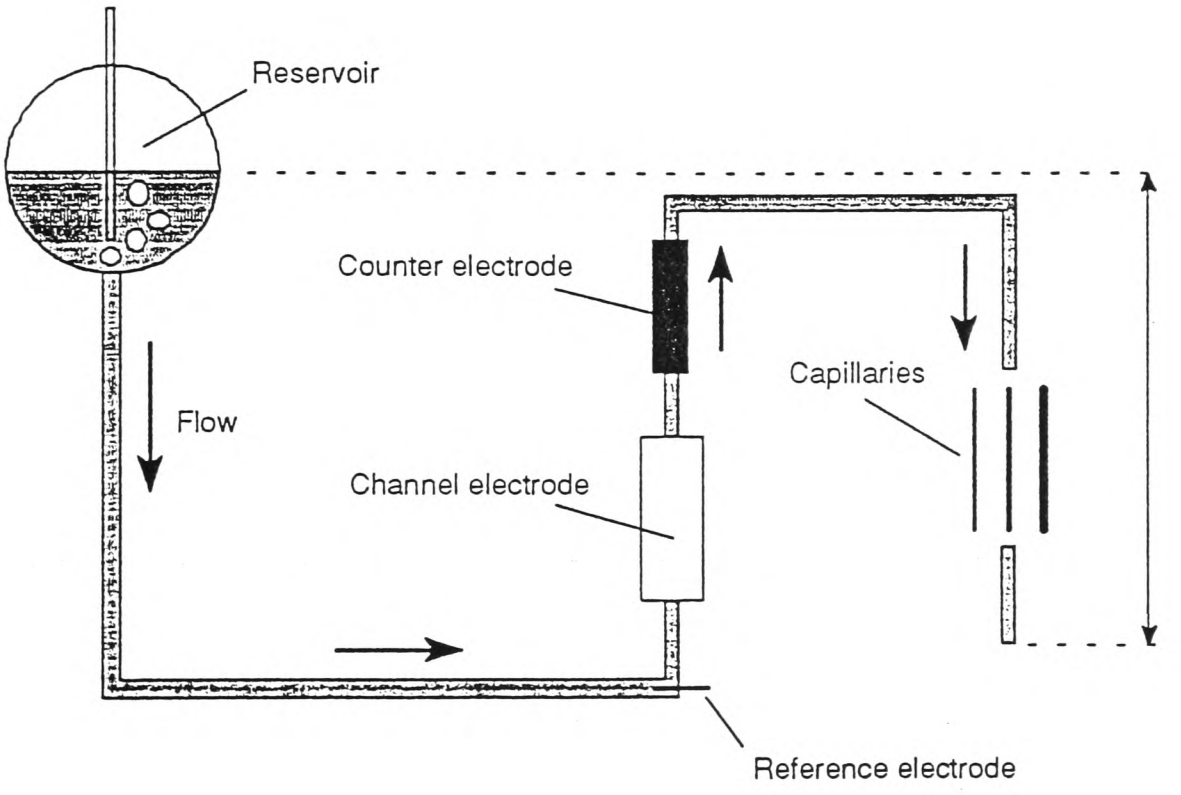

Figure 3.2. A schematic diagram of the channel electrode gravity fed flow system.

3.3 *In-Situ* Electrochemical Electron Spin Resonance (ESR)

The gravity flow channel electrode was also used to conduct simultaneous electrochemical ESR experiments. The simultaneous electrochemical ESR experiments

described in chapter 5 were carried out on a Bruker ER200D spectrometer with a 200 mW klystron operating in the frequency range 9.0 - 10.0 GHz, figure 3.3. A magnetic field moldulation of 100 KHz was used. The channel flow cell was carefully positioned in the centre of the rectangular cavity operating in the TE_{102} mode[3]. Two silica tubes of approximately 10 mm internal diameter were placed around the inlet and outlet portions of the flow cell to control the positioning of the cell within the cavity. The other details of the flow system used for the *in-situ* ESR experiments were essentially the same as those for the standard flow system described previously.

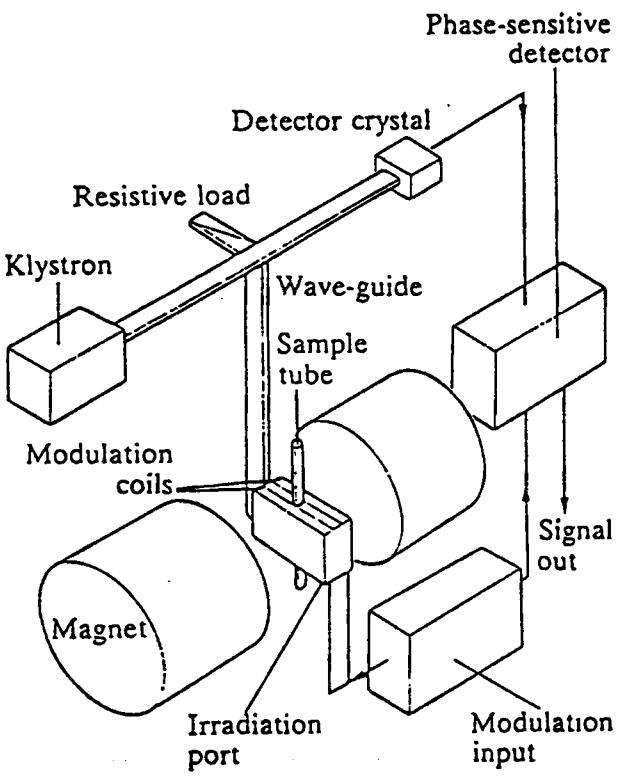

Figure 3.3. The ESR spectrometer.

3.4 Electronics

For the channel electrode measurements an Oxford Electrodes potentiostat and linear potential scan generator were used to obtain the voltammograms. For the conventional

---

3 J. E. Wertz and J. R. Bolton, *Electron Spin Resonance: Elementary Theory and Practical Applications,* Chapman and Hall, New York, (1986)

channel electrode experiments these were recorded on a Lloyd Instruments (Southampton) PL3 chart recorder, with a multimeter (Cirkit, Broxbourne, Herts), capable of a precision of 0.1 mV used to independently check the current and voltage measurements.

3.5 The High Speed Channel Flow Cell

The high speed channel flow cell used in chapters 4, 6, 7 and 8 has been introduced in chapter 1. The channel cell shown in figure 3.4 was fabricated in silica (Optiglass Ltd., Hainault, Essex) with the cross sectional area of the flow cell approximately 2 mm x 0.1 mm. The Pt microband electrodes were made by sealing a Pt foil strip (Goodfellow Metals, Cambridge) between two glass rods. The Pt foil was held in place using two metal-glass seals which formed a smooth seal between the glass and the Pt. The section of glass containing the electrode was then cut to form a rectangular shape using standard glass-working tools. The glass used was chosen to be soda-glass rather than Pyrex as the linear expansion coefficient of soda-glass is more compatible with that of Pt[4]. Pt has a linear expansion coefficient of 9 x 10^{-6} K^{-1} compared with 3.3 x 10^{-6} K^{-1} and 9 x 10^{-6} K^{-1} of Pyrex and soda-glass respectively. Another advantage of soda-glass is its lower softening temperature compared with that of Pyrex[4] (973 K vs. 1093 K) which further facilitates electrode fabrication.

The face of the glass containing the electrode was lapped to a flat surface and polished using silicon carbide and alumina abrasives by decreasing the particle sizes to 0.3 μm (Shandon Scientific Co. Ltd., London). The electrode was re-polished prior to each different experiment to ensure that the electrode surface was clean and reproducible. The exact dimensions of the

---

4 J. Moore, C. C. Davis, M. A. Coplan and S. C. Greer, *Building Scientific Apparatus*, Addison-Wesley: Redwood City, California, 2nd Edn., Chapter 2, (1989),

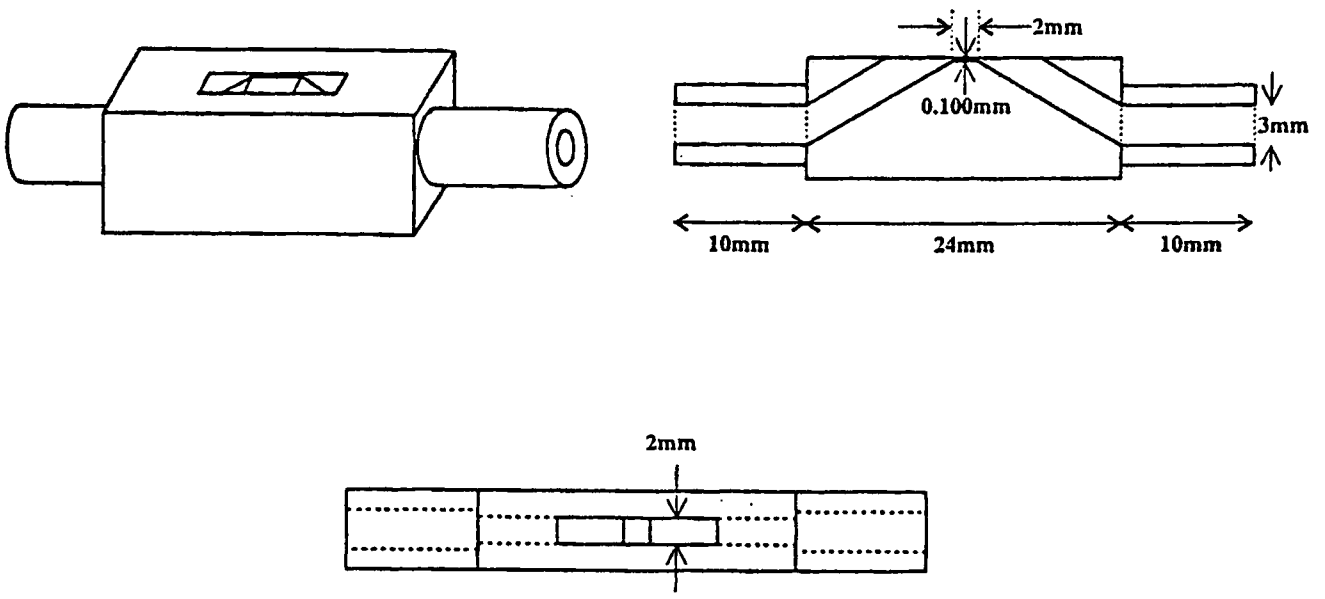

Figure 3.4. *The high speed channel flow cell showing a perspective view and the principal dimensions.*

electrode were measured using either a scanning electron microscope or a Topometrix AFM and are reported in the relevant chapters.

The experiments described in chapter 6 used a Hg/Cu electrode. This involved etching the surface of the Pt electrode using a 3 M KCN/ 1 M KOH solution to slightly recess the electrode prior to electroplating. The etching process lasted for 3 - 4 hours, with a current of 2 mA being drawn throughout. The Pt electrode was then electroplated with Cu for 20 minutes using an aqueous 5 mM cupric nitrate/ 0.1 M KCl / 20 mM ammonium hydroxide solution. Having produced a shiny Cu coating the electrode was plated with Hg for 1 minute using a 0.12 M KCN/ 0.15 M mercury(I) nitrate solution. The times involved in the plating procedures were obtained from previous reports[5].

The counter and reference electrodes were both coils of Pt wire (Goodfellow Metals, Cambridge), as described in chapter 1.

---

5 M. Donten and Z. Kublik, *J. Electroanal. Chem.*, **196**, (1985), 275

3.5.1 Delivery and Control of the Solution Flow

Flow rates of up to 10 cm^3 s^{-1} were achieved using the pressure driven flow delivery detailed in chapter 1. The chamber containing the channel cell and the solution reservoir was pressurised by cylinder nitrogen under computer control using two fast acting electromagnetic valves (Clippard Inc., Cincinnati, Ohio, USA). The chamber pressure was monitored using a silicon diaphragm pressure sensor (Entran Ltd., Watford). Oxygen was removed from the chamber by repeated cycles of pressurising and venting. A separate valve controlled the de-oxygenation of the solution by bubbling with nitrogen which was carried out with the chamber at atmospheric pressure to avoid supersaturation with nitrogen.

The flow rate was controlled by the combination of the chamber pressure with one of three pre-calibrated capillaries (appendix 2) through which the waste solution flows. The capillaries were selected using electromagnetic Teflon Valves (Neptune Research Inc., Maplewood, New Jersey, USA). These valves were normally closed so that solution was only consumed during the short time required to carry out a measurement.

The high speed channel flow cell was controlled using a Viglen 486DX33 computer equipped with the control software required to run the experiments along with the data analysis of the data obtained.

3.6 Platinum Single Crystals

The use of single crystals in electrochemical measurements requires high grade reagents and ultra-clean glassware. This section describes the equipment used to carry out such experiments along with the methods used to prepare the single crystals and glassware involved.

3.6.1 The Electrochemical Cell

The electrochemical cell used for the single crystal experiments, figure 3.5, was designed by Dr. Gary Attard at Cardiff University. The electrochemical cell was made of glass with the main body comprising of two compartments. The first contained the single crystal working electrode and the counter electrode with the reference electrode housed in the second small adjoining compartment.

(1) The Single Crystal Working Electrode

The single crystal working electrodes, Pt(111), Pt(110) and Pt(100), were prepared using the method described by Clavilier et al.[6]. The appropriate single crystal working electrode was then connected to a long Pt wire which was placed inside a glass capillary, figure 3.5. The capillary was held inside a Teflon holder which enabled the crystal to be moved up and down by loosening the screw connected to the Teflon holder.

(2) The Reference Electrode

The reference electrode used was a palladium/hydrogen (Pd/H) electrode as this could be kept clean and free of contamination. The (Pd/H) electrode was made from a Pd wire (Goodfellows, Cambridge) and sealed in a glass holder. After removing contaminants from the surface of the electrode by heating in a Bunsen flame the Pd electrode was charged with hydrogen via the gas inlet of the reference compartment, figure 3.5 (inlet 1), for 30 minutes.

(3) The Counter Electrode

The counter electrode was a Pt gauze (Goodfellows, Cambridge).

---

6 J. Clavilier, D. Armand, S. G. Sun and M. Petit, *J. Electroanal. Chem.*, **205**, (1986), 267

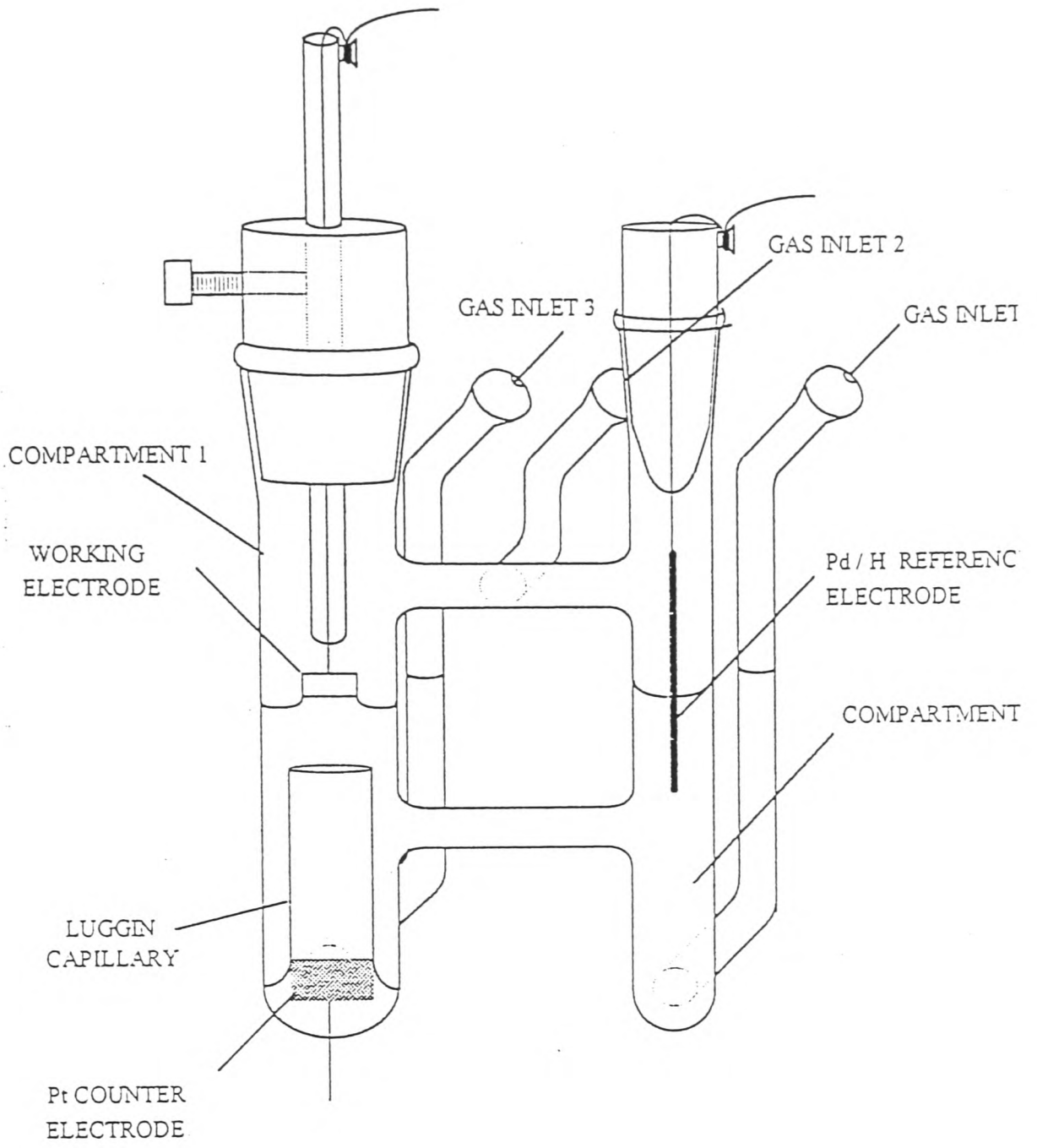

Figure 3.5. The electrochemical cell used for single crystal experiments.

3.6.2 The Cleaning Procedure

In order to remove any contaminants, particularly organic compounds, all of the glassware used in the single crystal experiments was soaked overnight in a dilute solution of potassium permanganate in concentrated sulphuric acid (AnalaR, 98%). After soaking the glassware was then rinsed thoroughly with water before it was steamed, using specially adapted glassware to mount the cell, for about 30 minutes using Elgastat (High Wycombe) UHQ water. The electrochemical cell was then steamed for a second time.

3.6.3 Preparation of Solutions

All of the electrolyte solutions were prepared using high quality reagents (Aristar, BDH). Before any electrochemical measurements were made the solutions were purged of oxygen by bubbling pureshield argon through inlet 3, figure 3.5, of the electrochemical cell for 20 minutes, (the gas line was fitted with an Oxisorb unit (Messer Griesheim, Germany) to ensure that no oxygen was present in the argon). The argon line was then swapped to inlet 2 to enable the argon to blow over the surface of the electrode.

3.6.4 Mounting the Single Crystal in the Electrochemical Cell

The single crystal electrode was annealed in the hottest part of a Bunsen flame, to red heat, for about a minute to remove any impurities form the surface. The stopper for compartment 1 was then removed and the hot electrode (in the glass capillary) was placed promptly into the electrochemical cell. The electrode was left in the argon flow for about 15 - 20 seconds to enable it to cool before it was quenched in the electrolyte solution. Quenching at too high a temperature over a period of time would induce crystal stresses which would eventually give rise to a polycrystalline sample. The height of the electrode was then adjusted to give a good meniscus, as shown in figure 3.6, by loosening the Teflon screw connected to the holder and moving the glass capillary tube containing the electrode. Once the single crystal electrode was in place cyclic voltammograms were recorded using the electronics described in section 3.4.

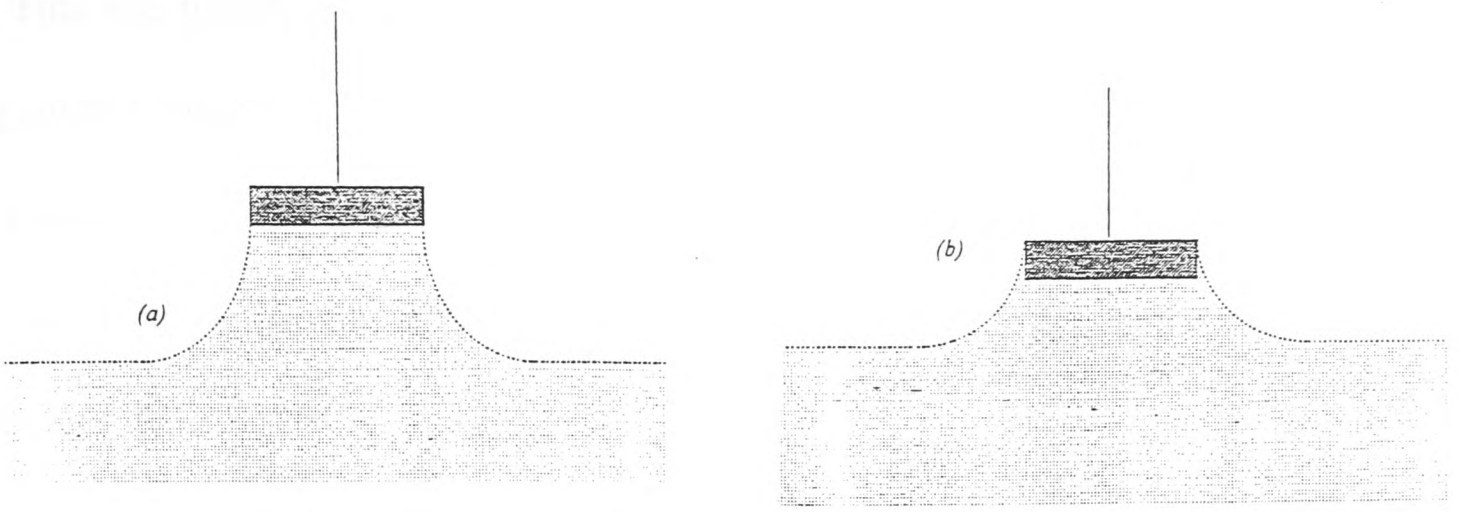

Figure 3.6. *(a)* *Formation of a good meniscus between crystal and electrolyte.*

(b) *Poor meniscus formation due to wetting of the crystal.*

3.7 Rotating Disc Electrode (RDE)

Rotating disc electrodes were used to estimate diffusion coefficients. This type of hydrodynamic system offers the advantage of being simple to use and capable of generating consistently reproducible results. The apparatus consisted of a small metallic disc, working electrode, embedded in the centre of a large Teflon cylinder, figure 3.7. The working electrode used was fabricated from Cu with the precise dimensions, measured using a travelling microscope. The Cu electrode was plated with Hg using the method described in section 3.5. The electrode was constructed such that the disc and the Teflon holder were flush, with only one face of the electrode exposed to the electrolyte solution. The electrode surface was polished prior to each experiment with diamond lapping compounds ranging in size from 25 - 0.25 μm (Kemet International, Kent). Traces of lapping compound were removed using nanopure water. The Teflon cylinder was then positioned within the main solution containing double walled glass vessel, figure 3.7, and rotated perpendicular to the face of the disc at a selected constant speed in the range of 0.5 - 50 Hz (to an accuracy of 0.01

Hz). This was maintained using a motor controller that employed proportional feedback with a Hg contact attached to a metal screw thread providing electrical contact to the RDE.

The counter electrode used was a Pt gauze (Goodfellow Metals, Cambridge) with a standard calomel electrode used as a reference electrode. Voltammograms were recorded using the electronics described in section 3.4.

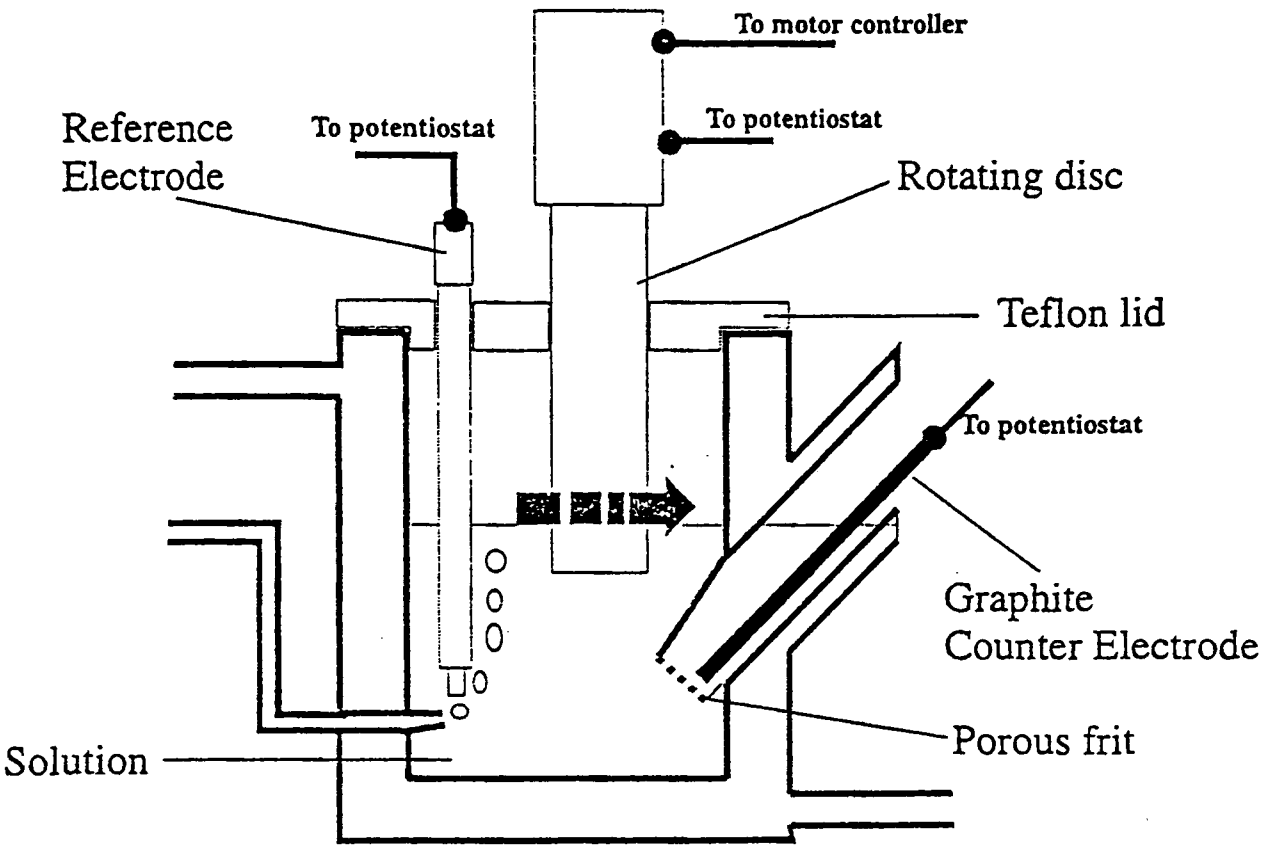

Figure 3.7. Schematic diagram of the rotating disc electrode.

3.8 pH Measurements

The pH of solutions was measured using a glass combination electrode (BDH Poole, Dorset) in conjunction with a Jenway 3030 pH meter (Jenway Ltd., Dunmow, Essex). The readings were made with a precision of ± 0.01 pH units.

3.9 Solvents and Solution Preparation

All of the aqueous solutions were made up using Elgastat (High Wycombe, Bucks) UHQ grade water (18 MΩ cm). For the nitromethane experiments described in chapters 5, 6, 7 and 8 the aqueous solutions were buffered using solutions based on the following: pH 1.8 - 0.2 M phosphoric acid/ 0.08 M KOH; pH 3 - 5 - 0.1 M citric acid/ 0.1 M potassium phosphate; pH 7 - 0.2 M potassium phosphate; pH 8 - 9 - 0.2 M boric acid. In each case the buffers were adjusted to the desired pH by the addition of KOH solution and additionally contained 1.0 M potassium chloride as supporting electrolyte. The solutions were thoroughly degassed for 30 minutes before use with nitrogen. An aqueous solution of 0.37 M nitromethane was prepared immediately prior to experimentation which was then added to 250 cm^3 of the degassed buffer solution to produce a 1.5 mM solution of nitromethane.

For the high speed channel flow measurements described in chapter 4 the solvent used was acetonitrile with tetabutylammonium perchlorate as the supporting electrolyte. Again the solutions were degassed with nitrogen for at least 30 minutes prior to electrochemical measurements to remove dissolved oxygen.

All of the chemicals used were weighed out using a Unimatic CL 41 electronic balance to a precision of ± 0.1 mg.

3.10 Computing

The computer programs for the numerical simulations described in the following chapters were written in FORTRAN 77. The programs were carried out on a Silicon Graphics Origin 2000.

3.11 Chemicals Used

A comprehensive list of all the chemicals used in the following chapters is given in the following tables.

CHEMICAL	GRADE	SUPPLIER
Argon	Pureshield	BOC
Hydrogen	High purity	BOC
Nitrogen	oxygen-free	BOC

Table 3.1. Gases used.

CHEMICAL	GRADE	SUPPLIER
Acetonitrile	98%	Fisons
Tetrabutylammonium perchlorate (TBAP)	puriss	Fluka
Ferrocene	98%	Aldrich
p-Bromonitrobenzene (*p*BNB)	99%	Aldrich
p-Chloronitrobenzene (*p*CNB)	99%	Aldrich
N,N,N',N'-Tetramethyl-1,4-phenylenediamine (TMPD)	99%	Aldrich

Table 3.2. Chemicals used in chapter 4.

CHEMICAL	GRADE	SUPPLIER
Ammonium Hydroxide	ACS	Aldrich
Boric acid	99.5%	Fluka
Citric acid	99.7%	BDH
Cupric nitrate	AnalaR	BDH
Deuterated nitromethane	99%	Aldrich
Deuterium oxide	99%	Aldrich
Fluorescein	p.a.	Fluka
Hydrochloric acid	37% wt. In solution	BDH
Mercury (I) nitrate	AnalaR	BDH
Nitric acid	GPR	BDH
Nitromethane	puriss, absolute	Fluka
pH 4 Buffer	± 0.01	Aldrich
pH 10 Buffer	± 0.01	Aldrich
Phosphoric acid	85% wt. In solution	Aldrich
Potassium chloride	99%	Aldrich
Potassium cyanide	98%	M&B
Potassium hydroxide	1.039 N	Aldrich
Potassium hydroxide pellets	AnalaR	BDH
Potassium phosphate	99%	Aldrich
Sodium hydroxide	0.0975N	Aldrich
Sulphuric acid	AristaR, 99.999%	Aldrich
Sulphuric acid	AnalaR	BDH

Table 3.3. *Chemicals used in chapters 5, 6, 7 and 8.*

4. Transient Measurements and the High Speed Channel Flow Cell

Contents

The work presented in this chapter has been published in J. Phys. Chem. B, 101, (1997), 5540

4.1 Introduction

As discussed in chapter 1, the voltammetric timescale accessible by *steady-state* measurements has recently been extended through the enhancement of mass transport to microelectrodes using forced convection in addition to diffusion[1-3]. This has enabled the investigation of rapid homogeneous processes coupled to electrochemistry and heterogeneous electron transfer reactions that were previously masked by mass transport control. The high speed channel flow cell, introduced in chapter 1, has been successfully employed for such investigations demonstrating that homogeneous first order rate constants as high as 10^4 - 10^5 s^{-1} and standard electrochemical rate constants as high as 1 cm s^{-1} are readily accessible through steady-state voltammetry[3,4].

This experimental chapter extends the application of the high speed channel flow cell to potential step transient measurements, described in chapter 2. The aim of this chapter is to confirm whether the neglect of axial diffusion under transient - as opposed to steady-state conditions is justified whilst investigating the possibility of accessing even faster rate constants using the high speed channel flow cell.

4.2 Theory

The electrochemical systems used to investigate the application of the high speed channel flow cell to potential step transient measurements involved simple reversible one electron transfer reactions of the form:

---

1 R. G. Compton, A. C. Fisher, R. G. Wellington, P. J. Dobson and P. A. Leigh, *J. Phys. Chem.*, **97**, (1993), 10410

2 R. G. Compton, R. A. W. Dryfe, J. A. Alden, N. V. Rees, P. J. Dobson and P. A. Leigh, *J. Phys. Chem.*, **98**, (1994), 1270

3 N. V. Rees, R. A. W. Dryfe, J. A. Cooper, B. A. Coles and R. G. Compton, *J. Phys. Chem.*, **99**, (1995), 7096

$$A \pm e^- \rightleftharpoons B$$

where the bulk solution contains only A. The transients were obtained by stepping the potential from a value at which no current flowed to one where the mass transport limiting current was obtained under steady-state conditions as described in section 2.3.2. The dimensions and co-ordinates of the high speed channel flow cell, described previously, are shown in figure 1.1. Using the co-ordinates assigned in figure 1.1 the time-dependent mass transport equation for species A can be written as:

$$\frac{\partial[A]}{\partial t} = D_A \frac{\partial^2[A]}{\partial x^2} + D_A \frac{\partial^2[A]}{\partial y^2} - v_x \frac{\partial[A]}{\partial x} \qquad (4.1)$$

where [A] is the concentration of species A, D_A is the diffusion coefficient of species A and v_x is the velocity component of the flow (x-direction). The equation above assumes that diffusion in the *z*-direction is negligible. However, diffusion in the x-direction is included in the mass transport equation as the significance of axial diffusion effects when carrying out transient measurements using the high speed channel flow cell had not been confirmed prior to the work carried out in this chapter. The boundary conditions for a potential step transient are discussed in section 2.5.2.

A rigorous approximation of equation (4.1) has been obtained by Bidwell[5] et al. for potential step transients at channel electrodes, using an implicit finite difference method based on a 3-point stencil. The resulting linear equations were solved using the strongly implicit procedure (SIP). As discussed in section 2.5, the backward implicit method (BI) does not allow the inclusion of axial diffusion effects. Bidwell et al. were able to show that transients normalised

---

4 N. V. Rees, J. A. Alden, R. A. W. Dryfe, B. A. Coles and R. G. Compton, *J. Phys. Chem.*, **99**, (1995), 14813

5 M. J. Bidwell, J. A. Alden and R. G. Compton, *J. Electroanal. Chem.*, **414**, (1996), 247

to their steady-state value in the absence of axial diffusion, as predicted using the Levich[6] equation:

$$I_{lim} = 0.925F[A]_{bulk} D_A^{2/3} \nu_f^{1/3} (h^2 d)^{-1/3} w x_e^{2/3} \qquad (4.2)$$

where F is the Faraday constant and the other parameters are defined in section 1.5.2, are a unique function, f, of two dimensionless parameters, p and τ, as shown below:

$$\frac{I}{I_{Lim,Lev}} = f(p,\tau) \qquad (4.3)$$

It should be noted that equation (4.3) assumes the Lévêque[7] approximation, defined in section 1.5.2.2, in which the convective flow profile is assumed to be linear instead of parabolic in the vicinity of the electrode.

The definitions of p and τ are given below:

$$p = \left(\frac{Dh}{2\nu_0 x_e^2}\right)^{2/3} \qquad (4.4)$$

$$\tau = t\left(\frac{4\nu_0^2 D}{h^2 x_e^2}\right)^{1/3} \qquad (4.5)$$

where the parameters are again defined in section 1.5.2. Therefore, using equations (4.4) and (4.5), Bidwell et al. were able to construct a working surface[5] as a contour plot of $I/I_{lim,\,Lev}$ against log(p) and log(τ), figure 4.1. This working surface can be used for the analysis of current-time transient data recorded at any flow rate or cell geometry, providing that the Lévêque approximation still holds, including cases in which axial diffusion effects are significant.

---

6 V. G. Levich, *Physicochemical Hydrodynamics*, Prentice-Hall, Englewood Cliffs, New Jersey, USA, (1962)

7 M. A. Lévêque, *Ann. Mines. Mem. Ser.*, **12/13**, (1928), 201

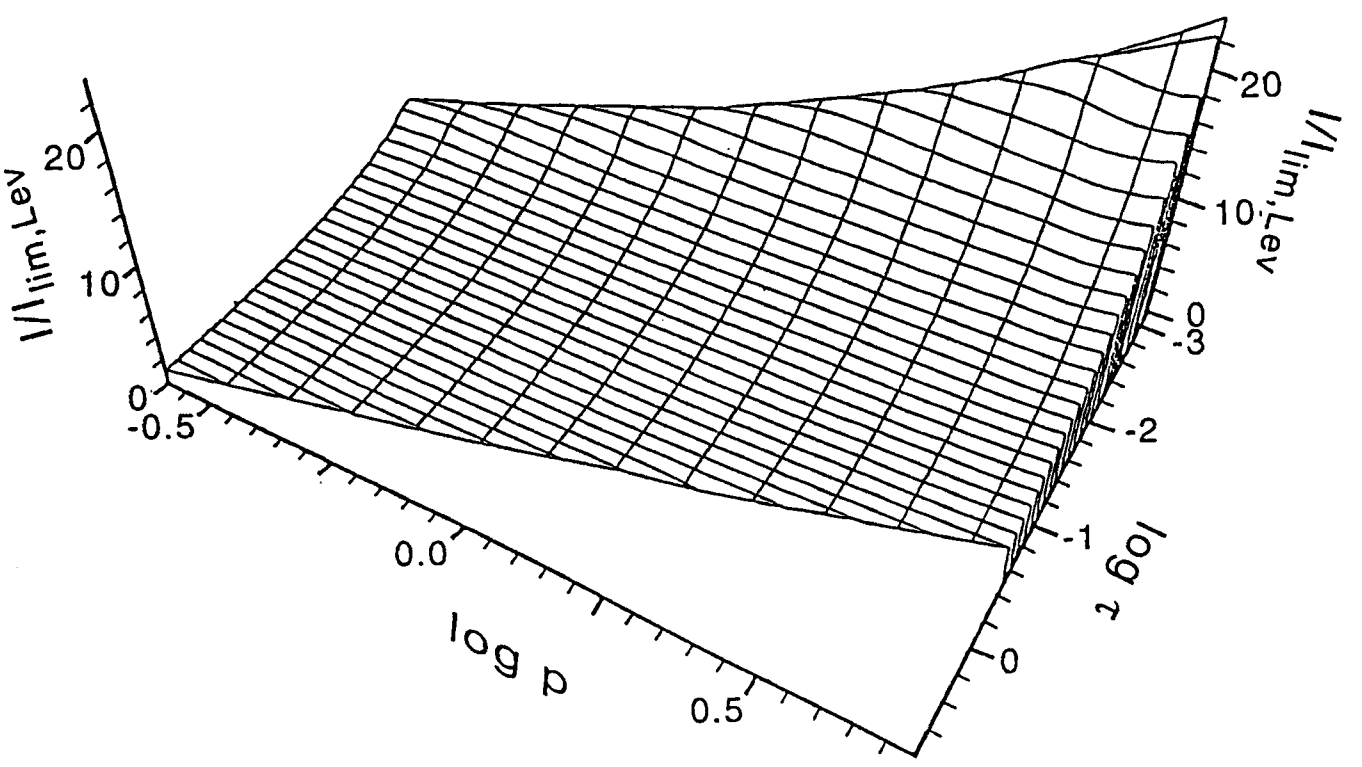

Figure 4.1. Working surface for potential step transients.

For cases where axial diffusion effects are significant, the steady-state current deviates from that predicted by equation (4.2) as the Levich equation does not take such effects into consideration. The parameter p in the complete working surface provides an estimation of the axial diffusion contribution to the mass transport equation (4.1). It therefore follows that for larger p values the effect of axial diffusion is greater and hence the steady-state current flowing is larger than that predicted by the Levich equation. Equation (4.4) shows that the size of the parameter p is inversely proportional to the rate of solution flow, implying that the relative contribution of axial diffusion effects to the mass transport equation decreases as the solution flow rate is increased. This is significant when considering the case of the high speed channel flow cell as it might be the case that axial diffusion effects in the high speed channel flow cell can be neglected in transient measurements in the same way that they are in steady-state measurements where the Levich equation holds[3], section 1.5.2. In this case the mass

transport along the x-axis only includes the convective term as shown in equation (2.44). The aim of this chapter is to examine experimentally whether or not axial diffusion can be neglected under transient conditions.

The mass transport equation for cases where axial diffusion can be neglected has been solved numerically using the backward implicit method (BI) described in section 2.5.2. In these cases the normalised transient current with respect to the transport limiting current $I/I_{lim,\ Lev}$ is a unique function of the normalised time, τ, defined by equation (4.5). Therefore, under conditions in which axial diffusion effects can be neglected, transient data can be analysed using the working curve given in figure 4.2[5].

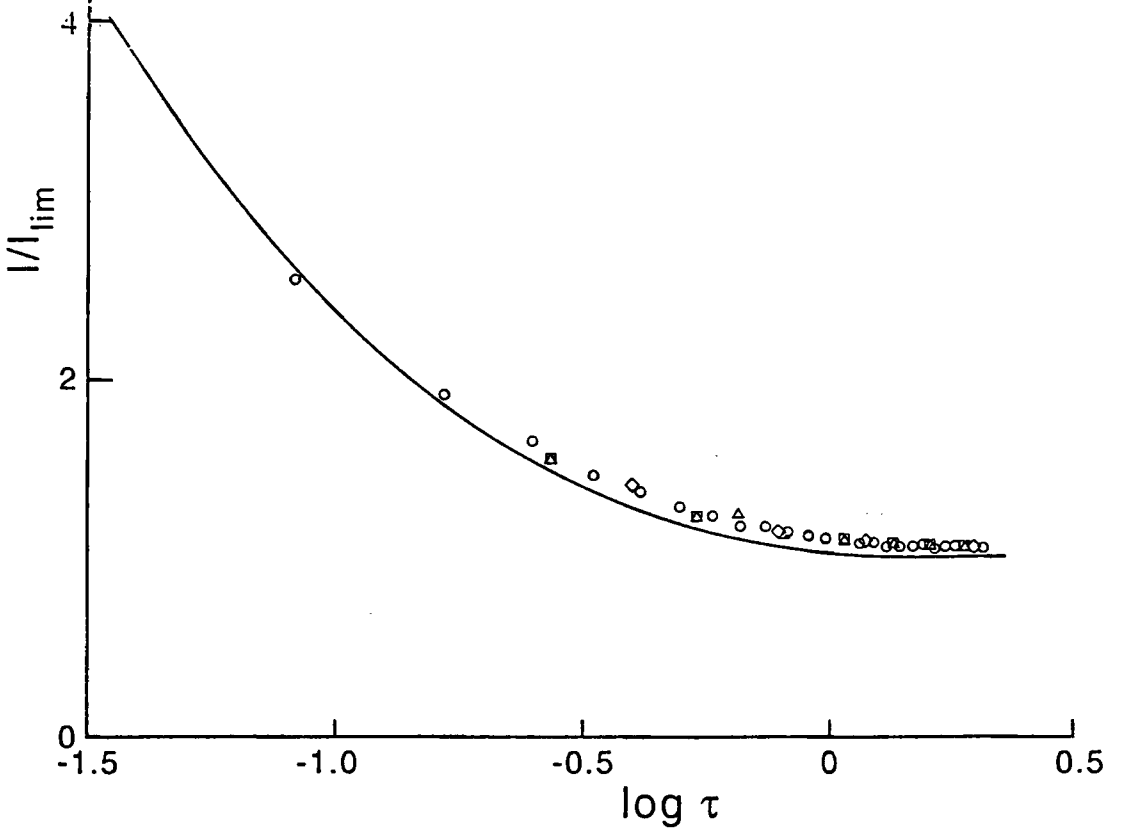

Figure 4.2. *Working curve for normalised transients (-) and experimental normalised transients for pCNB at four different flow rates: 0.1429 $cm^3\ s^{-1}$ (○), 0.3367 $cm^3\ s^{-1}$ (◊), 0.8448 $cm^3\ s^{-1}$ (□) and 1.5044 $cm^3\ s^{-1}$ (△).*

4.3 General Experimental Details

The experimental details of the high speed channel flow cell have been described in chapters 1 and 3. The microband electrode was made from a Pt foil strip (Goodfellow Metals, Cambridge) using the method described previously. A Topometrix atomic force microscope was used to measure the precise dimensions of the electrode: 40 μm length (x_e) and 0.94 mm width (w). The species studied were the one-electron oxidation of N,N,N',N'-tetramethyl-1,4-phenylendiamine (TMPD) and the one-electron reductions of *p*-bromonitrobenzene (*p*BNB) and *p*-chloronitrobenzene (*p*CNB).

4.4 Preliminary Steady-State Voltammetry

In order to calibrate the height of the high speed channel, steady-state experiments on the oxidation of 0.5 mM ferrocene in 0.1 M TBAP/ acetonitrile, a well established simple one-electron process[8,9] were carried out. The half-wave potential (the potential at half the limiting current value) measured was + 0.225 ± 0.01 V (vs. pseudoreference electrode) for a range of electrolyte flow rates up to 3.5 $cm^3\ s^{-1}$. The mass transport limited current showed a linear dependence on the cube root of the solution flow rate according to the Levich equation (4.2), figure 4.3. Hence, the application of equation (4.2) with the measured geometric parameters of the channel electrode (x_e, w, d), and a value of 2.3 x 10^{-5} $cm^2\ s^{-1}$ for the diffusion coefficient of ferrocene in acetonitrile[8,9], enabled the height of the channel cell to be calculated. In all cases a value of 95 ± 7 μm was found.

Steady-state voltammetric experiments were then recorded using 0.5 mM solutions of TMPD, *p*BNB and *p*CNB in 0.1 M TBAP/ acetonitrile. In all cases electrochemically reversible one-

---

8 P. Sharp, *Electrochim. Acta*, **28**, (1983), 301

9 H. Schull, K. Sochaj, *Electrochim. Acta.*, **34**, (1989), 915

electron waves were obtained, with half-wave potentials of +0.185, -1.390 and -1.230 V (vs. Pt pseudo reference electrode) for the oxidation of TMPD and the reduction of *p*BNB and *p*CNB respectively. Figure 4.4 shows a sample steady-state voltammogram for *p*CNB at a flow rate of 1.504 $cm^2\ s^{-1}$. The mass transport limited current dependence on the electrolyte flow rate was found to be in excellent agreement with the behaviour predicted by the Levich equation as shown in figures 4.5(a) - (c). This enabled the diffusion coefficient of each of the electroactive species used to be obtained from the slopes of the linear plots shown in figures 4.5(a) - (c) and the channel geometry parameters obtained previously. The diffusion coefficient values obtained for TMPD, *p*BNB and *p*CNB were 2.15, 2.30 and 2.05 (x 10^{-5} $cm^2\ s^{-1}$; ± 10%), respectively.

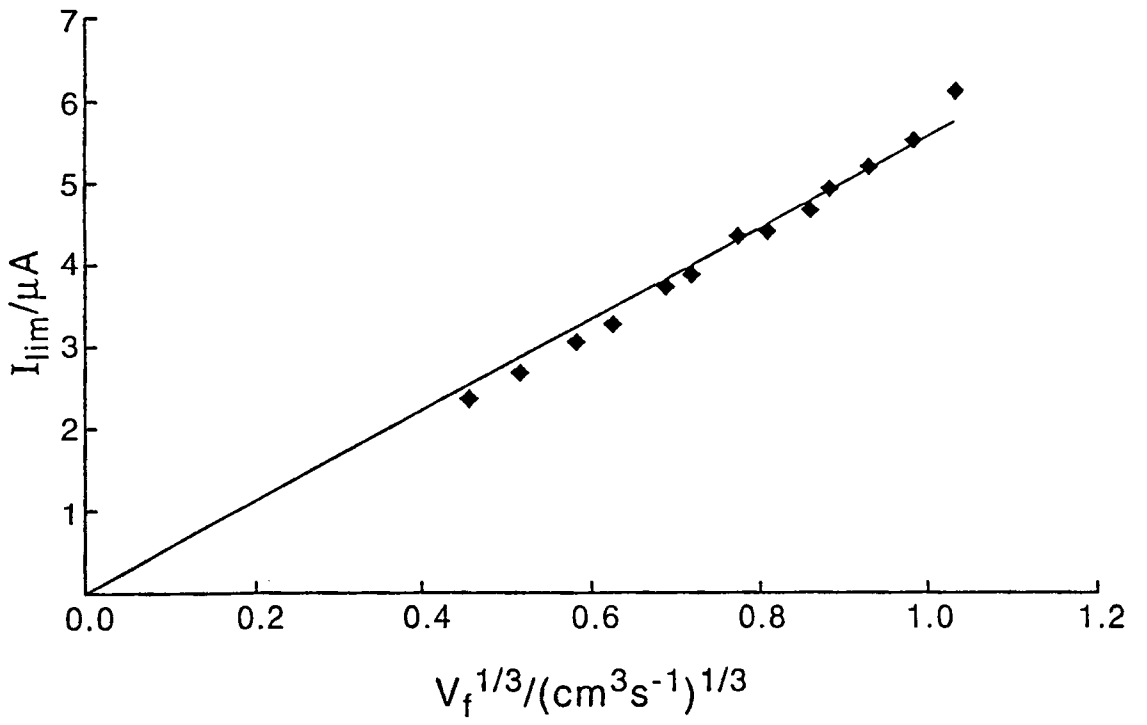

Figure 4.3. *The transport limiting current (I_{lim}) / flow rate (v_f) data obtained for the oxidation of ferrocene (0.5 mM) using a 40.6μm Pt channel electrode.*

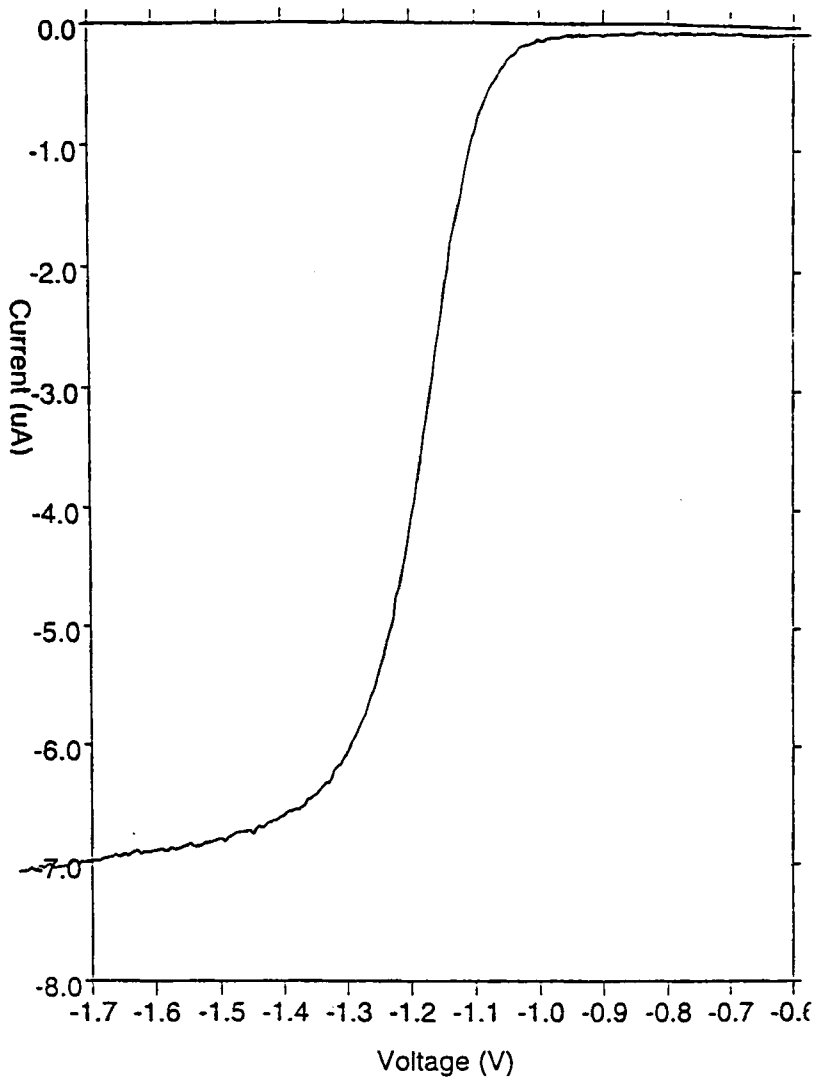

Figure 4.4. *The steady-state voltammogram for pCNB at a flow rate of 1.5044 $cm^3\ s^{-1}$.*

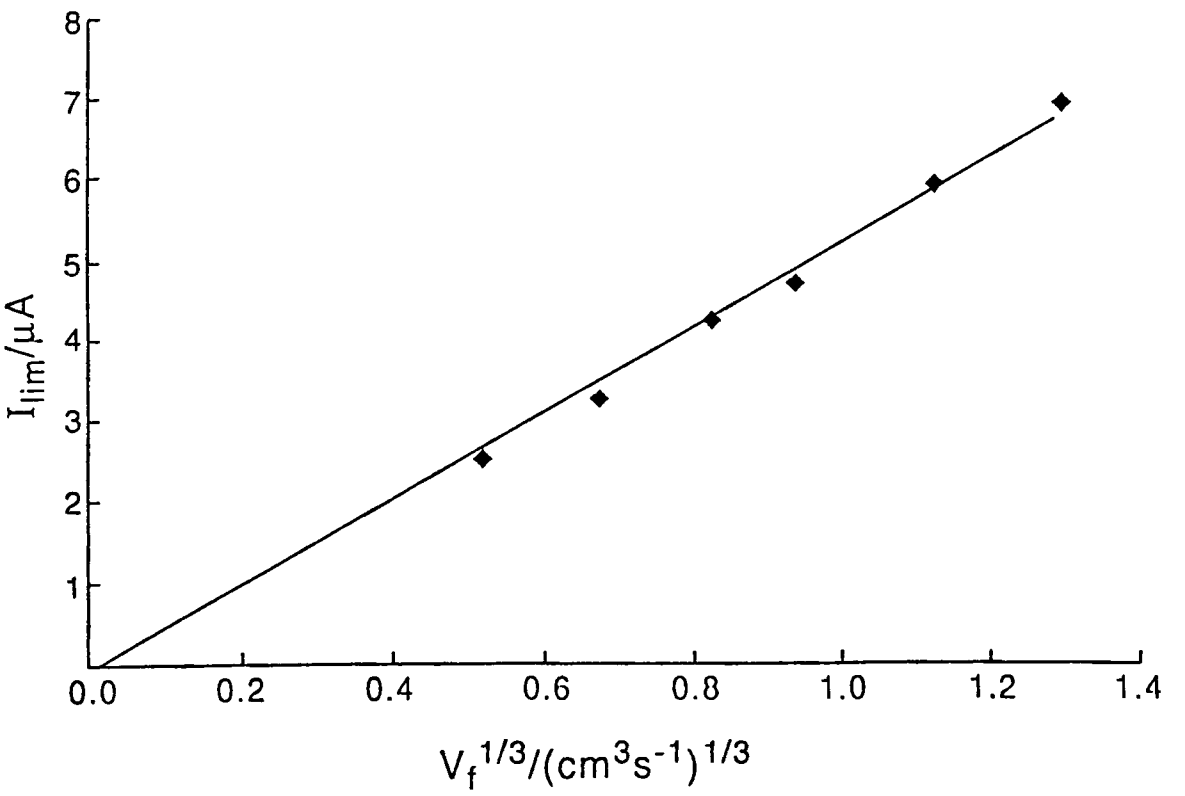

Figure 4.5. *(a)* *The transport limited current (I_{lim}) / flow rate (v_f) data obtained for the oxidation of TMPD (0.5 mM) in 0.1 M TBAP/ acetonitrile solution.*

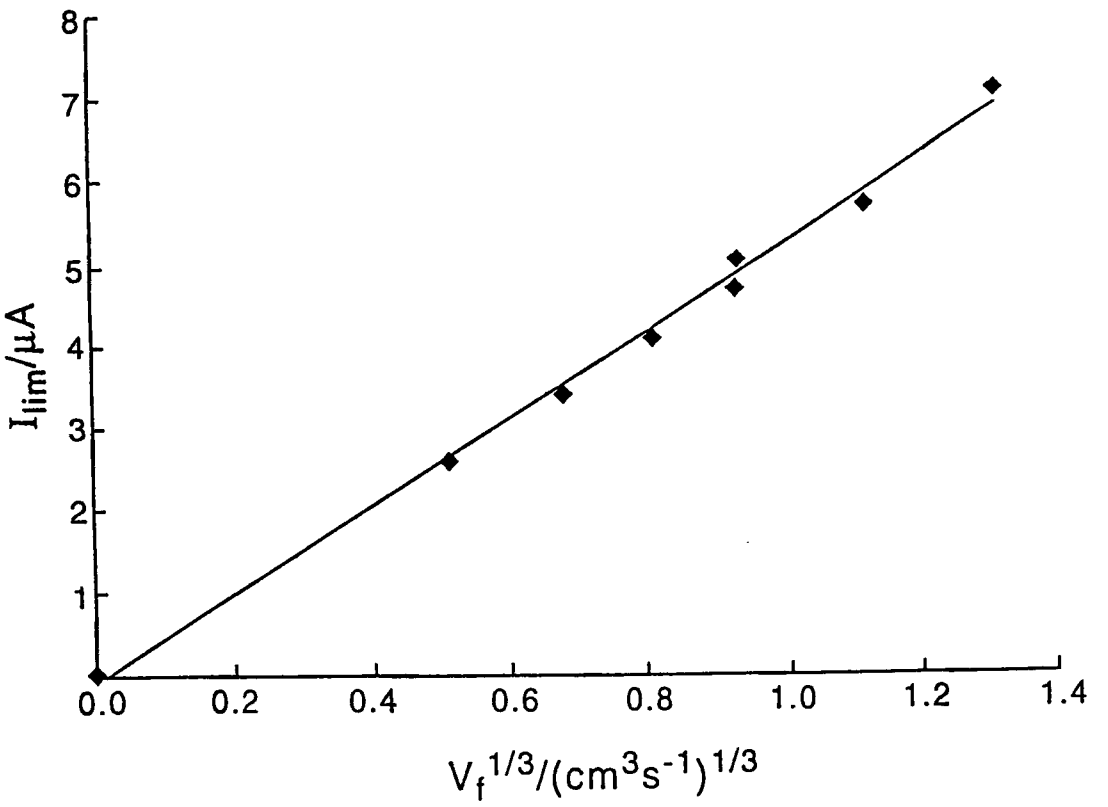

Figure 4.5. (b) The transport limited current (I_{lim}) / flow rate (v_f) data obtained for the reduction of pBNB (0.5 mM) in 0.1 M TBAP/ acetonitrile solution.

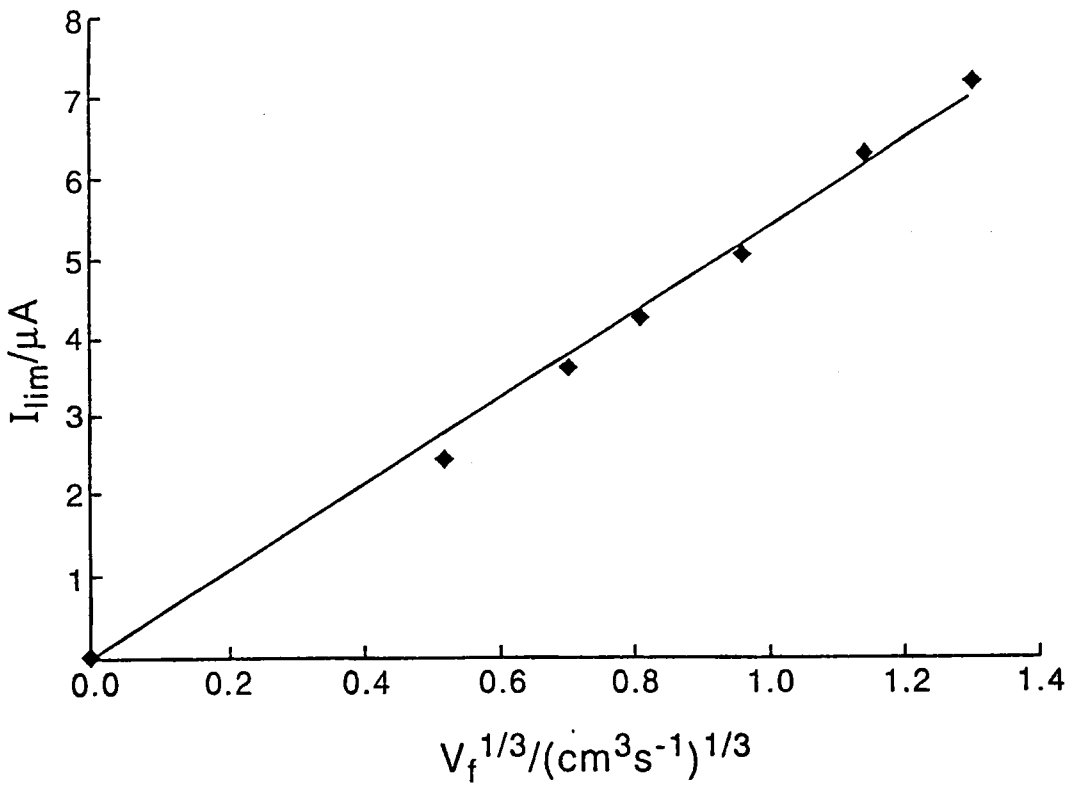

Figure 4.5. (c) The transport limited current (I_{lim}) / flow rate (v_f) data obtained for the reduction of pCNB (0.5mM) in 0.1 M TBAP/ acetonitrile solution.

It should be noted that as discussed in section 1.5.2, the basis of the Levich equation is that the dominant forms of mass transport are convection axially through the high speed cell and diffusion normal to the electrode surface. Axial diffusion is assumed to be negligible. The agreement between the experimental data shown in figures 4.5(a) - (c) and the Levich equation confirms the negligible axial diffusion effects when carrying out steady-state measurements using the high speed channel flow cell.

4.5 Potential Step Transient Measurements

Potential step experiments were carried out at a range of flow rates for each of the three species under investigation. The potential steps were made from an initial potential at which no current flowed, to a potential at which the mass transport limiting current was reached. The resulting transient current obtained was recorded as a function of time as discussed in section 2.3.2, which showed an extremely fast decay, figure 4.6. This rapid decay was observed to become faster as the electrolyte flow rate was increased as shown in figure 4.7.

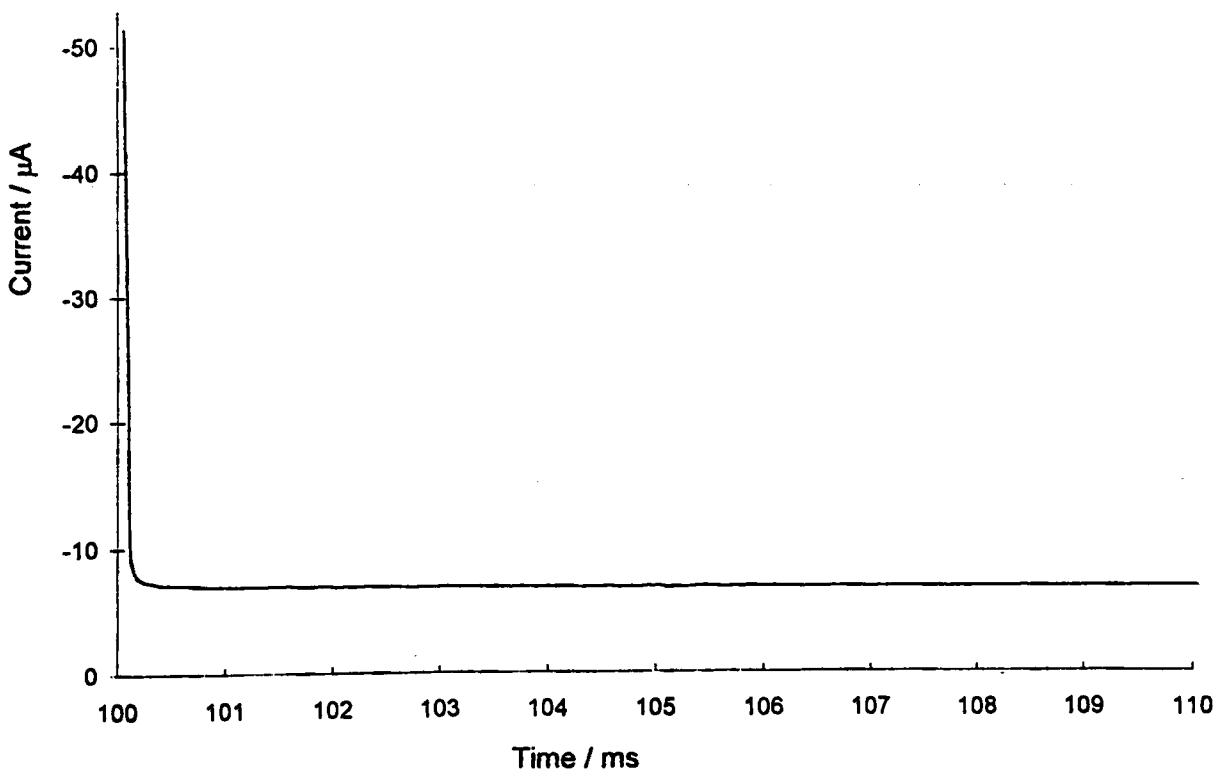

Figure 4.6. *The current-time transient recorded for pCNB at a flow rate of 1.5044 cm^3 s^{-1}*

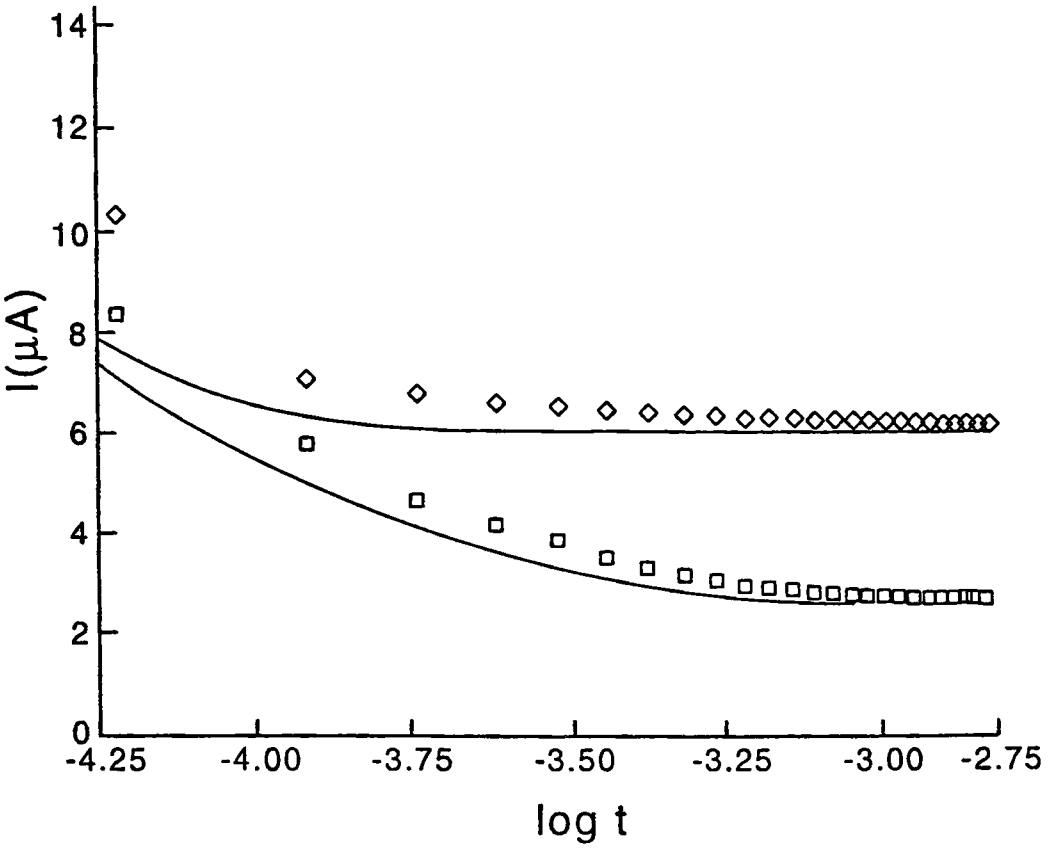

Figure 4.7. Current-time transients recorded using 0.5 mM TMPD in 0.1 M TBAP/ acetonitrile solution at a flow rate of 1.406 cm^3 s^{-1} (◇) and 0.5 mM pBNB in 0.1 M TBAP/ acetonitrile solution at a flow rate of 0.1418 cm^3 s^{-1} (□). The solid line represents the theoretically predicted transient as calculated using BI.

4.6 Numerical Simulation of the Potential Step Transients

The experimental current-time transients were modelled using the backward implicit (BI) method introduced in section 2.5.2. As shown in figure 4.7, good agreement between the simulated values and the experimental values was obtained in all of the conditions investigated. Again axial diffusion was not included in the simulation due to the constraints of BI discussed in section 2.5. The good agreement between the numerical and the experimental results suggests that axial diffusion effects can be neglected in transient experiments carried out using the high speed channel flow cell.

As mentioned in section 4.2, for experimental conditions using the high speed channel flow cell where the Lévêque[7] approximation holds, the normalised transient current with respect to the steady-state value predicted by the Levich equation, is a unique function of the dimensionless time parameter, τ, equation (4.5). This enables the experimental data obtained for such conditions to be analysed using the simple working curve given in figure 4.2. In figure 4.2 some of the experimental results obtained using the high speed channel flow cell, at different flow rates, are included. The experimental agreement found with the working curve generated by the BI method indicates once more the validity of the assumption of negligible diffusion effects in high speed channel flow cell experiments.

Using equation (4.4) the p values for the geometrical and flow parameters corresponding to the high speed channel flow cell were calculated. These were found to be lower than 1×10^{-3}. In the working surface given in reference 5 it can be seen that for such low values of p the transient response does not depend on the p value; it is a unique function of the dimensionless time parameter τ, as would be expected if axial diffusion effects are negligible.

An additional check to see if axial diffusion effects are significant when carrying out potential step transient measurements using the high speed channel flow cell was made through the comparison of the transient current simulated using the BI method, according to the procedure described in section 2.5.2, with those obtained using SIP following the numerical approximation of equation (4.1). The SIP simulations were carried out by Dr. John Alden. The least favourable case was chosen, to ensure a rigorous test, with one of the lower flow rates achieved using the high speed channel flow cell being used in the comparison. At the lower flow rates the relative effect of axial diffusion in the overall mass transport is higher.

The results for the geometric parameters of the high speed channel flow cell described previously are shown in figure 4.8.

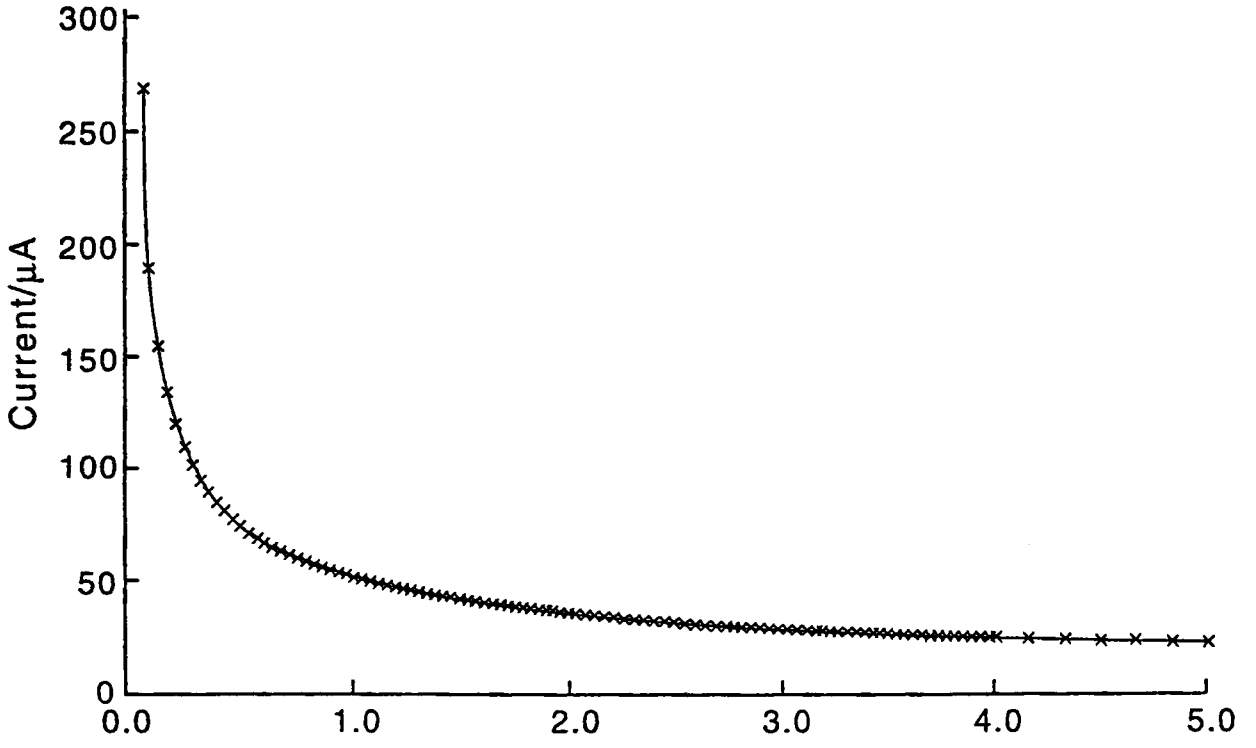

Figure 4.8. Current-time-transients simulated for a 40.6 μm electrode using BI which does not include axial diffusion effects (-) and SIP where axial diffusion effects were taken in to consideration (x).

The difference between the values predicted by both methods are negligible as was expected from the previous results obtained. This clearly demonstrates the validity of the assumption of no axial diffusion effect on the mass transport limited current for the transient experiments of the high speed channel flow cell.

4.7 Transient Measurements and the High Speed Channel Flow Cell

Summarising the work presented so far in this chapter it is possible to conclude that the BI method is an appropriate simulation method for the transient current data obtained

using the high speed channel flow cell. Axial diffusion effects were confirmed to be negligible when carrying out such potential step experiments enabling the BI method to be applied. The main advantages of using the BI method to analyse transient current data is the speed and stability of the method along with the ready incorporation of mechanistic changes. Therefore, a combination of high speed channel flow potential step measurements and BI modelling offers a powerful tool for investigating mechanistic problems that change the transient current response (CE, EC', ECE...). Such a technique promises to enable even higher rate constants to be measured. This is investigated further in the following section which considers the specific case of the $EC_{hom}E$ mechanism.

4.8 The Application of BI to the $EC_{hom}E$ mechanism

As mentioned in the previous section and section 2.5.2.1 it is possible to extend time-dependent (transient) BI theory to include homogeneous kinetics. The $EC_{hom}E$ mechanism is described by:

$$E \quad A \quad \pm \quad e^- \rightleftharpoons \quad B$$

$$C \qquad\qquad B \quad \rightarrow \quad C$$

$$E \quad C \quad \pm \quad e^- \rightleftharpoons \quad \text{products}$$

The mass transport equations for the species A, B and C are given below:

$$D_A \frac{\partial^2[A]}{\partial y^2} - v_x \frac{\partial[A]}{\partial x} = \frac{\partial[A]}{\partial t} \tag{4.6}$$

$$D_B \frac{\partial^2[B]}{\partial y^2} - v_x \frac{\partial[B]}{\partial x} - k[B] = \frac{\partial[B]}{\partial t} \tag{4.7}$$

$$D_C \frac{\partial^2[C]}{\partial y^2} - v_x \frac{\partial[C]}{\partial x} + k[B] = \frac{\partial[C]}{\partial t} \tag{4.8}$$

The time-dependent mass transport equations for species A, B and C take on the same form as those given in section 2.5.2 which describes the simple one-electron transfer reaction of a species A. However, in the case of species B there is an additional kinetic term -k[B] on the left hand side and for species C the additional term is +k[B]. The boundary conditions required to solve the finite difference form of the mass transport equations are shown below:

$t \leq 0$

$$0 < y < 2h, 0 < x < x_e; \; [A] = [A]_{bulk}, [B] = [C] = 0; \quad {}^{t}g^{A}_{j,k} = 1, {}^{t}g^{B}_{j,k} = {}^{t}g^{C}_{j,k} = 0 \qquad (4.9)$$

$t > 0$

$$x = 0; \qquad [A] = [A]_{bulk}, [B] = [C] = 0; \quad {}^{t}g^{A}_{j,k} = 1, {}^{t}g^{B}_{j,k} = {}^{t}g^{C}_{j,k} = 0 \qquad (4.10)$$

$$y = 0; \qquad [A] = [C] = 0, \frac{\partial [A]}{\partial y} = -\frac{\partial [B]}{\partial y}, {}^{t}g^{A}_{0,k} = {}^{t}g^{C}_{0,k} = 0 \qquad (4.11)$$

$$y = 2h; \qquad \frac{\partial [A]}{\partial y} = \frac{\partial [B]}{\partial y} = \frac{\partial [C]}{\partial y} = 0; \qquad {}^{t}g^{B}_{0,k} = {}^{t}g^{A}_{1,k} + {}^{t}g^{B}_{1,k}$$

$$(4.12)$$

$${}^{t}g^{A}_{J,k} = {}^{t}g^{A}_{J-1,k}$$

$${}^{t}g^{B}_{J,k} = {}^{t}g^{B}_{J-1,k}, {}^{t}g^{C}_{J,k} = {}^{t}g^{C}_{J-1,k}$$

The boundary condition at y = 0 affects the matrix elements for species B described in section 2.5.2. The values of b_1 and d_1 become $\lambda^y + \lambda^C_j + 1$ and ${}^{t}g^{B}_{1,k} + \lambda^C_j \left({}^{t+1}g^{B}_{1,k-1} \right) + \lambda^{y\,t+1} g^{A}_{1,k}$ respectively. All of the matrix elements for species A remain the same as those given in section 2.5.2 as species A is unaffected by the chemical kinetics. However, for species B and C the matrix elements are affected by the chemical kinetics producing the matrix elements shown on the following page.

For species B: $b_j = 2\lambda^y + \lambda^C_j + 1 + k$

For species C: $d_j = {}^t g^C_{1,k} + \lambda^C_j \left({}^{t+1} g^C_{1,k-1} \right) + k\, {}^{t+1} g^B_{j,k}$

Hence, knowing the relevant matrix elements given above and using the boundary conditions given in equations (4.9) - (4.12) the transient current for an ECE mechanism can be obtained using the method described in section 2.5.2.

4.9 The Determination of Fast Homogeneous Rate Constants via BI modelling of the High Speed Channel Flow Cell

The application of the BI method to homogeneous kinetics described in the previous section was used to demonstrate the use of the high speed channel flow cell in combination with the BI method in determining fast homogeneous rate constants. Figure 4.9, which was generated using the BI method shows the effective number of electrons corresponding to the transient response of a system following an ECE mechanism at a 40 μm band electrode versus time. The plot illustrates that provided the current-time transients can be experimentally recorded on the microsecond time scale, then homogeneous rate constants of ~ 1 x 10^6 s^{-1} are accessible. This is 1 order of magnitude higher than that corresponding to a steady-state experiment, 1 x 10^5. Further work is planned to reduce the length of the electrode used in the high speed channel flow cell to dimensions ~ 1 μm with the aim of reducing the timescale by a further order of magnitude.

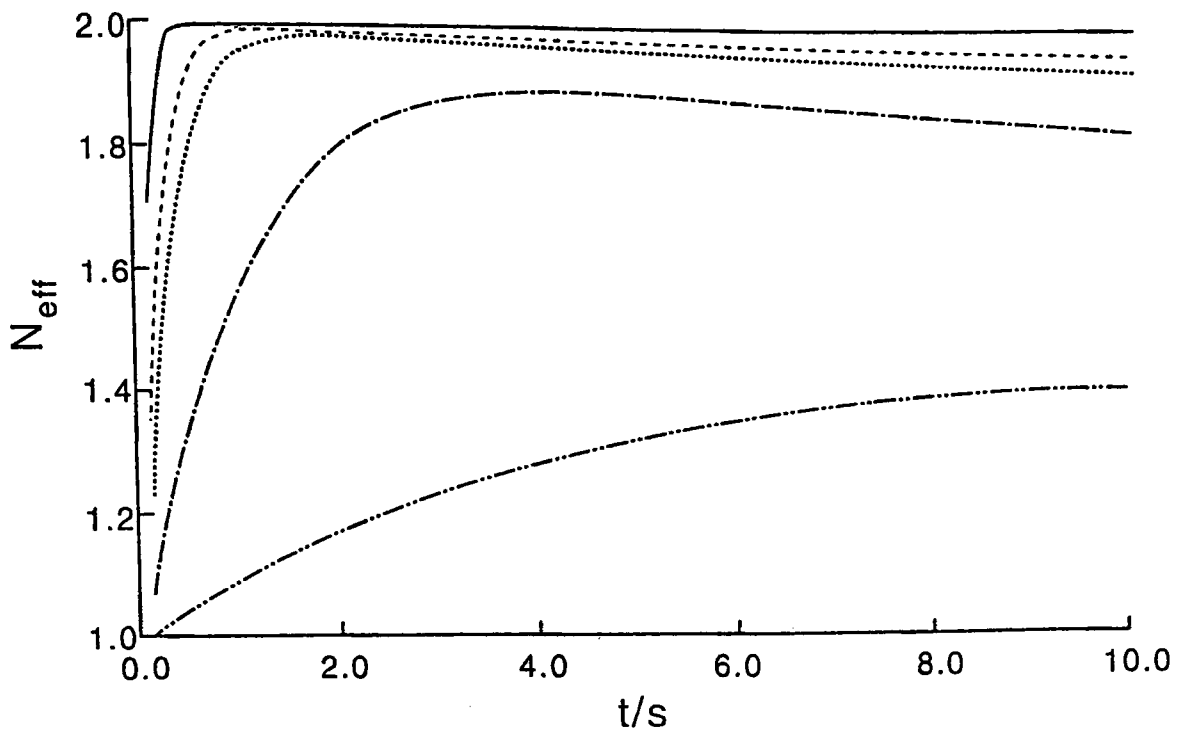

Figure 4.9. *Number of effective electrons vs. time corresponding to an ECE mechanism at a 40 μm electrode calculated using BI and the values for the homogeneous rate constant: 10^7 s^{-1} (—), 10^6 s^{-1} (– – –), 5 x 10^5 s^{-1} (•••), 10^5 s^{-1} (– • –), and 1 x 10^4 s^{-1} (–••–).*

5. The Reduction of Nitromethane in Basic Aqueous Solution

Contents

The work presented in this chapter has been published in J. Electroanal. Chem., 437, (1997), 183

5.1 Introduction

As discussed in the previous chapters electrochemical reactions often involve a complex sequence of electron transfers and coupled chemical kinetics that occur at the electrode surface (heterogenous kinetics) or in solution (homogeneous kinetics). The unambiguous description and interpretation of such complex reactions provides a challenging area of investigation for electrochemists. An extreme example of one such system is the electro-reduction of aliphatic nitro-compounds. This process has been studied extensively[1-5] as the resulting voltammetry has good potential for analytical determination enabling a considerable number of drugs to be analysed electrochemically after the preparation of their nitro-derivatives. Experiments carried out on the reduction of aliphatic nitro-compounds in aqueous solutions at a Hg electrode showed two waves. The first of which involves the uptake of four electrons and four protons along with the cleavage of a N-O bond, producing the corresponding hydroxylamine. The equation for the overall reaction is shown below:

$$RNO_2 \xrightarrow{4e^-,4H^+} RNHOH + H_2O \qquad (5.1)$$

The second wave appears only in basic or neutral solutions and involves further reduction of the hydroxylamine to the alkyl amine.

Clearly a large number of mechanistic possibilities present themselves in the study of aliphatic nitro-compounds due to the involvement of the four electrons, four protons, N-O bond breaking and the possibility of adsorption and desorption of intermediates at the electrode surface. Insight into the complex mechanism of a specific aliphatic nitro-compound, nitromethane, in aqueous solution was gained by Guidelli et al.[5]. They investigated the

---

1 F. Petru, *Collect. Czech. Chem. Commun.*, **12**, (1947), 62
2 M. Suzuki and P. J. Elving, *Collect. Czech. Chem. Commun.*, **25**, (1960), 3202
3 G. Battisuzzi, G. Grandi and R. Andreolli, *Collect. Czech. Chem. Commun.*, **36**, (1971), 730
4 S. Wawzonek and S. Tsung-Yuan, *J. Electroanal. Soc.*, **120**, (1973), 745

influence of the supporting electrolyte and the pH of the buffer on aqueous solutions of nitromethane at a Hg electrode. Their results were consistent with an ECE mechanism in which the radical anion $[CH_3NO_2]^{\bullet-}$, formed from an initial electron transfer step, diffuses away from the electrode surface and undergoes a protonation reaction to produce CH_3NO_2H. This compound is then immediately reduced to the hydroxylamine as shown in the scheme below:

$$CH_3NO_2 + e^- \rightleftharpoons CH_3NO_2^{\bullet-} \quad (5.2)$$

$$CH_3NO_2^{\bullet-} \xrightarrow{+H^+,k} CH_3NO_2H \quad (5.3)$$

$$CH_3NO_2H + ne^- \rightarrow \text{products} \quad (5.4)$$

More recently impedance voltammetry has been used by Prieto et al.[6-9] to unravel some of the key details of the mechanism for the reduction of nitromethane in aqueous solution at a Hg electrode. It was found that for basic solutions of nitromethane the electron transfer steps were Nernstian on the time scales studied and that the mechanism begins with an elementary one-electron transfer step as found by Guidelli, equation (5.2). However this was found to be followed by a fast heterogeneous chemical step, C1, as shown in the scheme on the following page. The radical formed from the initial chemical step is possibly $^{\bullet}CH_2N(O^-)OH$, which can undergo a further chemical step, C2 in the scheme, involving the breaking or an N-O bond and hence the loss of a hydroxide ion. The resulting product is then immediately reduced to the methylhydroxylamine involving the uptake of three protons and three electrons.

---

5 R. Guidelli and M. L. Foresti, *J. Electroanal. Chem.*, **88**, (1978), 65

6 M. Rueda, M. Sluyters-Rehbach and J. H. Sluyters, *J. Electroanal. Chem.*, **261**, (1989), 23

7 F. Prieto, M. Rueda, I. Navarro, M. Sluyters-Rehbach and J. H. Sluyters, *J. Electroanal. Chem.*, **327**, (1992), 1

8 F. Prieto, M. Rueda, I. Navarro, M. Sluyters-Rehbach and J. H. Sluyters, *J. Electroanal. Chem.*, **405**, (1996), 1

9 F. Prieto, I. Navarro and M. Rueda, *J. Phys. Chem.*, **100**, (1996), 16346

Investigations carried out on pure Hg electrodes showed that the second chemical step, C2, was relatively slow, enabling the inferred radical intermediate, $^{\bullet}CH_2N(O^-)OH$, to have time to diffuse from the electrode surface, resulting in the partial prevention of the second reaction. However, although the impedance measurements carried out by Prieto et al. provided an insight into the chemical kinetics involved in the reduction of nitromethane and strongly suggested the involvement of the second chemical reaction, no unambiguous distinction could be made between its heterogeneous or homogeneous character[10]. Considering the work of Guidelli[5] discussed earlier it was assumed that the chemical step was heterogeneous but clearly independent data from other techniques is required to enable clarification.

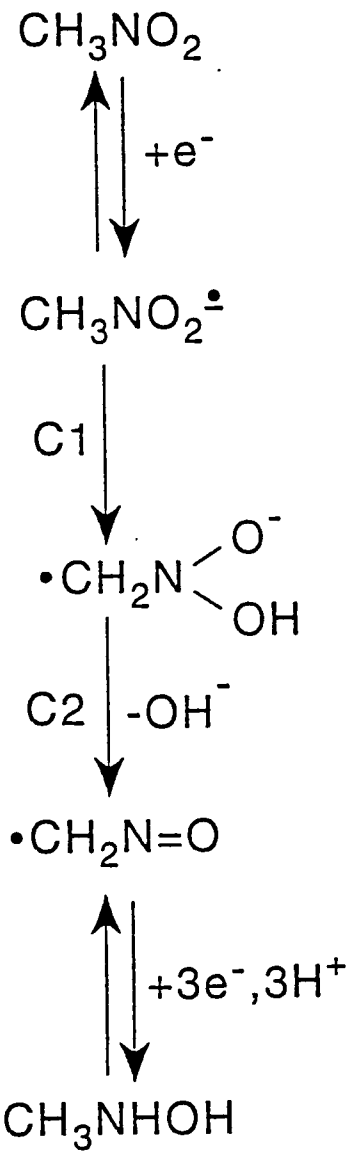

Figure 5.1. *The reduction decomposition mechanism of nitromethane.*

10 M. Rueda, Eds. R. G. Compton and G. Hancock, *Research in Chemical Kinetics,* **4**, (1997)

The difficulties involved in the resolution between homogeneous and heterogeneous chemical steps coupled to electrochemistry has been discussed by Laviron[11]. Laviron emphasised the advantage of using spectroelectrochemical methods, such as those discussed in chapter 1, when such a distinction is required.

The following chapter uses channel flow cell voltammetry and *in-situ* electrochemical ESR to investigate further the coupled kinetics involved in the reduction of nitromethane with the aim of independently assessing whether or not the chemical steps, C1 or C2 are involved in the mechanism and if they are surface catalysed processes.

5.2 Overview of Chapter

The work presented in the following chapter illustrates how a combination of computer simulations and electrochemical techniques including spectrochemical methodology can be successfully employed to probe complex electrochemical processes.

Initially the voltammetric theory for heterogeneous ECE (and ECEEE) processes at channel electrodes is developed. This enables a comparison to be made with the existing theory for the analogous homogeneous process which is well established[12]. The heterogeneous ECEEE theory is then applied to the reduction of nitromethane in aqueous solution at pH 8.3 carried out at a Hg plated Au electrode. Finally *in-situ* electrochemical ESR measurements are made to investigate the possibility of detecting the radical generated from the first electron transfer step to gain an insight into the involvement/ or not of a heterogeneous chemical step.

---

11 E. Laviron, *J. Electroanal. Chem.*, **391**, (1995), 187

12 W. M. Leslie, J. A. Alden, R. G. Compton and T. Silk, *J. Phys. Chem.*, **100**, (1996), 14130

5.3 General Experimental Details

All of the channel flow experiments reported were carried out using the Hg amalgamated Au channel electrode described in section 3.2. Solution flow rates between 10^{-4} and 10^{-1} cm^3 s^{-1} were employed. The *in-situ* electrochemical ESR measurements were made[13] using the system described in section 3.3. 5.5 mM solutions of nitromethane (puriss, absolute, Fluka) were prepared immediately prior to experimentation as described in section 3.9 and were buffered at pH 8.3 using 0.2 M H_3BO_3 and 0.04 M KOH. The supporting electrolyte was KCl. In the numerical simulations 1000 grid points were typically used over the electrode length and 500 over the fraction of the total channel depth which corresponds to no less than the maximum size of the diffusion layer thickness. These numbers of grid points were chosen to ensure that the programs were fully converged, so that the results of repeated simulations were consistent. The programs used in this chapter were written in collaboration with Dr. John Alden.

5.4 Theory

In this section the voltammetric theory for $EC_{het}E$ processes at channel electrodes in which the C step occurs at the electrode surface is developed. It should be noted that this theory is readily extendable to the case involving the transfer of more than one electron following the chemical step, as in the case of the reduction of nitromethane which will be shown subsequently to involve an ECEEE mechanism. The reaction scheme for a reductive $EC_{het}E$ mechanism is shown on the following page:

---

13 Experiments were carried out in collaboration with Dr. R. Webster

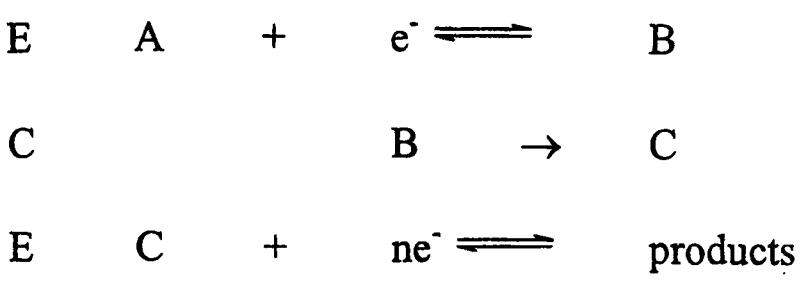

E A + e^- ⇌ B

C B → C

E C + ne^- ⇌ products

where n = 1 for and ECE mechanism and n = 3 for an ECEEE mechanism. The steady-state convective diffusion equations for species A and B are:

$$\frac{\partial[A]}{\partial t} = 0 = D_A \frac{\partial^2[A]}{\partial x^2} + D_A \frac{\partial^2[A]}{\partial y^2} - v_x \frac{\partial[A]}{\partial x} \qquad (5.5)$$

$$\frac{\partial[B]}{\partial t} = 0 = D_B \frac{\partial^2[B]}{\partial x^2} + D_B \frac{\partial^2[B]}{\partial y^2} - v_x \frac{\partial[B]}{\partial x} \qquad (5.6)$$

where D_A and D_B are the diffusion coefficients of species A and B respectively, v_x is the solution velocity in the x-direction and the co-ordinates x and y are defined in figure 1.1.

As discussed in chapter 1, channel electrodes are designed to ensure that a laminar flow is produced and that a sufficiently long lead in length exists upstream of the electrode to enable the development of Poiseuille flow. Therefore:

$$v_x = v_0 \left(1 - \frac{(h-y)^2}{h^2} \right) \qquad (5.7)$$

where h is the half height of the cell as shown in figure 1.1 and v_0 is the solution velocity at the centre of the channel. Equations (5.5) and (5.6) can be simplified by assuming that axial diffusion effects are negligible. This approximation is valid provided that the electrodes considered are not of microelectrode dimensions as discussed in section 1.5.2.2.

The boundary conditions for the transport limited electrolysis of A are given below:

all y, $x < 0$, $[A] = [A]_{bulk}$, $[B] = 0$ (5.8)

$y = 0$, $0 < x < x_e$, $[A] / [B] = \exp(\theta)$

$$D_A \frac{\partial[A]}{\partial y} = -D_B \frac{\partial[B]}{\partial y} + k_{het}[B] \quad (5.9)$$

$$y = 2h, \text{ all } x, \; D_A \frac{\partial[A]}{\partial y} = D_B \frac{\partial[B]}{\partial y} = 0 \quad (5.10)$$

where k_{het} is the heterogeneous rate constant for the chemical kinetics transforming B into C and the [A] / [B] redox couple is assumed to be electrochemically reversible so that $\theta = (F / RT)(E - E^0_{A/B})$ as described in section 2.2. A further assumption is that the electrode potential is such as to reduce species C in the final n-electron transfer step.

5.4.1 Numerical Simulation of the $EC_{het}E$ Mechanism

It is possible to solve the mass transport equations (5.5) and (5.6) for the boundary conditions above using the Backward Implicit method (BI) described in section 2.5. However the boundary condition (5.9) shows that the loss of species B at the electrode surface occurs by a combination of diffusion away from the electrode and chemical reaction at the electrode surface. The incoming flux of A is therefore equal to the sum of the two effects as shown in the equation. This condition implies that the concentration of species A at the electrode is dependent on the concentration of B above the surface and vice-versa. Therefore when calculating the transport limited current the concentration profiles of both A and B are required simultaneously. In order to overcome this problem the numerical solution is obtained

using a 'back-to-back' grid[14] as shown in figure 5.2 in place of the 2-D finite difference grid described previously. KE is the number of nodes along the electrode.

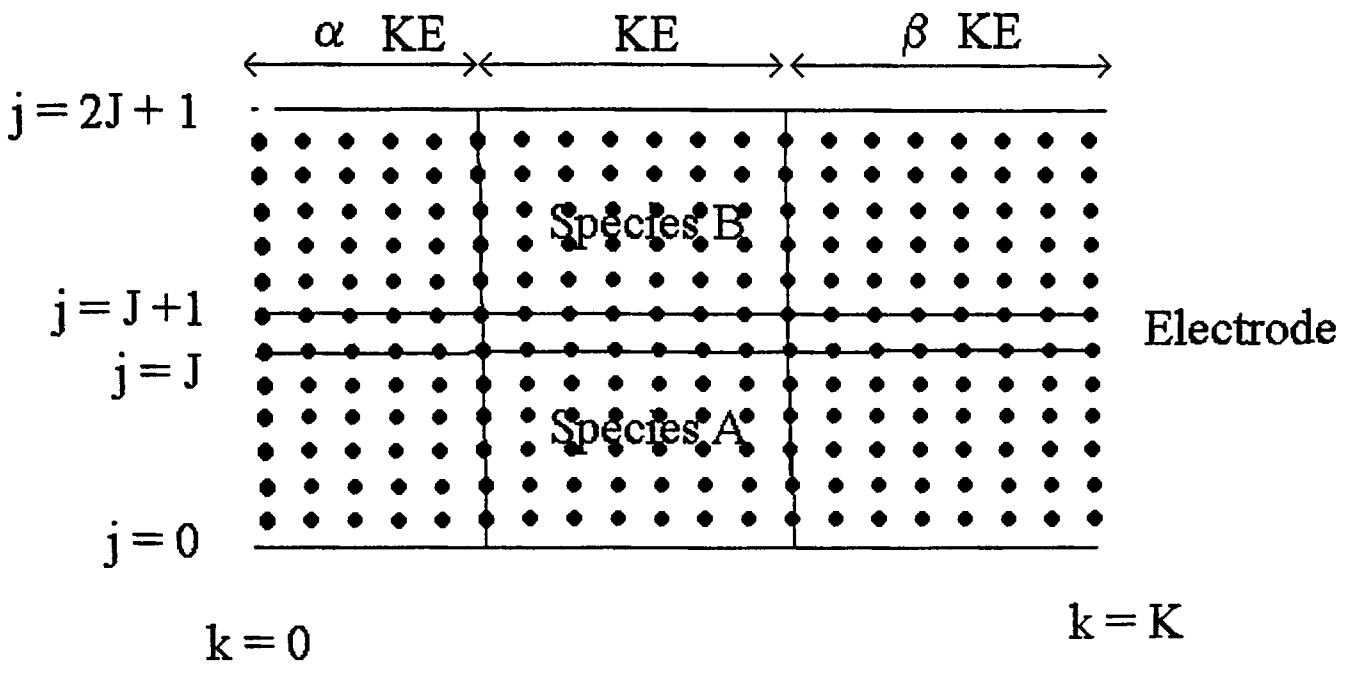

Figure 5.2. The back-to-back finite difference grid.

The back-to-back grid has the following differences from the 2-D grid:

(1) The grid runs form j = 1 to j = J.

(2) Species A is 'upside down' in the region j = 1 to j = J, and species B is in the top half of the grid from j = J + 1 to j = 2J.

(3) The points representing the channel wall, which are not actually simulated, are found at j = 0 for species A and j = 2J + 1, for species B. These boundaries are where the no flux boundary condition (5.10) applies.

(4) The points just above the electrode surface, j = 1 on a 2-D grid, are at j = J for species A and j = J + 1 for species B. Note that the electrode surface itself is not simulated.

Using the 'back-to-back' finite difference grid and the boundary conditions listed on the

---

14 R. A. W. Dryfe, *D. Phil. Thesis*, Oxford University, (1995), 82

previous page, the matrix elements for the $EC_{het}E$ mechanism can be generated using the method described in section 2.5.1.1. The Thomas Algorithm[14] (appendix 1) is then employed to solve the resulting matrix to enable the generation of the concentration profiles for species A and B. Having obtained the concentration profiles for species A and B the current produced at the electrode is calculated using the equation given below:

$$I = Fw\int_0^{x_e}\left(D_A\frac{\partial[A]}{\partial y} + nk_{het}[B]\right)_{y=0}\partial x \qquad (5.11)$$

5.4.2 Working Curves

Section 2.4 discussed the merits of using working curves for mechanistic investigations. Such curves enable the response at a channel electrode of any geometry and flow rate, providing that the Lévêque approximation is applicable, to be described using the normalised parameter K_{norm} for the particular mechanism considered. Using an analogous analysis to that described in section 2.4.1 for and $EC_{hom}E$ mechanism, the dimensionless kinetic parameter for an $EC_{het}E$ (or an $EC_{het}EEE$) mechanism can be written as:

$$K_{het} = k_{het}\left(2h^2x_e d / 3v_f D^2\right)^{1/3} \qquad (5.12)$$

Using the K_{het} parameter given above and the numerical theory described in the previous section working curves corresponding to an $EC_{het}E$ and $EC_{het}EEE$ mechanism were generated as shown in figures 5.3 and 5.4. The well established analogous working curves for the $EC_{hom}E$ and $EC_{hom}EEE$ mechanism[15] were included on the plots to enable a comparison between the two mechanisms to be made.

---

14 L. Lapidus and G. F. Pinder, *Numerical Analysis of Partial Differential Equations in Engineering and Science*, Wiley, New York, (1982)

15 R. G. Compton, M. B. G. Pilkington and G. M. Stearn, *J. Chem. Soc., Faraday Trans.* I, **84**, (1988), 2155

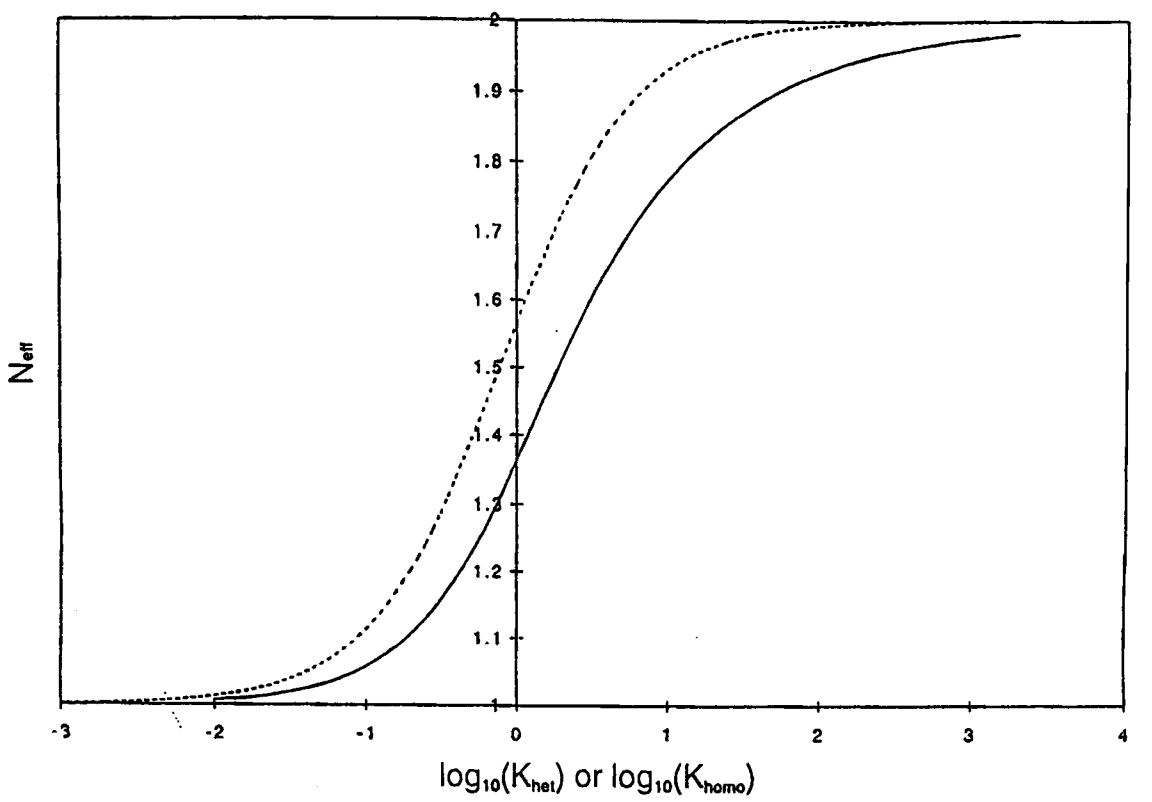

Figure 5.3. Dimensionless working curves describing the N_{eff} behaviour of an $EC_{het}E$ (.....) process and an $EC_{hom}E$ process (—) at a channel electrode.

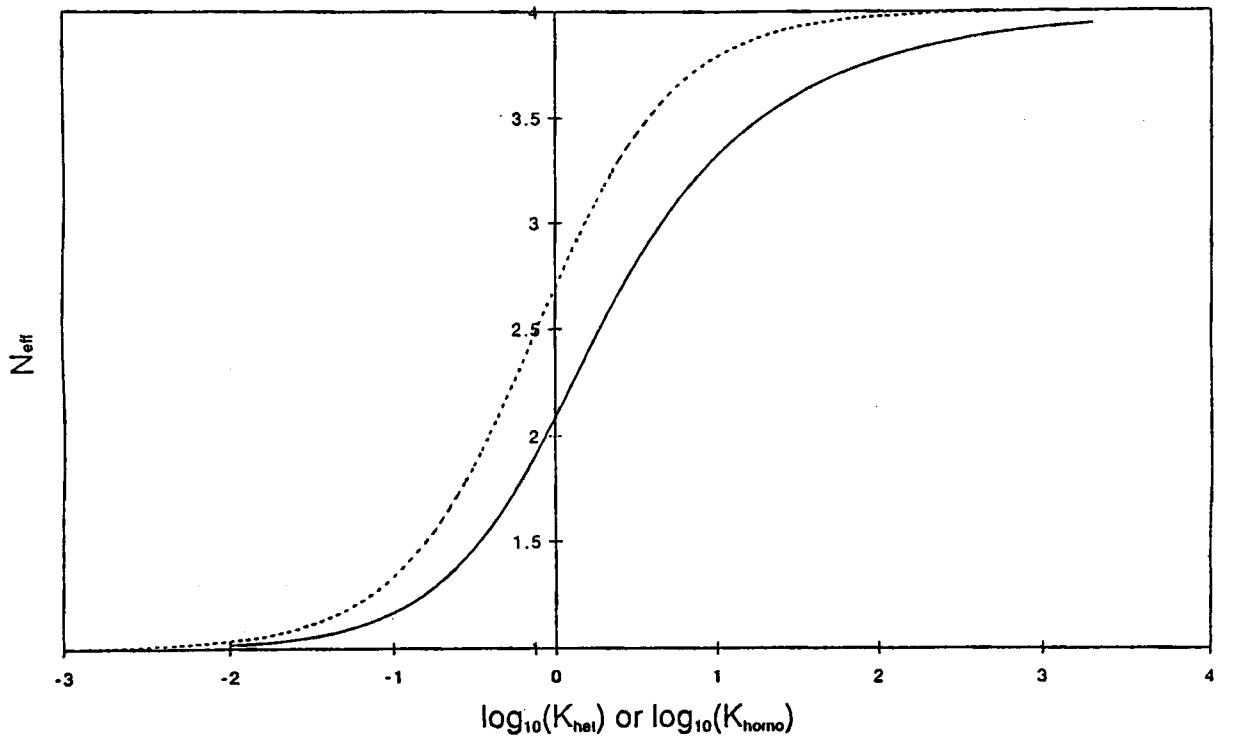

Figure 5.4. Dimensionless working curves describing the N_{eff} behaviour of an $EC_{het}EEE$ (.....) process and an $EC_{hom}EEE$ process (—) at a channel electrode.

Looking at the two figures 5.3 and 5.4, it is clear that a distinction between homogeneous and heterogeneous mechanisms may be possible using experimental limiting current measurements recorded over a sufficiently wide range of flow rates.

5.5 Channel Electrode Voltammetry

Steady-state voltammograms were recorded using the channel electrode for the reduction of 5.5 mM nitromethane in aqueous solution. The voltammograms obtained had a half-wave potential of -0.978 V at the faster flow rates employed. Less negative values were recorded at the slower flow rates as shown in figure 5.5. This dependence of the half-wave potential on the solution flow rate suggests the presence of coupled following kinetics. At the higher flow rates the product formed from the initial reduction of nitromethane, $[CH_3NO_2]^{\bullet-}$ is swept away from the electrode surface before the following chemical kinetics are able to take place. However, at the slower flow rates the reduction product $[CH_3NO_2]^{\bullet-}$ has time to undergo a chemical transformation resulting in a decrease in the concentration of $[CH_3NO_2]^{\bullet-}$. This decrease in concentration is balanced electrochemically by the positive shift in the potential of the nitromethane reduction.

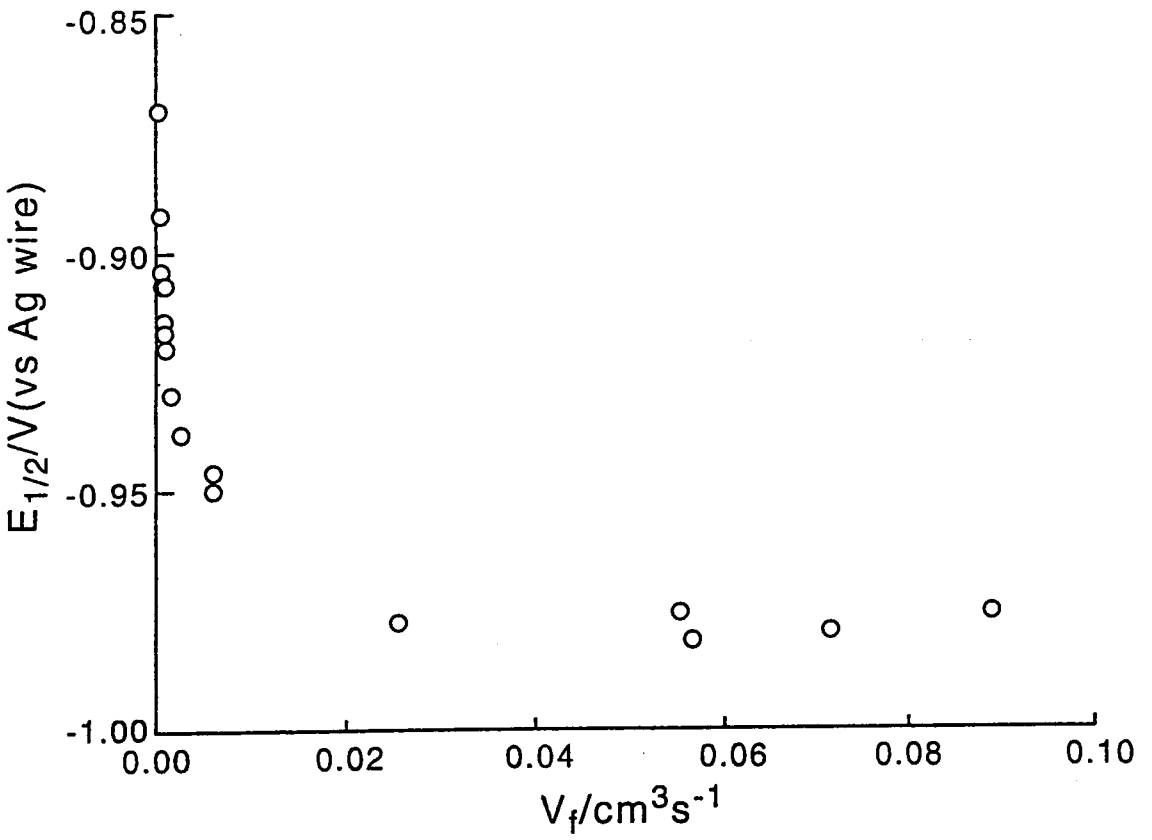

Figure 5.5. *The variation of the half-wave potential for the reduction of nitromethane (5.5 mM) in aqueous solution with the solution flow rate.*

The transport limiting current for the reduction of nitromethane was also measured over a range of flow rates as shown in figure 5.6. The plot revealed that at slower flow rates the data was consistent with the Levich equation, (1.12), where the number of electrons involved in the reduction was four and the diffusion coefficient for nitromethane[6] was 2 x 10^{-5} cm^2 s^{-1}. The diffusion coefficient of nitromethane was confirmed through rotating disk experiments carried out with a Au/Hg electrode in a boric acid buffer (pH 8.3). However it can be seen in figure 5.6 that at the higher flow rates there is a deviation from Levich behaviour as the number of electrons transferred drops increasingly below four as the flow rate increases. These results are qualitatively consistent with the plot expected for an ECEEE process.

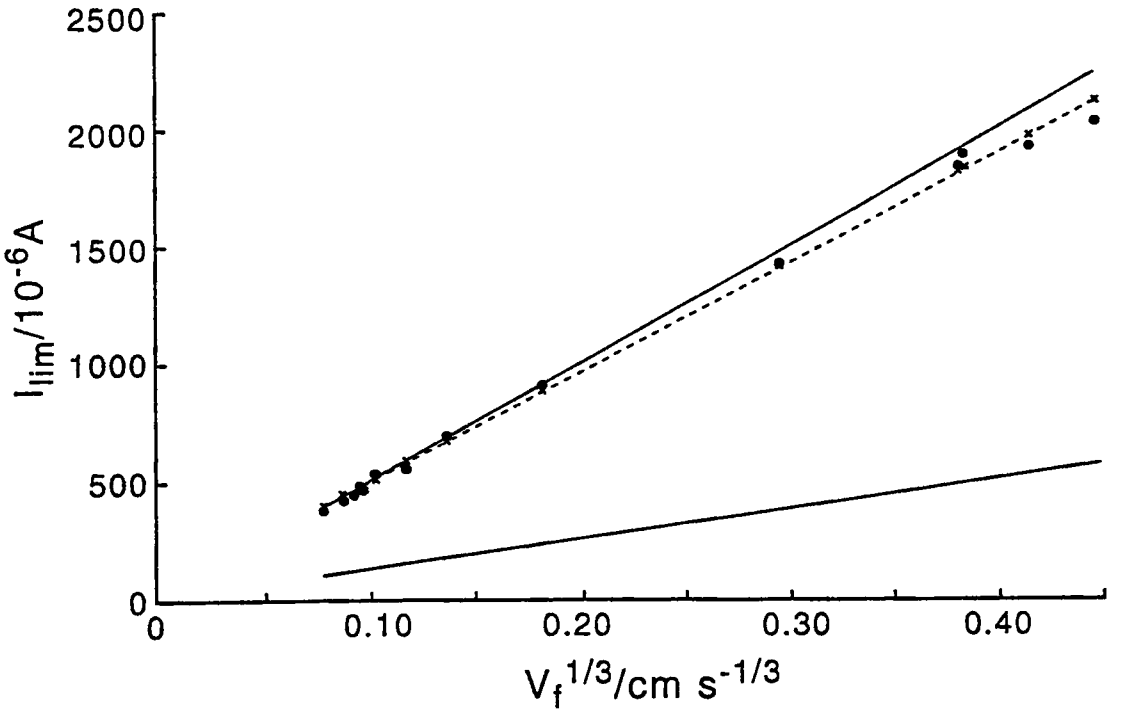

Figure 5.6. *The variation of the transport limiting current with solution flow rate (•) for the reduction of nitromethane (5.5 mM) in aqueous solution. The simulated currents (x) for an ECEEE process with k_{het} = 0.06 cm s^{-1} are also included. The two solid lines are those calculated for a pure one- and four-electron process.*

Although channel flow voltammetry was able to confirm the existence of coupled kinetics in the four-electron reduction of nitromethane alternative methods were required in order to probe the nature of the kinetics further. This is discussed in the following section in which *in-situ* electrochemical ESR experiments were applied to the nitromethane investigations.

5.6 *In-Situ* Electrochemical ESR Measurements

In-situ electrochemical ESR measurements were carried out using the experimental set-up described in section 3.3. An initial ESR spectrum was recorded at a potential held in the limiting current region of a 5.5 mM solution of nitromethane, using the Au/Hg channel electrode positioned close to the centre of the ESR cavity. Figure 5.7 shows the spectrum obtained which comprises of a triplet of 1:3:3:1 quartets consistent with the $[CH_3NO_2]^{\bullet-}$ radical anion[16] thought to be produced from the initial one-electron reduction step illustrated in figure 5.1. Analysis of the spectrum indicated the hyperfine splitting constants given in equation (5.13).

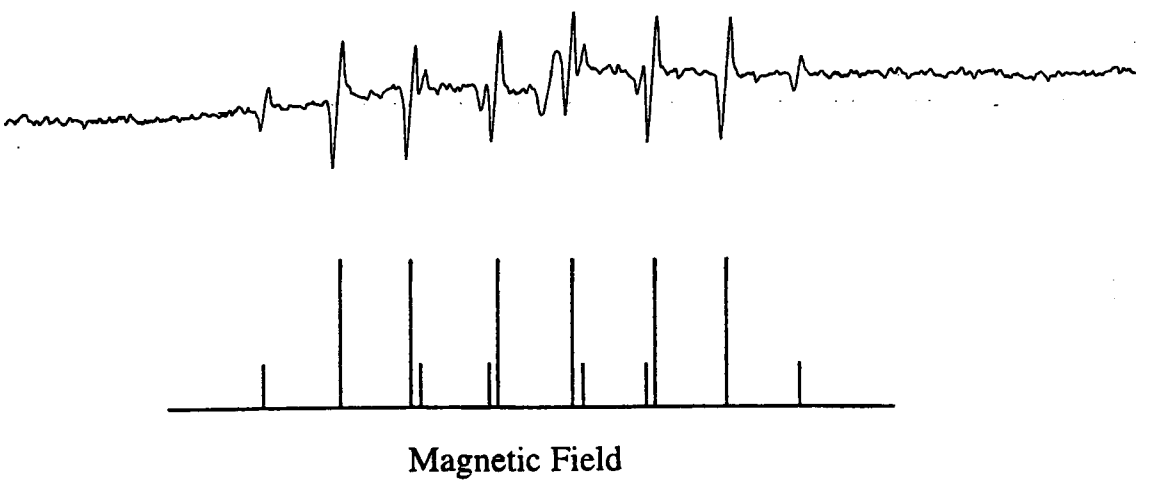

Figure 5.7. *The ESR spectrum for $[CH_3NO_2]^{\bullet-}$ obtained from the electrolyses of nitromethane at a Au/Hg channel electrode with the potential held in the limiting current region. Shown below is the spectrum predicted using the hyperfine splitting constants given in equation (5.13).*

$a_N = 26.3 \pm 0.1$ G $\qquad$ $a_H = 12.2 \pm 0.1$ G (5.13)

These constants are very close to those reported for other similar aliphatic nitro-radical anions in aqueous media[17]. For example nitroethane was reported to have the following hyperfine splitting constants.

$a_N = 25.5 \pm 0.1$ G $\qquad$ $a_H = 9.75 \pm 0.1$ G (5.14)

No further ESR signals were observed.

5.6.1 Investigation of Radical Stability Using *In-Situ* Electrochemical ESR

As discussed in section 1.5.3.4, it is possible to use channel flow cells with *in-situ* electrochemical ESR to deduce whether or not a radical is stable. For the case of a radical which is stable on the channel electrode timescale the variation of the ESR signal intensity (S) with both the solution flow rate (v_f) and the electrode current (I) is characterised by the expression given below:

$$S \propto \frac{I}{v_f^{2/3}} \qquad (5.15)$$

This relationship was applied to the nitromethane investigations with the aim of gaining further insight into the stability of the $[CH_3NO_2]^{\bullet -}$ radical and hence the mechanism involved in the reduction of nitromethane. *In-situ* electrochemical ESR spectra were recorded at a wide range of channel flow rates enabling the signal intensity and electrode currents to be recorded. A log-log plot of (S/I) against flow rate (v_f) was then generated as shown in figure 5.8.

---

16 J. B. Carroll, *PhD Thesis*, State Univ. of New York at Buffalo, (1983)

17 L. H. Piette, P. Ludwig and R. N. Adams, *J. Am. Chem. Soc.*, **94**, (1962), 4212

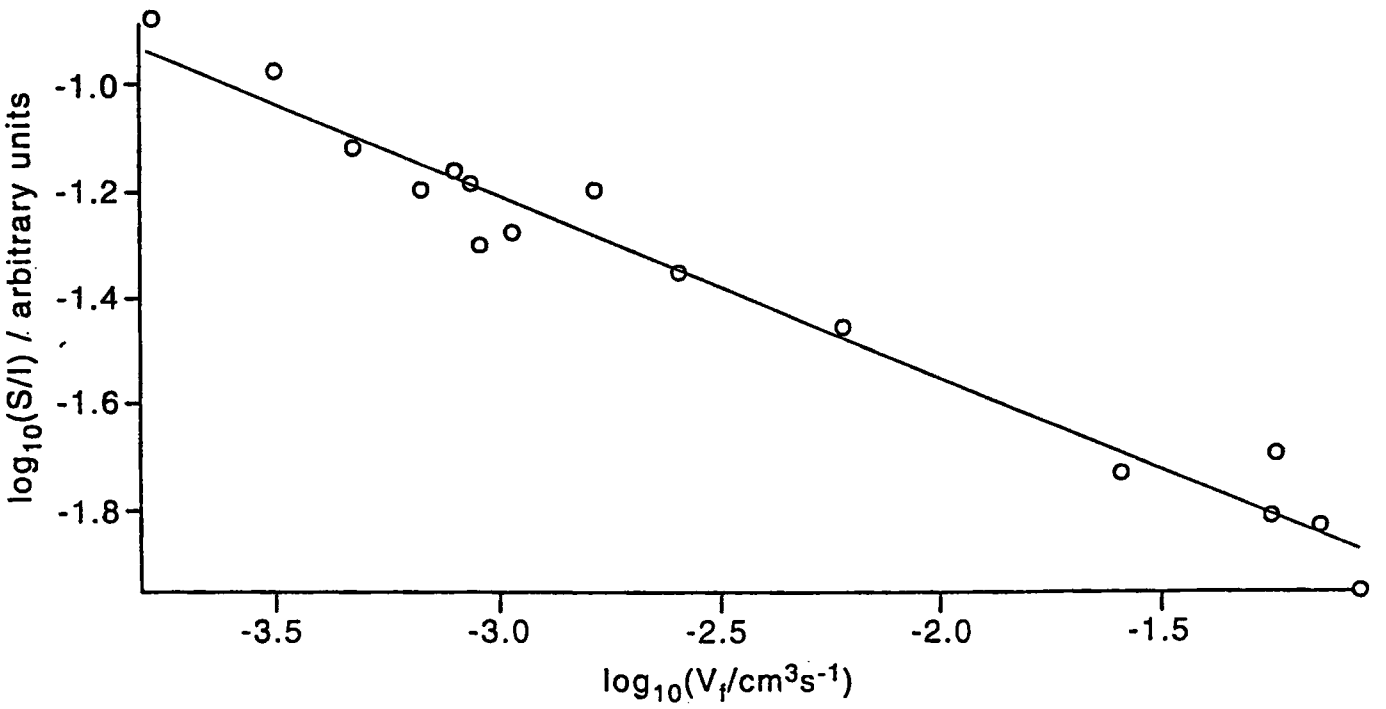

Figure 5.8. *A plot of log(S/I) against log(v_f) obtained from the electrolysis of a 5.5 mM solution of nitromethane at a Au/Hg channel electrode located close to the centre of the ESR cavity.*

Looking at figure 5.8 it is evident that the slope of the plot is not the (-2/3) value expected if the $[CH_3NO_2]^{\bullet-}$ radical was stable. Hence at this stage it was assumed that the $[CH_3NO_2]^{\bullet-}$ radical was unstable but further confamation was required. It was possible to confirm the instability of the $[CH_3NO_2]^{\bullet-}$ radical using a different relationship in which the signal intensity (S) was plotted against the solution flow rate (v_f) for electrode potentials corresponding to the transport limited current of nitromethane, figure 5.9. Looking at figure 5.9 it can be seen that the signal intensity is clearly insensitive to the solution flow rate unlike the steady decrease in signal intensity expected for a stable radical[18].

18 R. G. Compton and R. A. W. Dryfe, *Prog. Reaction Kinetics*, **20**, (1995), 245

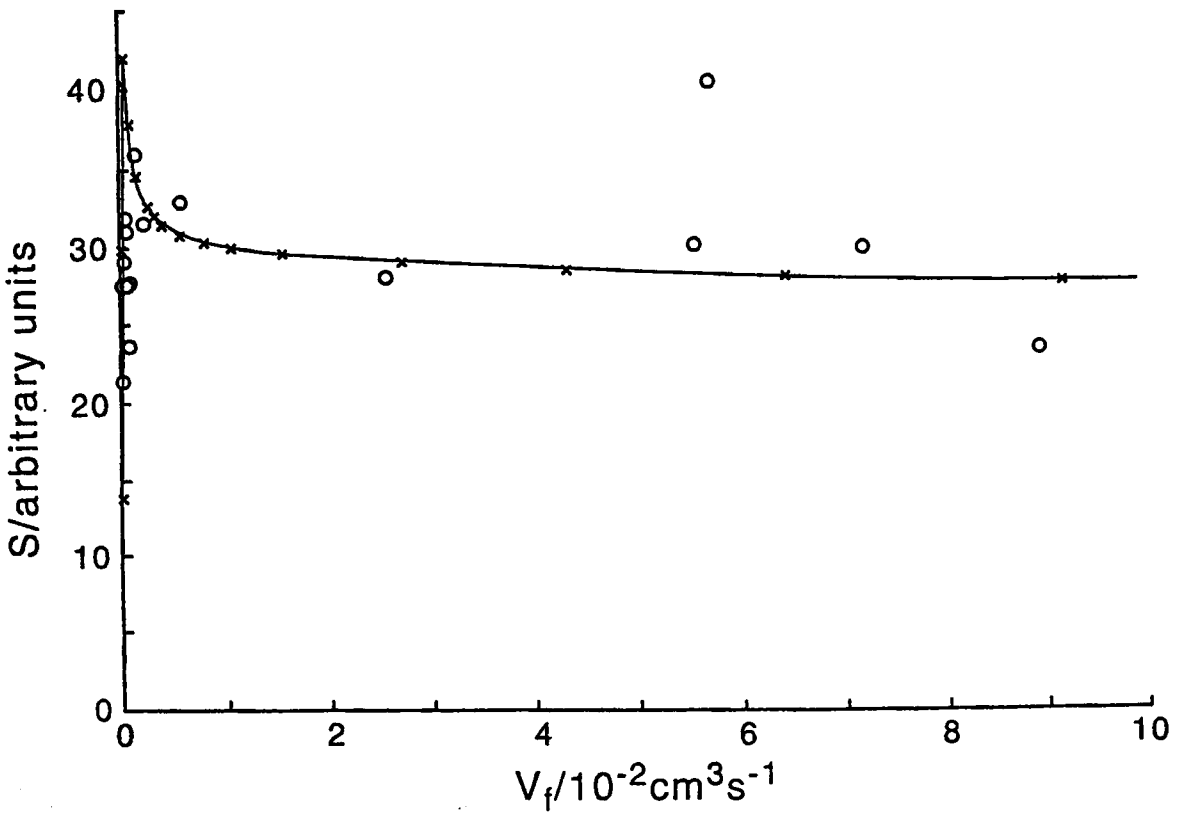

Figure 5.9. *A plot of ESR signal intensity (S) against flow rate (v_f) for the reduction of nitromethane (O). The values simulated for an ECEEE process with k_{het} = 0.06 cms $^{-1}$corresponding to the experimental conditions (—).*

It was possible to generate the signal expected for a stable radical by adapting the numerical theory described in section 5.4.1 so that there was no reaction at the electrode surface. The ESR signal due to a stable radical species was then found by integrating the concentration profile of the radical (as obtained from the BI numerical simulation), over the cavity dimensions as shown below[19]. (It should be noted that as the radical was assumed to be stable no kinetics were included in the simulation):

$$S = S_0 w \int_0^{x_d} \cos^2\left\{\left(x - 0.5x_e\right)/\left(x_d - 0.5x_e\right)\pi/2\right\} \int_0^{2h} \left[CH_sNO_2\right]^{\bullet -} dydx \qquad (5.16)$$

where x_d is the end of the cavity, S_0 is the signal due to one mole of radicals at the centre of the cavity and the $\cos^2$ represents the sensitivity profile of the TE_{102} ESR cavity, which

---

19 C. W. Lee, J. C. Eklund, R. A. W. Dryfe and R. G. Compton, *Bull. Korean Chem. Soc.*, **17**, (1996), 162

reaches a maximum at the cavity centre. The simulation produced for conditions corresponding to the channel flow cell employed experimentally, using a program written by Dr. John Alden, is shown in figure 5.10. A comparison of figures 5.9 and 5.10 clearly confirms the instability of the $[CH_3NO_2]^{\bullet-}$ radical.

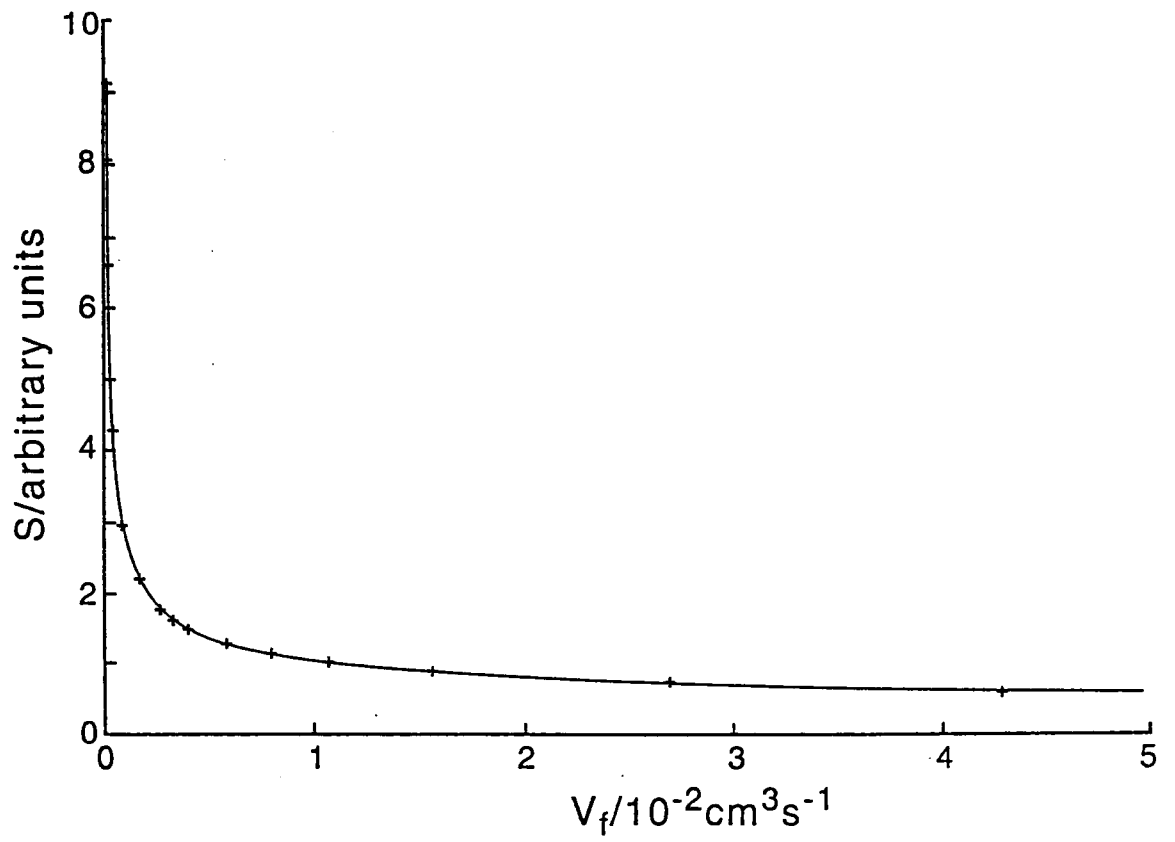

Figure 5.10. A simulation showing the characteristic fall-off of ESR signal with flow rate for the cell geometry used experimentally.

5.6.2 Quantification of the Heterogeneous Rate Constant

Having analysed the *in-situ* ESR measurements to confirm the instability of the $[CH_3NO_2]^{\bullet-}$ radical, further analysis of the ESR data was required to enable quantification of the heterogeneous rate constant for the chemical kinetics coupled to the reduction of nitromethane. Computer simulations of the ESR signals were obtained using the theory adapted from section 5.4, as described previously, for a heterogeneous ECEEE mechanism corresponding to a range of values for k_{het}. Corresponding transport limited current values were also simulated for the range of flow rates and k_{het} values using the theory developed in

section 5.4. The ESR signal data and that for the corresponding limiting current values were then plotted as log(S/I) against flow rate (v_f) as shown in figure 5.11. It should be noted that the vertical scale has an arbitrary offset corresponding to the sensitivity factor of the particular cavity employed[20].

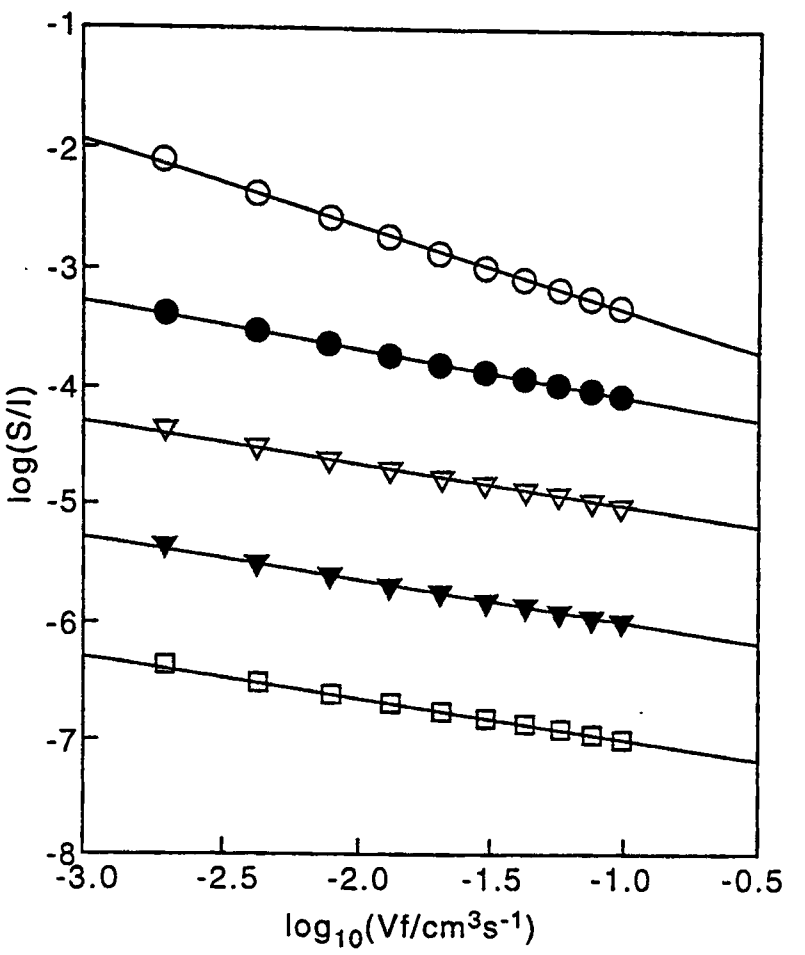

Figure 5.11. *The simulated plots of log(S/I) against log(v_f) generated using an ECEEE mechanism for different values of k_{het}/ cm s^{-1}: 5.0 (□), 0.5 (▼), 0.05 (▽), 0.005 (●) and 0.0 (○). The plots are closely linear in each case with slopes of -0.36, -0.36, -0.37, -0.4 and -0.7 respectively.*

Figure 5.11 shows the log(S/I) against log (v_f) data for the following k_{het} values; 5.0, 0.5, 0.05, 0.005 and 0.0 cm s^{-1}. Looking at figure 5.11 it is clear that the plots are closely linear with gradients of, -0.36, -0.36, -0.37, -0.4 and -0.7 respectively. The last plot generated for an ECEEE mechanism in which the heterogeneous rate constant was 0, corresponds to the case of the stable $[CH_3NO_2]^{\bullet-}$ radical anion investigated in section 5.6.1. As shown by equation (5.15) the log(S/I) versus log(v_f) plot expected for a stable radical has a gradient of -(2/3). The

20 B. A. Coles and R. G. Compton, *J. Electroanal. Chem.*, **144.** (1983), 87

data simulated for the stable radical, $k_{het} = 0$, generated a plot with a gradient of 0.7 which is consistent with that expected from equation (5.15). The slight deviation from the value of -(2/3) expected under pure Lévêque conditions is due to the relatively large length (6 mm) of the electrode used in the experimental investigations.

Examination of the different plots simulated for the range of k_{het} values indicates that the simulation using a value of $h_{het} = 0.05$ cm s^{-1} or greater closely reproduces the near-linear trend, with a slope of -0.34 ± 0.03 seen experimentally in figure 5.8. In figure 5.9 the ESR signal versus flow rate data simulated for a k_{het} value of 0.06 cm s^{-1} is included in the plot. On examination of figure 5.9 it is clear that a reasonable agreement between the experimental and the computer generated data can be seen. The consistency seen in the two sets of simulation data shown in figures 5.9 and 5. 11 for experimental values for $k_{ket} = 0.06$ cm s^{-1} is significant because the (S) versus (v_f) simulation is independent of the exact mechanism subsequent to the heterogeneous chemical step. However, the simulation of the log(S/I) against log(v_f) data make the assumption that a further three electrons have been transferred after the chemical step, which therefore contribute to the current measured. It should also be noted that the plots in figures 5.8 and 5.11 are all virtually linear. If the chemical reaction inducing the radical loss was homogenous the plots would be curved and for certain values of k_{het} pass through a maximum[22].

5.7 Conclusions

The experiments presented in this chapter demonstrate how channel electrode measurements in combination with ESR spectroscopy and numerical modelling make a powerful tool for mechanistic discrimination. The results obtained from such investigations

support the mechanism proposed by Prieto et al. for the reduction of the aliphatic nitro-compound, nitromethane, shown in figure 5.1. The reduction involves a chemical reaction sandwiched between two` reductions as previously proposed on the basis of impedance data[6-9]. In addition to the confirmation that the mechanism proceeds via an ECEEE mechanism the results presented in the previous sections indicate that the chemical step is heterogeneous rather than homogeneous in character. However, the rate constant for the heterogeneous chemical step was calculated to be 0.06 cm s^{-1} which is higher than that obtained by Prieto et al.[6-8] for C2 in the reduction of nitromethane at pure Hg electrodes, who proposed that C2 was the rate determining step. The value 0.06 cm s^{-1} is in fact identical to that obtained for C1, figure 1, by Prieto et al. This together with the fact that the detected radical anion is clearly that of the radical anion $[CH_3NO_2]^{\bullet -}$, suggests that the chemical step C1 rather than C2 is the rate determining chemical step in the reduction of nitromethane at Au plated Hg electrodes.

---

21 R. D. Webster, A. Bond, B. A. Coles and R. G. Compton, *J. Electroanal. Chem.*, **404**, (1996), 303

6. Heterogeneous ECE Processes at Channel Electrodes : Analytical Theory

Contents

The work presented in this chapter has been published in J. Phys. Chem., 102, (1998), 1515

6.1 Introduction

In the previous chapter the theory predicting the transport limited current for heterogeneous ECE (and ECEEE) processes at channel electrodes was developed using the backward implicit method (BI), discussed in section 2.5. This was applied to model the current generated from the reduction of nitromethane in aqueous solution (pH 8.3) at a channel electrode which contributed to the eventual conclusion that the mechanism follows a heterogeneous ECEEE pathway with a rate constant of k_{het} = 0.06 cm s^{-1}. This chapter extends the voltammetric theory for heterogeneous ECE (and ECEEE) processes to produce simple analytical expressions which allow the ready mechanistic interpretation of experimental data and the deduction of corresponding rate constants without the need for computer programs. Comparisons are made between the simple analytical solutions developed for the mass transport equations of a heterogeneous ECEEE mechanism and the numerical simulations described previously.

The working curves generated through the numerical simulation of a heterogeneous ECE (and ECEEE) mechanism and a homogeneous ECE (and ECEEE) mechanism presented in chapter 5 suggested that under favourable conditions a clear distinction between the two mechanisms would be achievable on the basis of experimental current measurements made as a function of flow rate. Using the simple analytical expressions developed, limiting current flow rate data was generated for the case of a conventional channel flow cell and the high speed channel flow cell to investigate this possibility of this mechanistic discrimination through variable mass transport measurements.

The proposed method of mechanistic investigation is then applied to the reduction of nitromethane in aqueous solution at a Hg/Cu electrode deposited on a Pt substrate. As

discussed in chapter 5 the reduction of nitromethane[1-3] involves a complex sequence of electron transfer and chemical steps including the uptake of four electrons and four protons and the cleavage of a N-O bond. The reaction scheme shown in figure 5.1 begins with a one-electron transfer step followed by coupled chemical kinetics and the production of the final product methylhydroxylamine from a reduction step involving the uptake of three electrons and three protons. In the previous chapter the coupled kinetics were shown to involve a rate determining heterogeneous chemical step. The high speed channel flow cell was used to carry out experiments on the reduction of nitromethane with the aim of bringing the effective number of electrons involved in the reduction into a range amenable to investigation by the variation of the mass transport and hence further investigate the heterogeneous character of the rate determining chemical step.

6.2 General Experimental Details

The experimental details of the high speed channel flow cell have been described in chapters 1 and 3. A 25 μm (x_e), 1.54 cm (d) Hg/Cu electrode was prepared using the procedure outlined in section 3.5. Solutions of nitromethane (1.5 mM) were prepared with pHs ranging from 1.8 to 9.0 using the buffers given in section 3.9.

6.3 Theory

In this section the voltammetric theory for a heterogeneous ECE process occurring at a

---

1 R. Guidelli and M. L. Foresti, *J. Electroanal. Chem.*, **88**, (1978), 65

2 F. Prieto, M. Rueda, M. Sluyters-Rehbach and J. H. Sluyters, *J. Electroanal. Chem.*, **327**, (1992), 1

3 F. Prieto, R. D. Webster, J. A. Alden, W. J. Aixill, G. A. Waller and R. G. Compton, *J. Phys. Chem.*, **437**, (1997), 183

channel electrode is developed. The reaction scheme for a heterogeneous ECE mechanism is shown in the scheme below:

E A ± e^- ⇌ B

C B → C

E C ± e^- ⇌ products

The steady-state convective-diffusion equations describing the distributions of species A and B are:

$$\frac{\partial[A]}{\partial t} = 0 = D_A \frac{\partial^2[A]}{\partial x^2} + D_A \frac{\partial^2[A]}{\partial y^2} - v_x \frac{\partial[A]}{\partial x} \qquad (6.1)$$

$$\frac{\partial[B]}{\partial t} = 0 = D_B \frac{\partial^2[B]}{\partial x^2} + D_B \frac{\partial^2[B]}{\partial y^2} - v_x \frac{\partial[B]}{\partial x} \qquad (6.2)$$

where D_A and D_B are the diffusion coefficients of species A and B respectively, v_x is the solution velocity in the x-direction and the co-ordinates x and y are defined in figure 1.1.

As explained previously v_x can be described in terms of the parabolic flow given in equation (5.7) and axial diffusion effects can be neglected provided the electrodes considered are not of microelectrode dimensions.

The boundary conditions relevant to the case of the transport limited electrolysis of A are as follows:

all y, $x < 0$, $[A] = [A]_{bulk}$, $[B] = 0$, $[C] = 0$ (6.3)

$y = 0$, $0 < x < x_e$, $[A] = 0$ (6.4)

$$D_A \frac{\partial[A]}{\partial y} = -D_B \frac{\partial[B]}{\partial y} + k_{het}[B]$$

$y = 0, \quad 0 < x < x_e, \qquad [C] = 0$

$$y = 2h, \text{ all } x, \quad D_A \frac{\partial[A]}{\partial y} = D_B \frac{\partial[B]}{\partial y} = 0 \tag{6.5}$$

It is possible to solve the mass transport equations (6.1) and (6.2) using the boundary conditions specified above by direct application of the finite difference method described in chapter 5. However this chapter is concerned with the analytical solution of equations (6.1) and (6.2) under steady-state conditions.

First the normalised variables χ, ξ and K given below are introduced.

$$\chi = x / x_e \tag{6.6}$$

$$\xi = (2\nu_0 / hDx_e)^{1/3} y \tag{6.7}$$

$$K_{het} = k_{het}(hx_e/2\nu_0 D^2)^{1/3} \tag{6.8}$$

where 2h is the channel height defined in figure 1.1. As described previously almost all practical channel flow cells designed for mechanistic investigations operate under conditions where the time to diffuse across the depth (2h) of the cell is long compared to the time taken to convect along the length of the electrode enabling the velocity profile in the x-direction, ν_x, to be simplified using the Lévêque[4] approximation:

$$\nu_x = \nu_0\left(1 - \frac{(h-y)^2}{h^2}\right) = \nu_0\left(\frac{h^2 - (h^2 - 2hy + y^2)}{h^2}\right) = \nu_0 \frac{y}{h}\left(2 - \frac{y}{h}\right) \approx 2\nu_0 \frac{y}{h} \tag{6.9}$$

for $y \approx 0$

Using the normalised parameters, (6.6), (6.7) and (6.8) and the Lévêque approximation, equations (6.1) and (6.2) simplify to the following:

---

4 M. Lévêque, *Ann. Mines Mem. Ser.*, **12/13**, (1928), 201

$$0 = \frac{\partial^2[A]}{\partial\xi^2} - \xi\frac{\partial[A]}{\partial\chi} \tag{6.10}$$

$$0 = \frac{\partial^2[B]}{\partial\xi^2} - \xi\frac{\partial[B]}{\partial\chi} \tag{6.11}$$

It is assumed that $D = D_A = D_B$.

6.3.1 Application of the Laplace Transform Technique to the Mass Transport Equation for Species A

The mass transport equations given above can be solved using the Laplace transform technique[5]. These solutions generate an expression for the transport limited current produced at a channel electrode which can in turn be used to write the simple expressions for the effective number of electrons being transferred, as a function of the rate constant K_{het}.

The Laplace transform with respect to χ of the concentration of species A is defined as:

$$L[A] = \int_0^\infty \exp(-p\chi)[A]d\chi \tag{6.12}$$

where p is the transformed variable of χ.

Application of this Laplace transform to equations (6.10) and (6.11) together with the boundary conditions given in equations (6.3) - (6.5) is described below.

Considering the derivative $\frac{\partial[A]}{\partial\chi}$ from equation (6.10) the Laplace transform technique can be used to rewrite the derivative as:

$$L\left(\frac{\partial[A]}{\partial\chi}\right) = \int_0^\infty \exp(-p\chi)\frac{\partial[A]}{\partial\chi}\partial\chi \tag{6.13}$$

---

5 J. Miles, *Integral Transforms in Applied Mathematics*, Cambridge University Press, London, (1971)

Therefore integrating by parts transforms the equation (6.13) to the following expression:

$$L\left(\frac{\partial[A]}{\partial\chi}\right) = \left[\exp(-p\chi)[A]\right]_{\chi=0}^{\chi=\infty} + pL[A] \qquad (6.14)$$

The first term on the right hand side of equation (6.14) reduces to $-[A]_{bulk}$ (as $[A]_{\chi=0} = [A]_{bulk}$) giving:

$$L\left(\frac{\partial[A]}{\partial\chi}\right) = p\left[L[A] - \frac{[A]_{bulk}}{p}\right] \qquad (6.15)$$

Taking a Laplace transform with respect to χ of both sides of equation (6.10) using equation (6.15) yields overall differential equation:

$$\frac{\partial^2 y}{\partial \xi^2} = p\,\xi\,y \quad \text{where } y = L[A] - \frac{[A]_{bulk}}{p} \qquad (6.16)$$

If $x = p^{1/3}\xi$ is substituted into equation (6.16) then a simpler equation results:

$$\frac{\partial^2 y}{\partial x^2} = xy \qquad (6.17)$$

This second order differential equation is now solvable as it takes the form of the Airy equation defined below:

$$\frac{\partial^2 Ai(x)}{\partial x^2} = xAi(x) \qquad (6.18)$$

where Ai(x) denotes the Airy function[6] (defined in appendix 3):

$$Ai(x) = \frac{1}{3^{2/3}\pi}\sum_{0}^{\infty}\frac{\Gamma(n/3+1/3)}{n!}\cdot\sin\left[\tfrac{2}{3}(n+1)\pi\right]\cdot\left(3^{1/3}x\right)^n \qquad (6.19)$$

Equation (6.16) is readily solved (see appendix 3) to give a solution of the form of equation (6.19). The general solution to the Airy equation, $\frac{\partial^2 y}{\partial x^2} = xy$, takes the form:

---

6 M. Abramowitz and A. I. Stegun, *Handbook of Mathematical Functions*, Dover, New York, (1970)

$y = aAi(x) + bBi(x)$

where a and b are arbitrary constants and the function Bi(x) is defined in appendix 3. However since the function Bi tends to infinity as x increases (see appendix 3) and the concentration of A is required to tend to its bulk value as ξ tends to infinity the arbitrary constant b is set to zero and only solutions of the form y = aAi(x) are considered. Hence:

$$y = const.Ai(p^{1/3}\xi) \qquad (6.20)$$

Considering equations (6.20) and (6.16) it is possible to equate the two expressions for y, producing:

$$L[A] = \frac{[A]_{bulk}}{p} + aAi(p^{1/3}\xi) \qquad (6.21)$$

The boundary condition given in equation (6.4) states that when y = 0, [A] = 0, therefore the Laplace transform of [A] is also 0 at this point, enabling an expression for the Laplace transform of the concentration of A to be written in terms of constants and the Airy function:

$$0 = \frac{[A]_{bulk}}{p} + aAi(0) \qquad (6.22)$$

Hence:

$$a = -\frac{[A]_{bulk}}{pAi(0)} \qquad (6.23)$$

6.3.2 Application of the Laplace Transform Technique to the Mass Transport Equation for Species B

Considering species B, the boundary condition (6.4) can be written in terms of the normalised parameters as shown on the following page:

$$\left(\frac{2V_0}{hDx_e}\right)D\left.\frac{\partial[A]}{\partial\xi}\right|_{\xi=0} = -\left(\frac{2V_0}{hDx_e}\right)D\left.\frac{\partial[B]}{\partial\xi}\right|_{\xi=0} + k_{het}[B] \qquad (6.24)$$

The introduction of a dimensionless form of the heterogeneous rate constant k_{het}, defined in equation (6.25) enables simplification of equation (6.24) to (6.26):

$$K_{het} = \frac{k_{het}}{D}\left(hDx_e/2V_0\right)^{1/3} \qquad (6.25)$$

$$\left.\frac{\partial[A]}{\partial\xi}\right|_{\xi=0} = -\left.\frac{\partial[B]}{\partial\xi}\right|_{\xi=0} + K_{het}[B] \qquad (6.26)$$

The overall mass transport equation for species B given in equation (6.2) is the same as that for species A. Therefore the solution of equation (6.2) is obtained using the same method described for species A. The result is the general expression for the Laplace transform of the concentration of species B:

$$L[B] = bAi(p^{1/3}\xi) \qquad (6.27)$$

Taking Laplace transforms of both sides of equation (6.26) and substituting the expression for the Laplace transform of $[A]$ as derived above results in the following relation.

$$\frac{-[A]_{bulk}Ai'(0)p^{1/3}}{pAi(0)} = -bAi'(0)p^{1/3} + bK_{het}Ai(0) \qquad (6.28)$$

Equating both sides of the resulting equation gives the constant b as given below:

$$b = -\frac{[A]_{bulk}Ai'(0)}{p^{2/3}Ai(0)\left[Ai(0)K_{het} - Ai'(0)p^{1/3}\right]} \qquad (6.29)$$

The Laplace transforms for species A and B are summarised below:

$$L[A] = \frac{[A]_{bulk}}{p} - \frac{[A]_{bulk}}{p}\cdot\frac{Ai\left(p^{1/3}\xi\right)}{Ai(0)} \qquad (6.30)$$

$$L[B] = -\frac{[A]_{bulk}\,Ai'(0)}{p^{2/3}Ai(0)} \cdot \frac{Ai\left(p^{1/3}\xi\right)}{\left[Ai(0)K_{het} - Ai'(0)p^{1/3}\right]} \tag{6.31}$$

where $Ai'(x)$ denotes the first derivative of $Ai(x)$ with respect to ξ.

6.3.3 Calculation of the Effective Number of Electrons Transferred in an $EC_{het}E$ Reaction (or an $EC_{het}EEE$ Reaction)

The current generated at the electrode surface is proportional to the influx of species A, and the rate of formation of species C. Hence the transport limiting current can be evaluated using the expression below:

$$I = Fw\int_0^{x_c}\left(D\frac{\partial[A]}{\partial y} + k_{het}[B]\right)_{y=0} dx \tag{6.32}$$

Transforming this expression by inserting the normalised variables defined earlier gives the relation:

$$I \propto Fw\int_0^1 L^{-1}\left(\partial L[A]/\partial\xi\right)_{\xi=0} d\chi + \int K_{het}L^{-1}L[B]_{\xi=0}\,d\chi \tag{6.33}$$

where L^{-1} denotes the inverse Laplace transform.

The current expression above applies to a heterogeneous ECE mechanism. The case of a simple one electron transfer is evaluated using the equation below:

$$I_{one\,e^-} \propto Fw\int_0^1 L^{-1}\left(\partial L[A]/\partial\xi\right)_{\xi=0} d\chi \tag{6.34}$$

Using the two equations (6.33) and (6.34) it is possible to define the effective number of electrons transferred in a heterogeneous ECE process as the ratio of the overall ECE current to the one electron current as in equation (6.35).

$$N_{eff} = \frac{\int_0^1 L^{-1}\left(\partial L[A]/\partial\xi\right)_{\xi=0} d\chi + \int_0^1 L^{-1}(K_{het} L[B]_{\xi=0}) d\chi}{\int_0^1 L^{-1}\left(\partial L[A]/\partial\xi\right)_{\xi=0} d\chi} \tag{6.35}$$

Integrating equation (6.35) in Laplace space[5] and making use of the general rule that,

$$L^{-1}\frac{f(p)}{p} = \int_0^t F(t)dt \quad \text{where } L\{F(t)\} = f(p) \tag{6.36}$$

in other words division by p has the effect of integrating F(t) from 0 to t, leads to the following expression for N_{eff}:

$$N_{eff} = \frac{\left[L^{-1}\frac{1}{p}\left(\partial L[A]/\partial\xi\right)_{\xi=0}\right]_{\chi=1} + \left[L^{-1}\frac{1}{p}K_{het}L[B]_0\right]_{\chi=1}}{\left[L^{-1}\frac{1}{p}\left(\partial L[A]/\partial\xi\right)_{\xi=0}\right]_{\chi=1}} \tag{6.37}$$

Using equation (6.30):

$$\left.\frac{\partial L[A]}{\partial\xi}\right|_{\xi=0} = \frac{-[A]_{bulk}\,Ai'(0)}{p^{2/3}Ai(0)} \tag{6.38}$$

Substituting equation (6.38) into equation (6.37) gives:

$$N_{eff} = \frac{\left[-L^{-1}\frac{1}{p}\frac{[A]_{bulk}\,Ai'(0)}{p^{2/3}Ai(0)}\right]_{\chi=1} + \left[L^{-1}\frac{1}{p}K_{het}L[B]\right]_{\chi=1}}{\left[-L^{-1}\frac{1}{p}\frac{[A]_{bulk}\,Ai'(0)}{p^{2/3}Ai(0)}\right]_{\chi=1}} \tag{6.39}$$

In order to solve equation (6.39) the standard inverse Laplace transform[5] result given below is employed.

$$L^{-1}\Gamma(v+1)p^{-v-1} = \chi^{v} \qquad \text{for } v > -1 \tag{6.40}$$

where the function Γ denotes a Gamma Function defined by equation (6.41).

$$\Gamma(n) = \int_0^{\infty} u^{n-1}e^{-u}du \qquad \text{where } n > 0 \tag{6.41}$$

Using the standard Laplace transform equation (6.40) and the expression for L[B], (6.31) defined earlier, equation (6.39) then becomes:

$$N_{eff} = \left[1 - \frac{\Gamma(5/3)Ai(0)K_{het}}{Ai'(0)} L^{-1}\frac{1}{p^2}\cdot\frac{1}{\left[1-\frac{Ai(0)K_{het}}{Ai'(0)p^{1/3}}\right]}\right]_{\chi=1} \tag{6.42}$$

Note the expression above gives an N_{eff} range between 1 and 2 electrons since:

when $K_{het} = 0$, $N_{eff} = 1$, but,

$$\text{when } K_{het} \to 4,\ N_{eff} \to \left[1-\frac{\Gamma(5/3)Ai(0)K_{het}}{Ai'(0)}L^{-1}\left(-\frac{1}{p^2}\frac{Ai'(0)p^{1/3}}{Ai(0)K_{het}}\right)\right]_{\chi=1}$$

$$= \left[1-\frac{\Gamma(5/3)Ai(0)K_{het}}{Ai'(0)}L^{-1}\left(-\frac{1}{p^{5/3}}\frac{Ai'(0)}{Ai(0)K_{het}}\right)\right]_{\chi=1} \tag{6.43}$$

Thus using the inverse Laplace transform result of (6.40), $L^{-1}(p^{-5/3}) = 1/\Gamma(5/3)$, $N_{eff} \to 2$.

To evaluate N_{eff} over the full range more simplistic expressions valid for both small and large K_{het} values are derived as shown on the following pages. The nature of the expression for N_{eff} also makes the direct application of the inverse Laplace transform in (6.42) difficult and so approximations are necessary.

6.3.3.1 The Low K Approximation

Equation (6.42) indicates that an inverse Laplace transform of the type shown below is required:

$$L^{-1}\frac{1}{p^2\left[1+Ap^{-1/3}\right]} \qquad \text{where } A=\frac{-K_{het}Ai(0)}{Ai'(0)} \tag{6.44}$$

Using binomial expansion theory it is possible to rewrite this expression in the following form:

$$L^{-1}\frac{1}{p^2}\left[1-\sum_{n=1}^{\infty}a_n p^{-n/3}\right] \tag{6.45}$$

It can be shown that for a series of this kind a simple inverse Laplace transformation[5] exists as given below:

$$L^{-1}\left(\sum_{n=1}^{\infty}c_n p^{-n/r}\right)=\sum_{n=1}^{\infty}\frac{c_n\chi^{(n/r-1)}}{\Gamma\left(\frac{n}{r}\right)} \qquad \text{given } p\to\infty, r>0 \tag{6.46}$$

This result used in conjunction with equation (6.40) implies expression (6.45) becomes

$$\frac{1}{\Gamma(2)}-\sum_{n=1}^{\infty}\frac{a_n\chi^{\left(\frac{n+2}{3-1}\right)}}{\Gamma\left(\frac{n+2}{3}\right)} \tag{6.47}$$

It should be noted that both the gamma function and the power to which χ is raised contain (n+2) terms. This is due to the incorporation of the $1/p^2$ term from outside the bracket in equation (6.45).

As $\chi=1$ the equation simplifies to:

$$\frac{1}{\Gamma(2)} - \sum_{n=1}^{\infty} \frac{a_n}{\Gamma\left(\frac{n+2}{3}\right)} \tag{6.48}$$

Hence equation (6.42) becomes:

$$N_{eff} = 1 - \frac{\Gamma\left(\frac{5}{3}\right) Ai(0) K_{het}}{Ai'(0)} \left\{ \frac{1}{\Gamma(2)} - \sum_{n=1}^{\infty} \frac{a_n}{\Gamma\left(\frac{n+2}{3}\right)} \right\} \tag{6.49}$$

The standard gamma functions defined in appendix 4 are then used to simplify equation (6.49) to the low K approximation (6.50).

$$N_{eff} = 1 - \frac{\frac{2}{3}\Gamma\left(\frac{2}{3}\right) Ai(0) K_{het}}{Ai'(0)} \left\{ 1 - \sum_{n=1}^{\infty} \frac{a_n}{\Gamma\left(\frac{n+2}{3}\right)} \right\} \tag{6.50}$$

The summation part of this expression is then calculated by evaluating the summation series computationally to convergence using the airy function solutions given in appendix 3. The result is the following expression for low K values:

$$N_{eff} = 1 + 1.2377 K_{het}^{1} - 1.6982 K_{het}^{2} + 2.6085 K_{het}^{3} - 4.3867 K_{het}^{4} + ... \tag{6.51}$$

6.3.3.2 The High K Approximation

This approximation is conducted in an analogous manner to that of the low K approximation but first equation (6.42) is rearranged into the form:

$$N_{eff} = 1 + \Gamma\left(\frac{5}{3}\right) L^{-1} \frac{1}{p^{5/3}} \left[1 - \frac{Ai'(0) p^{1/3}}{Ai(0) K_{het}} \right]^{-1} \tag{6.52}$$

Binomial theory is applied again resulting in the following:

$$N_{eff} = 1 + \Gamma\left(\frac{5}{3}\right) L^{-1} \frac{1}{p^{5/3}} \left[1 + \sum_{n=1}^{\infty} (-1)^n b_n \frac{p^{n/3}}{K_{het}{}^n} \right] \qquad (6.53)$$

Note in (6.53) b1 $\frac{b_1}{K_{het}{}^1} = \alpha / K_{het}$ where $\alpha = -Ai'(0)/Ai(0)$

Inverse Laplace transforms are performed as in the high K case giving rise to the following expression for N_{eff}.

$$N_{eff} = 1 + \Gamma\left(\frac{5}{3}\right) \left\{ \frac{1}{\Gamma\left(\frac{5}{3}\right)} + \sum_{n=1}^{\infty} \frac{(-1)^n b_n}{\Gamma\left(\frac{5-n}{3}\right) K_{het}{}^n} \right\} \qquad (6.54)$$

In this high K approximation there is the problem that the summation cannot proceed indefinitely as the high K expression is restricted to the order of K^{-5}. This is due to equation (6.40) only being valid for v > -1 resulting in the limiting of the summation at the $\Gamma(0)$ term. Again the summation is converged by computational methods and the following expression for the high K approximation follows:

$$N_{eff} \cong 2 - 0.7369 K_{het}^{-1} + 0.4797 K_{het}^{-2} - 0.2583 K_{het}^{-3} + 0.0952 K_{het}^{-4} - 0.01856 K_{het}^{-5} \qquad (6.55)$$

6.4 Comparison of the Analytical Expressions for N_{eff} with Numerical Simulations

In the previous chapter the backwards implicit finite difference (BI) method was applied to the voltammetric theory for heterogeneous ECE (and ECEEE) processes. Figure 6.1 shows a comparison between the working curve generated using this numerical method and the analytical expressions generated previously.

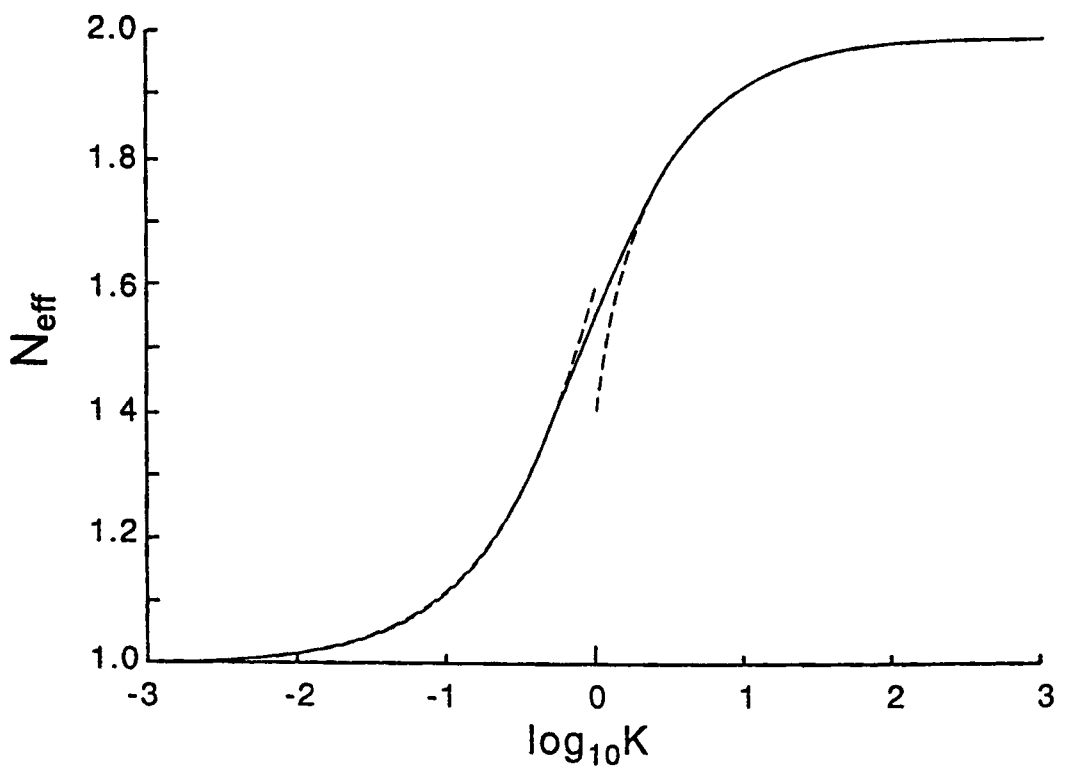

Figure 6.1. *Working curve showing the relationship of N_{eff} and K_{het} for a heterogeneous ECE process as calculated from numerical simulation (—) and from equations (6.51) and (6.55) respectively (...).*

Comparison of the analytical and numerical predictions shown in figure 6.1 shows that the low K expression holds to within 0.1 % for $\log(K_{het}) < -0.35$ while the high K equation describes the simulated data to within 0.1 % for $\log(K_{het}) > 0.45$. In the range $-0.35 < K_{het} < 0.45$ the simulated curve is described by equation (6.56):

$$N_{eff} = 1.5602 + 0.5439 \log (K_{het}) \qquad (6.56)$$

to within 0.85 %. It may therefore be concluded that equations (6.51) and (6.55) are adequate to describe the experimental behaviour for almost all experimental purposes.

Equations (6.51), (6.55) and (6.56) define the channel electrode voltammetric response for the heterogeneous ECE mechanism. Analogous expressions have been derived previously by Leslie et al.[7] for the homogeneous case. It is therefore possible to examine whether it is

---

7 W. Leslie, J. A. Alden, R. G. Compton and T. Silk, *J. Phys. Chem.*, **100**, (1996), 14310

possible to confidently distinguish between the two mechanisms on the basis of limiting current flow rate data alone. In order to do so it is noted that experiments may be conducted using either a conventional electrode characterised by a typical geometry of 2h = 0.1 cm, w = 0.3 cm, d = 0.6 cm and x_e = 0.3 cm and a volume flow rate, v_f, range of 4 x 10^{-4} to 25 cm^3 s^{-1}. Alternatively the high speed channel electrode described previously may be used with a typical geometry of 2h = 0.0125 cm, w = 0.15 cm, d = 0.2 cm, x_e = 0.0025 cm and a volume flow rate range of $0.1 < v_f / cm^3 s^{-1} < 2.5$. To investigate the possibility of mechanistic resolution, N_{eff} versus flow rate data was generated for authentic heterogeneous ECE processes with D = 2 x 10^{-5} cm^2 s^{-1} and for rate constants of k_{het} = 0.0004 and 0.0014 cm s^{-1} for the conventional channel electrode case and k_{het} = 0.014 and 0.055 cm s^{-1} for the high speed channel electrode system. Figures 6.2 and 6.3 show the plots of N_{eff} variation with v_0 for the two cases.

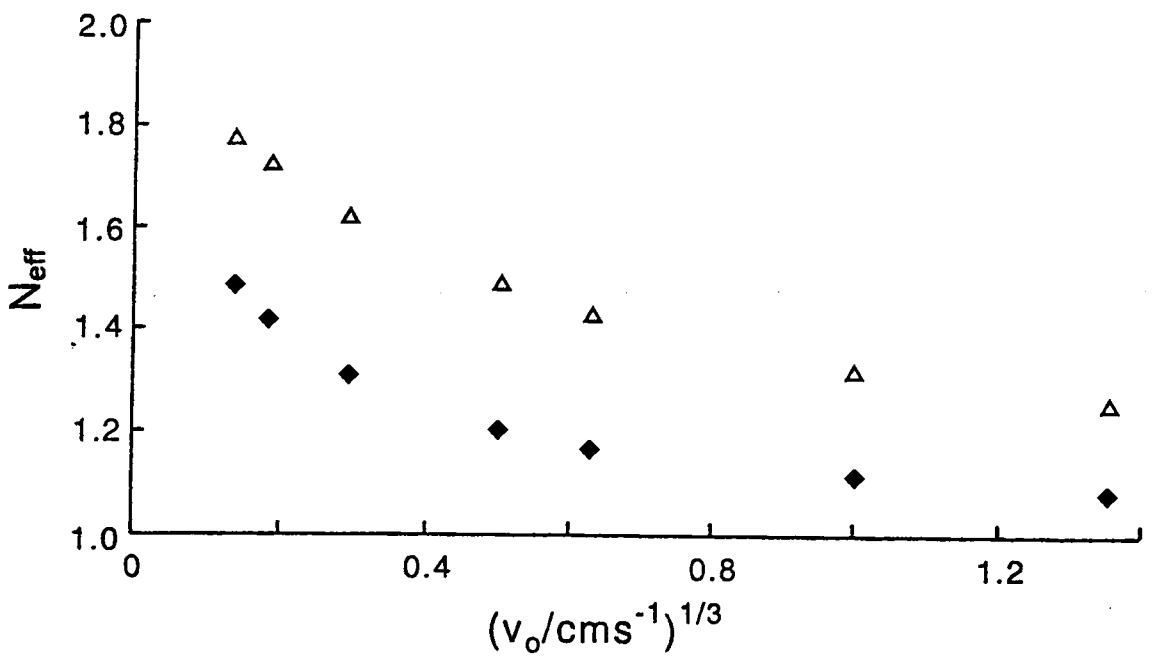

Figure 6.2. *Variation of N_{eff} with $v_0^{1/3}$ for an authentic heterogeneous ECE process with k_{het} / cm s^{-1} = 0.0004 and 0.0014 for a conventional channel flow cell of the geometry described in the text.*

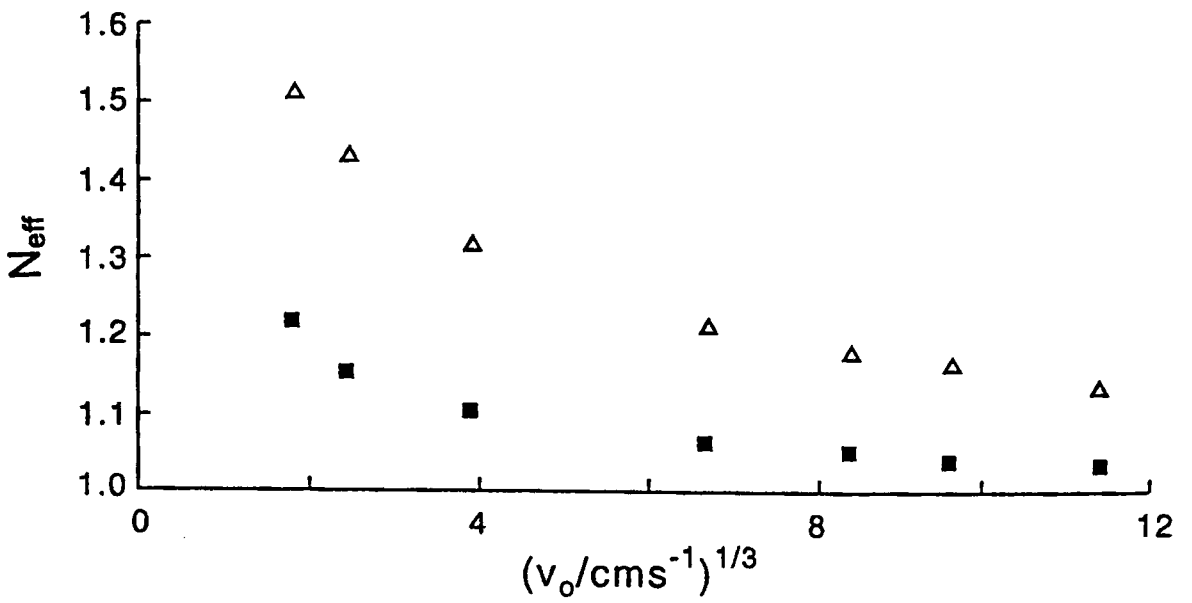

Figure 6.3. *Variation of N_{eff} with $v_0^{1/3}$ for an authentic heterogeneous ECE process with k_{het} / cm s^{-1} = 0.014 and 0.055 for a high speed channel electrode of the geometry described in the text.*

The data generated was then analysed according to the homogeneous theory[7] which suggests N_{eff} is a unique function of the dimensionless rate constant given in equation (6.57):

$$K_{homo} = k_{homo}(4h^4x_e^2/9v_f^2D)^{1/3} \qquad (6.57)$$

where $V_f = 4v_0hd/3$. The known working curves[7] allow the inference of K_{homo} as a function of flow rate for the "synthetic" heterogeneous ECE data. If the latter were indistinguishable from a homogeneous ECE process, then a plot of K_{homo}, against (flow rate)$^{-2/3}$ would be a straight line passing through the origin. Figures 6.4 and 6.5 show that this is not the case but rather that significantly curved plots are obtained. This observation suggests that, provided N_{eff} data can be obtained which is sufficiently far from the limiting values of 1 or 2 electrons, then variable mass transport measurements should permit a clear resolution of homogeneous and heterogeneous ECE mechanisms.

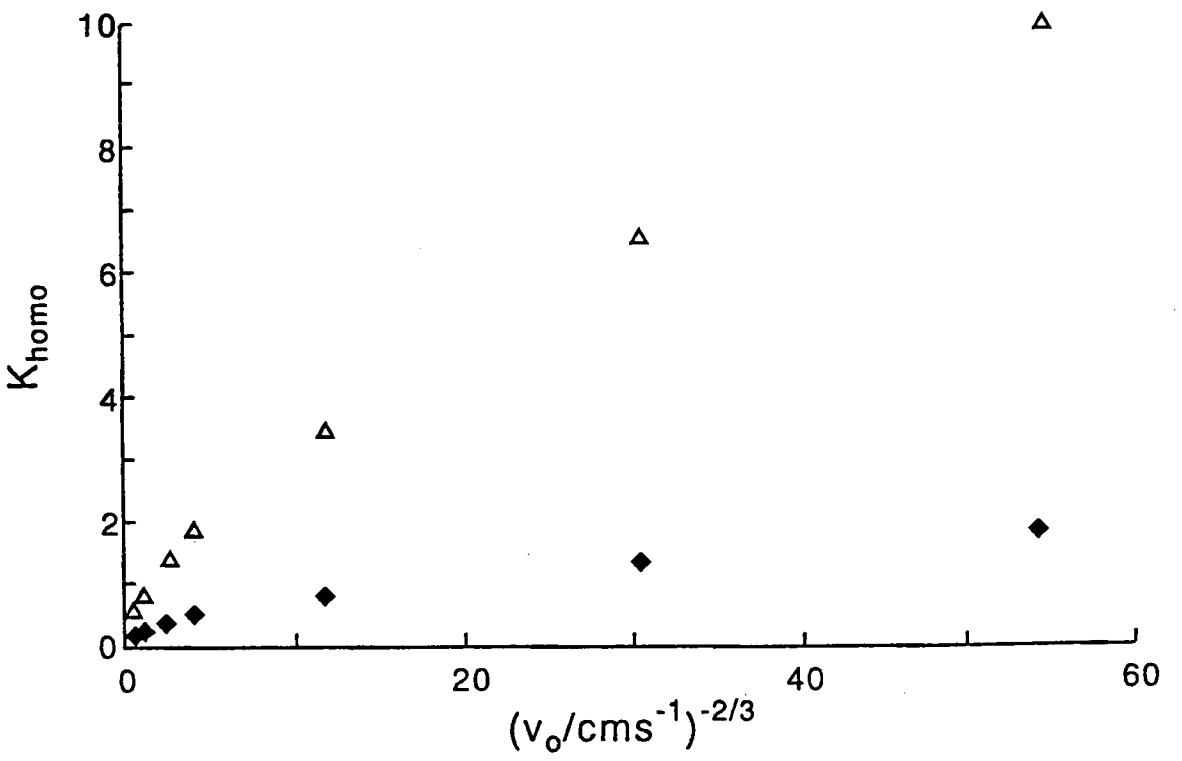

Figure 6.4. *The data of figure 6.2 analysed in terms of a homogeneous ECE reaction.*

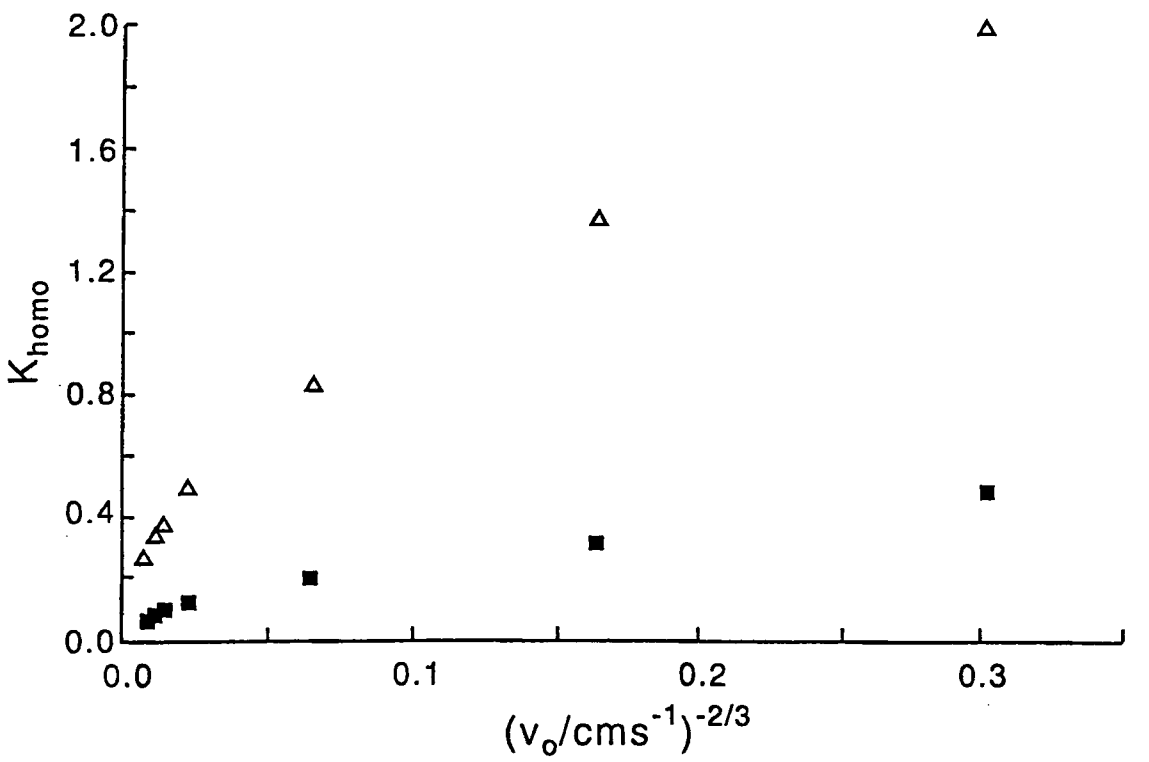

Figure 6.5. *The data of figure 6.3 analysed in terms of a homogeneous ECE reaction.*

6.5 High Speed Channel Investigations of Nitromethane

As described in chapter 5, experiments carried out using a conventional channel electrode to investigate the reduction of nitromethane in aqueous solution (pH 8.3) at a Au/Hg electrode indicated that the mechanism followed an $EC_{het}EEE$ reaction scheme. The theoretical work presented in this chapter suggests that experiments conducted in such a way as to bring the effective number of electrons transferred into a range, $1 < N_{eff} < 4$, would be amenable to investigation by variation of the mass transport and hence permit a clear resolution between a homogeneous ECEEE reaction and a heterogeneous ECEEE reaction.

In order to probe the nitromethane reaction scheme on a much shorter timescale than previous experiments described in chapter 5 and hence bring the effective number of electrons transferred into the range, $1 < N_{eff} < 4$, voltammetric measurements were performed using the high speed channel flow cell. Experiments were carried out on 1.5 mM solutions of nitromethane buffered at various pHs between 1.8 and 9.0 to investigate any pH dependence of the mechanism at a Cu/Hg electrode.

Prior to each nitromethane experiment the height of the high speed channel flow cell was calibrated using the reduction of 1 mM fluorescein in 0.1 M NaOH with KCl as supporting electrolyte. Steady-state experiments were recorded with a half-wave of -1.05 ± 0.5 V (vs. Pt pseudoreference electrode) for a range of electrolyte flow rates up to 3.5 $cm^3\ s^{-1}$. The mass transport limited current showed a linear dependence on the cube root of the solution flow rate according to the Levich equation[8] (1.12). Hence, the application of equation (1.12) with the measured geometric parameters of the channel electrode (x_e, w, d), and a value of 4.0×10^{-6} $cm^2\ s^{-1}$ for the diffusion coefficient of fluorescein in NaOH obtained from rotating disk

---

8 V. G. Levich, *Physicochemical Hydrodynamics*, Prentice Hall, Englewood Cliffs, New Jersey, (1962)

measurements, enabled the height of the channel cell to be calculated. In all cases a value of 0.0125 ± 0.005 cm was found.

The steady-state voltammograms recorded for the different pH solutions in the range of 1.8 - 9.0 of nitromethane had a half-wave potential of -1.3 ± 0.1 V (vs. Pt pseudo-reference electrode) with no systematic variation with pH. For each solution pH the transport limiting current was measured as a function of flow rate (v_f) as in the case of the gravity flow investigations reported in chapter 5. Typical plots of limiting current vs. $vf^{1/3}$ are shown in figures 6.6(a) - (f). It can be seen that in all cases there is a steady increase in an approximately linear fashion with N_{eff} values lying in the range of 1.04 - 1.61 (pH 1.8), 1.39 - 1.88 (pH 3.0), 1.62 - 1.93 (pH 4.0), 2.34 - 2.92 (pH 5.0), 2.00 - 2.92 (pH 7.0), 2.32 - 2.87 (pH 9.0).

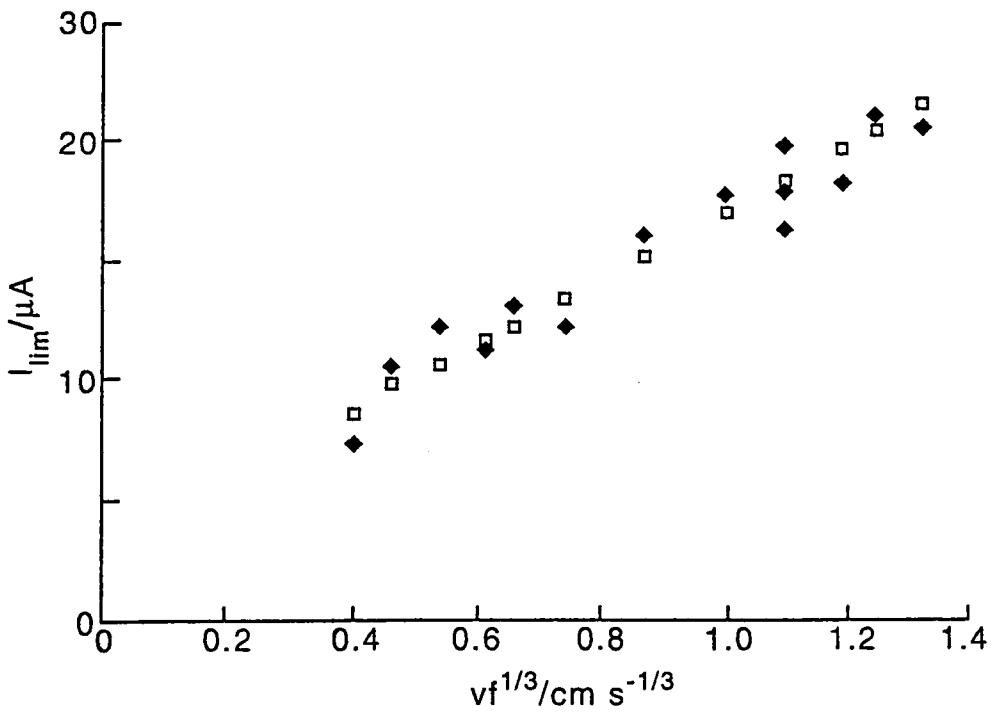

Figure 6.6(a). *The variation of the transport limited current with the electrolyte flow rate as measured (♦) in buffered solution of pH 1.8. The open symbols (□) show the behaviour simulated for an ECEEE mechanism using the values of k_{hel} plotted in figure 6.7.*

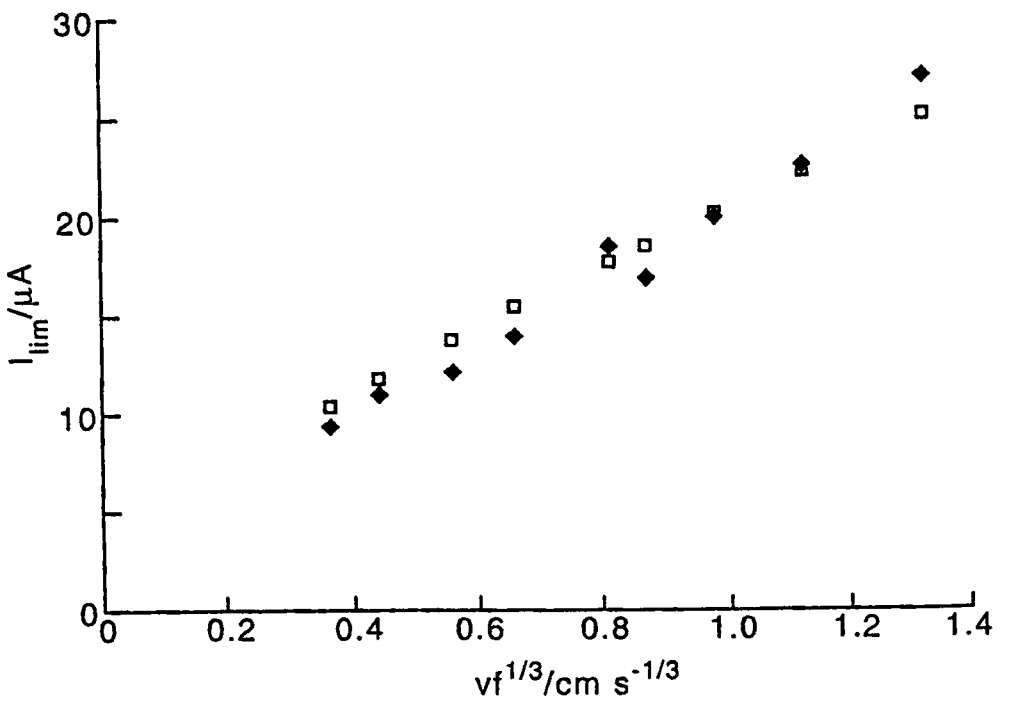

Figure 6.6(b). The variation of the transport limited current with the electrolyte flow rate as measured (♦) in buffered solution of pH 3.0. The open symbols (□) show the behaviour simulated for an ECEEE mechanism using the values of k_{het} plotted in figure 6.7.

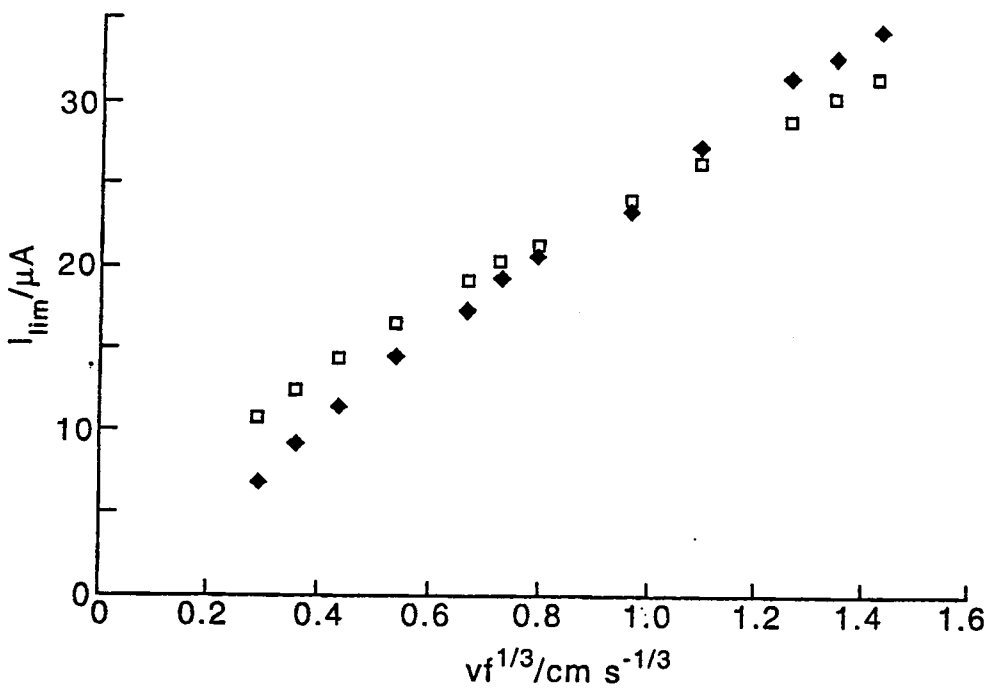

Figure 6.6(c). The variation of the transport limited current with the electrolyte flow rate as measured (♦) in buffered solution of pH 4.0. The open symbols (□) show the behaviour simulated for an ECEEE mechanism using the values of k_{het} plotted in figure 6.7.

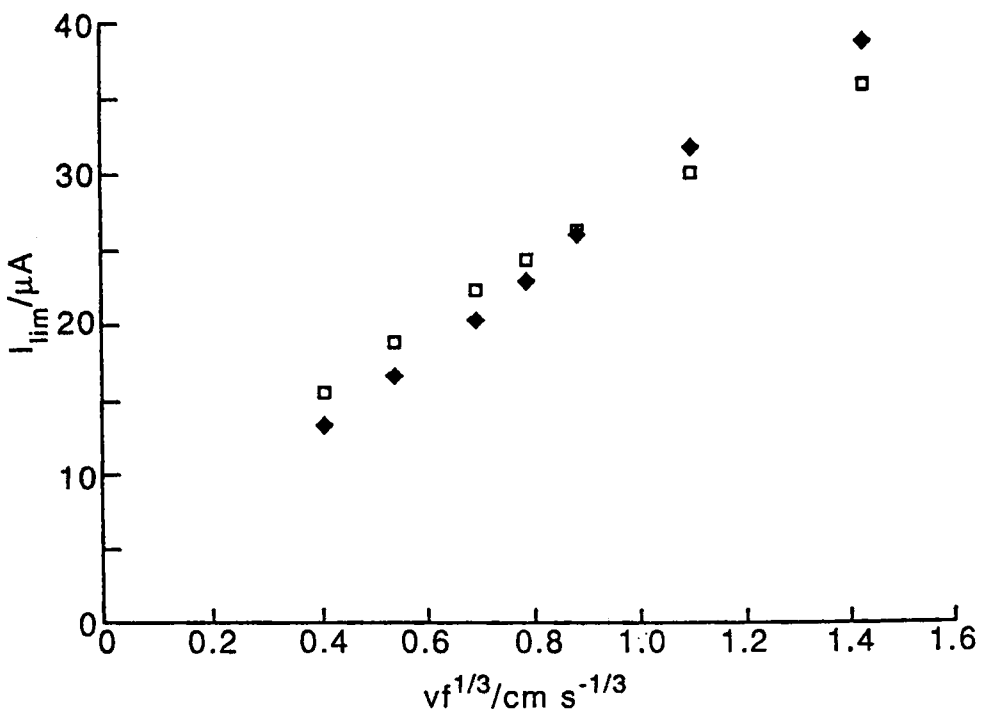

Figure 6.6(d). *The variation of the transport limited current with the electrolyte flow rate as measured (♦) in buffered solution of pH 5.0. The open symbols (□) show the behaviour simulated for an ECEEE mechanism using the values of k_{het} plotted in figure 6.7.*

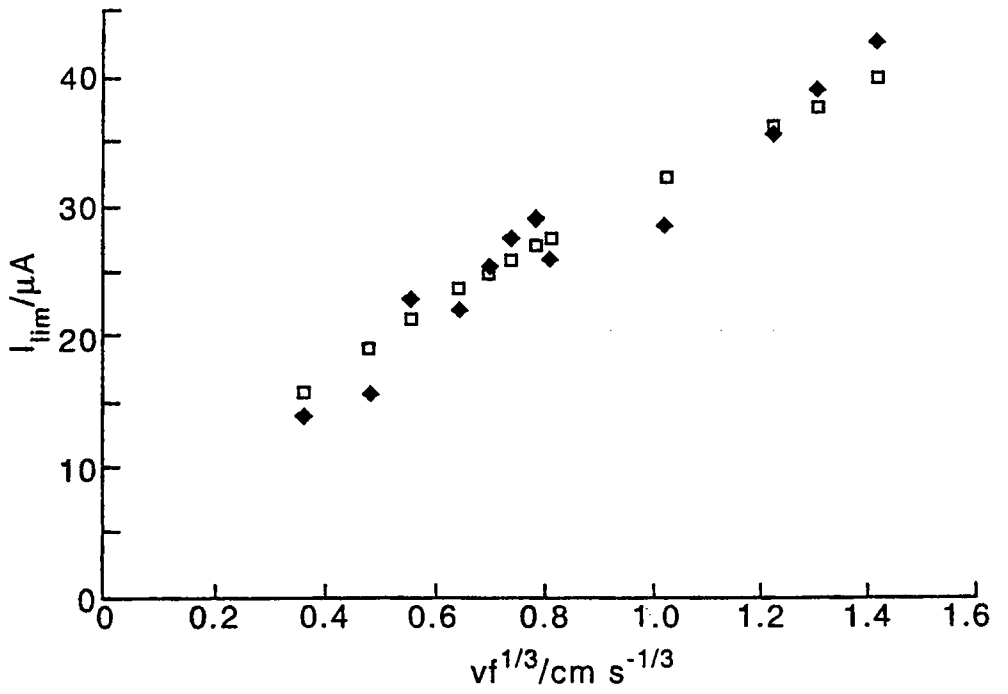

Figure 6.6(e). *The variation of the transport limited current with the electrolyte flow rate as measured (♦) in buffered solution of pH 7.0. The open symbols (□) show the behaviour simulated for an ECEEE mechanism using the values of k_{het} plotted in figure 6.7.*

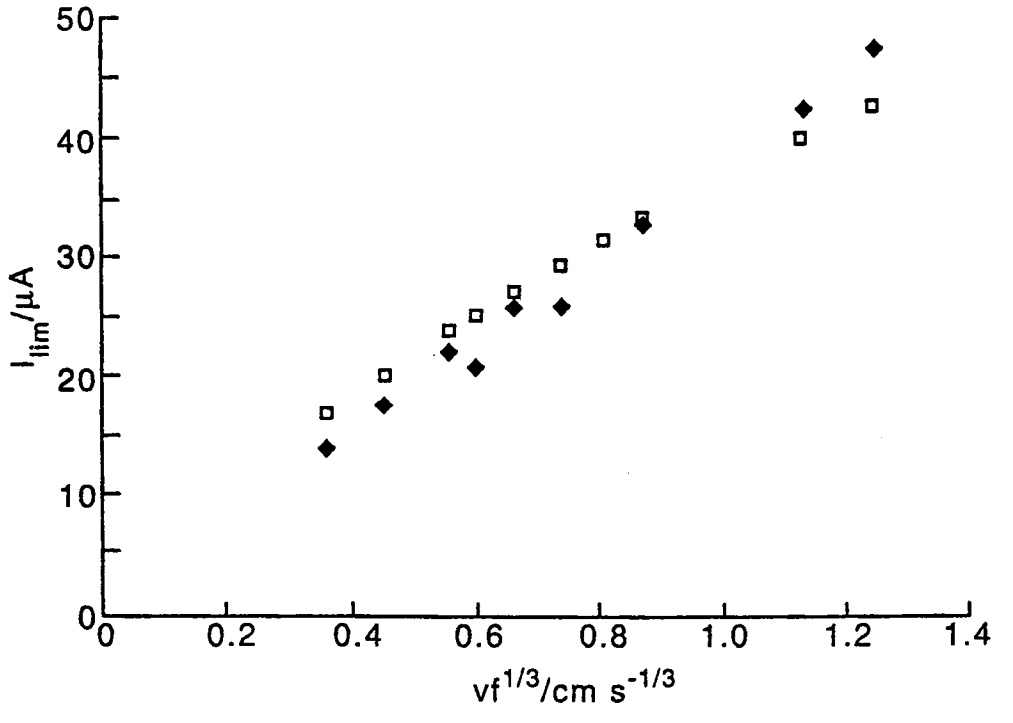

Figure 6.6(f). *The variation of the transport limited current with the electrolyte flow rate as measured (♦) in buffered solution of pH 9.0. The open symbols (□) show the behaviour simulated for an ECEEE mechanism using the values of k_{het} plotted in figure 6.7.*

The approximate cube root dependence of the transport limiting current values on the volume flow rate shown in figures 6.6(a)-(f) arises from the relatively weak dependence of N_{eff} on flow rate recognised above for electrode processes in which electron transfer steps are separated by heterogeneous (but not homogeneous) chemical steps. The possibility of mistaking any of the plots shown in figure 6.6 for simple Levich type behaviour should be apparent. More importantly the near linearity of the plots in figures 6.6(a)-(f) provides a clear indication that the multi-electron process involved in the reduction of nitromethane does not contain any kinetically significant coupled homogeneous steps. Instead the deviation of the N_{eff} values below 4 must result from heterogeneous coupled kinetics where, as discussed above, the sensitivity of N_{eff} towards the flow rate is much weaker.

In order to analyse the limiting current flow rate data show in figures 6.6(a)-(f) the working curve shown in figure 6.1 was adapted for an ECEEE process[3] and best fit values of k_{het} values found for each pH. The corresponding theoretical plots are shown in figure 6.6(a)-(f). Good agreement can therefore be seen across the entire flow rate range indicating that the data is consistent with a heterogeneous ECEEE mechanism. Figure 6.7 shows a plot of the best fit k_{het} values versus pH, which indicates that the C1 step defined in chapter 5 shows a very weak increase with pH. In chapter 5 the experiments carried out at a Au/Hg electrode enabled a k_{het} value of 0.06 cm s^{-1} to be deduced for a nitromethane solution at pH 8.3 which suggests that the Cu/Hg electrode surfaces prepared for the work presented in this chapter showed a little more electrocatalytic activity in respect of the C1 step.

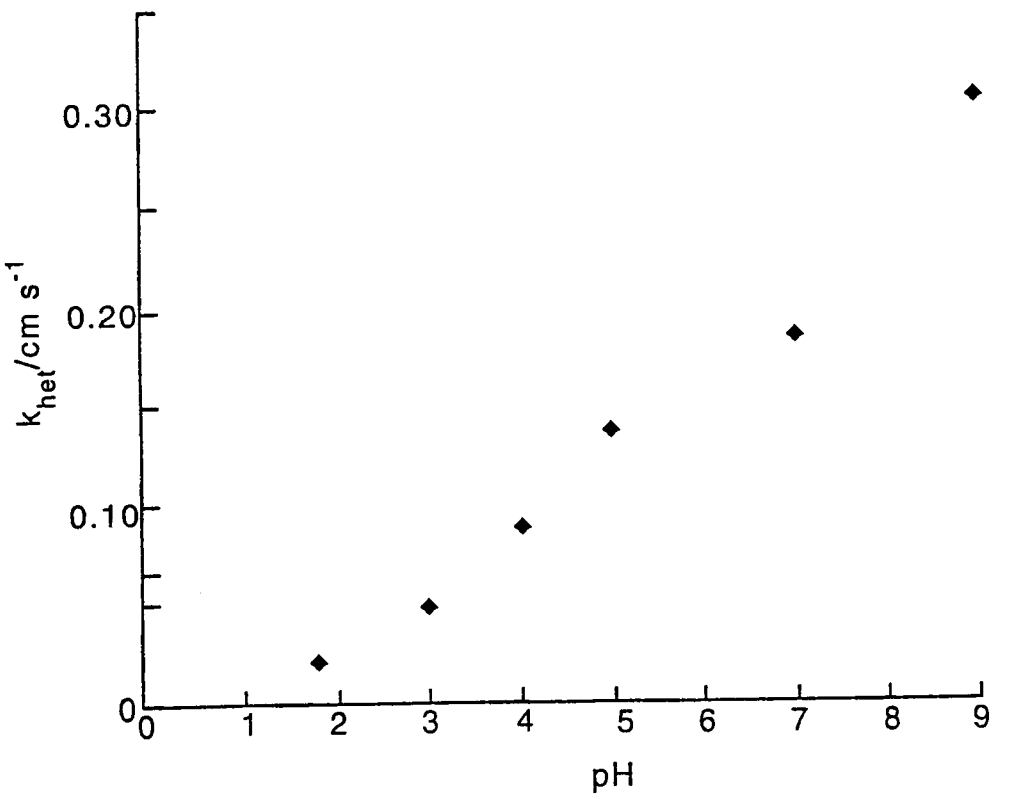

Figure 6.7. *The variation of k_{het} with pH.*

6.6 Conclusions

The work presented in this chapter has shown that variable flow rate channel electrode voltammetry can successfully distinguish the character of the chemical step in ECE type mechanisms as homogeneous or heterogeneous. In particular, in the latter case the effective number of electrons transferred is only weakly sensitive to solution flow rate so that the transport limited current approximately follows a cube root (Levich) behaviour as expected in the absence of coupled kinetics .

7. The Application of Voltammetric Waveshape Theory to the Reduction of Nitromethane

Contents

The work presented in this chapter has been accepted for publication in J. Phys. Chem.

7.1 Introduction

In the previous two chapters the voltammetric theory for a heterogeneous ECEEE process was developed using both analytical and numerical methods. The new voltammetric theory was applied to the complex reduction pathway of nitromethane which was thought to proceed via a heterogeneous ECEEE[1,2] mechanism. Analysis of the current flow rate data recorded for the reduction of aqueous solutions of nitromethane at a Hg/Au[3] conventional channel electrode and a Hg/Cu[4] high speed channel electrode enabled the deduction of the heterogeneous rate constant for the coupled chemical kinetics. A value of 0.06 cm s^{-1} was found for the kinetics occurring at the Hg/Au electrode with a slightly higher rate constant for the Hg/Cu electrode.

However, the investigation and characterisation of complex electrochemical mechanisms would be considerably assisted if the additional and essentially independent information gained from the analysis of voltammetric waveshapes was included in the data analysis. This proposal is addressed in the following sections in which the voltammetric theory for heterogeneous ECEEE processes is extended further to include the prediction of voltammetric waveshapes, as characterised by the half-wave potential and the Tafel slope as a function of the rate of mass transport and the cell geometry. In particular the latter is shown to be a sensitive probe of the nature and magnitude of the coupled kinetics involved. Two working surfaces are developed which allow the ready mechanistic interpretation of experimental data

---

1 R. Guidelli and M. L. Foresti, *J. Electroanal. Chem.*, **88**, (1978), 65

2 F. Prieto, M. Rueda, M. Sluyters-Rehbach and J. H. Sluyters, *J. Electroanal. Chem.*, **327**, (1992), 1

3 F. Prieto, R. D. Webster, J. A. Alden, W. J. Aixill, G. A. Waller and R. G. Compton, *J. Phys. Chem.*, **43**, (1997), 183

4 W. J. Aixill, J. A. Alden, F. Prieto, G. A. Waller, R. G. Compton and M. Rueda, *J. Phys. Chem.*, **102**, (1998), 151

recorded at a channel flow cell and the deduction of corresponding rate constants through the analysis of voltammetric waveshapes.

As with the previous two chapters the theory developed is applied to experiments carried out on the reduction of aqueous solutions of nitromethane. However in this chapter the effect of different electrode surfaces on the kinetics involved in the reduction of nitromethane is also investigated. Steady-state voltammetry is recorded at both Pt and Au high speed channel electrodes with the aim of gaining more information about the coupled kinetics involved and the standard electrochemical rate constant for the initial reduction step. Any significant effects brought about due to the differences in the metal electrodes are discussed.

7.2 General Experimental Details

The experimental details of the high speed channel flow cell were described in chapters 1 and 3. The microband electrodes were made from a Pt foil strip (Goodfellow Metals, Cambridge) and a Au foil strip (Goodfellow Metals, Cambridge) using the method described previously. A Topometrix atomic force microscope was used to measure the precise dimensions of the electrodes; 40 μm length (x_e) and 0.94 mm width (w) for the Pt electrode and 25 μm length (x_e) and 1.04 mm width (w) for the Au electrode. Solutions of nitromethane (1.5 mM) were prepared with pHs ranging from 6.0 to 9.0 using the buffers given in section 3.9.

7.3 Theory

In this section the voltammetric theory for a heterogeneous ECE reaction is developed

to enable the simulation of voltammetric waves produced at a channel electrode. As with the previous two chapters the heterogeneous ECE reaction pathway shown below is considered.

E A ± e^- ⇌ B

C B → C

E C ± e^- ⇌ products

The steady-state convective-diffusion equations describing the distributions of species A and B at a channel electrode are:

$$\frac{\partial[A]}{\partial t} = 0 = D_A \frac{\partial^2[A]}{\partial x^2} + D_A \frac{\partial^2[A]}{\partial y^2} - \nu_x \frac{\partial[A]}{\partial x} \qquad (7.1)$$

$$\frac{\partial[B]}{\partial t} = 0 = D_B \frac{\partial^2[B]}{\partial x^2} + D_B \frac{\partial^2[B]}{\partial y^2} - \nu_x \frac{\partial[B]}{\partial x} \qquad (7.2)$$

where D_a and D_B are the diffusion coefficients of species A and B respectively, ν_x is the solution viscosity in the x-direction and the co-ordinates x and y are defined in figure 1.1.

In this chapter it is assumed that the Butler-Volmer kinetics, described in chapter 2, apply to the charge transfer reaction at the electrode surface so that, considering a reduction process,

$$A + e^- \underset{k_b}{\overset{k_f}{\rightleftharpoons}} B \qquad (7.3)$$

The electrochemical rate constants are given by:

$$k_f = k_s \exp(-\alpha\theta) \qquad (7.4)$$

and

$$k_b = k_s \exp(+\beta\theta) \qquad (7.5)$$

where the dimensionless electrode potential is defined in equation (7.6).

$$\theta = (F/RT)(E-E^{0'}) \qquad (7.6)$$

E is the electrode potential, $E^{0'}$ is the formal potential of the A/B redox couple and α and β are transfer coefficients, discussed in chapter 2. The formal potential, $E^{0'}$, is related to the standard electrode potential, E^0, by the equation below:

$$E^{0'} = E^0 - \frac{RT}{F}\ln\frac{\gamma_B}{\gamma_A} \qquad (7.7)$$

where γ_A and γ_B are the activity coefficients for species A and B respectively. E^0 assumes that the solution under investigation is behaving ideally which is not the case experimentally hence $E^{0'}$ is quoted for the data investigated in this chapter.

The Butler-Volmer expressions given above are significant when considering voltammetric waveshapes as the shape of a voltammogram obtained at a channel electrode is dependent on the reversibility of the electron transfer step. The wave becomes stretched along the potential axis with increasing irreversibility, as k_s becomes smaller shown below in figure 7.1.

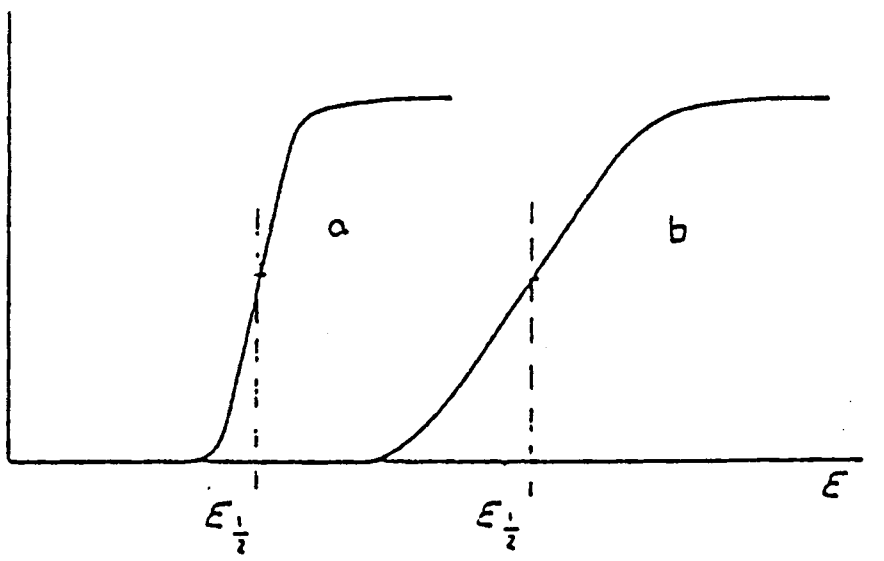

Figure 7.1. *Hydrodynamic voltammograms for (a) a reversible reduction, large k_s and (b) an irreversible reduction, small k_s.*

As the transport limiting current remains constant, the irreversibility of a voltammetric wave can be quantified by the dimensionless half-wave potential:

$$\theta_{1/2} = (F/RT)(E_{1/2}-E^{0'}) \qquad (7.8)$$

The reversibility of the electron transfer step involved in a heterogeneous reaction is incorporated in the boundary conditions for the electrode surface using the equation below where the flux of species A to the electrode surface is expressed by:

$$y = 0, \quad 0 < x < x_e, \qquad D_A \frac{\partial[A]}{\partial y} = k_f[A]_{y=0} - k_b[B]_{y=0} \qquad (7.9)$$

The other boundary conditions for the species considered for a heterogeneous ECE reaction are given in the previous chapter in equations (6.3) - (6.5).

Using the boundary condition above and those given in chapter 6 the mass transport equations (7.1) and (7.2) can be solved by the direct application of the finite difference method described in chapter 5.

In this chapter computer programs written by Dr. John Alden were used to simulate steady-state voltammetric waves for a heterogeneous ECE reaction. The programs involved 1000 grid points over the electrode length and 500 over the fraction of the total channel depth which correspond to no less than the maximum size of the diffusion layer thickness. Voltammograms were computed for a range of rate constants, k_{het} and k_s, by systematically changing the electrode potential θ for different channel electrode geometries. The electrode currents flowing under the various conditions were evaluated using the current expression given in equation (7.10).

$$I(\theta) = Fw\int_0^{x_e} D\frac{\partial[A]}{\partial y} + k_{het}[B]_{y=0}\,dx \qquad (7.10)$$

The current for an ECEEE process is modified to:

$$I(\theta) = Fw\int_0^{x_e} D\frac{\partial[A]}{\partial y} + 3k_{het}[B]_{y=0}\,dx \qquad (7.11)$$

7.4 Development of a Working Surface Showing the Variation of the Dimensionless Half-Wave Potential ($\theta_{1/2}$) with the Dimensionless Heterogeneous Rate Constant (K_{het}) and the Dimensionless Standard Electrochemical Rate Constant (K_s)

In this section the theory discussed above for a heterogeneous ECE (and ECEEE) mechanism is developed further to enable a working surface showing the variation of $\theta_{1/2}$ with K_{het} and K_s to be developed.

7.4.1 Dependence of the Dimensionless Half-Wave Potential ($\theta_{1/2}$) on the Dimensionless Heterogeneous Rate Constant (K_{het}) and the Dimensionless Standard Electrochemical Rate Constant (K_s)

In general the flux of species A to the electrode surface can be described using the boundary condition given in equation (7.9) as shown below:

$$\left.\frac{\partial[A]}{\partial y}\right|_{\xi=0} = k_f[A]_{y=0} - k_b[B]_{y=0} + K_{het}[B]_{y=0} \qquad (7.12)$$

Using the normalised parameters ξ and K_{het} defined by equations (6.7) and (6.8) in chapter 6, equation (7.12) can be written as:

$$\left.\frac{\partial[A]}{\partial \xi}\right|_{\xi=0} = \frac{1}{D}\left(\frac{2V_0}{Dhx_e}\right)^{-1/3}\left[k_f[A]_{y=0} - k_b[B]_{y=0}\right] + K_{het}[B]_{y=0} \qquad (7.13)$$

Substituting for equations (7.4) and (7.5) defined previously gives:

$$\left.\frac{\partial[A]}{\partial\xi}\right|_{\xi=0} = k_s\left(\frac{hx_e}{2V_0D^2}\right)^{1/3}\left[e^{-\alpha\theta}[A]_{y=0} - e^{+\beta\theta}[B]_{y=0}\right] + K_{het}[B]_{y=0} \qquad (7.14)$$

By defining K_s as

$$K_s = k_s\left(\frac{hx_e}{2V_0D^2}\right)^{1/3} \qquad (7.15)$$

the expression then becomes

$$\left.\frac{\partial[A]}{\partial\xi}\right|_{\xi=0} = K_s\left(e^{-\alpha\theta}[A]_{\xi=0} - e^{+\beta\theta}[B]_{\xi=0}\right) + K_{het}[B]_{\xi=0} \qquad (7.16)$$

Looking at equation (7.16) it can be clearly seen that the concentration of species A, [A], is a function of χ, ξ, θ, K_{het} and K_s.

The effective number of electrons transferred for a heterogeneous ECEEE reaction at the half-wave potential (n_{eff}) is equal to $N_{eff}/2$ which can be expressed using equation (7.17):

$$\frac{N_{eff}}{2} = \frac{\text{I at half - wave potential}}{\text{Transport limited I (at infinite } \theta)} = \frac{\left[\int_0^1 \left.\frac{\partial[A]}{\partial\xi}\right|_{\xi=0} d\chi + 3\int_0^1 K_{het}[B]_{\xi=0}\, d\chi\right]_{\theta_{1/2}}}{\left[\int_0^1 \left.\frac{\partial[A]}{\partial\xi}\right|_{\xi=0} d\chi + 3\int_0^1 K_{het}[B]_{\xi=0}\, d\chi\right]_{\theta\to\infty}} \qquad (7.17)$$

where N_{eff} is the effective number of electrons transferred for the whole wave and I is the current at the relevant point on the wave.

As

$$\int_0^1 \left.\frac{\partial[A]}{\partial\xi}\right|_{\xi=0} d\chi = \int_0^1 [K_s(e^{-\alpha\theta}[A]_{\xi=0} - e^{+\beta\theta}[B]_{\xi=0}) + K_{het}[B]_{\xi=0}]d\chi \qquad (7.18)$$

or at the half-wave potential:

$$\int_0^1 \left.\frac{\partial[A]}{\partial\xi}\right|_{\xi=0} d\chi = \int_0^1 [K_s(e^{-\alpha\theta_{1/2}}[A]_{\xi=0} - e^{+\beta\theta_{1/2}}[B]_{\xi=0}) + K_{het}[B]_{\xi=0}]d\chi \qquad (7.19)$$

it can be seen that $\frac{N_{eff}}{2}$ is a function of $\theta_{1/2}$, K_{het} and K_s only as [A] and [B] are only dependent on χ, ξ, θ, K_{het} and K_s and integration removes the dependence on χ and ξ. Therefore a function of $\theta_{1/2}$, K_{het} and K_s , $f(\theta_{1/2}, K_{het}, K_s)$ can be defined:

$$f(\theta_{1/2}, K_{het}, Ks) = \frac{\int_0^1 [K_s(e^{-\alpha\theta_{1/2}}[A]_{\xi=0} - e^{+\beta\theta_{1/2}}[B]_{\xi=0}) + K_{het}[B]_{\xi=0}]d\chi + 3\int_0^1 K_{het}[B]_{\xi=0}\,d\chi}{\left[\int_0^1 [K_s(e^{-\alpha\theta_{1/2}}[A]_{\xi=0} - e^{+\beta\theta_{1/2}}[B]_{\xi=0}) + K_{het}[B]_{\xi=0}]d\chi + 3\int_0^1 K_{het}[B]_{\xi=0}\,d\chi\right]_{\theta\to\infty}} - \frac{N_{eff}}{2} = 0. \qquad (7.20)$$

From $f(\theta_{1/2}, K_{het}, K_s) = 0$ it is evident that $\theta_{1/2}$ is a function of K_{het} and K_s only.

The derivation above demonstrates that for conditions in which the Lévêque approximation[5] holds $E_{1/2}$ is a function of K_{het} and K_s only. Hence analysis of $E_{1/2}$ data from channel electrode experiments should enable values for K_{het} and K_s for a heterogeneous ECEEE reaction to be calculated. It follows that the reaction rate constants k_{het} and k_s may be deduced.

7.4.2 Generation of the Working Surface

Using the theory developed in section 7.3, $\theta_{1/2}$ values were generated for a range of K_{het} and K_s values resulting in the working surface shown in figure 7.2. Looking at figure 7.2 it can be seen that in the case of a reduction, at sufficiently large values of K_s (corresponding to electrochemically reversible conditions) the effect of the following chemical step is to shift the half-wave potential to less negative potentials than the formal potential ($E^{0'}$). However, as the value of K_s is decreased, the effect of the following kinetics (in comparison to the

situation of no heterogeneous kinetics) becomes less and less. In particular, when the limit of essentially irreversible electrochemical kinetics ($K_s << 1$) is reached, the observed half-wave potential is entirely insensitive to the surface catalysed loss of B and, as expected, occurs at overpotentials negative of $E^{0'}$.

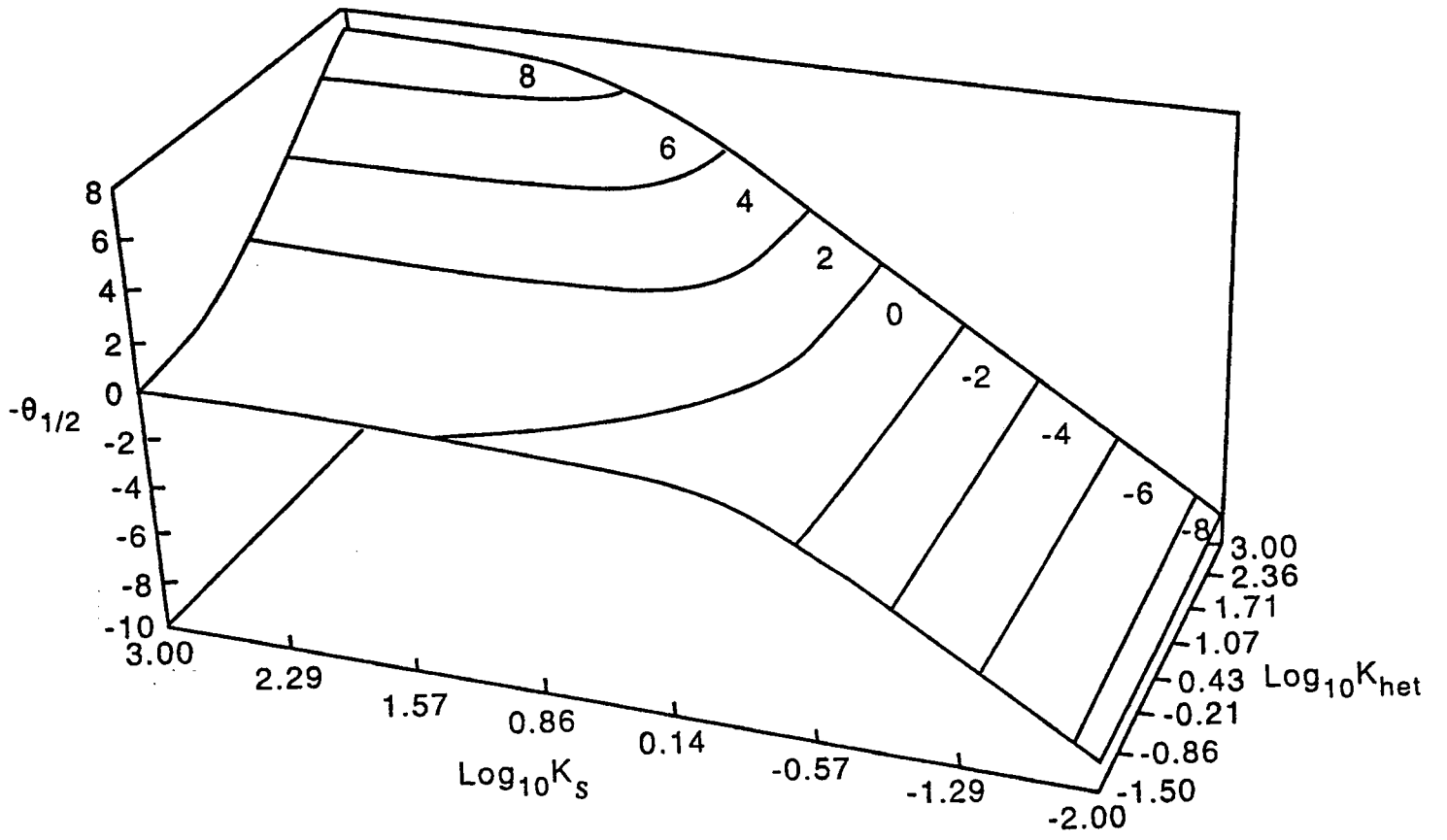

Figure 7.2. Working surface showing the variation of $\theta_{1/2}$ with the dimensionless rate constants K_{het} and K_s.

7.5 Development of a Working Surface Showing the Variation of the Tafel Slope with the Dimensionless Heterogeneous Rate Constant (K_{het}) and the Dimensionless Standard Electrochemical Rate Constant (K_s)

In this section the theory discussed in section 7.3 is developed further to enable a working surface showing the variation of the Tafel slope with K_{het} and K_s to be developed.

---

5 M. Lévêque, *Ann. Mines Mem. Ser.*, **12/13**, (1928), 201

The use of the Tafel law when investigating the rate of electron transfer was introduced in chapter 2. Analysis of hydrodynamic voltammograms for a simple one electron process at a uniformly accessible electrode shows that for an irreversible (small k_s) electron transfer the reductive case is given by:

$$-\log\left(\frac{1}{I}-\frac{1}{I_{lim}}\right)=-\frac{\alpha FE}{RT}+c \qquad (7.21)$$

similarly for an oxidation:

$$-\log\left(\frac{1}{I}-\frac{1}{I_{lim}}\right)=\frac{\beta FE}{RT}+c \qquad (7.22)$$

where I_{lim} is the transport limiting current. Hence the slope of a Tafel plot, which displays the potential (E) against $\log\left(\frac{1}{I}-\frac{1}{I_{lim}}\right)$ is:

$$\left[\frac{dE}{d\left(\log\left(\frac{1}{I}-\frac{1}{I_{lim}}\right)\right)}\right] \qquad (7.23)$$

Similarly using the dimensionless half-wave potential defined in equation (7.8) the Tafel slope can be written as:

$$\left[\frac{d\theta}{d\left(\log\left(\frac{1}{I}-\frac{1}{I_{lim}}\right)\right)}\right] \qquad (7.24)$$

Therefore the variation in the Tafel slope would be expected to be an indication of at least the value of k_s and will be shown in the following theory to also have a dependence on k_{het} for the heterogeneous ECEEE reaction considered.

7.5.1 Dependence of the Tafel Slope on the Dimensionless Heterogeneous Rate Constant (K_{het}) and the Dimensionless Standard Electrochemical Rate Constant (K_s)

Using equations (7.18) and (7.19) defined previously the Tafel parameter can be written as[6]:

$$\log\left(\frac{I_{lim}}{I}-1\right)=\log\left[\frac{\left[\int_0^1[K_s(e^{-\alpha\theta}[A]_{\xi=0}-e^{+\beta\theta}[B]_{\xi=0})+K_{het}[B]_{\xi=0}]d\chi+3\int_0^1 K_{het}[B]_{\xi=0}\,d\chi\right]_{\theta\to\infty}}{\left[\int_0^1[K_s(e^{-\alpha\theta}[A]_{\xi=0}-e^{+\beta\theta}[B]_{\xi=0})+K_{het}[B]_{\xi=0}]d\chi+3\int_0^1 K_{het}[B]_{\xi=0}\,d\chi\right]}-1\right] \quad (7.25)$$

Hence it can be seen that $\log\left(\frac{I_{lim}}{I}-1\right)$ is a function of θ, K_{het} and K_s and therefore the slope of a Tafel plot relating θ to $\log\left(\frac{I_{lim}}{I}-1\right)$ will only be dependent on K_{het} and K_s. This result suggests that further information about K_{het} and K_s could be deduced from the Tafel slope analysis of voltammetric waves generated at a channel electrode.

7.5.2 Generation of the Working Surface

Using the theory developed in section 7.3 Tafel slope values were generated for a range of K_{het} and K_s values resulting in the working surface shown in figure 7.3.

---

6 $$\log\left[\frac{I_{lim}}{I}-1\right]=\log\left(\left[\frac{1}{I}-\frac{1}{I_{lim}}\right]I_{Lim}\right)=\log\left[\frac{1}{I}-\frac{1}{I_{lim}}\right]+\log I_{lim}$$

$$\therefore \frac{dE}{d\log\left[\frac{I_{lim}}{I}-1\right]}=\frac{dE}{d\log\left[\frac{1}{I}-\frac{1}{I_{lim}}\right]}$$

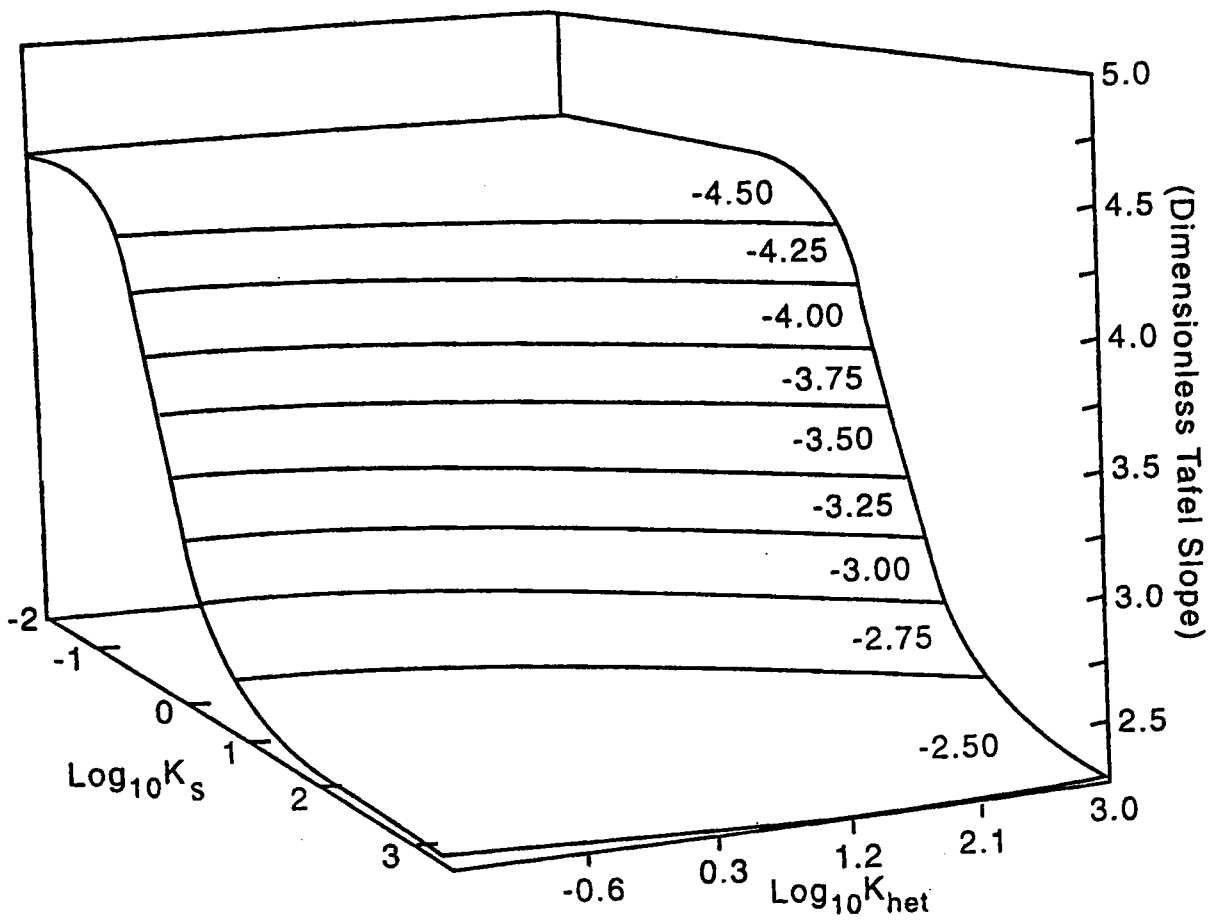

Figure 7.3. Working surface showing the variation of the Tafel slope with the dimensionless rate constants K_{het} and K_s.

Figure 7.3 shows that at low values of K_s larger values for the Tafel slope are seen, as expected for an electrochemically irreversible process at a channel electrode[7]. As K_s increases the Tafel slope drops to that corresponding to an electrochemically reversible charge transfer and in this limit the Tafel slope is again independent of K_s. However, the value of K_s required in order to observe an electrochemically reversible charge transfer is greater when appreciable heterogeneous kinetics are present due to the loss of species B through chemical reaction at the electrode surface. An implication of this is that a redox couple, which has a K_s value sufficiently high to give rise to electrochemical reversibility under given mass transport conditions, can appear to be electrochemically irreversible if the electrode surface is highly efficient towards the decomposition of B.

---

7 M. J. Bidwell, J. A. Alden and R. G. Compton, *J. Electroanal. Chem.*, **417**, (1996), 119

Figures 7.2 and 7.3 together with the working curve relating the effective number of electrons transferred under mass transport limited conditions to K_{het} for a heterogeneous ECE mechanism, developed in chapter 5, permit the qualitative analysis of experimental data for such processes. In particular it is hoped that mutually consistent values of K_{het} can be obtained from such current and waveshape data analysis so providing a strong indication of the veracity of the mechanistic assignment. This is investigated further in the following section in which experiments carried out on the reduction of aqueous solutions of nitromethane at a channel electrode are analysed using the working surfaces developed above with the aim of gaining further insight into the mechanism involved.

7.6 High Speed Channel Investigations of Nitromethane at a Pt Electrode

Steady-state experiments were conducted on the reduction of nitromethane (1.5mM) in aqueous solution (7 $0 < pH < 9.0$) using a 40 μm Pt microband electrode in the high speed channel flow cell described previously. Voltammograms were recorded over a range of flow rates from 0.03 to 2.5 cm s^{-1} with half-wave potentials in the range of (-0.75) - (-0.85) V (vs. Pt pseudo-reference electrode) with no systematic change with pH.

7.6.1 Analysis of the Limiting Current Flow Rate Data

Initially analysis of the limiting current flow rate data obtained for the reduction of nitromethane at the Pt electrode was carried out using the theory developed in chapters 5 and 6. The limiting flow rate data for pHs 7.0 - 9.0 along with the best fit k_{het} value calculated form the theory developed previously is shown in figures 7.4(a) - (e).

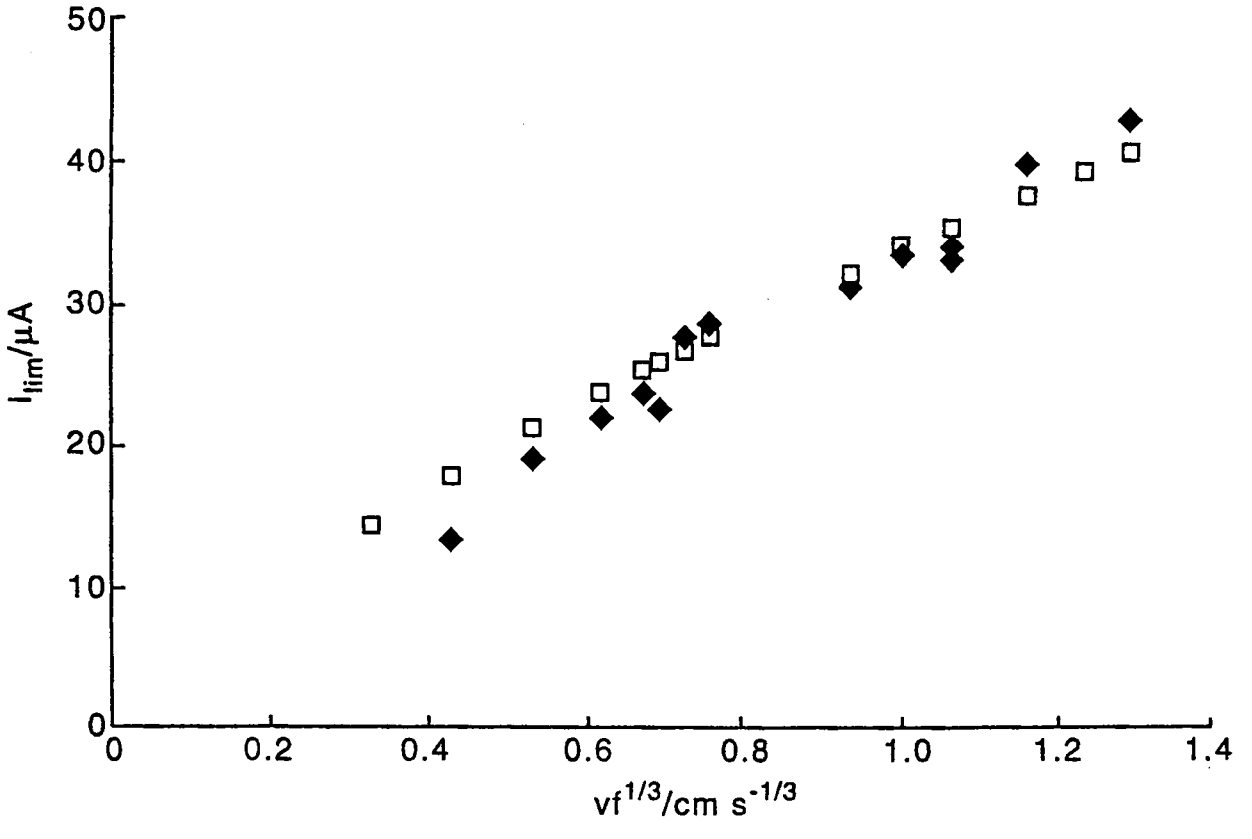

Figure 7.4(a). The variation of the transport limited current with the electrolyte flow rate as measured (♦) in buffered solution of pH 7.0. The open symbols (□) show the behaviour simulated for an ECEEE mechanism using the best fit value of 0.24 cm s^{-1} for k_{het}.

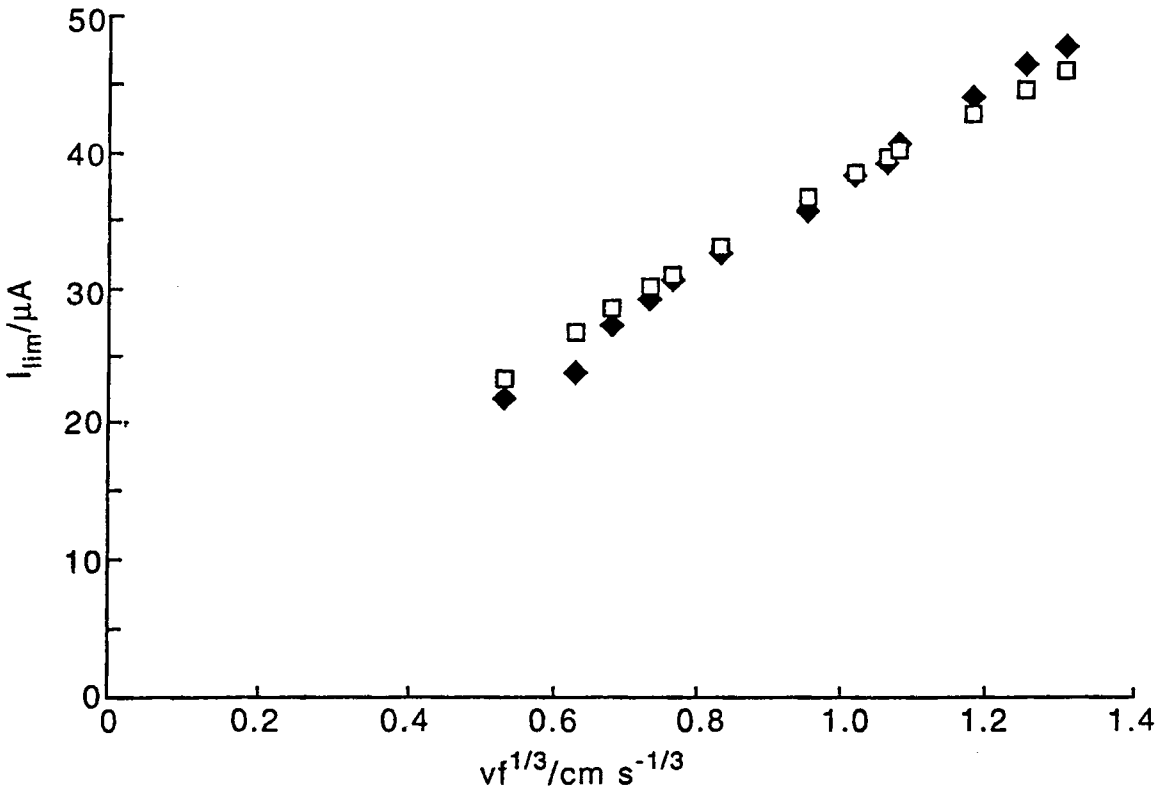

Figure 7.4(b). The variation of the transport limited current with the electrolyte flow rate as measured (♦) in buffered solution of pH 7.5. The open symbols (□) show the behaviour simulated for an ECEEE mechanism using the best fit value of 0.36 cm s^{-1} for k_{het}.

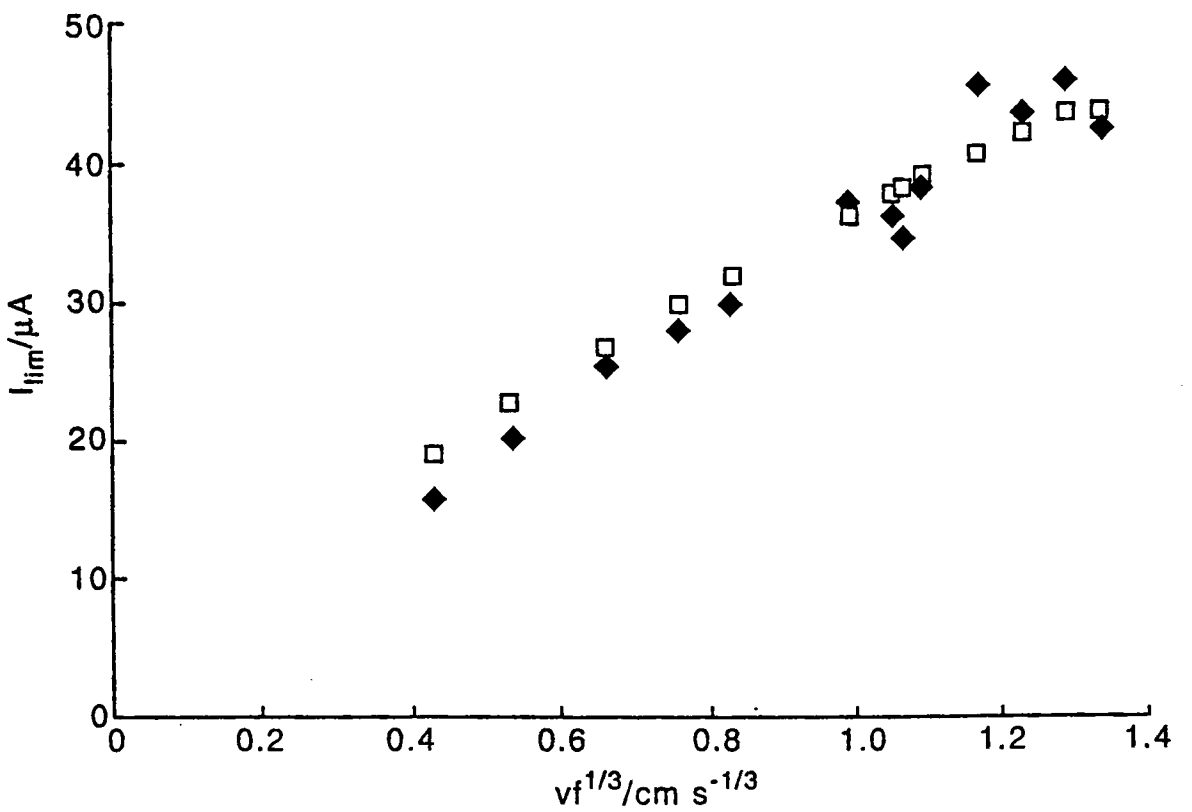

Figure 7.4(c). *The variation of the transport limited current with the electrolyte flow rate as measured (♦) in buffered solution of pH 8.0. The open symbols (□) show the behaviour simulated for an ECEEE mechanism using the best fit value of 0.32 cm s^{-1} for k_{het}.*

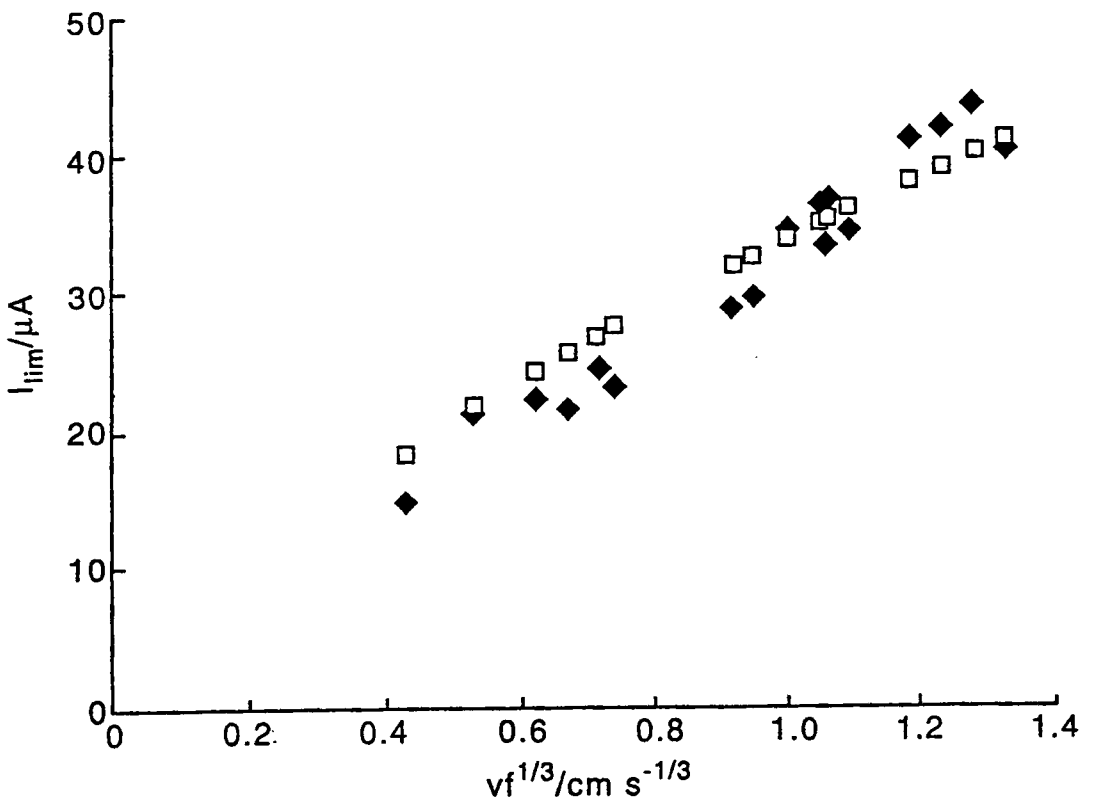

Figure 7.4(d). *The variation of the transport limited current with the electrolyte flow rate as measured (♦) in buffered solution of pH 8.5. The open symbols (□) show the behaviour simulated for an ECEEE mechanism using the best fit value of 0.24 cm s^{-1} for k_{het}.*

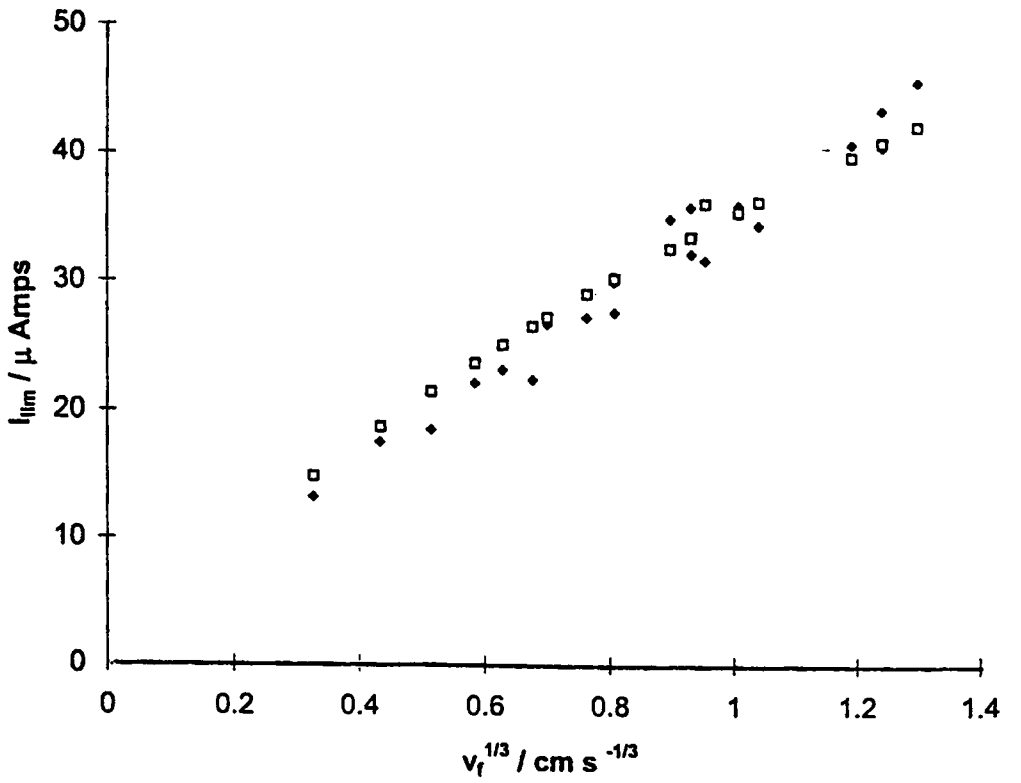

Figure 7.4(e). *The variation of the transport limited current with the electrolyte flow rate as measured (♦) in buffered solution of pH 9.0. The open symbols (□) show the behaviour simulated for an ECEEE mechanism using the best fit value of 0.28 cm s^{-1} for k_{het}.*

Looking at figures 7.4(a) - (e) it can be seen that the heterogeneous rate constants k_{het} lie between 0.24 and 0.36 cm s^{-1} and display no systematic trend with pH. It should be noted that as with the limiting current data obtained at a Hg/Cu electrode presented in chapter 6 the approximate linear dependence of the transport limiting current with flow rate is strong evidence for a heterogeneous as opposed to homogeneous rate determining chemical step.

7.6.2 Analysis of the Tafel Slope Data

In order to carry out an independent check on the heterogeneous rate constants obtained from the current flow rate data, Tafel slopes were measured for all of the voltammetric waves by evaluating the expression in equation (7.24) from plots of E against $\log(\frac{1}{I} - \frac{1}{I_{lim}})$. Good linear plots were found in all cases as typified by the data in figure 7.5.

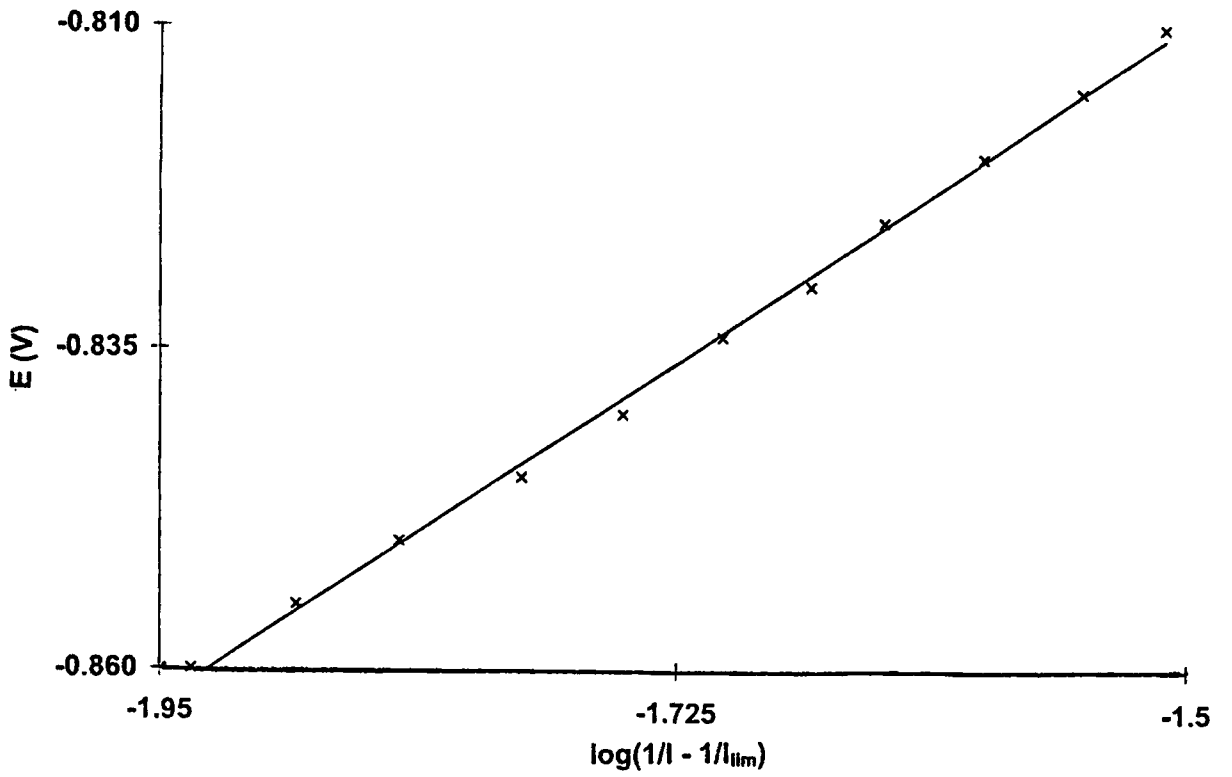

Figure 7.5(a). A Tafel plot recorded at a flow rate of 0.57 $cm^3 s^{-1}$ for a solution of pH 8.0.

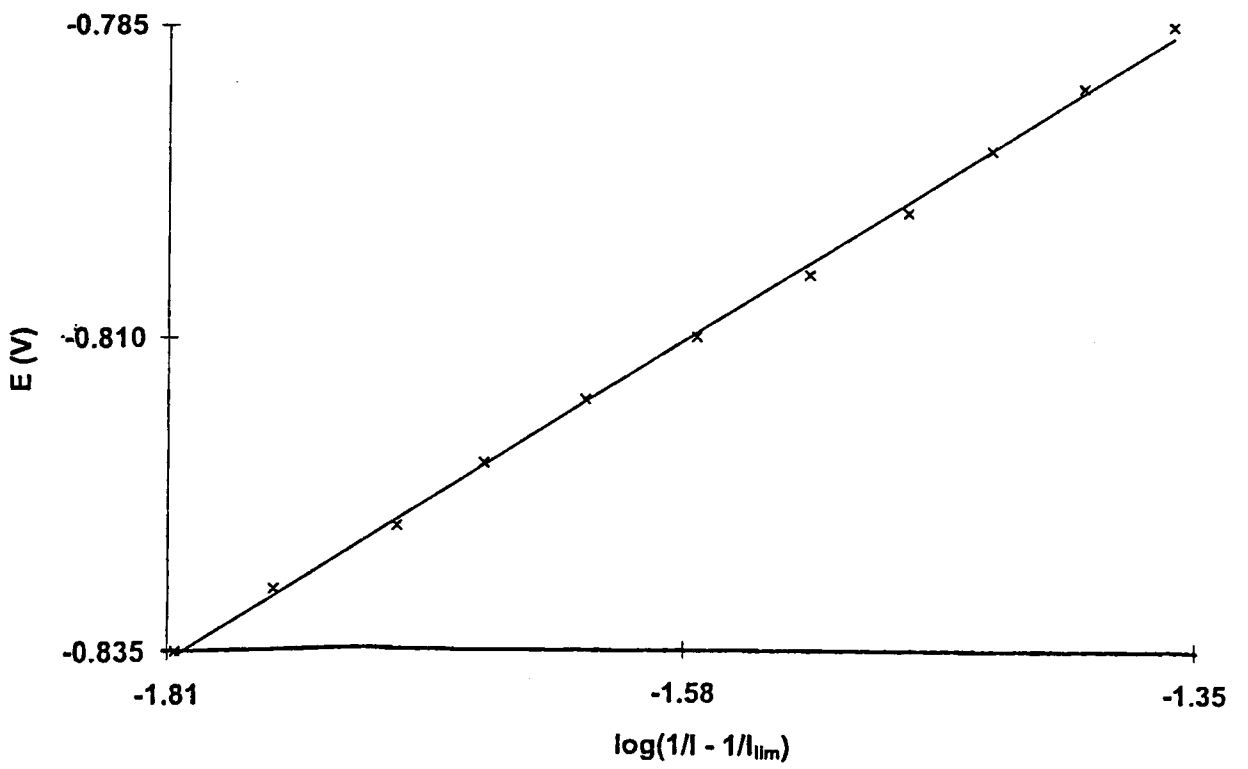

Figure 7.5(b). A Tafel plot recorded at a flow rate of 0.079 $cm^3 s^{-1}$ for a solution of pH 8.0.

The Tafel plots generated for the voltammetric waves recorded at the high speed channel electrode were analysed in terms of a simple quasi-reversible E process using the relevant theory for a channel electrode[7]. The values of k_s obtained from the analysis were found to systematically increase in size at higher flow rates, as shown in figure 7.6. However, when the analysis of the Tafel plots was conducted using the working curve developed in section 7.5 for a heterogeneous ECEEE process using the values of k_{het} gained from the transport limiting current data, the values of k_s were found to be independent of the flow rate. These consistencies provide strong evidence that the mechanism is indeed of the heterogeneous type. Sample values showing the variation in k_s with flow rate for the E and the heterogeneous ECEEE mechanism are displayed in table 7.1.

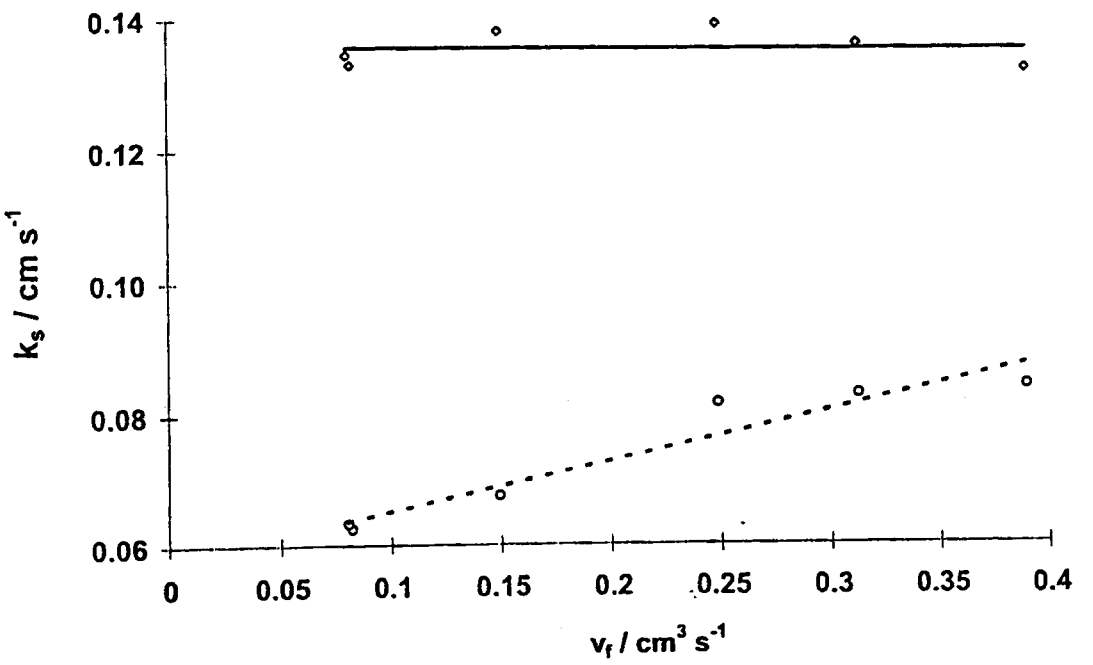

Figure 7.6(a). Dependence of k_s on flow rate as analysed for a simple E process (----) and a heterogeneous ECEEE process (—) at pH (7.0), k_{het} = 0.24 cms^{-1}.

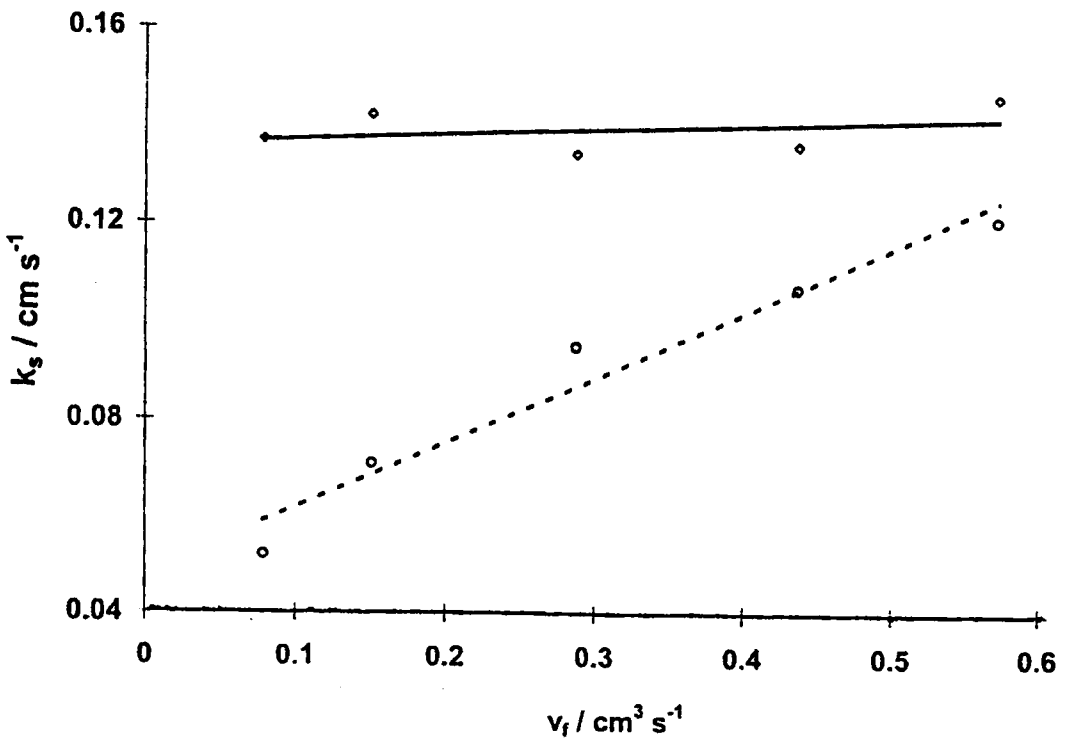

Figure 7.6(b). Dependence of k_s on flow rate as analysed for a simple E process (----) and a heterogeneous ECEEE process (—) at pH (8.0).

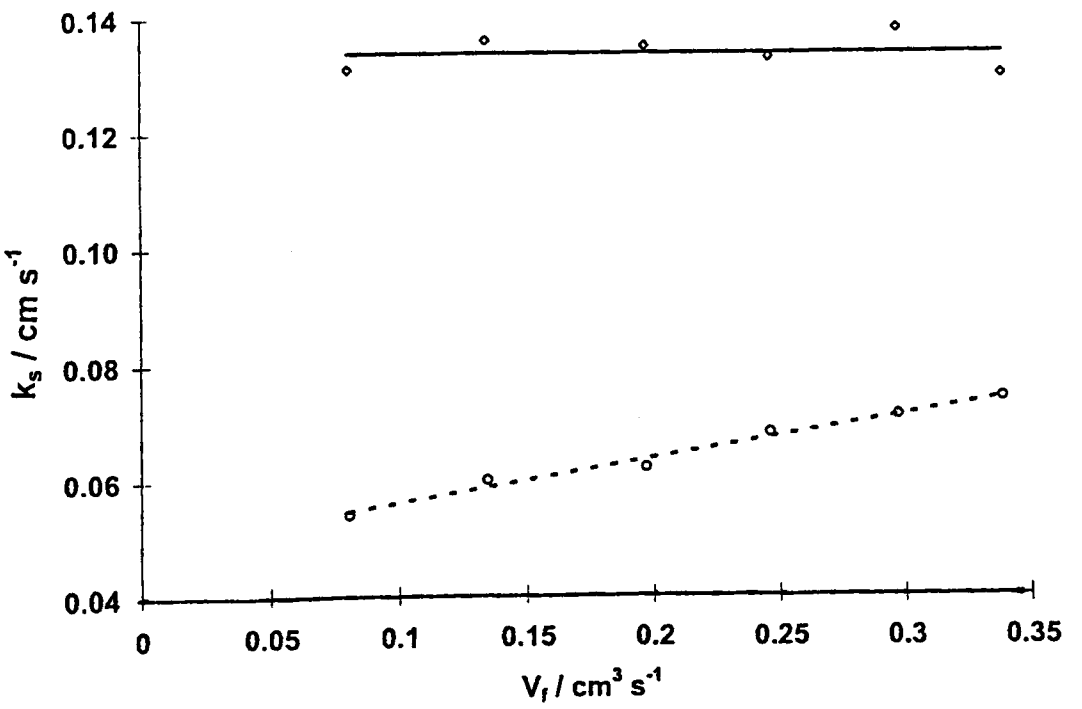

Figure 7.6(c). Dependence of k_s on flow rate as analysed for a simple E process (----) and a heterogeneous ECEEE process (—) at pH (9.0).

	pH = 7.0			**pH = 8.0**	
v_f / $cm^3 s^{-1}$ (± 0.001)	E k_s (± 0.001)/ cm s^{-1}	$Ec_{het}EEE$ k_s (± 0.001)/ cm s^{-1}	V_f/ $cm^3 s^{-1}$ (± 0.001)	E k_s (± 0.001)/ cm s^{-1}	$Ec_{het}EEE$ k_s (± 0.001)/ cm s^{-1}
0.390	0.079	0.127	0.571	0.121	0.146
0.312	0.078	0.131	0.436	0.107	0.136
0.249	0.072	0.134	0.287	0.095	0.134
0.149	0.063	0.133	0.151	0.071	0.142
0.082	0.058	0.128	0.079	0.052	0.137

Table 7.1. A summary of the Tafel analysis data obtained for pH 7.0 and 8.0.

The Tafel slope data was analysed for pHs 7.0, 8.0 and 9.0 resulting in the k_s values of 0.130, 0.139 and 0.134 cm s^{-1} respectively with a mean values of k_s calculated as 0.134 cm s^{-1}.

7.6.3 The Variation of the Half-Wave Potential with the Solution Flow Rate

The final analysis carried out on the high speed channel data recorded for the reduction of nitromethane at a Pt electrode was the variation of the half-wave potentials with the solution flow rate. The recorded voltammograms showed half-wave potentials in the range -0.75 - -0.85 V (vs. pseudo reference electrode) with no systematic change in pH. The values of k_{het} and k_s generated from the limiting current and Tafel slope analyses were used to simulate the flow rate dependence of the half-wave potential. The fits obtained enabled the deduction of a mean value of -0.87 ± 0.05 V (vs. Pt pseudo reference electrode) for the formal potential, $E^{0'}$, of the CH_3NO_2/ $[CH_3NO_2]^{\bullet-}$ redox couple.

7.7 High Speed Channel Investigations of Nitromethane at a Au electrode

After investigating the reduction of nitromethane at a Pt electrode similar steady-state experiments were then carried out at a Au electrode. The experiment was conducted using a (1.5 mM) aqueous solution of nitromethane at pH 6.0 under conditions described previously. The data analysis process used was the same carried out for the Pt electrode investigations.

7.7.1 Analysis of the Limiting Current Flow Rate Data

Initially analysis of the limiting current flow rate data obtained for the reduction of nitromethane at the Au electrode was carried out using the theory developed in chapters 5 and 6. The best fit k_{het} value calculated form the theory developed previously is shown in figure 7.7.

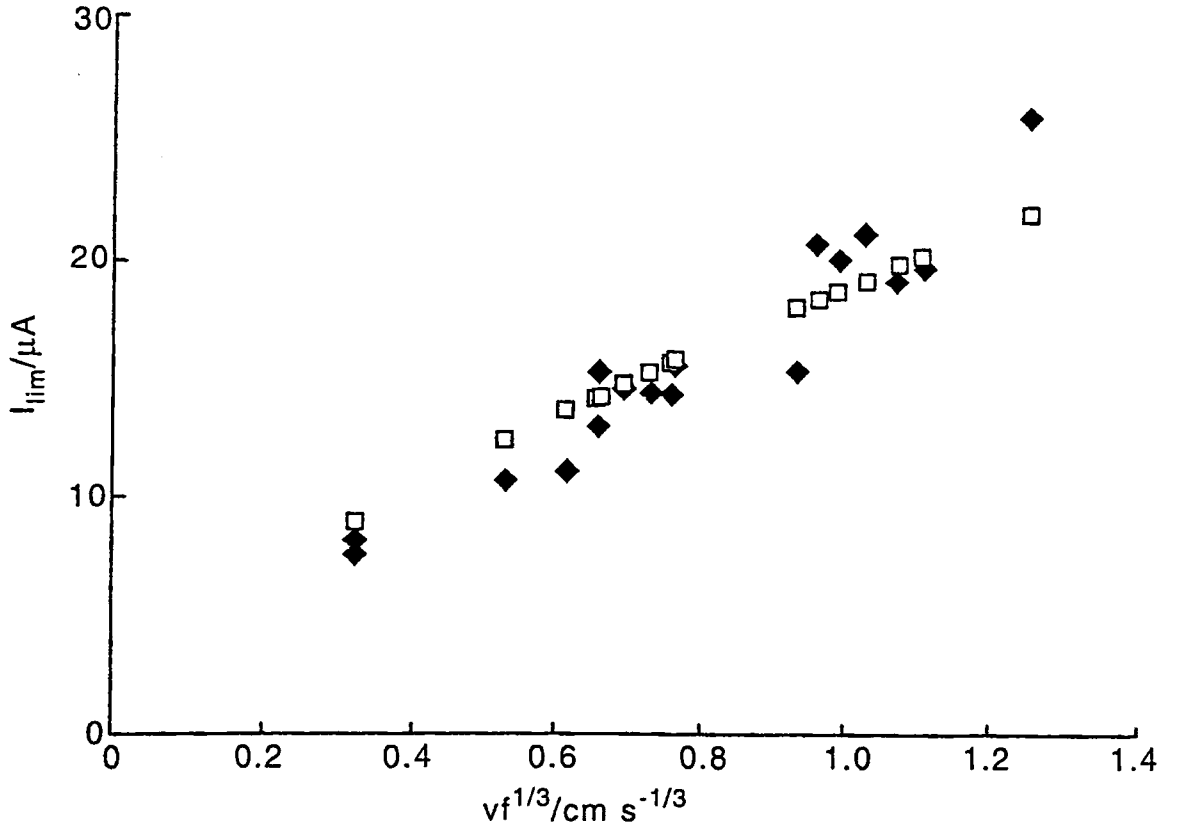

Figure 7.7. *The variation of the transport limited current with the electrolyte flow rate as measured (♦)in buffered solution of pH 6.0. The open symbols (□) show the behaviour simulated for an ECEEE mechanism using the best fit value of 0.095 cm s^{-1} for k_{het}.*

As discussed for the Pt electrode data analysis the approximately linear dependence of the transport limited currents with the cube root of the flow rate is again evidence for a heterogeneous as opposed to homogeneous rate determining chemical step.

7.7.2 Analysis of the Tafel Slope Data

The k_{het} value deduced in the previous section was employed in order to calculate the optimum value for k_s as described for the case of the Pt electrode. Analysis of the Tafel slope gave a value of 0.196 ± 0.001 cm s^1 for k_s and the variation of k_s with flow rate is shown in figure 7.8. The plots show that the best fit values of k_s are independent and unchanging with flow rate over the range examined for the heterogeneous ECEEE process, whereas as with the Pt data the E analysis shows a strong flow rate dependence. These provide strong evidence that the mechanism is indeed of the $EC_{het}EEE$ type.

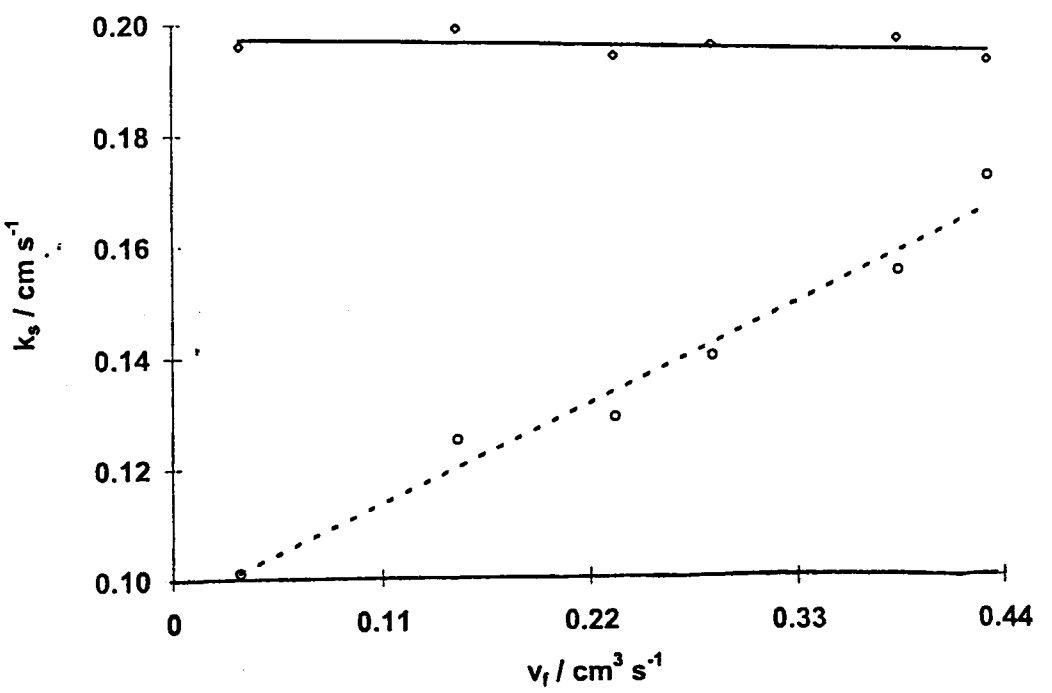

Figure 7.8. *Dependence of k_s on flow rate as analysed for a simple E process (----) and a heterogeneous ECEEE process (—) at pH (6.0).*

7.7.3 The Variation of the Half-Wave Potential with the Solution Flow Rate

A half-wave of -0.87 ± 0.01 V (vs. a Pt pseudo-reference electrode) was deduced for the formal potential, $E^{0'}$, of the CH_3NO_2/ $[CH_3NO_2]^{\bullet-}$ redox couple at the Au electrode. This was achieved using the values of k_{het} and k_s generated in the previous two sections together with the working surface developed.

7.8 Conclusions

The work presented in this chapter has shown that heterogeneous ECE type processes can be voltammetrically well-characterised if both the flow rate dependence of the transport limited current and the Tafel slope are examined in parallel. Values of the heterogeneous rate constant, k_{het}, and the standard electrochemical rate constant, k_s can be deduced.

The reduction of nitromethane in aqueous solution in the pH range of 7.0 to 9.0 at Pt electrodes appears to follow a heterogeneous ECEEE mechanism with $k_s = 0.13 \pm 0.01$ cm s^{-1} and $k_{het} = 0.26 \pm 0.07$ cm s^{-1}. Similarly the reduction of nitromethane in aqueous solution at pH 6.0 at a Au electrode appears to follow a heterogeneous ECEEE mechanism with $k_s = 0.19 \pm 0.01$ cm s^{-1} and $k_{het} = 0.095 \pm 0.05$ cm s^{-1}. The overall mechanism is thus of the same type as determined at Hg electrodes and at Hg/Cu or Au/Hg electrodes discussed in the previous chapters.

Consideration of the values of k_{het} calculated for the reduction of nitromethane at different electrode surfaces shown in table 7.2 reveals a surprising independence of k_{het} on the chemical identity of the surface. This paradox, a surface indifferent heterogeneous reaction, will be addressed in the following chapter with the aid of kinetic isotope measurements.

Electrode	Hg - pH 8.3	Hg/Cu - pH 7.0	Au/Hg - 8.3	Pt - pH 8.0	Au - pH 6.0
k_{het}	0.06	0.18	0.06	0.32	0.095

Table 7.2. A summary of the k_{het} values obtained for the different electrode surfaces considered.

8. The Reduction of Nitromethane: A Surface Indifferent Electrocatalytic Reaction

Contents

The work presented in this chapter has been submitted for publication in J. Phys. Chem.

8.1 Introduction

In the previous chapter the reduction of nitromethane in aqueous solution at a Pt high speed channel electrode was investigated. Limiting current and Tafel slope analysis techniques were used to conclude that the reaction pathway follows a heterogeneous ECEEE mechanism with k_{het} values at pH 7.0, 8.0 and 9.0 found to be, 0.24, 0.32 and 0.28 cm s^{-1} respectively. This chapter probes the reduction of nitromethane at a Pt electrode further through the application of Pt single crystals (appendix 5) to cyclic voltammetry. Pt (100), (110) and (111) crystal planes are employed with the aim of determining any surface sensitivity of the ECEEE heterogeneous mechanism.

In chapters 5 - 7 the reduction of nitromethane in aqueous solution has been investigated at a diverse range of electrode materials including Au, Pt[1], Hg/Cu[2] and Hg/Au[3]. In all of these cases it was possible to measure the value of the heterogeneous rate constant, k_{het}, describing the chemical step in the reaction mechanism. For Pt in the pH range 7.0 - 9.0 this value was 0.3 ± 0.06 cm s^{-1}. For Hg/Cu it was 0.18 cm s^{-1}, for Au/Hg it was 0.06 cm s^{-1} and for Au it was 0.095 cm s^{-1}. Consideration of these values shows a surprising independence of the heterogeneous rate constant on the chemical identity of the surface with all of the values being similar to within less than an order of magnitude.

The possible reasons for the apparent paradox of the observed surface indifference of the electrocatalysis are considered in this chapter. Kinetic isotope measurements are investigated in order to gain further insight into the complex reduction pathway of nitromethane. High speed channel experiments involving the reduction of CD_3NO_2 in D_2O at a Pt electrode are

---

1 P. B. Mills, W. J. Aixill, F. Prieto, J. A. Alden, R. G. Compton and M. Rueda, *J. Phys. Chem.*, in press

2 W. J. Aixill, J. A. Alden, F. Prieto, G. A. Waller, R. G. Compton and M. Rueda, *J. Phys. Chem.*, **102**, (1998), 1515

compared to the isotopically light analogue reported in the previous chapter with the aim of determining a *conclusive description* of the complicated reaction mechanism for the reduction of nitromethane in aqueous solution and explaining the surface indifference.

8.2 General Experimental Details

Cyclic voltammetry was carried out at (100), (110) and (111) single crystal Pt electrodes supplied by Dr. Gary Attard (University of Cardiff). The experimental set-up is described in section 3.6. Solutions of 1.5 mM nitromethane at pH 8.0 were prepared using the buffer described in section 3.9.

The experimental details of the high speed channel flow cell were described in chapters 1 and 3. The microband electrode was made from a Pt foil strip (Goodfellow Metals, Cambridge) using the method described previously. A Topometrix atomic force microscope was used to measure the precise dimensions of the electrode; 40 μm length (x_e) and 0.94 mm width (w). Solutions of deuterated nitromethane (3.7 mM) were prepared from deuterium oxide with pHs of 8.5 and 9.0 using the buffers given in section 3.9.

8.3 Cyclic Voltammetry of Aqueous Sulphuric Acid

Prior to the cyclic voltammetry experiments carried out on nitromethane the surface integrity of the single crystals was verified using aqueous sulphuric acid as described in the following section.

---

[3] F. Prieto, R. D. Webster, J. A. Alden, W. J. Aixill, G. A. Waller, R. G. Compton and M. Rueda, *J. Electroanal. Chem.*, **437**, (1997), 183

8.3.1 Cyclic Voltammetry of Aqueous Sulphuric Acid at a Polycrystalline Pt Electrode

The electrochemistry of polycrystalline Pt in aqueous sulphuric acid is well established[4]. There are three main characteristic regions of a typical cyclic voltammogram for aqueous sulphuric acid that have been attributed to an oxygen species and two forms of hydrogen which adsorb onto the electrode surface with different strengths. After an initial activation procedure of rapidly cycling the potential between the oxide and the hydrogen regions the voltammogram reaches a stable state as shown in figure 8.1.

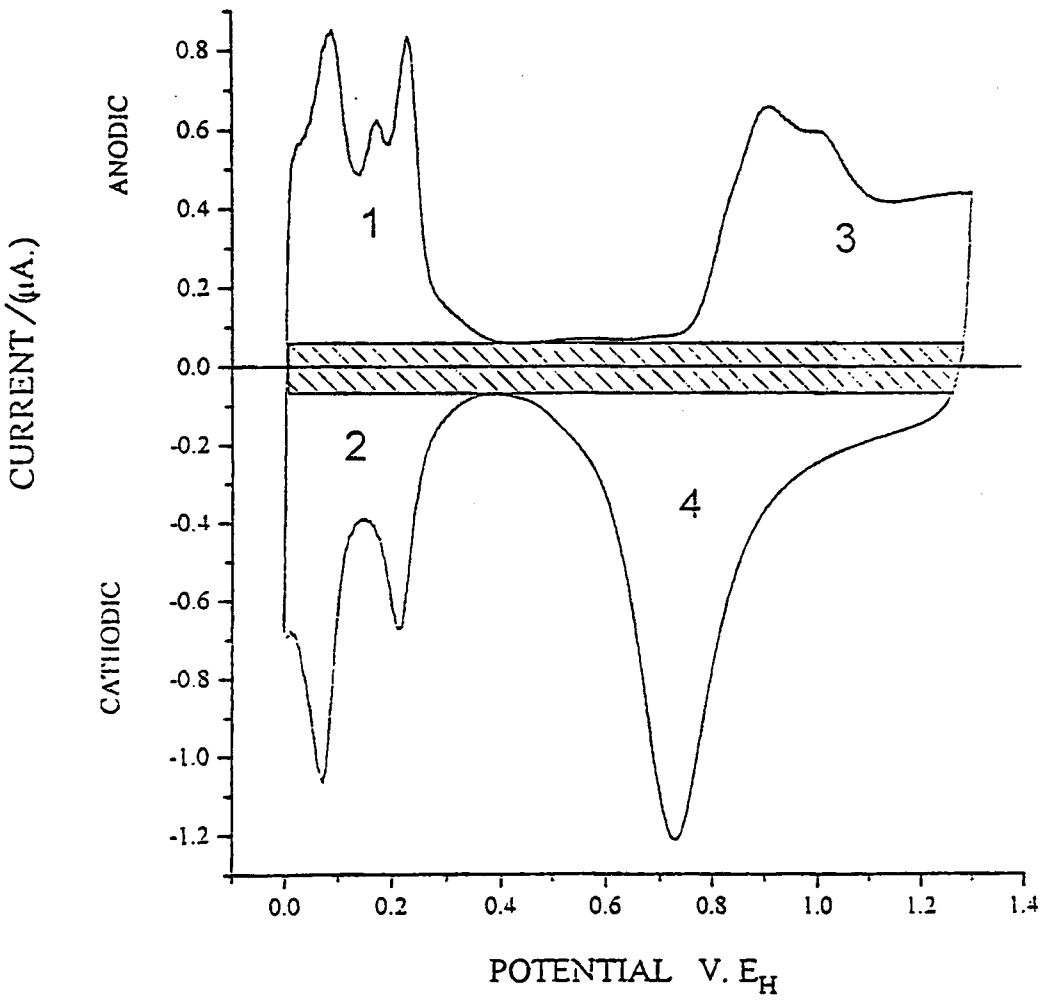

Figure 8.1. Cyclic Voltammogram of a Clean Polycrystalline Pt Electrode in 0.5 M H_2SO_4.

Each of the regions shown in figure 8.1 have been attributed as follows.

Regions 1 and 2 are due to the desorption and adsorption of hydrogen respectively. The symmetrical nature of the peaks indicates that the processes are reversible and the two

different peaks are due to the different types of hydrogen adsorbed. The peaks at the more negative potential correspond to the 'weakly' adsorbed hydrogen which has been shown to be at Pt(110) sites whereas the peaks at the more positive potential correspond to the 'strongly' adsorbed hydrogen, at Pt(100) sites.

Region 3 is due to the formation of a surface oxide:

$$H_2O \rightarrow OH_{ads} + H^+ + e^-$$

A place exchange then occurs between the Pt and the oxygen causing the oxygen atoms to become strongly chemisorbed.

Region 4 is due to the place-exchange oxide phase:

$$Pt - O + 2H^+ + 2e^- \rightarrow Pt + H_2O$$

The shaded area shown on figure 8.1 corresponds to charging of the electrical double layer.

8.3.2 Cyclic Voltammetry of Aqueous Sulphuric Acid at a Single Crystal Pt Electrode

In contrast to that of polycrystalline Pt, cyclic voltammetry at single crystal Pt surfaces has been the subject of considerable controversy. Clavilier at al.[5] proposed that the range of different peaks reported for the cyclic voltammetry of aqueous sulphuric acid at a Pt(111) electrode, the most sensitive of the single crystals used in this chapter, was due to the insufficient cleaning procedures employed. In order to overcome this problem Clavilier et al.[5] developed a novel surface preparation technique that involved annealing the single crystal in a Bunsen flame as described in chapter 3. This method was shown to produce the long range surface order required to produce the characteristic cyclic voltammetry for the relevant single

---

4 F. G. Will and C. F. Knorr, *Z. Electrochem.*, **64**, (1960), 258

crystals. The cyclic voltammograms for aqueous sulphuric acid at the (100), (110) and (111) Pt single crystals used in this chapter as established by Clavilier are shown in figure 8.2 [6].

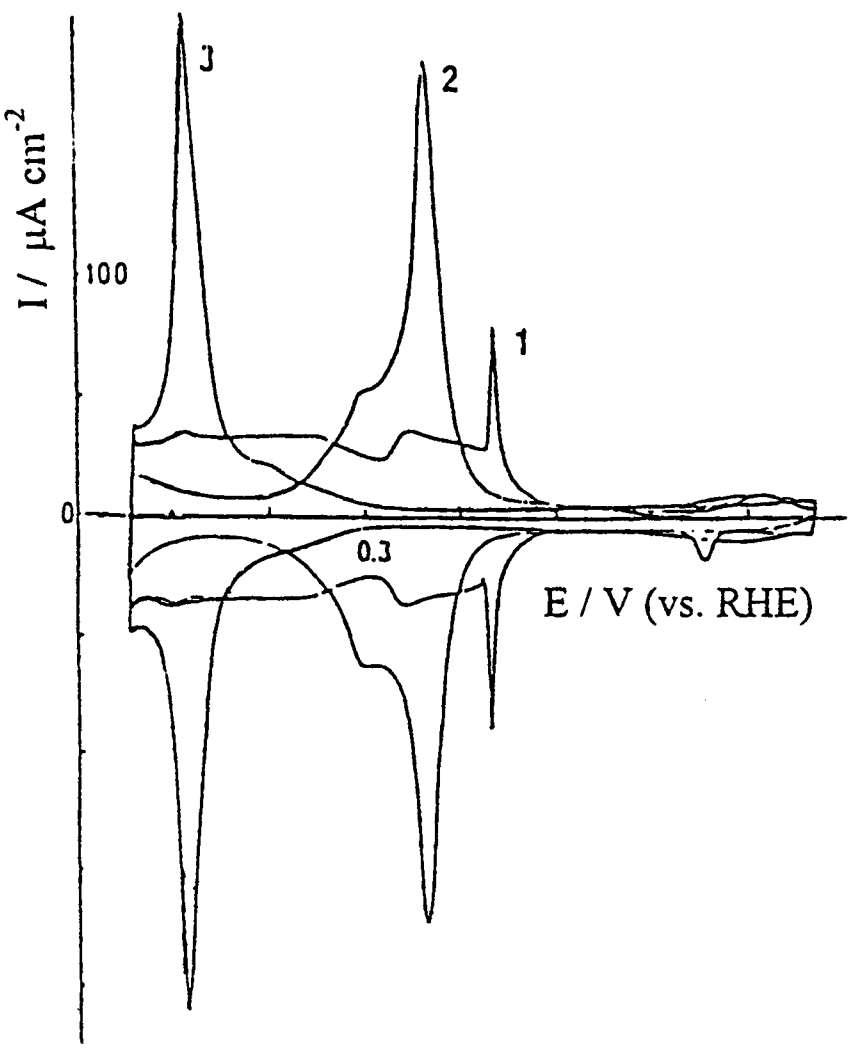

Figure 8.2. Cyclic voltammograms for 0.5 M aqueous sulphuric acid as reported by Clavilier et al.[6]. [1 = Pt(111), 2 = Pt(100) and 3 = Pt(110).

Prior to the experiments carried out on nitromethane the surface integrity of the single crystals used was tested by running cyclic voltammograms on 1.0 M aqueous sulphuric acid using the procedure described in chapter 3 and comparing the results obtained with those in figure 8.2. The flame annealing procedure developed by Clavilier was employed. This also provided an opportunity to become familiar with the precise experimental technique required when using single crystals in electrochemistry. Any contamination from the glassware, solution or atmosphere would have resulted in surface defects and prevented the production of accurate

---

5 J. Clavilier, R. Faure, G. Guinet and R. Durand, *J. Electroanal. Chem.*, **107**, (1980), 205

6 J. Clavilier, A. Rodes, K. El. Achi and M. A. Zamakhchari, *J. Chim. Phys.*, **88**, (1991), 1291

voltammograms. Care was also taken to keep the potential applied to the single crystal within the range shown in figure 8.2 as higher potentials would have resulted in the adsorption and subsequent desorption of oxygen to the surface of the electrode and hence the loss of the surface order. An example of the cyclic voltammograms obtained for 1.0 M aqueous sulphuric acid on the Pt(111), Pt(110) and Pt(100) single crystals employed are shown in figure 8.3.

Figure 8.3. Cyclic voltammograms for 1.0 M aqueous sulphuric acid. [1 = Pt(111), 2 = Pt(100) and 3 = Pt (110)].

Comparing figures 8.2 and 8.3 it is clear that the single crystals used in the experiments reported in the following section had a good surface integrity.

8.4 Cyclic Voltammetry of Nitromethane at Single Crystal Pt Electrodes

Experiments were conducted under diffusion only conditions using the experimental set-up described in chapter 3. Cyclic voltammograms were recorded for solutions of 1.5 mM nitromethane in both acetonitrile with 0.1M tetrabutylammonium perchlorate (TBAP) as supporting electrolyte, and in the pH 8.0 buffer described in section 3.9 with KCl as the supporting electrolyte.

In the potential range accessible before the solvent breakdown occurred no wave was observed in any of the voltammograms which could be attributed to the reduction of nitromethane, figure 8.4. Experiments conducted using a polycrystalline electrode were also unsuccessful under the same conditions.

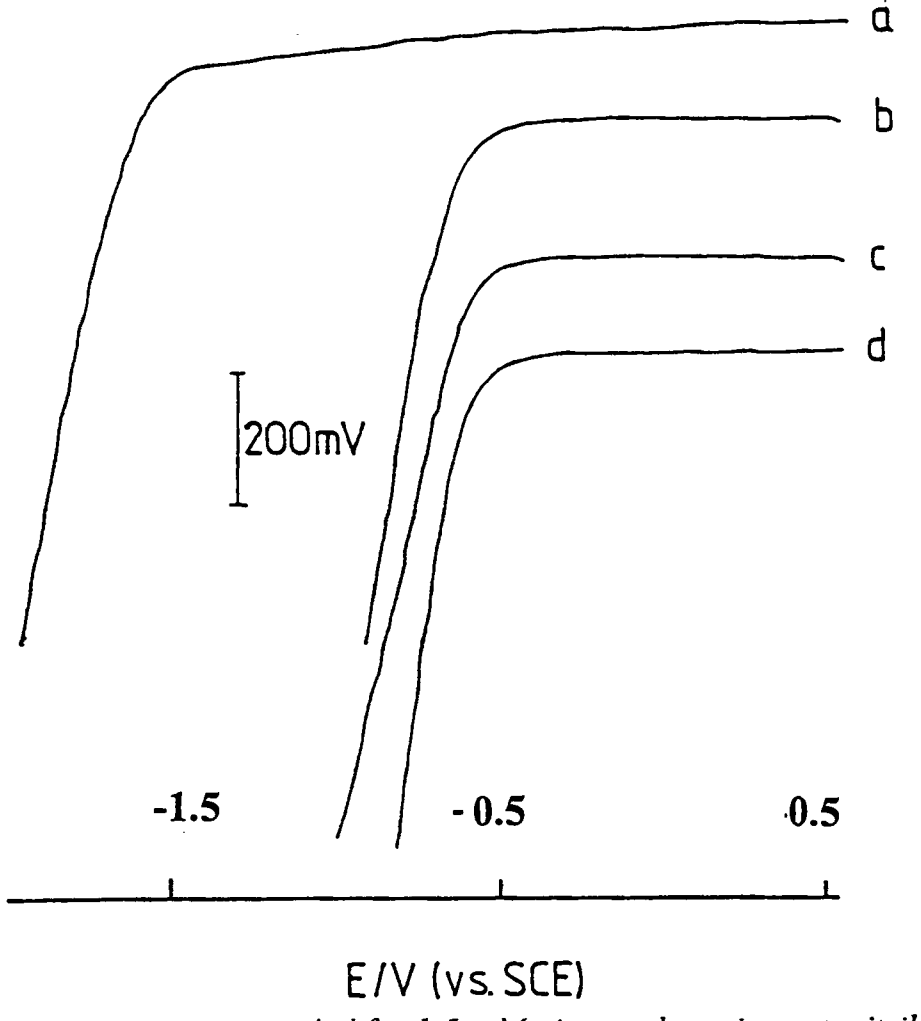

Figure 8.4. *Voltammograms recorded for 1.5 mM nitromethane in acetonitrile. [a - polycrystalline, b - Pt(111), c- Pt (110) and d - Pt (100)].*

This observation can be explained by considering the potential at which the solvent breakdown occurs in comparison to the reduction of nitromethane. As the mass transport to the electrode surface increases the potential required to induce a redox reaction becomes larger with the increase becoming greater for more irreversible reactions. This difference between the formal electrode potential $E^{0'}$ and the observed potential needed to promote reaction is known as the overpotential, described in chapter 2. To interpret the experimental observations it is noted that the overpotential for the irreversible solvent breakdown increases faster with higher mass transport than the overpotential for the quasi-reversible reduction of nitromethane. Therefore, with the low mass transport conditions employed in the single crystal experiments the nitromethane reduction is not visible before the solvent breakdown occurs. In contrast for conditions of high mass transport such as the high speed channel electrode experiments described in the previous chapter, the nitromethane wave is observed as the solvent breakdown shifts to a higher potential than the relative potential required for the nitromethane reduction.

In order to investigate the reduction of nitromethane at single crystal electrodes a long term solution to the mass transport problem discussed above would be to incorporate the single crystal electrode into the high speed channel flow cell.

8.5 Deuterated Nitromethane Experiments to Probe the Chemical Reaction Step of the Proposed Heterogeneous ECEEE Mechanism

The investigations into the complex reduction pathway of nitromethane in aqueous solution presented in the previous chapters have enabled the conclusion that the mechanism follows a heterogeneous ECEEE reaction pathway. The chemical step was suggested to

involve the C1 and C2 steps shown in scheme 5.1. In order to probe the kinetics of the chemical step, C1, further, steady-state experiments were carried out for solutions of deuterated nitromethane in deuterium oxide at pHs 8.5 and 9.0 at a Pt high speed channel electrode. Steady-state voltammograms were recorded at a range of flow rates with the aim of comparing the number of effective electrons transferred in the reduction, N_{eff}, with the results obtained for the isotopically light analogue reported in chapter 7. It was thought that such an investigation would provide information as to whether or not the C1 chemical step involves a rate determining hydrogen transfer step and hence enable further clarification of the mechanism involved in the reduction of nitromethane in aqueous solution.

8.5.1 Steady-State Voltammetry of Deuterated Nitromethane at a Pt Electrode

In order to insure that reliable interpretation of the data was achieved the high speed channel flow cell was re-calibrated for a volume flow rate range, v_f, of 0.015 - 2.5 cm^3 s^{-1} using samples of deuterated water as shown in appendix 2. Steady-state voltammograms were then recorded at pH 8.5 and 9.0 with a half-wave potential of -1.05 ± 0.1 V (vs. Pt pseudo-reference electrode). The pH of the solutions, 8.5 and 9.0 correspond to pD values of 8.9 and 9.4 respectively[7,8]. For each pD solution the transport limiting current was measured as a function of flow rate (v_f). as shown in figure 8.5.

---

7 A. K. Covington, M. Paabo, R. A. Robinson and R. G. Bates, *Analyt. Chem.*, **40**, (1968), 700

8 H. Kahihana, M. Maeda and T. Amaya, *Bull. Chem. Soc. Japan*, **43**, (1970), 1377

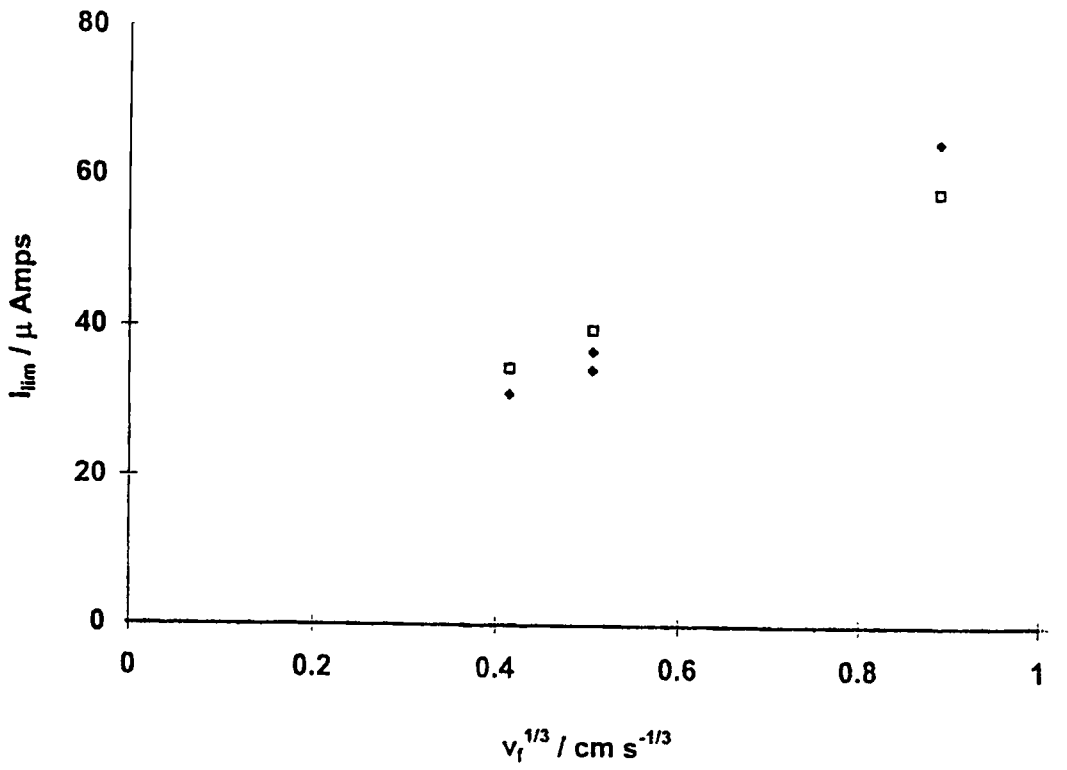

Figure 8.5 (a). *The transport limiting current(I_{lim}) / flow rate (v_f) data obtained for the reduction of deuterated nitromethane (1.5mM) at pD = 8.9 using a 40.6μm Pt high speed channel electrode (♦). The open symbols (□) show the behaviour simulated for an ECEEE mechanism with a k_{het} of 0.12 cm s^{-1}.*

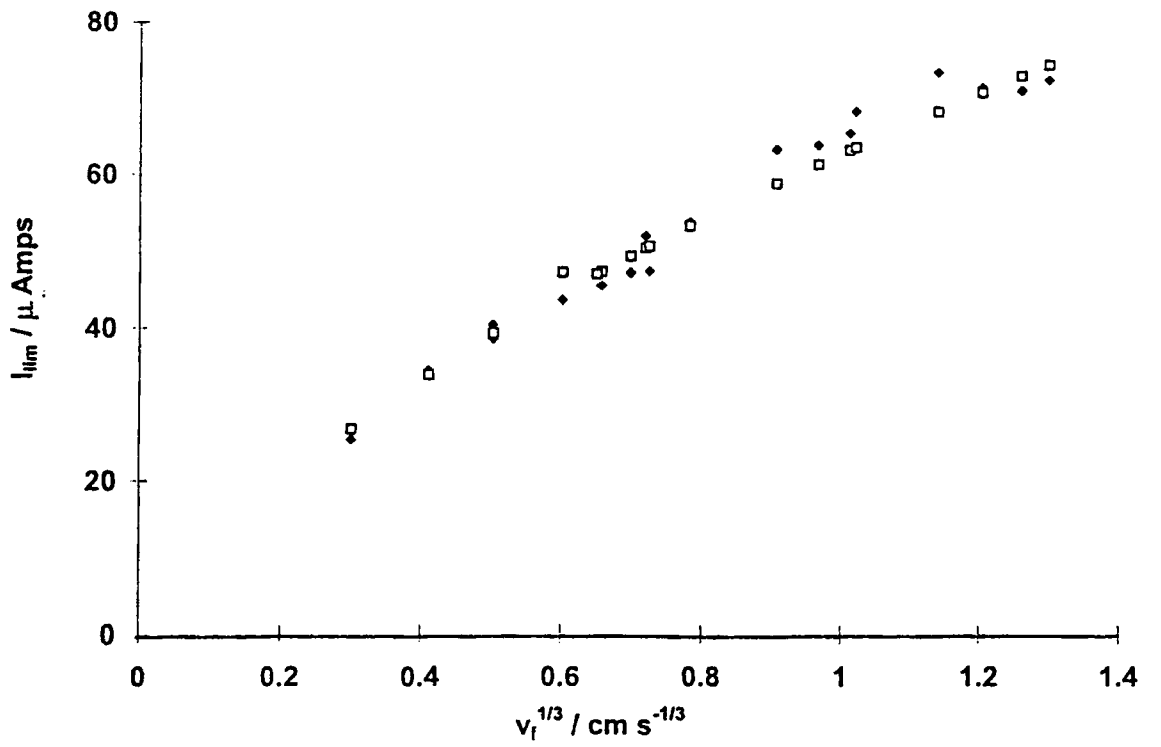

Figure 8.5 (b). *The transport limiting current(I_{lim}) / flow rate (v_f) data obtained for the reduction of deuterated nitromethane (1.5mM) at pD = 9.4 using a 40.6μm Pt high speed channel electrode (♦). The open symbols (□) show the behaviour simulated for an ECEEE mechanism with a k_{het} of 0.13 cm s^{-1}.*

In order to analyse the flow rate data generated for the deuterated nitromethane solutions the diffusion coefficient for deuterated nitromethane in deuterated water was required. This was calculated using the Stokes-Einstein equation described in appendix 6. The Stokes-Einstein equation relates diffusion coefficients to the solvent viscosity as shown below:

$$D = \frac{k_B T}{6r\eta\pi} \qquad (8.1)$$

where D is the diffusion coefficient, k_B is the Boltzman constant, r, is the radius of the solvated molecule and η is the solvent viscosity. Assuming that $r_{CD_3NO_2}$ and $r_{CH_3NO_2}$ are comparable, the ratio of diffusion coefficients for CD_3NO_2 and CH_3NO_2 given by the Stokes-Einstein equation is:

$$\frac{D_{D_2O}}{D_{H_2O}} = \frac{\eta_{H_2O}}{\eta_{D_2O}} \qquad (8.2)$$

so

$$D_{D_2O} = D_{H_2O}\frac{\eta_{H_2O}}{\eta_{D_2O}} \qquad (8.3)$$

The high speed channel experiments carried out at pD = 8.9 were conducted at 20 °C, whereas the pD = 9.4 experiment was conducted at 25 °C. The viscosity values of D_2O[9] and H_2O[10] at the relevant temperatures are shown in table 8.1.

Therefore the values shown in table 8.2 for the diffusion coefficient of CD_3NO_2 in D_2O can be estimated from the previously determined value[11] of 2 x 10^{-5} cm^2 s^{-1} for the diffusion coefficient of CH_3NO_2 in H_2O.

---

9 *J. Phys. Chem. Ref. Data*, **12**, (1983), 952

10 C.R.C., *Handbook of Chemistry and Physics*, (74th Edition), 6-10, (1993)

Temperature (°C)	Viscosity of H_2O (10^{-6} Pa s^{-1})	Viscosity of D_2O (10^{-6} Pa s^{-1})
20	1002	1185
25	894	1095

Table 8.1. The viscosity values of D_2O[9] and H_2O.

Temperature (°C)	Diffusion coefficient of CD_3NO_2 in D_2O (cm^2s^{-1})
20	1.7×10^{-5}
25	1.6×10^{-5}

Table 8.2. The diffusion coefficients of CD_3NO_2 in D_2O.

8.5.2 Comparison of the Heterogeneous Rate Constants for the ECEEE Mechanism

Knowledge of the diffusion coefficient for nitromethane in D_2O permitted the quantitative modelling of the transport limited current data to find the values of k_{het} for comparison with the data obtained in chapter 7. The heterogeneous rate constants, k_{het} were calculated for the pD 8.9 and 9.4 data using the method described in chapter 6 as shown in figure 8.5. The values obtained are shown in table 8.3 along with the values reported in chapter 7 for non-deuterated nitromethane.

pH of the CH_3NO_2 solution	k_{het} / cm s^{-1}	pD of the CD_3NO_2 solution	k_{het} / cm s^{-1}
8.5	0.24	8.9	0.12
9.0	0.28	9.4	0.13

Table 8.3. *The k_{het} values calculated for the deuterated nitromethane and non-deuterated nitromethane high speed channel flow data.*

Looking at table 8.3 it is clear that there is a large decrease in the size of the heterogeneous rate constant for the deuterated nitromethane mechanism when compared to the isotopically lighter analogue, non-deuterated nitromethane. It is therefore evident that a significant isotope effect operates for the electro-reduction on Pt with the chemical step being two or more times slower in deuterated solution.

8.6 Overall Inference of the Reaction Mechanism for the Reduction of Nitromethane in Aqueous Solution

All of the mechanistic evidence concerning the electro-reduction of nitromethane in aqueous solution presented in this thesis suggests that the reaction mechanism follows an ECEEE type process with the chemical step proceeding on the electrode surface as shown in the scheme below.

(i) E $A + e^- \rightleftharpoons B$

(ii) C $B \xrightarrow{-k_{het}} C$

(iii) EEE $C + 3e^- \rightleftharpoons$ products

Consistent with this *in-situ* electrochemical ESR experiments discussed in chapter 5 revealed both the presence of the $[CH_3NO_2]^{\bullet-}$ radical anion during the reduction of nitromethane at Hg/Au electrodes and the fact that in homogeneous solution this species was stable on the voltammetric timescale with the loss of the radical ion only being observed at the electrode surface. The heterogeneous nature of the kinetic decay is also evident from the hydrodynamic voltammetry, discussed in the relevant chapters, where the dependence of the transport limited current on the rate of the mass transport is quite different from that expected for a coupled homogeneous chemical reaction. However as discussed in this chapter if the reaction *is* heterogeneous it must occur in such a manner that the chemical nature of the electrode surface exerts very little influence on the overall kinetics of the mechanism.

Considering this surface indifference and taking into account the significant isotope effect measured between H_2O and D_2O, it is proposed that the transition state for the reaction involves the transfer of $H^{\bullet}$ (or $D^{\bullet}$) from carbon to oxygen as shown in the scheme in figure 8.6. In homogenous solution this occurs only very slowly so that the anion radical $[CH_3NO_2]^{\bullet-}$ is stable on the voltammetric timescale as found in the investigations reported in chapter 5. However if the reaction occurs in solution but adjacent to the electrode surface then the species $^{\bullet}CH_2N(OH))^-$ may absorb onto the electrode surface so ensuring the irreversibility of the chemical step. Clearly if the energy barrier to adsorption is less than that required for the H (D) atom transfer then the reaction rate will be insensitive to the adsorption step and hence to the chemical identity of the electrode surface. The schematic reaction profile shown in figure 8.7 summarises the proposed mechanism. The slow step in the electrode reaction corresponds to the transition state TS1 with the transition state for adsorption, TS2, being of lower energy, at least for the electrode materials studied. In contrast for homogeneous

solution the transition state corresponding to further reaction of $^{\bullet}CH_2N(OH))^-$ is of higher energy than TS1 so that $^{\bullet}CH_2N(OH))^-$ is then unstable with respect to reconversion to the radical anion $[CH_3NO_2]^{\bullet-}$ so explaining the observed relative stability of the latter in the absence of an adsorbing surface.

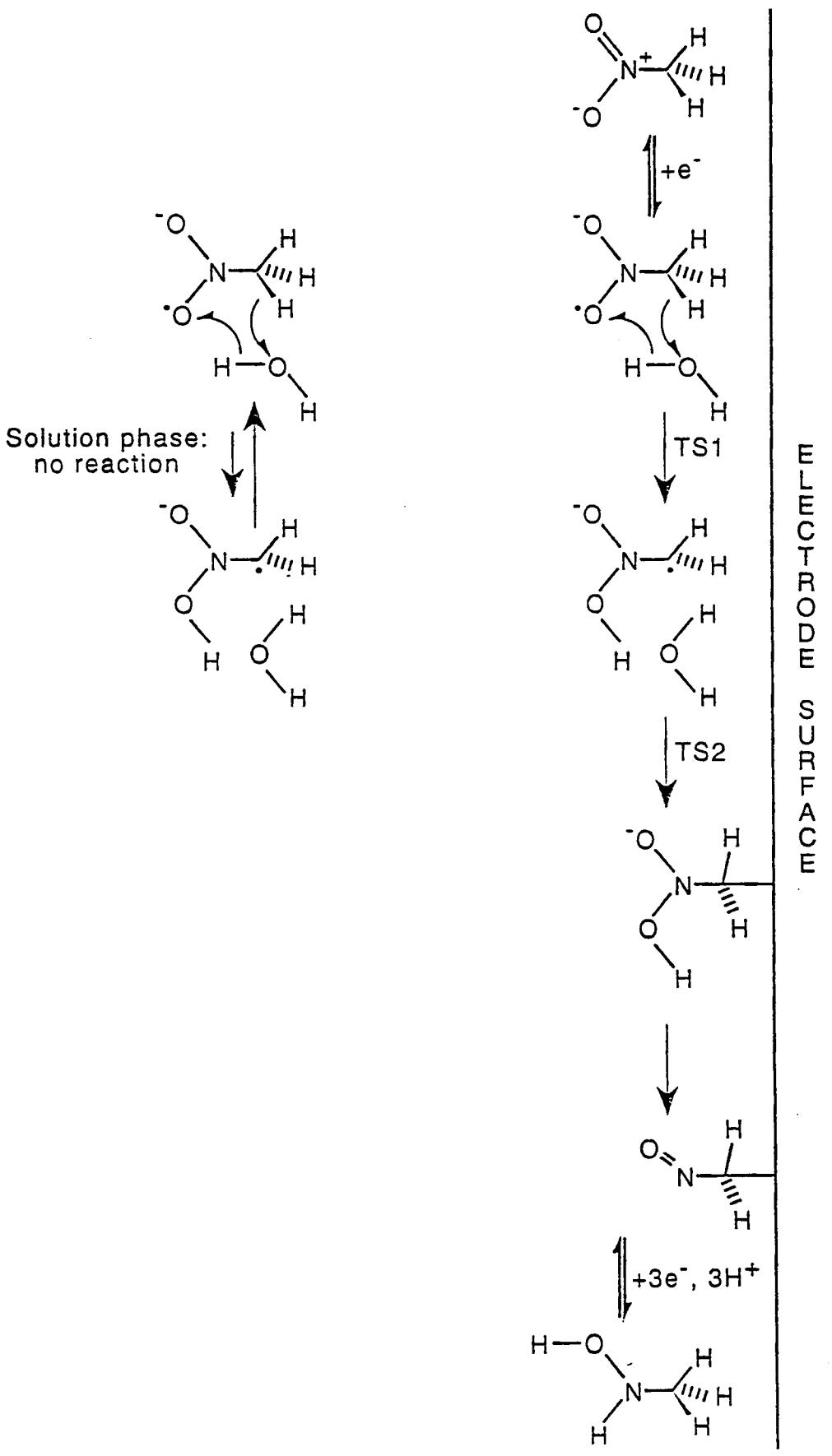

Figure 8.6. *The proposed reaction mechanism for the reduction of nitromethane in aqueous solution.*

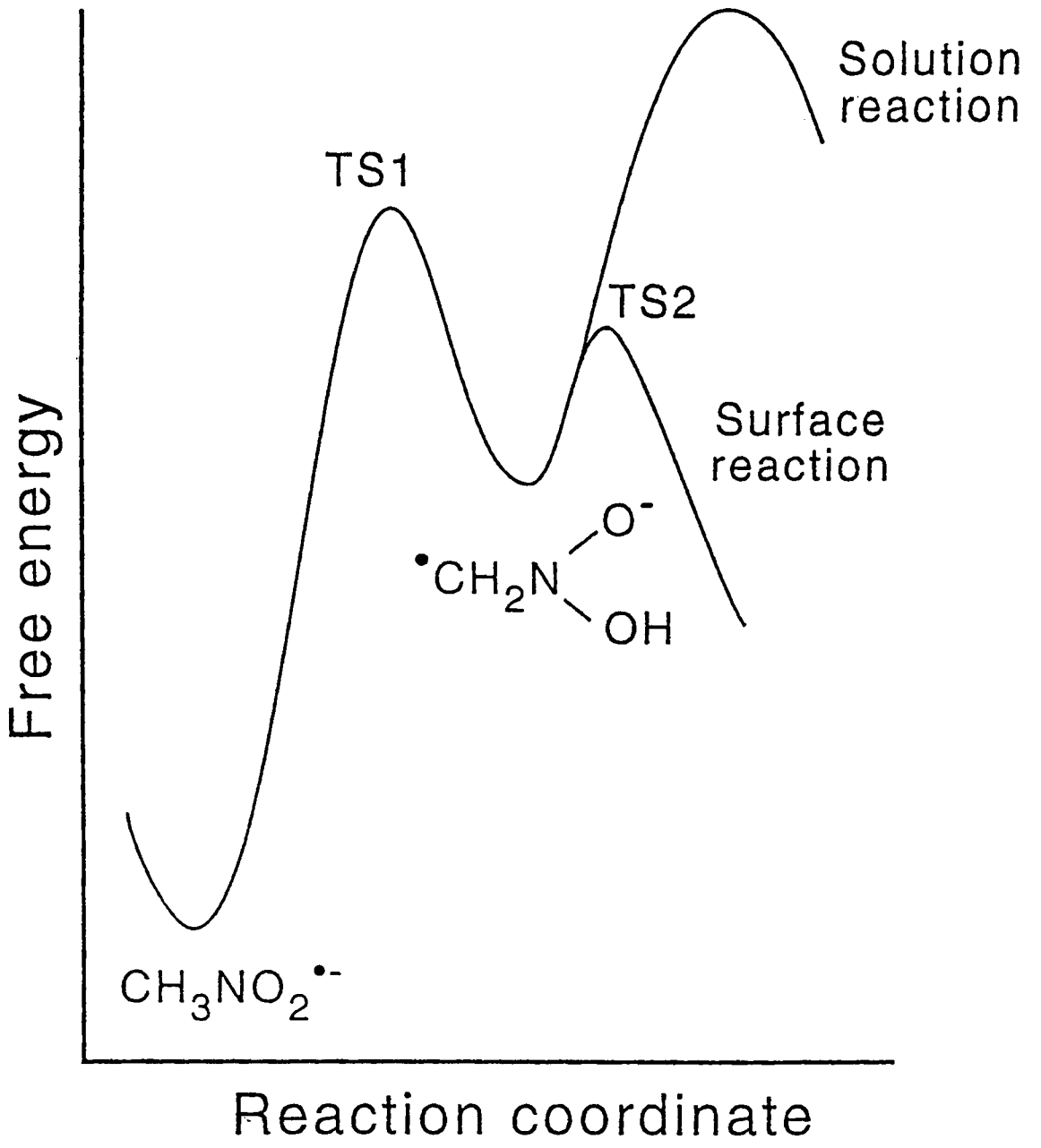

Figure 8.7. *Schematic reaction profile showing the proposed mechanism for the electro-reduction of nitromethane.*

It is useful to note that the observed 'heterogeneous' kinetics inferred voltammetrically and summarised by equation (8.4)

$$I = F\int\left(D\frac{\partial[A]}{\partial y} + 3k_{het}[B]\right)_{y=0} dA \qquad (8.4)$$

are consistent first with a conventional heterogeneous reaction in which there is adsorption of the intermediate B formed in reaction (ii):

(iv) B(aq) $\rightleftharpoons$ B(ads)

before conversion into species C:

(v) B(ads) → C(ads)

and further electrochemical reaction. In this case the net rate constant

$k_{het} = K_{(iv)}k_{(v)}$ (8.5)

reflecting both the adsorption constant, $K_{(iv)}$ for reaction (iv) and the heterogeneous rate constant, $k_{(v)}$ for reaction (v). Second the kinetic formulation is also compatible with the reaction mechanism proposed above for nitromethane in which the slow chemical reaction (ii) in the ECEEE pathway occurs homogeneously in the layer of the solution immediately adjacent to the electrode solution:

(vi) B(aq) → C(aq)

followed by rapid irreversible adsorption of the species C

(vii) C(aq) → C(ads)

and subsequent irreversible transformation leading to a flow of current beyond that expected for a simple one-electron process. In this case k_{het} simply reflects the rate of step (vi). It follows that a voltammetrically inferred current behaviour given by equation (8.4) does not itself indicate that the rate of the determining step occurs on the electrode surface.

Returning to the case of the nitromethane reduction it should be noted that the mechanism proposed in the scheme shown in figure 8.7 is consistent with all of the presently known experimental data relating to the reaction at a diversity of electrode surfaces and that the surface indifference of the reaction can be explained by a homogenous chemical transformation of the $[CH_3NO_2]^{\bullet -}$ radical anion occurring in an electrode reaction layer and which is rendered irreversible, and so kinetically visible, by adsorption onto any suitable electrode surface.

The elucidation of the complex reaction mechanism for the reduction of nitromethane in aqueous solution presented in this thesis demonstrates the power of voltammetric techniques when such clarification is required. In chapters 5 - 8 the synergistic application of experimental and numerical methods to the nitromethane investigations has enabled the determination of a novel mechanism that prior to the work presented in this thesis was unknown.

The reduction of nitromethane in aqueous solution has provided a challenging area of investigation for electrochemists for some time due to the complex sequence of electron transfers, adsorption/ desorption phenomena and chemical reactions including N-O bond breaking and the proton loss/ uptake involved. The mechanistic scheme presented in this thesis offers the most conclusive description of the reduction pathway to date whilst introducing the concept of a whole new electrochemical process; *the surface indifferent electrocatalytic reaction.*

APPENDICES

Contents

The Thomas Algorithm

The Thomas algorithm is a useful and efficient means of solving tri-diagonal matrices. It was employed to calculate current in the computer programs shown in appendix 7. The matrix equation derived is of the form:

$\{d\} = [T]\{u\}$

It is a simplified form of Gaussian elimination and operates by factorising the matrix [T] into two bi-diagonal matrices, $[T_L]$ and $[T_U]$ such that:

$[T] = [T_L][T_U]$

A solution for the vector, {v}, is then found for

$[T_L]\{v\} = \{d\}$

and {v} is used to give a final solution $[T_U]\{u\} = \{v\}$

Since $[T_L]^{-1}\{d\} = \{v\}$ and $[T_U]\{u\} = [T_L]^{-1}\{d\}$

thus $([T_L][T_U])\{u\} = \{d\}$

The matrix [T] of $(J-1)^2$ elements can be written as

$$[T] = \begin{bmatrix} b_1 & c_1 & 0 & & & & \\ a_2 & b_2 & c_2 & 0 & & & \\ 0 & \ddots & \ddots & \ddots & 0 & & \\ & 0 & a_j & b_j & c_j & 0 & \\ & & 0 & \ddots & \ddots & \ddots & 0 \\ & & & 0 & a_{J-2} & b_{J-2} & c_{J-2} \\ & & & & 0 & a_{J-1} & b_{J-1} \end{bmatrix}$$

On factorisation, [T] takes the form:

$$[T] = [T_L][T_U] = \begin{bmatrix} \alpha_1 & & & & 0 \\ a_2 & \alpha_2 & & & \\ & \ddots & \ddots & & \\ & & a_{J-2} & \alpha_{J-2} & \\ 0 & & & a_{J-1} & \alpha_{J-1} \end{bmatrix} \begin{bmatrix} 1 & \beta_1 & & & 0 \\ & 1 & \beta_2 & & \\ & & \ddots & \ddots & \\ & & & 1 & \beta_{J-2} \\ 0 & & & & 1 \end{bmatrix}$$

where α_J and β_J are to be determined. By equating both the left and the right hand sides, the following relations are obtained :

$\alpha_J \rightarrow b_1$ $\qquad$ $\beta_J \rightarrow c_1 / \alpha_1$

$\alpha_J = b_j - a_j\beta_{j-1}$ $\qquad$ $j = 2,3...J-1$

$\beta_j = c_1 / \alpha_j$ $\qquad$ $j = 2,3...J-2 \quad (a_j \neq 0)$

After obtaining α_J and β_J, the equation for $\{v\}$ is solved

$[T_L]\{v\} = \{d\}$

where the elements v_j of $\{v\}$ are given by

$v_1 = d_1 / \alpha_1$

$v_j = (d_1 - a_j v_{j-1}) / \alpha_j$

$\{v\}$ is then used to determine the elements u_J of $\{u\}$

$u_{J-1} = v_{J-1}$

$u_j = v_j - \beta_j u_{j+1}$

By this procedure the matrix equation $[T]\{u\} = \{d\}$ is solved for $\{u\}$ and hence the Thomas algorithm can be used successfully to calculate solutions to the mass transport equations arising from diffusion around the electrode in electrochemical experiments.

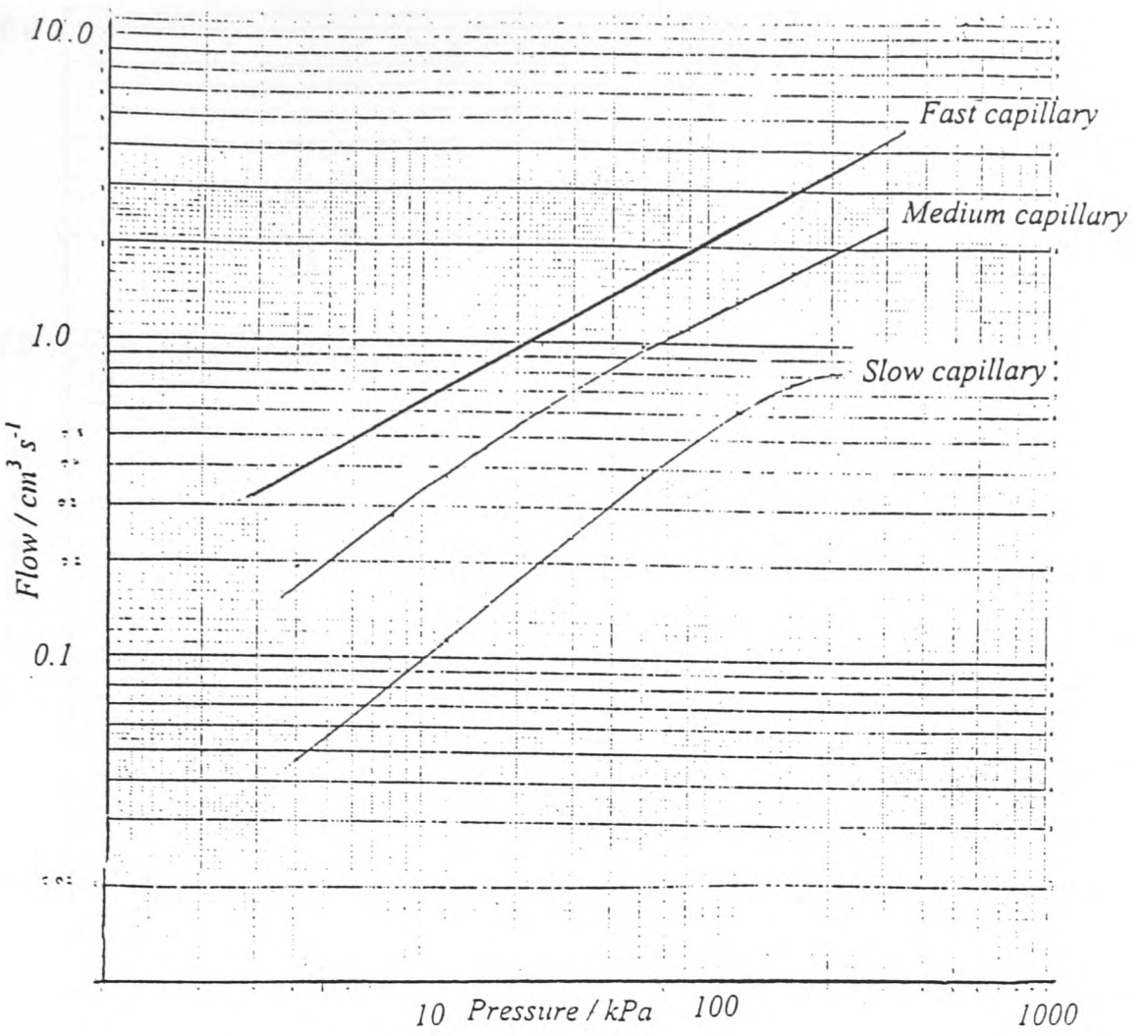

MeCN flow calibration for the high speed channel flow cell.

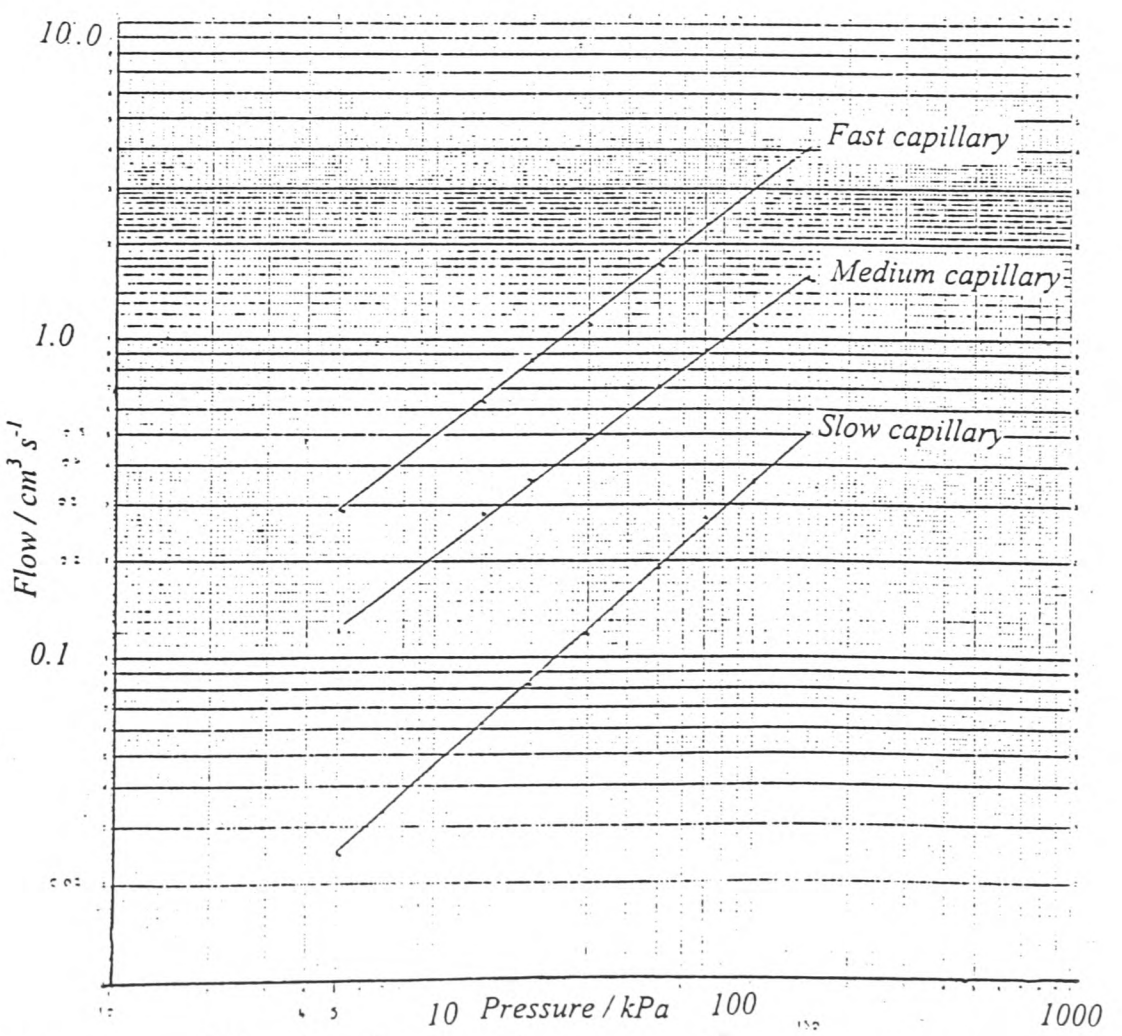

H_2O flow calibration for the high speed channel flow cell.

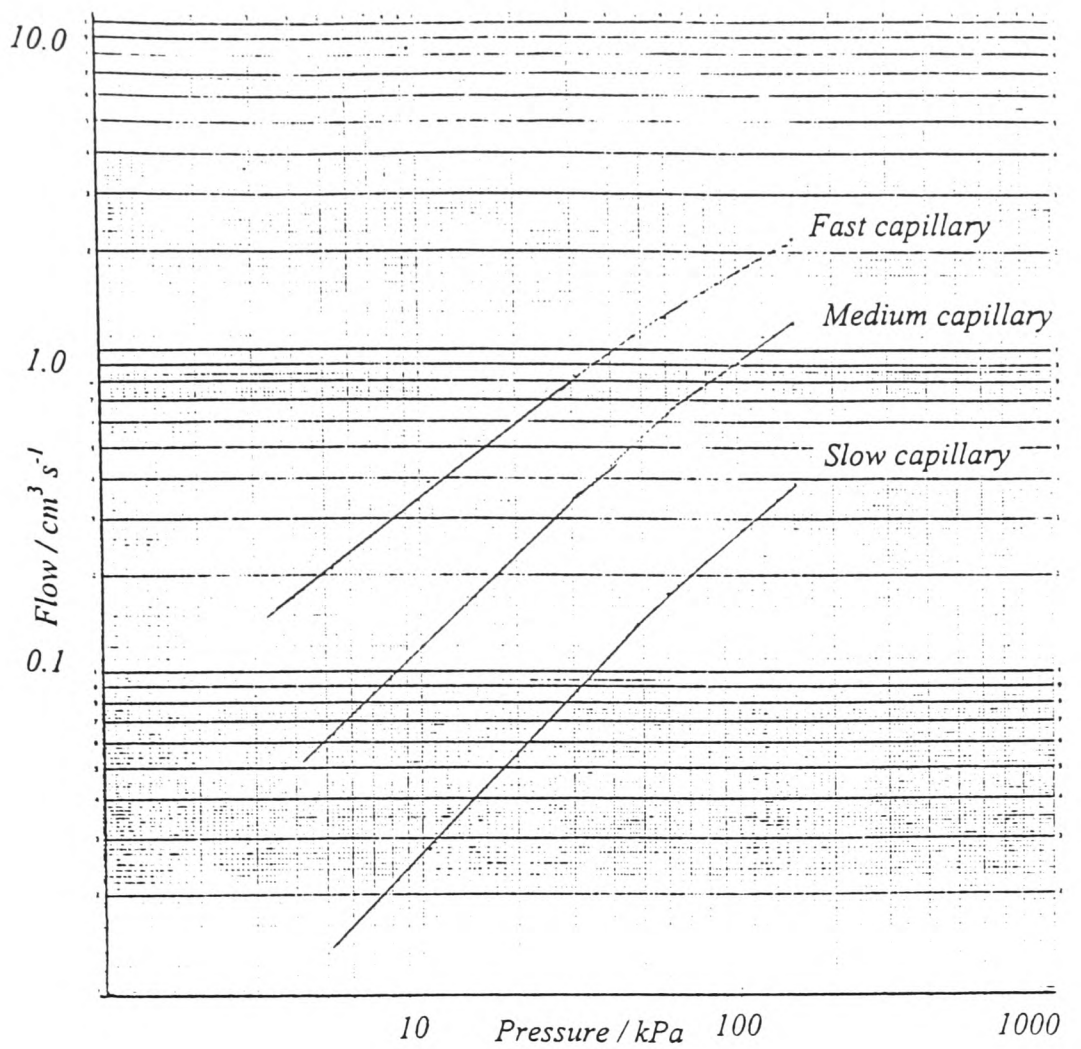

D_2O flow calibration for the high speed channel flow cell.

Airy Functions

Airy functions arise in the solution of the differential equation:

$$\frac{d^2w}{dz^2} - zw = 0$$

Pairs of solutions to this equation are:

$Ai(z), Bi(z)$

$Ai(z), Bi(ze^{2\pi i/3})$

$Ai(z), Bi(ze^{-2\pi i/3})$

In terms of ascending series,

$Ai(z) = c_1 f(z) - c_2 g(z)$

$Bi(z) = \sqrt{3}[c_1 f(z) + c_2 g(z)]$

where

$$f(z) = 1 + \frac{1}{3!}z^3 + \frac{1.4}{6!}z^6 + \frac{1.4.7}{9!}z^9 + \ldots\ldots$$

$$f(z) = \sum_0^\infty 3^k \left(\frac{1}{3}\right)_k \frac{z^{3k}}{(3k)!} \qquad g(z) = z + \frac{2}{4!}z^4 + \frac{2.5}{7!}z^7 + \frac{2.5.8}{10!}z^{10} + \ldots\ldots$$

$$g(z) = \sum_0^\infty 3^k \left(\frac{2}{3}\right)_k \frac{z^{3k+1}}{(3k)!}$$

$(\alpha + 1/3)_0 = 1$

$(\alpha + 1/3)_k = (3\alpha+1)(3\alpha+4)\ldots\ldots(3\alpha+3k-2)$

(α arbitrary; $k = 1,2,3\ldots\ldots$)

It follows that as $z \to \infty$, $Ai(z) \to 0$ whereas $Bi(z) \to \infty$. For the problems in this thesis, the boundary conditions stipulate that as $z \to \infty$, $w \to 0$, and thus $Ai(z)$ represents the required solution.

Gamma Functions

Integer values

$\Gamma(n+1) = 1.2.3.... (n-1)\ n = n!$

Fractional values

$$\Gamma(n + \frac{2}{3}) = \frac{2.5.8.11....(3n-1)}{3^n}\Gamma\left(\frac{2}{3}\right)$$

$$\Gamma(\frac{2}{3}) = 1.3542$$

$$\Gamma(n + \frac{1}{3}) = \frac{1.4.7.10....(3n-2)}{3^n}\Gamma\left(\frac{1}{3}\right)$$

$$\Gamma(\frac{n}{3}) = \Gamma(\frac{n}{3} + \frac{1}{3} - \frac{1}{3}) = (n' + \frac{1}{3}) \qquad n' = \frac{n-1}{3}$$

$$\Gamma(n' + \frac{1}{3}) = \frac{1.4.7.10....(3n'-2)}{3^{n'}}\Gamma\left(\frac{1}{3}\right)$$

$$\Gamma(\frac{1}{3}) = 2.6789$$

Miller Indices

When the metal crystal is cut at different angles, the exposed surfcaes can possess a wide variety of atomic arrays, as described by Miller indices[1]. The Miller indices of a particular plane are best interpreted by considering the set of axes in figure A5.1.

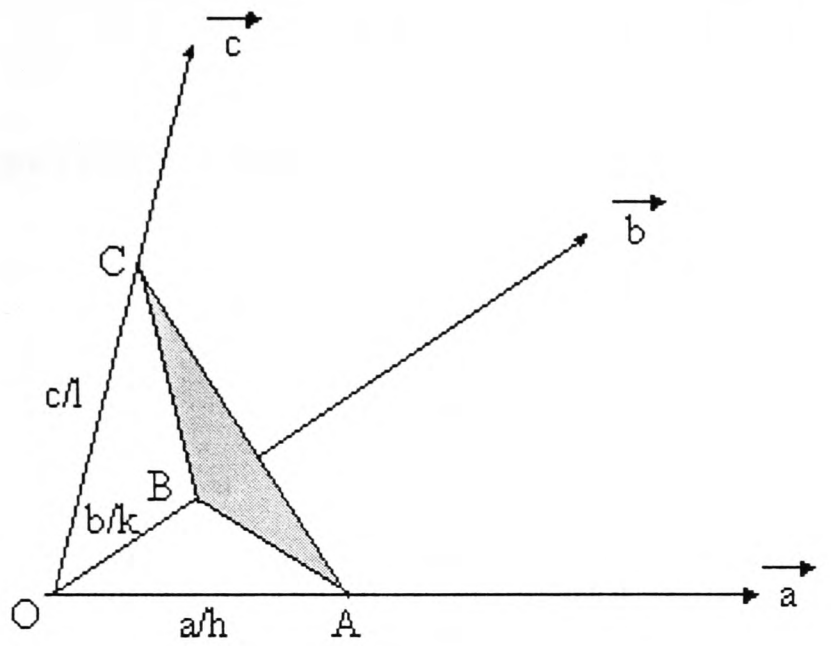

Figure A5.1. Crystal axes intercepted by a crystal plane.

The plane ABC intersects the axes at A, B and C, with the distances of the intercepts from the origin being OA, OB and OC respectively. If the unit cell is chosen with dimensions a, b, and c, then these lenghts are OA/a. OB/b and OC/c. Hence the reciprocals of the lengths would be a/OA, b/OB and c/OC, which are defined as the integers h, k and l. (i.e.: h = a/OA, k = b/OB and l = c/OC). The triple (hkl) is referred to as the Miller index and hence defines the surface planes. Figure A5.2 shows the (100), (110) and (111) planes relevant to this thesis.

---

1 M. A. Buerger, *Elementary Crystallography*, Wiley, New York, (1963)

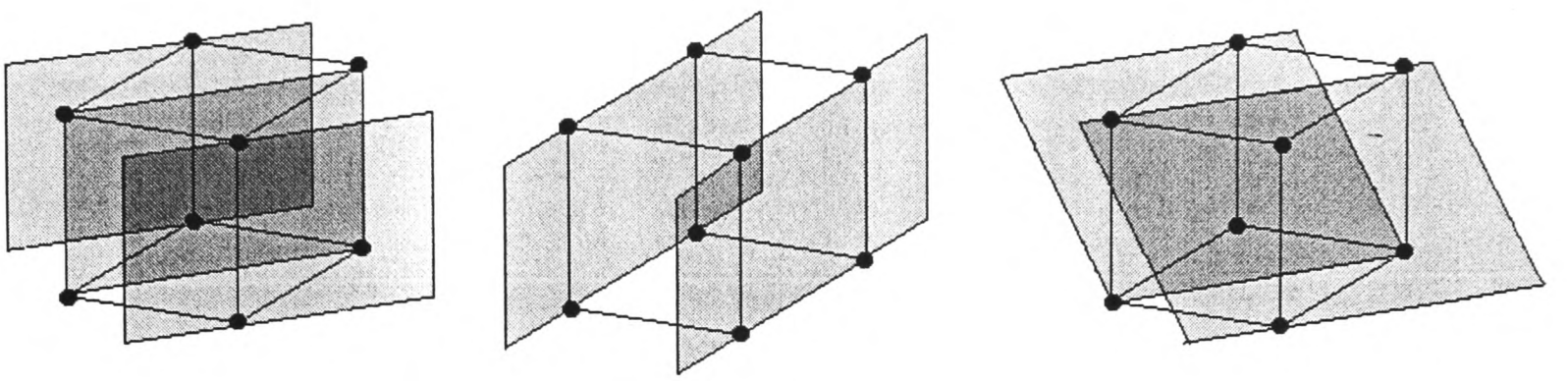

Figure A5.2. (100), (110) and (111) Miller planes.

The Stokes-Einstein Equation

Considering an isolated ion of charge $z_i e$, the force, f, due to the electric field, E, is

$$f = z_i eE.$$

This is counterbalanced by a viscous force, which is given by the Stokes' equation

$$f = 6r_i \pi \eta v_i,$$

where η is the solution viscosity, r_i is the radius of the solvated ion and v_i is the velocity vector. If other retarding effects are neglected, the maximum velocity is therefore:

$$v_i = \frac{z_i eE}{6r_i \pi \eta} \qquad \text{or} \qquad v_i = u_i E$$

where u_i is the ion mobility, the proportionality constant between velocity and electric field strength.

The flux of charge, j_i, for a solution of concentration c_i is given by

$$j_i = z_i e v_i c_i N_A,$$

and as

$$eN_A = F,$$

where F is Faraday's number, this expression can be rewritten as

$$j_i = z_i c v_i F \qquad \text{or} \qquad j_i = z_i c_i u_i FE.$$

As the concentration gradient is also a chemical potential gradient, the following equation is applicable, presuming a sufficiently dilute solution,

$$\mu_i = \mu_i^{\phi} + RT \ln c_i,$$

where μ_i is the chemical potential of i and μ^{ϕ}_i is its standard chemical potential.

Differentiation with respect to distance, at constant temperature and pressure, gives

$$\left(\frac{\partial \mu_i}{\partial x}\right)_{P,T} = \frac{RT}{c_i}\left(\frac{\partial c_i}{\partial x}\right)_{P,T}.$$

As the diffusive force experienced by the particle i is given by

$$f = -\left(\frac{\partial \mu_i}{\partial x}\right)$$

this can be re-expressed as

$$f = -\frac{RT}{c_i}\left(\frac{\partial c_i}{\partial x}\right).$$

The number flux of ions, J_i, is given by

$$J_i = \frac{j_i}{z_i e N_A} = c_i u_i E$$

substituting in the expression for j_i with respect to the electric field intensity gives

$$J_i = \frac{c_i u_i f}{z_i e}.$$

Incorporating the expression for the diffusive force produces the following equation

$$J_i = -\frac{u_i RT}{z_i F}\left(\frac{\partial c_i}{\partial x}\right)_{P,T}.$$

Comparing this to Fick's first law of diffusion

$$J_i = -D_i\left(\frac{\partial c_i}{\partial x}\right),$$

gives the Einstein relation,

$$D_i = \frac{u_i RT}{z_i F}.$$

Substituting this relation into the definition for the ion mobility, gives the Stokes-Einstein relation,.

$$D_i = \frac{kT}{6r_i\pi\eta}$$

where k is the Boltzman constant. This expression can be used to determine diffusion coefficients from experimental measurements of solution viscosity.

(1) BI Modelling of Potential Transients

```
**************
TRANSIENT BI
**************
PARAMETER(NJ=1000,NK=500)

    INTEGER NB,NP,NT,T,J,K,STEPS
    REAL*8
AO,XE,W,DD,DIFF,TWOH,VF,VX,VO,LAM
Y
    REAL*8
LAMJ(NJ),ALPHA(NJ),BETA(NJ),D(NJ),F(N
)
    REAL*8  U(NJ,NK),UOLD(NJ,NK)
    REAL*8
SIMT,DX,DY,DT,H,Y,ACCUM,CURR

* COPY PARAMS *

    NB=8
    NP=NJ*NK

* TIME *

    NT=200
    SIMT=0.1

* CELL PARAMETERS *

    XE   = 0.4
    TWOH = 0.04
    W    = 0.4
    DD   = 0.6
    DIFF = 2.E-5
    VF   = 0.01
    AO   = 1.E-6

* CALCULATE CONSTANTS *

    DX    = XE/NK
    DY    = TWOH/NJ
    DT    = 1.0/NT
    STEPS = NT*SIMT
    LAMY  = DIFF*DT/DY/DY

* SCREEN OUTPUT *

    PRINT *
    PRINT *,'TRANSIENT BI'
    PRINT *,'------------'
    PRINT *
    PRINT *,'NO OF TIME STEPS : ',STEPS
    PRINT *

* PARABOLIC FLOW *

        H=TWOH/2
        VO=3*VF/4/H/DD

        DO 10 J=1,NJ-1
        Y=J*DY
        VX=VO*(1-(H-Y)*(H-Y)/H/H)
        LAMJ(J)=VX*DT/DX
        10   CONTINUE

        * INITIAL CONCENTRATION = 1
        EVERYWHERE *

        DO 25 K=1,NK
        DO 20 J=1,NJ
        UOLD(J,K)=1.0
20      CONTINUE
25      CONTINUE
* TRANSIENT ALPHA & BETA *

        ALPHA(1) = 2*LAMY+1+LAMJ(1)
        BETA(1) = -LAMY/ALPHA(1)

        DO 30 J=2,NJ-2
         ALPHA(J)=(2*LAMY+1+LAMJ(J)) +
LAMY*BETA(J-1)
        BETA(J)=-LAMY/ALPHA(J)
30      CONTINUE
        ALPHA(NJ-1)=1+LAMY+LAMJ(NJ-
1) - (-LAMY*BETA(NJ-2))

        *************
        * TIME LOOP *
        *************

        DO 500 T=1,STEPS

        ACCUM=0

        ***********
        ** K LOOP*
        ***********

        DO 200 K=1,NK

        ** LHS INPUT VECTOR = 1 *

        IF(K.EQ.1) THEN
        DO 110 J=1,NJ-1
        D(J)=UOLD(J,K)+LAMJ(J)
110     ONTINUE
        ELSE
        DO 120 J=1,NJ-1
        D(J)=UOLD(J,K)+LAMJ(J)*U(J,K-1)
120     ONTINUE
        ENDIF

        ** THOMAS ALGORITHM *
F(1)=D(1)/ALPHA(1)
```

```
      DO 130 J=2,NJ-1
      F(J)=(D(J) + LAMY*F(J-1))/ALPHA(J)
130   CONTINUE

      U(NJ-1,K)=F(NJ-1)
      DO 140 J=NJ-2,1,-1
      U(J,K)=F(J)-BETA(J)*U(J+1,K)
140   CONTINUE

      ACCUM=ACCUM+U(1,K)

200   CONTINUE

*     * COPY U -> UOLD *

*     CALL COPY(NP,NB,U,UOLD)

      DO 310 K=1,NK.
      DO 300 J=1,NJ
      UOLD(J,K)=U(J,K)
300   CONTINUE
310   CONTINUE

      ** CALCULATE CURRENT IN UA *

      CURR                                    =
ACCUM*AO*96485*W*DIFF*1.E6*DX/DY

      PRINT *,'TIME : ',REAL(T*DT),'
CURRENT : ',CURR

500   CONTINUE

      STOP

      END
```

(2) SIP Modelling of Potential Transients

```
**********
TRANSIENT SIP
**********

      INTEGER NK,NJ,ITS,OPF,CPF
PARAMETER(NJ=800,NK=200,ITS=200)

      INTEGER
N1,N2,ITMAX,ITCOUN,ITUSED,NDIR,IXN,
IYN,IFAIL
      INTEGER
NT,P,N1M,J,K,TIME,FLAG

      REAL*8
A(NJ,NK),B(NJ,NK),C(NJ,NK)
      REAL*8
D(NJ,NK),E(NJ,NK),LAMCON(NJ)
      REAL*8
Q(NJ,NK),T(NJ,NK),LAM,LAMAX,CON,VF
      REAL*8
APARAM,CONRES,CONCHN,AL,BE
      REAL*8 RESIDS(ITS),CHNGS(ITS)
      REAL*8
WRKSP1(NJ,NK),WRKSP2(NJ,NK),WRKSP3
(NJ,NK)

      REAL*8 CURR,DX,DY,DT,Simt,PHI
      REAL*8
W,CONC,H,XE,DIFF,CW,VF3

      CHARACTER *20 FNAME

*****  Cell parameters

      W = 0.094D0
      CONC = 0.510D-6
      H = 0.0050
      XE = 0.00406
      DIFF = 2.400D-5
      CW = 0.20D0
      VF = 0.05
*****  Convergence parameters
      AL = 3
      BE = 3
      PHI= 1.00e-1
      NT = 33333333
      Simt=0.001

*****  User Controls

      FNAME="005SIPk.dat"
      FLAG=0
      CPF=40
      OPF=1

***** Calculated variables

      N1 = NJ
      N1M = NJ
      N2 = NK
      KE = NK/(AL+BE+1)
      DX = XE/KE
      DY = 2.0D0*H*PHI/NJ
      DT = 1.0D0/NT

*****  CALCULATE LAMDA VALUES

      TWOH = 2.0D0*H
      CON                                     =
(6.0D0*VF*DY*DT)/(TWOH*TWOH*TWOH*
CW*DX)
      LAM = (DIFF*DT)/(DY*DY)
      LAMAX = (DIFF*DT)/(DX*DX)
      DO 10 J=1,NJ-1
      LAMCON(J)                               =
CON*REAL(J)*(TWOH - REAL(J)*DY)
```

```
 10     CONTINUE
****************************************
******
*****  CALCULATION     OF     ARRAYS
A,B,C,D,E
****************************************
******

      DO 60 J = 1,NJ-1
        DO 40 K = 1,N2-1

*****  INTERNAL NODES

        A(J,K)    =    0.5D0*LAMCON(J)    -
LAMAX
        B(J,K) = - LAM
        C(J,K) = 1.0D0 +   2.0D0*LAM +
2.0D0*LAMAX
        D(J,K) = - LAM
        E(J,K)    =    -0.5D0*LAMCON(J)    -
LAMAX

*****  BOUNDARY NODES

*****  WESTERN BOUNDARY - ALL J,
K=1

        A(J,1) = 0.0D0

*****  EASTERN BOUNDARY - ALL J,
K=N2-1 - NO FLUX

        C(J,N2-1) = 2.0D0*LAM + 1.0D0 -
0.5D0*LAMCON(J) + LAMAX
        E(J,N2-1) = 0.0D0

*****  NORTHERN BOUNDARY - ALL K,
J=NJ-1 - NO FLUX

        C(NJ-1,K) = 2.0D0*LAMAX + LAM
+ 1.0D0
      C(NJ-1,N2-1) = LAMAX + LAM +
1.0D0 - 0.5D0*LAMCON(NJ-1)
        D(NJ-1,K) = 0.0D0

*****  SOUTHERN BOUNDARY - ALL K,
J=1

*****  BEFORE ELECTRODE - NO FLUX

        IF (K.LT.(AL*KE+1)) THEN
        B(1,K) = 0.0D0
        C(1,K) = 2.0D0*LAMAX + LAM +
1.0D0
        ENDIF

*****  ON ELECTRODE - NO CONC IN 1,K

        IF
((K.GT.(AL*KE)).AND.(K.LT.((AL+1)*KE+1
))) THEN
         B(1,K) = 0.0D0
        ENDIF

*****  AFTER ELECTRODE - NO FLUX

        IF (K.GT.((AL+1)*KE)) THEN
        B(1,K) = 0.0D0
        C(1,K)  =  2.0D0*LAMAX  +  LAM
+1.0D0
      C(1,N2-1) = LAMAX + LAM + 1.0D0 -
0.5D0*LAMCON(1)
        ENDIF

40      CONTINUE
60      CONTINUE


*****  NAG ROUTINE VARIABLES

        APARAM = 10.0D0
        ITMAX =  ITS
        ITCOUN = 0
        NDIR = 1
        CONRES = 1.0D-6
        CONCHN = 1.0D-5
        IFAIL = 0

***** OPEN FILE FOR CURR-TIME DATA

      OPEN
(15,FILE=FNAME,STATUS='UNKNOWN')
     if          (flag.eq.1)          OPEN
(16,FILE='listing',STATUS='OLD')

***** INITIALISE T ARRAY: STARTS
BEING ONE EVERYWHERE AS 1ST
APPROX ***

        DO 130 J = 1, N1-1
        DO 120 K = 1, N2-1
        T(J,K) = 1.0D0
120     CONTINUE
130     CONTINUE

****************************************
***
**************    T-I-M-E        L-O-O-P
!!!********
****************************************
***

        DO 1000 TIME = 1,Simt*NT
********** PUT IN Q (RHS) ARRAY:
ALWAYS SET TO OLD T VALUE
        DO 110 J = 1, N1-1
        DO 100 K = 1, N2-1
        Q(J,K) = T(J,K)
        IF (K.EQ.1) THEN
```

```
      Q(J,1) = T(J,1) - 0.5D0*LAMCON(J)
+ LAMAX
                    ENDIF
100   CONTINUE
110   CONTINUE


*****  CALL SUBROUTINE FROM NAG

      CALL
D03EBF(N1,N2,N1M,A,B,C,D,E,Q,T,APARA
M,ITMAX,

+ITCOUN,ITUSED,NDIR,IXN,IYN,CONRES,
CONCHN,RESIDS,

+CHNGS,WRKSP1,WRKSP2,WRKSP3,IFAIL)

*****  CALCULATE THE CURRENT FROM
THE T ARRAY

      CURR = 0.0D0
      DO 150 K = (AL*KE+1),((AL+1)*KE)
            CURR = CURR + T(1,K)
150   CONTINUE
      CURR                              =
96485.0D0*W*CONC*DX*DIFF*CURR*1.0D
6/DY

*****  WRITE TO FILE
      IF (MOD(TIME,OPF).EQ.0) THEN
      WRITE(15,*) TIME*dt,CURR
 152  FORMAT(1X,1F12.3,3X,1F9.5)
      PRINT*,TIME*dt,CURR
      CALL FLUSH(15)
      ENDIF

**** Dump conc profile ****

      IF (FLAG.eq.1) THEN
      IF
((MOD(time,40).EQ.0).AND.(time.GT.0))
THEN
       PRINT *,'DUMPING CP.....'
      READ (16,*) fname
      IF (fname.EQ.'END') FLAG=0
      OPEN
(12,FILE=fname,STATUS="UNKNOWN")
      DO 920 j=1,N1-1,5
      DO 910 k=1,N2-1,5
      WRITE (12,*) T(j,k)
 910  CONTINUE
 920  CONTINUE
      CLOSE(12)
      PRINT *,'CP DUMP SUCCESSFUL'
      ENDIF
      ENDIF


 1000 CONTINUE
      STOP
      END
```

(3) BI Modelling of $EC_{het}E$ Mechanism to Give Working Curve, then Calculating the Value of K_{het} From I_{lim} Data

```
**************************************
 STEADY-STATE BI: EChetE MECHANISM
      **
**************************************


   REAL*8 A(1000,4),B(1000,4),C(1000,4),
          U(1000,4),D(1000,4)
   REAL*8 ALPHA(1000,4),BETA(1000,4),
          F(1000),LAM(1000),LAMk(1000)
   REAL*8 AO,XE,W,DD,DIFF,TWOH,VF,
          b0,EVF(100),ILIMIT(100)
   REAL*8 VX,VO,H,LAMY,DY,DX,Y,
          ACCUM(4),CURR,Neff,ILIM
   REAL*8 GAM,GAMMIN,GAMMAX,
          GAMSTEPS,VAR,BESTVAR,
          KHET,BESTKHET
   INTEGER J,K,L,M,S,CPFLAG,CH

**     NJ & NK VALUES

       NK=1000
       NJ=1000
       CH=NJ/1

**     CELL PARAMETERS
       DO 5 I=1,M
       READ(11,*) EVF(I),ILIMIT(I)
       PRINT*,EVF(I),ILIMIT(I)
 5     CONTINUE
       CLOSE(11)

       CPFLAG=1
       BESTVAR=1000

**     CONC PROFILES

       IF (CPFLAG) THEN
       OPEN(11,FILE='cpa.dat',
      STATUS='UNKNOWN')
       OPEN(12,FILE='cpb.dat',
      STATUS='UNKNOWN')
       OPEN(13,FILE='cpc.dat',
      STATUS='UNKNOWN')
       OPEN(14,FILE='cpd.dat',
      STATUS='UNKNOWN')
       OPEN(15,FILE='sum.dat',
      STATUS='UNKNOWN')
       ENDIF

**     Cartesian Grid
```

```
      Xe      = 0.00406
      twoH    = 0.01
      W       = 0.094
      dd      = 0.2
      Diff    = 2.e-5
      Ao      = 1.48e-6

      PRINT*
      PRINT*,"ENTER      RANGE      OF
VALUES
     FOR GAMMA : (GAMMA=KHET/2)"
      PRINT*
      PRINT*,"Enter min value"
      READ (*,*) GAMMIN
      PRINT*,"Enter max value"
      READ (*,*) GAMMAX
      PRINT*,"Enter number of steps to        **
     sample"
      READ (*,*) GAMSTEPS
      PRINT*,"Enter number of sets of
data"
      READ (*,*) M

      PRINT*
      PRINT*,"  READING ",M," POINTS  10
OF
     EXPERIMENTAL DATA"                       **
      PRINT*
      PRINT*,"          FLOW      RATE
ILIM"
      PRINT*

      u(j,1)=1
      u(j,2)=0
      u(j,3)=0
      u(j,4)=0
20    CONTINUE

**    A,B & C for 4 species
      DO 40 s=1,4
      DO 30 J=1,CH-1
      a(j,s)=-LAM(j)
      b(j,s)=1+2*LAM(j)
      c(j,s)=-LAM(j)
30    CONTINUE
       b(CH-1,s)=b(CH-1,s)+c(CH-1,s)
40    CONTINUE

**    Production of B from A
     [eq & opp fluxes]
      b(1,2)=b(1,2) + a(1,2)/(1+GAM)

**    Production of D from C
     [eq & opp fluxes]
      b(1,4)=b(1,4) + a(1,4)

**    Standard Alpha & beta calculation
     [beta of CH-1 isn't used]
      DO 70 s=1,4
      accum(s)=0
      alpha(1,s) = b(1,s)
      beta(1,s) = c(1,s)/alpha(1,s)

      dx=Xe/NK
      dy=twoH/NJ
      LAMy=Diff/dy/dy

      PRINT*
      PRINT*," KHET                VAR"
      PRINT*
      DO 2000 L=0,GAMSTEPS
      GAM=GAMMIN+L*(GAMMAX-
     GAMMIN)/GAMSTEPS
      KHET=GAM/dy*Diff
      VAR=0
      DO 1000 I=1,M
      Vf=EVF(I)
      ILIM=ILIMIT(I)

**    Parabolic flow
      h       = twoH/2.
      Vo= 3*Vf/4/h/dd
      DO 10 j=1,CH-1
      y = j*dy
      Vx = Vo*(1-(h-y)*(h-y)/h/h)
      LAM(j) = LAMy*dx/Vx
      LAMk(j) = KHET*dx/Vx
      CONTINUE

**    Initial Concentrations
      DO 20 j=1,CH
      DO 110 J=2,CH-1
      f(j)=(d(j,s)-a(j,s)*f(j-1))
           /alpha(j,s)
110   CONTINUE

      u(CH-1,s)=f(CH-1)
      DO 120 J=CH-2,1,-1
      u(j,s)=f(j) - beta(j,s)*u(j+1,s)
120   CONTINUE
150   CONTINUE

**    CONC PROFILES

    IF (CPFLAG.AND.MOD(K,NK/50).EQ.0)
     THEN
      DO 160 J=1,CH,CH/50
      WRITE (11,*) U(J,1)
      WRITE (12,*) U(J,2)
      WRITE (13,*) U(J,3)
      WRITE (14,*) U(J,4)
      WRITE (15,*)U(J,4)+U(J,3)
                  +U(J,2)+U(J,1)
160   CONTINUE
      ENDIF

**    Accumulators for current **
      b0=(u(1,1)+u(1,2))/(1+GAM)
      accum(1)=accum(1)+u(1,1)
      accum(2)=accum(2)+u(1,2)
      accum(3)=accum(3)+GAM*b0
200   CONTINUE

*     End of k loop *
*     Calculate current in uA *
```

```
      DO 60 j=2, CH-1
       alpha(j,s)=b(j,s) - a(j,s)*beta(j-1,s)
       beta(j,s)=c(j,s)/alpha(j,s)
60    CONTINUE
70    CONTINUE

**  k loop  **
      DO 200 k=1,NK

**    SETUP D FROM U :
**  HOMOGENEOUS KINETICS
**  (There aren't any)

      DO 100 j=1,CH
      d(j,1)=u(j,1)
      d(j,2)=u(j,2)
      d(j,3)=u(j,3)
      d(j,4)=u(j,4)
100   CONTINUE

**    N species Thomas Algorithm
      DO 150 s=1,4
**    Species B&D made at electrode
      if(s.eq.2) d(1,2)=u(1,2)-
          a(1,2)*u(1,1)/(1+GAM)
      if(s.eq.4) d(1,4)=u(1,4)-
                          a(1,4)*u(1,3)
      f(1) = d(1,s)/alpha(1,s)
      curr=(accum(1)+(3*accum(3)))*Ao*
      96485*W*Diff*1.e6*dx/dy

*     Calculate Variance
      VAR=VAR+((CURR-ILIM))**2
      IF (CPFLAG) THEN
      CLOSE(11)
      CLOSE(12)
      CLOSE(13)
      CLOSE(14)
      CLOSE(15)
      ENDIF
1000  CONTINUE

      PRINT*, KHET,VAR
      IF (VAR.LT.BESTVAR) THEN
      BESTVAR=VAR
      BESTKHET=KHET
      ENDIF
2000 CONTINUE

  PRINT*, "THE BEST FITTING KHET IS :"
  PRINT*," BESTKHET          BESTVAR"
  PRINT*, BESTKHET,BESTVAR
  END
```

(4) Working Surface Showing the Variance of $\Delta\theta_{1/2}$ with Log K_{het} and Log Ks.

```
**********************
*PROGRAM SURFACE*
**********************
      REAL*8 N,EVF(100),EEHALF(100)
      COMMON /EDATA/ N,EVF,EEHALF
      REAL*8 VAR,KCHET,KEHET,
     KCHETMIN,KCHETMAX,KEHETMIN,
     KEHETMAX
      REAL*8
Tmin,Tmax,TOL,VF,Xe,twoH,
     dd,Diff,Ao,CONV,CALCVAR
      REAL*8 EHETSTEPS,CHETSTEPS,
     CALCTHALF,LOGKEHET,LOGKCHET
      CHARACTER*30 FILENAME

*     USER INTERFACE

      PRINT*,"Enter output data file name"
      READ (*,*) FILENAME
      PRINT*
      PRINT*,"CHEMICAL
HETEROGENEOUS
           RATE CONSTANT (Khet)"
      PRINT*
      PRINT*,"Enter      log(10)      of
dimensionless
           min value"
      READ (*,*) KCHETMIN
      PRINT*,"Enter      log(10)      of
      WRITE(10,*)"    KHET          K0
DTH"
      DO 20 I=0,CHETSTEPS
      DO 10 J=0,EHETSTEPS
    LOGKCHET=KCHETMIN+I*
    (KCHETMAX-KCHETMIN)/CHETSTEPS
    LOGKEHET=KEHETMIN+J*
    (KEHETMAX-KEHETMIN)/EHETSTEPS
      KCHET=CONV*(10**(LOGKCHET))
      KEHET=CONV*(10**(LOGKEHET))
      Tmin=-20
      Tmax=10
      DTH=CALCTHALF(VF,KCHET,
           KEHET,Tmin,Tmax,TOL)
      WRITE(10,*) LOGKCHET,
                  LOGKEHET,DTH
      CALL FLUSH(10)
10    CONTINUE
20    CONTINUE
      CLOSE(10)
      END

*     Binary search for Theta-half
      REAL*8                FUNCTION
CALCTHALF(VF,
          KCHET,KEHET,Tmin,Tmax,TOL)
      REAL*8 VF,KCHET,KEHET,TH,Tmin,
           Tmax,TOL
```

```
dimensionless
              max value"
        READ (*,*) KCHETMAX
        PRINT*,"Enter number of steps to
              sample"
        READ (*,*) CHETSTEPS
        PRINT*
        PRINT*,"ELECTROCHEMICAL
              HETEROGENEOUS RATE
              CONSTANT (K0)"
        PRINT*
        PRINT*,"Enter        log(10)        of
dimensionless
              min value"
        READ (*,*) KEHETMIN
        PRINT*,"Enter        log(10)        of
dimensionless
              max value"
        READ (*,*) KEHETMAX
        PRINT*,"Enter number of steps to
              sample"
        READ (*,*) EHETSTEPS

**      CELL PARAMETERS
        Xe      = 0.00406
        twoH    = 0.01
        dd      = 0.2
        Diff    = 2.0e-5
        Ao      = 1.48e-6
        CONV = ((0.5*twoH*twoH*Xe*dd)/
             (3.0*VF*Diff*Diff))**(-1.0/3.0)

        OPEN (10,FILE="results2.dat",
             STATUS="UNKNOWN")
IF(VERBOSE) PRINT *,Tmin,Tmax," ",
       Error
3010    CONTINUE
        CALCTHALF = Tmax
        IF(ERmin.LT.ERmax) CALCTHALF =
       Tmin
        IF(VERBOSE) PRINT *,"DELTA-
       THETA-HALF = ",CALCTHALF
        RETURN
        END

*       Simulation code
        REAL*8                  FUNCTION
SIMI(VF,KCHET,
     KEHET,THETA)
        REAL*8 VF,KCHET,KEHET
        INTEGER NK,NJ,NGY
        PARAMETER(NK=1000,NJ=500,
                  NGY=2*NJ)
        REAL*8 A(NGY),B(NGY),C(NGY),
             U(NGY),D(NGY),LAMJ(NGY)
        REAL*8 ALPHA(NGY),BETA(NGY)
             ,F(NGY)
        REAL*8
AO,XE,W,DD,DIFF,Rc,TWOH,
             PHI,FAR,R,T
        REAL*8 VX,VO,H,LAMY,DY,DX,Y,
             ACCUM,CURR,ACCUM2
        REAL*8 I,IMIN,IMAX,ITARG,Error,
             SIMI,ERmax,ERmin
        INTEGER VERBOSE
        VERBOSE=0
        TH=-80.0
        ITARG=SIMI(VF,KCHET,KEHET,TH)
/2
        IF(VERBOSE) PRINT *
        IF(VERBOSE)    PRINT    *,"Binary
Search:
       Ilim = ",ITARG*2,";  TOL=",TOL
        IF(VERBOSE) PRINT *
        IMIN=SIMI(VF,KCHET,KEHET,Tmin)
        ERmin=ABS(IMIN-ITARG)/ITARG
        IMAX=SIMI(VF,KCHET,KEHET,Tma
x)
        ERmax=ABS(IMAX-ITARG)/ITARG
        ERROR=MIN(ERmin,ERmax)
        IF(VERBOSE) PRINT *,Tmin,Tmax,"
",
      Error
        DO 3010 WHILE (ERROR.GT.TOL)
        TH=(Tmin+Tmax)/2.0
        I=SIMI(VF,KCHET,KEHET,TH)
        ERROR=ABS(I-ITARG)/ITARG
        IF (I.LT.ITARG) THEN
        Imax=I
        Tmax=TH
        ERmax=ERROR
        ELSE
        Imin=I
        Tmin=TH
        ERmin=ERROR
        ENDIF
**      Parabolic flow
        h       = twoH/2.
        Vo      = 3*Vf/4/h/dd

*       [A] : Upside down
        DO 10 j=1,NJ
        y = (NJ+1-j)*dy
        Vx = Vo*(1-(h-y)*(h-y)/h/h)
        LAMj(j) = LAMy*dx/Vx
10      CONTINUE

*       [B] : Right way up
        DO 20 j=NJ+1,NGY
        y = (j-NJ)*dy
         Vx = Vo*(1-(h-y)*(h-y)/h/h)
        LAMj(j) = LAMy*dx/Vx
20      CONTINUE

**      A,B and C
        DO 30 j=1,NGY
        a(j)=-LAMj(j)
        b(j)=1+2*LAMj(j)
        c(j)=-LAMj(j)
30      CONTINUE

**      No flux conditions
        b(1)=b(1)+a(1)
        a(1)=0
```

```
      REAL*8 THETA,STEPS,Tmin,Tmax,
     Ko,ATC,Co
      REAL*8 ka1,ka2,kb1,kb2,kf,kb,Ly,
     n1,n2,Q,B0
      INTEGER J,K

**    CELL PARAMETERS
      PHI    = 0.1
      Xe     = 0.00406
      twoH   = 0.01
      W      = 0.154
      dd     = 0.2
      Diff   = 2.0e-5
      Ao     = 1.48e-6
      Rc     = KCHET

** ELECTROCHEMICAL HETEROGENEOUS
   KINETICS

      n1     = 1
      n2     = 3
      Ko     = KEHET
      ATC    = 0.5

**    PHYSICAL CONSTANTS

      FAR=96485
      T=298
      R=8.314

**    Cartesian Grid
      dx=Xe/NK
      dy=twoH*PHI/(NJ+1)
      LAMy=Diff/dy/dy
      beta(j)=c(j)/alpha(j)
110   CONTINUE

*  k loop  *

      DO 500 k=1,NK

**    Thomas Algorithm
      f(1) = d(1)/alpha(1)
      DO 150 J=2,NGY
      f(j)=(d(j)-a(j)*f(j-1))/alpha(j)
150   CONTINUE
      u(NGY)=f(NGY)
      DO 160 J=NGY-1,1,-1
      u(j)=f(j) - beta(j)*u(j+1)
160   CONTINUE

**    Copy u -> d **
      DO 170 j=1,NGY
      b(NGY)=b(NGY)+c(NGY)
      c(NGY)=0

****  Potential  ****

      Q=kf+Ly+kb+Rc+(Rc*kf/Ly)
      kf=ko*exp(-ATC*THETA)
      kb=ko*exp((1.-ATC)*THETA)
      Ly=Diff/dy
      ka1=(Ly+kb+Rc)/Q
      ka2=kb/Q
      kb1=(Ly+kf)/Q
      kb2=kf/Q

**    Initial Concns
      DO 100 j=1,NJ
      d(j)=1.
      d(j+NJ)=0.
100   CONTINUE

**    Electrode boundary conditions
      b(NJ)=1+2*LAMj(NJ)
LAMj(NJ)*ka1
      c(NJ)=-LAMj(NJ)*ka2
      b(NJ+1)=1+2*LAMj(NJ+1)
LAMj(NJ+1)*kb1
      a(NJ+1)=-LAMj(NJ+1)*kb2

**    Alpha & Beta
      alpha(1) = b(1)
      beta(1) = c(1)/alpha(1)
      DO 110 j=2, NGY
      alpha(j)=b(j)-a(j)*beta(j-1)
      d(j)=u(j)
170   CONTINUE

**    Accumulator for current **
      Co=1-((U(NJ))*(ka1))-
((U(NJ))*(kb2))-
        (U(NJ+1)*kb1)-(U(NJ+1)*ka2)
      B0 = (((U(NJ))*kf)+((U(NJ+1))*
        (kf+Ly)))/Q
      accum=accum + (1-ka1)*U(NJ) - ka2*
          U(NJ+1) + (n2*Rc*B0*dy/Diff)
500   CONTINUE

*  End of k loop  *

*     Calculate current in uA *
curr=accum*Ao*96485*W*Diff*1.e6*dx/dy
   SIMI=CURR
   RETURN
   END
```

(5) Fitting Experimental Data To The $\Delta\theta_{1/2}$ Working Surface

```
**    SCAN FOR MINIMUM VARIANCE

      PROGRAM SURFACE
      REAL*8 EVF(100),EEHALF(100)
      READ (*,*) K0MAX
      PRINT*,"Enter number of steps to
          sample"
      READ (*,*) K0STEPS
```

```
      INTEGER*8 N,NVALID
      COMMON /EDATA/ N,EVF,EEHALF
      REAL*8
Xe,TwoH,DD,DIFF,Ao,T,n1,n2
      COMMON                    /CELL/
Xe,TwoH,DD,DIFF,
                  Ao,T,n1,n2,Khet
      REAL*8 VAR,Khet,E0,K0,E0MIN,
     E0MAX,K0MIN,K0MAX,CALCVAR
      REAL*8
E0STEPS,KOSTEPS,BESTE0,
           BESTKO,BESTVAR
      CHARACTER*30 EXPTNAME

*     USER INTERFACE
      PRINT*
      PRINT*,"Fitting of Experimental data
to
           theoretical E1/2 data"
      PRINT*
      PRINT*,"Standard          Electrode
Potential"
      PRINT*
      PRINT*,"Enter min value"
      READ (*,*) E0MIN
      PRINT*,"Enter max value"
      READ (*,*) E0MAX
      PRINT*,"Enter number of steps to
           sample"
      READ (*,*) E0STEPS
      PRINT*
      PRINT*,"Electrochemical
Heterogeneous
           Rate Constant (K0)"
      PRINT*
      PRINT*,"Enter min value"
      READ (*,*) K0MIN
      PRINT*,"Enter max value"
      BESTVAR=VAR
      BESTE0=E0
      BESTK0=K0
      ENDIF
      WRITE(10,*) E0,K0,VAR
      CALL FLUSH(10)
10    CONTINUE
20    CONTINUE
      PRINT*, "THE BEST FITTING
           PARAMETERS ARE :"
      PRINT*,"    BESTE0        BESTK0
BESTVAR"
      PRINT*, BESTE0,BESTK0,BESTVAR
      CLOSE(10)
      END

*     Compute variance
      REAL*8                    FUNCTION
CALCVAR(E0,K0)
      REAL*8 E0,K0
      REAL*8 EVF(100),EEHALF(100)
      INTEGER *8 N,NVALID
      COMMON /EDATA/ N,EVF,EEHALF
      REAL*8
      PRINT*,"Enter number of sets of
data"
      READ (*,*) N

** EXPERIMENTAL: Alpha is assumed to be
                  be 0.5 (in surface data)
      Xe     = 0.00406
      twoH   = 0.01
      dd     = 0.2
      Diff   = 2.0e-5
      Ao     = 1.48e-6
      T      = 298
      n1     = 1
      n2     = 3
      Khet   = 0.24
      BESTVAR = 1

      CALL READSURF()
      CALL READFILE(EXPTNAME)
      PRINT*
      PRINT*," E0    K0    Error"
      OPEN (10,FILE="variance.dat",
          STATUS="UNKNOWN")
      WRITE(10,*)" E0    K0    Err"
      DO 20 I=0,E0STEPS
      DO 10 J=0,K0STEPS
      E0=E0MIN+I*(E0MAX-E0MIN)/
         E0STEPS
      K0=K0MIN+J*(K0MAX-K0MIN)/
          K0STEPS
      VAR=CALCVAR(E0,K0)
      PRINT*,E0,K0,VAR
      IF (VAR.LT.BESTVAR) THEN
      CLOSE(11)
      PRINT*
      END
*
*     READ WORKING SURFACE into
    COMMON block
*
      SUBROUTINE READSURF()
      INTEGER*8 i,j,NX,NY
      REAL*8 Xmin,Xstep,Ymin,Ystep,
           Z(500,500)
      COMMON                    /SURFDATA/
NX,NY,Xmin,
     Xstep,Ymin,Ystep,Z
      OPEN(12,FILE='surface.dat',
          STATUS='OLD')
      READ (12,*) NX,NY
      READ (12,*) Xmin,Xstep
      READ (12,*) Ymin,Ystep
      DO I=1,NX
      DO J=1,NY
      READ(12,*) Z(I,J)
      END DO
      END DO
      CLOSE(12)
      END
*
*     Bilinear Interpolation function
*
```

```
EHALF,SUM,CALCEHALF,VF
      NVALID=N
      SUM=0
      DO 110 I=1,N
      VF=EVF(I)
      EMIN=-2
      EMAX=2
      EHALF=CALCEHALF(VF,E0,K0)
      IF                          (EHALF.EQ.-
99)NVALID=NVALID-1
      IF                    (EHALF.EQ.-99)
EHALF=EEHALF(I)
      PRINT*, NVALID
      SUM=SUM+((EHALF-EEHALF(I))/
          EEHALF(I))**2
110   CONTINUE
      IF (NVALID.GT.0) THEN
      CALCVAR=SUM/NVALID
      ELSE
      CALCVAR=-1
      ENDIF
      END
*
*     Read Expt data into COMMON block
*
      SUBROUTINE
READFILE(EXPTNAME)
      CHARACTER*20 EXPTNAME
      REAL*8 EVF(100),EEHALF(100)
      INTEGER *8 N
      COMMON /EDATA/ N,EVF,EEHALF
      OPEN(11,FILE=EXPTNAME,
         STATUS="OLD")
      PRINT*
      PRINT*,"READING ",N," POINTS OF
           EXPERIMENTAL DATA"
      PRINT*
      PRINT*,"  FLOW RATE            E
1/2"
      DO 210 I=1,N
      READ(11,*) EVF(I),EEHALF(I)
      PRINT*,EVF(I),EEHALF(I)
210   CONTINUE
      dx1=0
      i=nx-1
      endif
      if (j.eq.ny) then
    dy=1
    dy1=0
    INTER=Z(i,j)*dx1*dy1+Z(i+1,j)*dx*dy1
    INTERP=INTER+Z(i,j+1)*dx1*dy
           +Z(i+1,j+1)*dx*dy
      END

*     Replacement for Simulation code :
    Interpolate Ehalf
      REAL*8                FUNCTION
CALCEHALF(VF,E0,K0)
      REAL*8 VF,E0,K0,Khet
      REAL*8
Xe,TwoH,DD,DIFF,Ao,T,n1,n2
      COMMON                    /CELL/
*   X=LGKhet  Y=LGK0

      REAL*8 FUNCTION INTERP(X,Y)
      INTEGER*8 i,j,NX,NY
      REAL*8 x,y,INTER
      REAL*8 dx,dx1,dy,dy1
      COMMON              /SURFDATA/
NX,NY,Xmin,
    Xstep,Ymin,Ystep,Z
      REAL*8 Xmin,Xstep,Ymin,Ystep,
           Z(500,500)

*     Extrapolation Of Surface
      IF (X.LT.XMIN) X=XMIN
      IF     (Y.GT.YMIN+(NY-1)*YSTEP)
Y=(YMIN+(NY-1)*YSTEP)

*     Ignoring Points Off Surface
      IF (Y.LT.YMIN) INTERP=-10
      IF (X.GT.XMIN+(NX-1)*XSTEP)
      INTERP=-10
      IF (INTERP.eq.-10) RETURN

      i=1+((x-xmin)/xstep)
      j=1+((y-ymin)/ystep)
      dx=(x-xmin)/xstep -(i-1)
      dx1=1-dx
      dy=(y-ymin)/ystep -(j-1)
      dy1=1-dy

*     Drop index if on very edge
      if (i.eq.nx) then
      dx=1
      R=8.314

**  COMPUTE LOG DIMENSIONLESS RATE
    CONSTANTS = CO-ORDINATES ON
     SURFACE

      OPEN (11,FILE="dim.dat",
          STATUS="UNKNOWN")
      CONV = ((0.5*twoH*twoH*Xe*dd)/
           (3.0*VF*Diff*Diff))**(2.0/3.0)
      LGK0=LOG(CONV*K0)
      LGKhet=LOG(CONV*Khet)
      WRITE(11,*) LGK0,LGKhet,VF

**    PERFORM                  BILINEAR
INTERPOLATION
    FOR SHIFT IN THETA-HALF

      THALF=INTERP(LGKhet,LGK0)
      IF (THALF.EQ.-10) THEN
      CALCEHALF=-99
      ELSE
    CALCEHALF=(THALF*R*T/FAR/n1)+E0
      ENDIF
      RETURN
      END
```

```
Xe,TwoH,DD,DIFF,
                    Ao,T,n1,n2,Khet
      REAL*8 THALF,LGK0,LGKhet
      REAL*8 INTERP

**    PHYSICAL CONSTANTS

      FAR=96485
```

(6) Program To Find Tafel Slope From I_{lim} Data

```
**    PROGRAM TO FIND TAFEL SLOPE

 PARAMETER(NK=500,NJ=1000,NGY=2*NJ)
 REAL*8 A(NGY),B(NGY),C(NGY),U(NGY),
  D(NGY),LAMJ(NGY)
 REAL*8 ALPHA(NGY),BETA(NGY),F(NGY)
 REAL*8 AO,XE,W,DD,DIFF,Rc,TWOH, PHI
 REAL*8 VF,VX,VO,H,LAMY,DY,DX,Y,
        ACCUM, CURR,ACCUM2,Ilim
 REAL*8 THETA,STEPS,Tmin,Tmax,Ko,ATC,
        Co,TAFEL,B0
 REAL*8 ka1,ka2,kb1,kb2,kf,kb,Ly,n1,n2,Q
 INTEGER J,K

**    CELL PARAMETERS
      PHI    = 0.1
      Xe     = 0.00406
      twoH   = 0.01
      W      = 0.104
      dd     = 0.2
      Diff   = 2.0e-5
      Vf     = 0.27
      Ao     = 1.48e-6
      Rc     = 0.184
      n1     = 1
      n2   = 3

**    Scan parameters
      K = 0.1
      ATC= 0.5
      Vo = 3*Vf/4/h/dd

*     [A] : Upside down
      DO 10 j=1,NJ
      y = (NJ+1-j)*dy
      Vx = Vo*(1-(h-y)*(h-y)/h/h)
      LAMj(j) = LAMy*dx/Vx
10    CONTINUE

*     [B] : Right way up
      DO 20 j=NJ+1,NGY
      y = (j-NJ)*dy
      Vx = Vo*(1-(h-y)*(h-y)/h/h)
      LAMj(j) = LAMy*dx/Vx
20    CONTINUE

**    A,B and C

      DO 30 j=1,NGY

      Tmin=-1
      Tmax=0
      Steps=10

      PRINT*
      PRINT*,"ENTER K0"
      PRINT*
      READ (*,*) Ko

      OPEN(12,FILE='cp.dat',
          STATUS='UNKNOWN')
      OPEN(13,FILE='wshape.dat',
         STATUS='UNKNOWN')
      WRITE (13,*) "  Theta      Current"
      WRITE (13,*)
      OPEN(14,FILE='tafel.dat',
         STATUS='UNKNOWN')
      WRITE (14,*) "  Tafel      Theta"
      WRITE (14,*)
      PRINT*
      PRINT*,"  Tafel    Theta    Current"
      PRINT*

**    Cartesian Grid
      dx=Xe/NK
      dy=twoH*PHI/(NJ+1)
      LAMy=Diff/dy/dy

**    Parabolic flow
      h  = twoH/2.
**    Alpha & Beta
      alpha(1) = b(1)
      beta(1) = c(1)/alpha(1)
      DO 110 j=2, NGY
      alpha(j)=b(j)-a(j)*beta(j-1)
      beta(j)=c(j)/alpha(j)
110   CONTINUE

*  k loop  *
      DO 500 k=1,NK

**    Thomas Algorithm
      f(1) = d(1)/alpha(1)
      DO 150 J=2,NGY
      f(j)=(d(j)-a(j)*f(j-1))/alpha(j)
150   CONTINUE
      u(NGY)=f(NGY)
      DO 160 J=NGY-1,1,-1
      u(j)=f(j) - beta(j)*u(j+1)
```

```
      a(j)=-LAMj(j)
      b(j)=1+2*LAMj(j)
      c(j)=-LAMj(j)
30    CONTINUE

**    No flux conditions
      b(1)=b(1)+a(1)
       a(1)=0
      b(NGY)=b(NGY)+c(NGY)
      c(NGY)=0

****  Potential Loop    ****

      DO 1000, p=-1,Steps
      THETA=Tmin + (Tmax-Tmin)/Steps*p
      IF (p.eq.-1) THEN
      THETA=-1000
      ENDIF
      kf=ko*exp(-ATC*THETA)
      kb=ko*exp((1.-ATC)*THETA)
      Ly=Diff/dy
      Q=kf+Ly+kb+Rc+(Rc*kf/Ly)
      ka1=(Ly+kb+Rc)/Q
      ka2=kb/Q
      kb1=(Ly+kf)/Q
      kb2=kf/Q

**    Initial Concns
      DO 100 j=1,NJ
      d(j)=1.
      d(j+NJ)=0.
100   CONTINUE

**    Electrode boundary conditions
      b(NJ)=1+2*LAMj(NJ)
LAMj(NJ)*ka1
      c(NJ)=-LAMj(NJ)*ka2
      b(NJ+1)=1+2*LAMj(NJ+1)
             - LAMj(NJ+1)*kb1
      a(NJ+1)=-LAMj(NJ+1)*kb2
      accum=0

160   CONTINUE

**    Copy u -> d **
      DO 170 j=1,NGY
      d(j)=u(j)
170   CONTINUE

**    Accumulator for current **
 Co=1-((U(NJ))*(ka1))-((U(NJ))*(kb2))
      -(U(NJ+1)*kb1)-(U(NJ+1)*ka2)
 B0 = (((U(NJ))*kf)+((U(NJ+1))*(kf+Ly)))/Q
 accum=accum+(1-ka1)*U(NJ)-ka2*U(NJ+1)
        + (n2*Rc*B0*dy/Diff)

*     Write out concentration strip
      IF (MOD(k,NK/50).EQ.0) THEN
      DO 190 J=1,NGY,NGY/100
      WRITE(12,*) U(J)
190   CONTINUE
      ENDIF
500   CONTINUE

*  End of k loop  *

*  Calculate current in uA *
   curr=accum*Ao*96485*W*Diff*1.e6*dx/dy
   IF (p.eq.-1) THEN
      Ilim=curr
   ENDIF
   TAFEL=LOG10((1/curr)-(1/Ilim))
   print*, TAFEL,Theta,curr
   WRITE (13,*) Theta,curr
   WRITE (14,*) TAFEL,Theta
   CALL FLUSH (13)
   CALL FLUSH (14)

**  Next Potential  **

1000  CONTINUE
      END
```